5-13-2014

Synthesis of Modified Indocyanine Green Dyes and Targeting Hypoxia in Tumor Cells And Influence of Distal Methyl Group on Base Induced Isomerization of Terminal Alkynes

Innus Mohammad
University of Connecticut - Storrs, innus.mohammad@uconn.edu

Synthesis of Modified Indocyanine Green Dyes and Targeting Hypoxia in Tumour Cells

And

Influence of Distal Methyl Group on Base Induced Base Isomerization of Terminal Alkynes

Innus Mohammad, Ph.D.

University of Connecticut 2014

Abstract

Tumor hypoxia is a major indicator of treatment resistance to chemotherapeutic drugs and fluorescence optical tomography has tremendous potential to provide clinically useful functional information by targeting tumor hypoxia. The current techniques to detect hypoxia involve invasive and non-invasive probes, for example MRI, PET (non-invasive) and polarographic needle electrodes (invasive). The polarographic needle electrode technique is limited to superficial tumors, such as cervix, neck, and head. Non-invasive techniques such as Magnetic Resonance Imaging (MRI) and Positron Emission Tomography (PET) are expensive for routine clinical use and these techniques suffers from low spatial resolution, high back ground counts, needs an injection of radioactive tracer. Therefore there is a need for a cheap and non-invasive and safe technique for imaging hypoxia in tumors which would improve the cancer therapy outcomes. The aim of this dissertation is to design a cheap and non-invasive method to image hypoxia in tumor cells. In this dissertation, synthesis, photophysical characterization and hypoxia evaluation of a series of 2-nitroimidazole coupled indocyanine green dyes (first, second and third generation) is presented. In the first generation, 2-nitroimidazoles were coupled to indocyanine gree (ICG) via ethanolamine

linker and in the third generation ethanolamine was replaced with a piperazine unit. The third generation has the same piperazine linker but linked to a rigid dye (pentamethine dye). Among the three generations, the third generation dyes are effective in providing a strong fluorescence signal and stayed much longer (up to 24h) in the hypoxic regions of tumor cells.

We have observed that incorporation of a methyl group distal to a terminal long-chain alkyne leads to an increased rate of isomerization to the corresponding internal alkyne upon treatment with a strong base, in DMSO. When compared to a long-straight chain terminal alkyne, the isobranch analog isomerizes about three times faster under identical conditions. In both cases, equilibration to a 95-97:5-3 mixture of internal:terminal alkyne follows isomerization. The difference in rate may be due to conformational effects that involve folding of the alkyne, bringing the distal substituent close to the alkyne moiety. The isobranch may provide steric hindrance that disrupts such folding, making the propargylic proton or the terminal alkyne proton more available for reaction with base.

Synthesis of Modified Indocyanine Green Dyes and Targeting Hypoxia in Tumor Cells

And

Influence of Distal Methyl Group on Base Induced Isomerization of Terminal Alkynes

Innus Mohammad, B.S., M.S.

B.S. Andhra University, Vizag, India, 2001

M.S. University of Hyderabad, India, 2004

A Dissertation Submitted

In Partial Fulfillment

Of the Requirements

For the Degree of

Doctor of Philosophy

At the University of Connecticut

2014

Approval Page

Doctor of Philosophy Dissertation

Synthesis of Modified Indocyanine Green Dyes and Targeting Hypoxia in Tumor Cells

And

Influence of Distal Methyl Group on Base Induced Isomerization of Terminal Alkynes

Presented by

Innus Mohammad

Major Advisor _____

Michael B. Smith

Associate Advisor _____

Christian Brückner

Associate Advisor _____

Quing Zhu

University of Connecticut

(2014)

Acknowledgements

This dissertation would not have been possible without the guidance and the help of several individuals who in one way or another contributed and extended their valuable assistance in the preparation and completion of this study.

First and foremost, my utmost gratitude to my Ph.D. advisor Dr. Michael B. Smith, his sincerity and encouragement will never be forgotten. Dr Smith has always been supportive as I hurdled through obstacles in the completion of this research work.

I owe my deepest gratitude to my associate advisor Dr. Christian Brückner, for his kind concern and consideration of my requests and questions. Dr. Brückner has taught me how to format the thesis using Microsoft word automatic settings, which made my life easier when I was writing my thesis. He was always there for me whenever I needed help and he also gave me access to his lab to use the UV-VIS and other instruments.

I am grateful to Dr. Mark Peczuh, whom I took the major organic courses with. He is an excellent teacher and made me feel comfortable with the difficult concepts of organic chemistry. I have gained incredible knowledge from him.

I am thankful to our collaborator Dr. Quing Zhu for giving me an opportunity to work with her. She has been always kind and helpful in many aspects.

I would like to thank Dr. Fatma Selampinar for being a general examiner in my committee and also for being an example and motivation for me to acquire the ability of multi-tasking and time management.

My journey wouldn't have been this far if Mr. Isukapalli Thatharao garu (ITR) had not supported me for my BS and MS degrees. He had provided me the basic needs for my education. The caring and responsibility he took for me is invaluable. I am indebted to him for the rest of my life.

I am thankful to Dr. Anwar Beshir, Kaddy Camara, Rozita Ramli and the Smart family (Kelley, Kevin, Luke, Lisa, Keri, Janet and James) for their incredible efforts in creating a family atmosphere for me, here in the United States.

I am indebted to my best friend Dr. Santosh Keshipeddy for being such a good friend. Santosh supported me in both good and bad times. He has been advised me in making important decisions in my life. I am honored to be his friend and he is an example of true a friend. I would like to thank Jagadish Kona and Dr. Vamsi Krishna Mudhivarthi for the care and help that I got from them. Both Jagadish and Vamsi were there to help me in both good and bad times. I am grateful to Dr. Prashant Deshmukh who has been such a wonderful friend and colleague Prashant taught me the dos and donts of presenting research work at conferences, thanks for teaching me the tips and all the fun we had in driving down to New Orleans, ACS meeting. Prashant has been checking on me to make sure that I am aware of the necessary things that I need to do for the thesis defense and finding a postdoc.

I thank my past and current lab mates, Courtney Stanford and Chris Dietz for creating a healthy working environment. Thank you for all the fun we had working together with deadlines to submit molecules to our collaborator.

I am thankful to many of my colleagues and seniors especially Dr. Nick Eddy for his encouragement. Nick and I have had numerous discussions about problem solving skills in

organic chemistry from which I learned valuable tricks. I would like to thank Drs. Yanke Liang, Sampada Chitale, Lalith Palitha Samankumara, Inoka Deshipriya. I wanted to thank Annifer Magpusao, Raghu Vanam, Vijay Jasti, Harsha Mamidipalli, Bhaskara Chikkaveeraiah., and all other friends in the chemistry department for their help in providing me the rides and cheering me up in my difficult times. I would like to thank my PG friends Basu Keluth, Phani Pavan, Venu Srinivas and others. I want to thank my childhood friends Murthy, Abbas, Arif, Malleswarrao, Seshu, Subbarao, G Venkat, Nagaraju, Kishore, Bujjinna Trinath, Prasad. Rajesh and others.

Special thanks to Mr. Tamma Ravi Kumar, my high school tutor and mentor for his motivation and the help he has been offering me over the years. Ravi Kumar and his family treats me as one of their family members, I thank you from my bottom of heart for such an honor.

Last but not the least; I would like to thank my parents Magbul Basha, Rahamtunnisa Begum, brother Ismail and my lovely sister Shamshad Begum for their continuous support and unconditional love. And the one above all of us, the omnipresent God, for answering my prayers for giving me the strength to plod on despite my constitution wanting to give up and throw in the towel, thank you so much Dear Lord.

To My Father and Mother

Table of contents

List of figures

List of tables

List of schemes

COMMON ABBREVIATIONS

Other, less common abbreviations are given in the text when the term is used.

Ac	Acetyl
Ac_2O	Acetic anhydride
AcOH	Aceticacid
aq.	aqueous
Bn	Benzyl
Boc	*tert*-Butoxycarbonyl
Bu	*n*-Butyl
Bz	Benzoyl
^{13}C NMR	Carbon nuclear magnetic spectroscopy
Cp	Cyclopentadienyl
Cy	Cyclohexyl
°C	Temperature in Degrees Celcius
3D	Three-dimensional
DCC	1,3-Dicyclohexylcarbodiimide
DCM	Dichloromethane
DEA	Diethylamine
Dibal-H	Diisobutylaluminum hydride
DIPEA	Diisoproply ethylamine
DMAP	4-Dimethylaminopyridine
DME	Dimethoxyethane
DMF	*N,N′*-Dimethylformamide
DMS	Dimethyl sulfide
DMSO	Dimethyl sulfoxide
EDCI. HCl	1-Ethyl-3-(3-dimethylaminopropyl)carbodiimide hydrochloride
ESI	Electrospray ionization mass spectrometry
Et	Ethyl
EtOAc	Ethylacetate
GC	Gas chromatography

h	Hour (hours)
hv	Irradiation with light
HCl	Hydrochloric acid
^{1}H NMR	Proton Nuclear Magnetic Resonance Spectroscopy
HOBt	Hydroxybenzotriazole
HPLC	High performance liquid chromatography
HRMS	High resolution mass spectrometry
Hz	Hertzs
i-Pr	Isopropyl
IR	Infrared spectroscopy
LDA	Lithium diisopropylamide
Me	Methyl
min	minutes
IUPAC	international union of pure and applied chemistry
MS	Molecular Sieves (3Å or 4Å)
MeOH	Methanol
NMR	nuclear magentic resoaonce spectroscopy
NBS	*N*-Bromosuccinimide
O.N.	Overnight
Ph	Phenyl
PhH	Benzene
PhMe	Toluene
PPA	Polyphosphoric acid
Pr	*n*-Propyl
PyBOP	benzotriazol-1-yl-oxytripyrrolidinophosphonium hexafluorophosphate
Py	Pyridine
quant	Quantitative yield
NHS	N-hydroxysuccinimide
r.t.	Room temperature
s	seconds

TBAF	Tetrabutylammonium fluoride
t-Bu	*tert*-Butyl
T1	Longitudinal or spin-lattice relaxation
TEA	Triethylamine
TEAI	tetraethylammonium iodide
TFA	Trifluoroacetic acid
.tfa	trifluoroacetyl as a counter anion in the salt
THF	Tetrahydrofuran
UV-VIS	Ultraviolet and visible light spectroscopy

Chapter 1.

INTRODUCTION

1.1 Cancer

The human body is made up of trillions of living cells. Every day, these cells grow, divide or die in an orderly fashion. Cells divide at a much higher rate in children, allowing for growth in human body. After a certain age, cells divide to replace the dying cells or, to repair the injuries. On average, an adult human body creates 60 billion new cells each day; an equal number must die to maintain the cell count. When cells divide/grow, errors can happen in the DNA (deoxyribonucleic acid) sequence, which results the damaged DNA. The causes for DNA damage are diverse and complex; some of them are UV radiation, nuclear radiation, smoking, and carcinogenic chemicals. When DNA gets damaged, the cell can either repairs the DNA or it will die by apoptosis, which is a programmed cell death process. If apoptosis fails, the cell with defective DNA starts making new cells, all these new cells contains the DNA defect. These cells multiply abnormally, which results the accumulation of mass called a tumor (Figure 1.1). All tumors are not cancerous; tumors that cannot invade other tissues are called benign tumors. Benign tumors are not life threatening, except for the fact that they grow very large and stress healthy tissues and organs.[1]

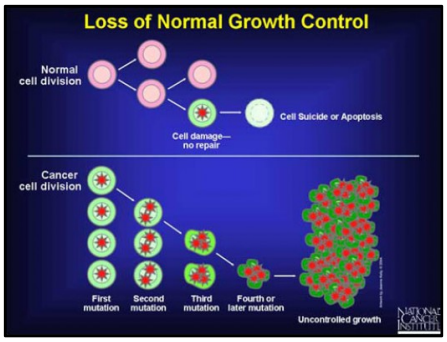

Figure 1.1. Loss of normal growth control in the cell[2]

Cancer cells can migrate to other parts of the body through the bloodstream and lymph vessels, which is called metastasis (Figure 1.2). Metastasis usually involves several steps, for invasion of cancer cells into normal tissues, including an intravasation step that involves movement of cancer cells through the walls of lymph vessels or blood vessels, and a circulation step in which cancer cells move through the lymphatic system and blood stream to other parts of the body. Cancer cells stop migrating in small blood capillaries and then invade the walls of the capillaries to migrate into the surrounding tissue, which is called as extravasation. Proliferation is the step where cancer cells multiply to form small tumors known as micrometastases. All cancers are not same. For example, lung cancer and skin cancer differ in terms of their growth rate and the way they respond to treatment techniques.[3]

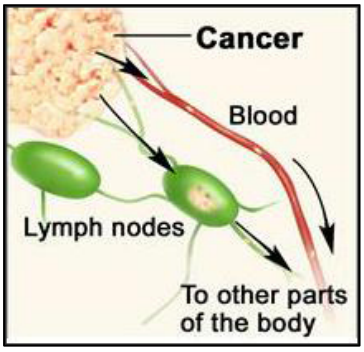

Figure 1.2. Migration of cancer cells to different parts of the body[3]

1.2 Hypoxia

Blood supply is vital for tumor growth and its sustenance. As a tumor grows, new blood vessels form through the process called angiogenesis (angio means blood vessel, and genesis means generation). The quick and uncontrolled growth of tumor cells results in irregular and leaky vascular networks. As a result, when tumor grows bigger, the oxygen supply to its vascular network will be reduced, which impedes biological functions of cancer

cells and leads to a tumor specific hypoxic region. This microenvironment of low oxygen, low pH and low glucose concentration in the tumor cell is characterized as *hypoxia* (Figure 1.3).[4-8]

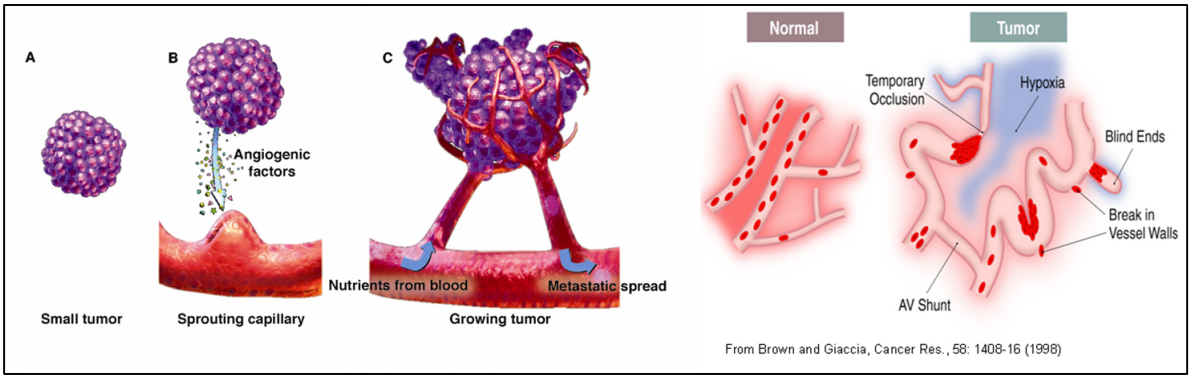

Figure 1.3. Angiogenesis and hypoxia

Cells in the hypoxic regions are relatively inactive compared to highly proliferative cells. The slow growth rate in hypoxic regions and decreasing perfusion inhibits the effectiveness of the chemotherapy drugs. In radiation therapy, radiation produces hydroxyl radicals from oxygen (O_2) and these radicals cause damage to the DNA of cancer cells, which eventually leads to cell death. The slow growth rate and low levels of oxygen are the reasons for the ineffectiveness of chemotherapy and radiotherapy. Studies have shown that prolonged hypoxia eventually leads to drug resistance, enhanced metastatic ability and treatment failure.[9] Given its significant role in tumor progression and resistance to the traditional anti-cancer agents, hypoxia is emerging as an important and high priority target for cancer therapy.

1.3 Hypoxia detection and Imaging techniques

Radiation therapy is one of the current treatments available for cancer; this treatment uses photons to ionize atoms in the DNA molecule. Upon irradiation an oxygen molecule forms an excited state singlet oxygen, which generates hydroxyl radicals; these hydroxyl radicals are effective in killing the cells in their immediate area by damaging the DNA. The lifetime of singlet oxygen in aqueous media is short, so it cannot diffuse very far, which enables targeting of specific areas in the body. Radiation therapy has little effect on treating hypoxic cells because of low levels of oxygen, and the free radicals formed recombine without causing damage to the DNA. Hypoxic cells are less than three times more resistant to radiation therapy than well oxygenated cancer cells. Therefore, it is important to have an understanding of tumor hypoxia to treat cancer effectively.

Current techniques to detect hypoxia involve invasive and non-invasive probes. Invasive techniques employ polarographic needle electrodes to measure partial pressure of oxygen in human tissue hypoxia. This technique is limited to superficial tumors, such as cervix,[10] head and neck.[11] Non-invasive techniques, Magnetic Resonance Imaging (MRI) and Positron Emission Tomography (PET) have been used to image hypoxia.

In PET technique, a positron-emitting radioactive tracer is injected into the patient's body, and radiation released by the tracer results in a three dimensional image of the body. The most commonly used PET scan imaging agent is ^{18}F-labeled fluoromisonidazole **1** (Figure 1.4). Nitroreductase activity (NO_2 group reduction on imidazole ring) influences the retention time of fluoromisonidazole within the tissues and it's delivery is not limited by perfusion.[12] There are several limitations, which include low spatial resolution, a high

retention in the liver, high background counts, and a day long resting period between repeated doses.[13]

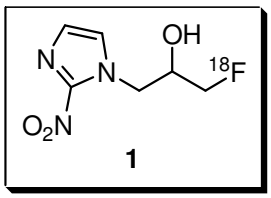

Figure 1.4. Fluoromisonidazole

In an MRI technique, a magnetic field lines up the electrically charged particles (protons) of hydrogen nucleus and a radio frequency field is used to alter their alignment systematically. When protons relax back in to their ground state, energy is given out that will be used in constructing the three dimensional image of the body. With the help of contrasting agents and tracers, an estimation of tumor permeability can be determined. There are several types of MRIs and each type provides different characteristics of a tumor. For example, fluorine-containing contrast agents are sensitive to oxygen concentration; so the ^{19}F-MRI can show the differences in oxygen concentration. Dynamic contrast-enhanced MRI (DCE-MRI) is a technique which provides the information about the properties of tumors such as distribution volume, permeability, and perfusion. Oxygen rich blood and oxygen poor blood behave differently in a magnetic field. BOLD-MRI (Blood oxygen level dependent MRI) works based on the difference between paramagnetic deoxyhemoglobin and diamagnetic oxyhemoglobin to image tumors, however this technique is not quantitative.[12]

Both PET and MRI techniques have their own limitations. They are expensive for the routine clinical use, and PET system suffers from low spatial resolution, high background counts and needs an injection of radioactive tracer. Therefore, there is a great need for a

cheap, non-invasive and safe technique for imaging hypoxia in tumors which would improve the cancer therapy outcomes.

Optical imaging is a non-invasive biomedical technique, which examines the cellular processes in a living animal. Near Infrared (NIR) Fluorescence Diffuse Optical Tomography (FDOT) is an optical imaging technique in which a fluorescence dye (fluorophore >700 nm) is irradiated with near infrared light and the remitted fluorescence collected for imaging. This technique has a potential to be of great use in the detection of hypoxia.

In the near infrared range, human tissue has relatively low absorption and high scattering, thus allowing an efficient penetration for near infrared light to pass through the tissue.[14] With the combination of a hypoxia marker that has the ability to target hypoxic regions of the tumor and a fluorescent dye, this technique can provide great sensitivity and specificity about the hypoxic regions of the tumor tissue. The signals from a fluorescent dye can be detected up to 2 to 3 cm from the skin surface and can be reconstructed in to an image to get the insight of the microenvironment of the tumor. Near infrared (NIR) Fluorescence Diffuse Optical Tomography (FDOT) is cost effective and has tremendous potential for probing tumor molecular markers.

Indocyanine dyes are an important class of NIR probes, among them indocyanine green (ICG, **2**) (Figure 1.5) is the only clinically approved dye for imaging purposes. Because of its high molar absorptivity and low toxicity, ICG **2** has various applications in fluorescence imaging[15-18] and it is the only FDA approved dye can be used in humans to administer the imaging studies.

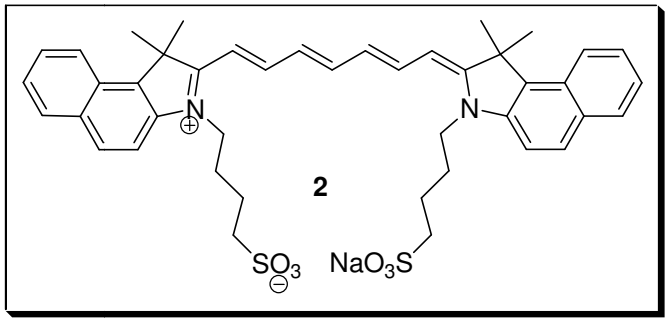

Figure 1.5. Indocyanine green (ICG)

1.4 Indocyanine Green and Nitroimidazoles

The light penetrate through the tissues as a function of wavelength, the shorter wavelength light absorbs on the surface of the tissue, which is not useful to image the biological processes that happen in the tissues. The longer wavelength light travels underneath the tissue and useful for imaging purpose (Figure 1.6). Major components of human tissue are hemoglobin and water, hemoglobin strongly absorbs at wavelengths lower than 650 nm and water absorbs strongly at wavelengths higher than 900 nm. The optical window between 650-900 nm is optimum for cell imaging experiments.

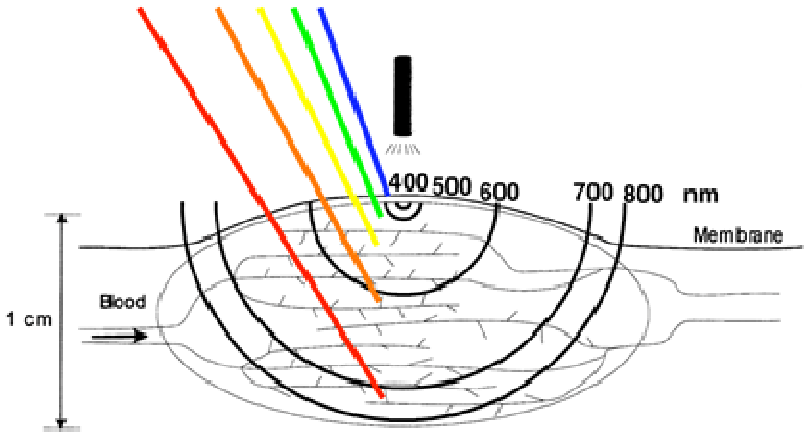

Figure 1.6. Penetration of light in tissue as a function of wavelengths[19]

Indocyanine green (ICG, **2**) meets the requirements of an NIR-FDOT dye, it absorbs at 760 nm and emits at ~807 nm, ICG has high molar absorptivity (250,000 cm^{-1} M^{-1}), which makes ICG a good contrasting dye to conduct fluorescence imaging deep under the surface of the skin. Studies in animals[20,21] and humans[22,23] have demonstrated that ICG has the ability to enhance contrast in tumor imaging. However, there are limitations to the use of ICG, **2** as a contrasting agent; it is highly non-specific, binds to plasma proteins, quickly washes out of the body and tumor site, the photostability in aqueous medium is low, and it has a low quantum yield.[24,25] These issues can be resolved with a dye that can target tumors specifically, and can be retained in the body for longer durations of time.

Hypoxic regions in tumors can be targeted with 2-nitroimidazoles. These compounds have a high affinity and sensitivity towards hypoxic cells. The sensitivity towards hypoxic cells is due to an enzyme-mediated four-electron reduction, which accumulates the nitroimidazoles in hypoxic regions of a tumor. A P-450 reductase is responsible for the reduction of nitroimidazoles, the actual mechanism for the nitro reduction is not known but the outline of a plausible mechanism is shown in Scheme 1-1.[26,27] Oxygen in normal tissue quickly reverses the reduction of nitroimidazoles, which prevents the congregation of reduced nitroimidazoles and blocks the reduction of nitroimidazoles. This observation accounts for the increase in sensitivity of nitroimidazoles towards hypoxic cells. Eventually these reduced nitroimidazoles bind with macromolecules and are retained in the hypoxic regions.[28,29] Low oxygen levels in hypoxic regions produces less hydroxyl radicals, which limits the effectiveness of radiation therapy. However, the effectiveness of radiation therapy can be increased by utilizing radiosensitizers that mimics the hydroxyl radicals.

Nitroimidazoles are known bioactive radiosensitizers that makes tumor cells more sensitive to radiation therapy.[30]

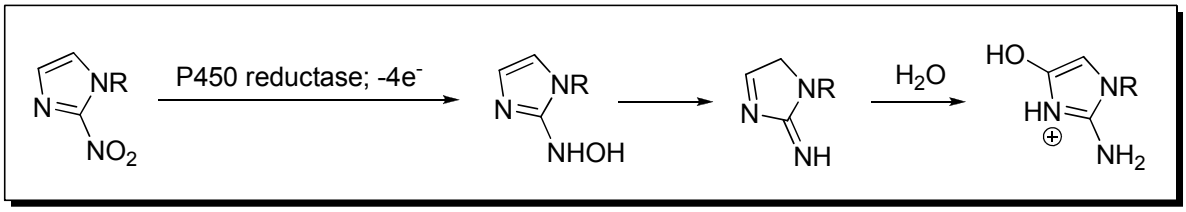

Scheme 1-1. Plausible mechanism for the reduction of nitroimidazoles

Among the members of nitroimidazole family, metronidazole (**3)** was the first one discovered in the late 1950's. It was used as an antibiotic initially and also as amebicide and antiprotozoal. Other members of this family are 5-nitroimidazole containing compounds tinidazole (**4)**, and ornidazole (**5)**, both have been serving effectively as antiprotozoal drugs.[30] (Figure 1.7)

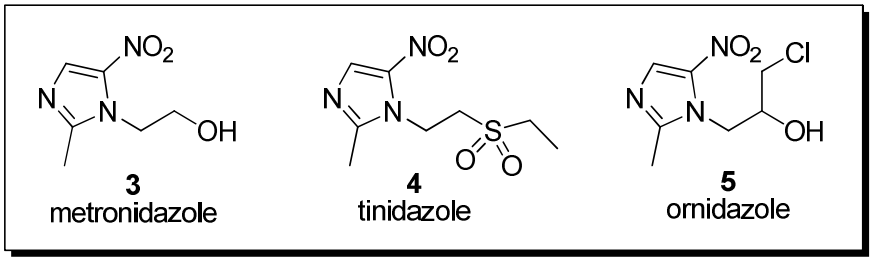

Figure 1.7. Structures of 5-nitroimidazoles: metronidazole, tinidazole, and ornidazole

Metronidazole acts as a hypoxic sensitizer at higher doses.[31] Studies have shown that among other nitroimidazoles such as misonidazole (**6)**,[31] pimonidazol (**7)**,[32] and etanidazole (**8)**,[33] (Figure 1.8) 2-nitroimidazoles are effective sensitizers, and have low cytotoxicity. Etanidazole (**8)** is of great interest because it is less toxic compared to other compounds of the family.[33]

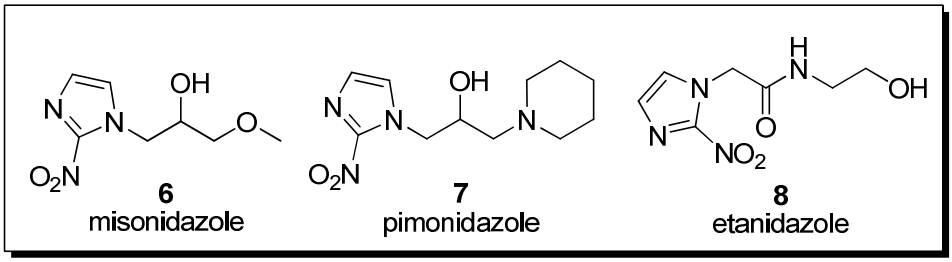

Figure 1.8. Structures of 2-nitroimidazoles: misonidazole, pimonidazole, and etanidazole

If nitroimidazoles can couple to indocyanine green dye, it would provide a method to target and image hypoxia in tumor cells. Since ICG (**2**) lacks reactive functional groups to couple nitroimidazoles, a chemical modification is needed in order to functionalize ICG (**2**) (Figure 1.10). This problem was solved by using a structural analogue of ICG (**2**) called ICG bis-carboxylic acid (**9**).[34] (Figure 1.9)

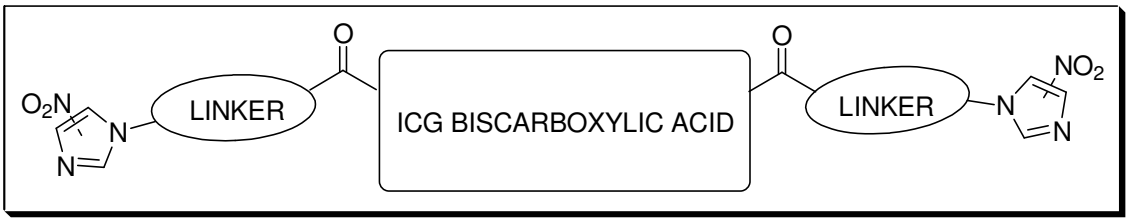

Figure 1.9. Design of hypoxia targeting dye conjugates

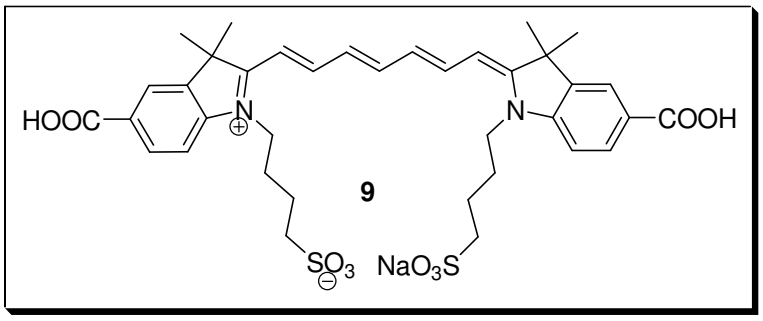

Figure 1.10. Structure of ICG bis-carboxylic acid (**9**)

Independent contributions from Lindsey et.al.;[34] Ozinskas et al.;[35] Licha et al.;[36] and Smith et al.;[24] have provided synthetic routes for the synthesis of the ICG bis-carboxylic acid (**9**). The Smith group has also developed a method for coupling nitroimidazoles to ICG bis-carboxylic acid (**9**), and the resulting dyes were labeled as "first generation dye conjugates". In the first generation dye conjugates, the nitroimidazole moiety and ICG bis-carboxylic acid were connected by an ethanolamine linker **10a**, **10b** (Figure 1.11).[24,37]

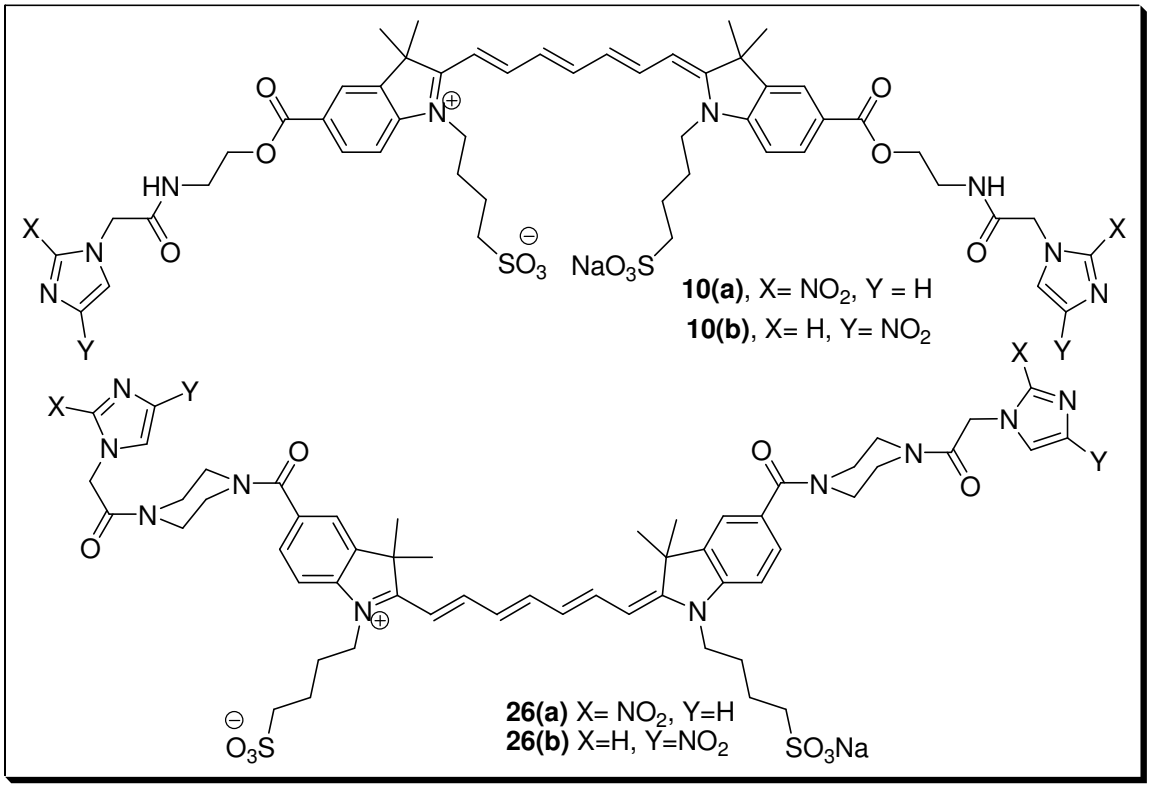

Figure 1.11. Structure of 2-nitroethanolamine ICG dye conjugates

The same strategy was applied to make piperazine analogs **26a**, **26b** with piperazine as a linker instead of ethanolamine and the resulting dye conjugates are labelled as "second generation dye conjugates". It was believed that piperazine analogue would have a longer lifetime in the mice relative to ethanolamine dye conjugates **10a**, **10b** because of the stable amide bonds, which are less susceptible to hydrolysis. The ICG bis-carboxylic acid (**9**) has a

slightly higher extinction coefficient and quantum yield than the commercially available ICG (**2**) however there is room for the development of photophysical properties of ICG bis-carboxylic acid (**9**) (Table 1-1). In the "third generation", attempts were made to improve the photophysical properities of ICG bis-carboxylic acid (**9**). Our approach was to introduce a ring system into the polyene chain so that it increases rigidity in the molecule and thereby increasing the quantum yield.

Table 1-1. Photophysical properties of indocyanine green dyes

Dye	λ_{abs} (nm)	λ_{em} (nm)	Extinction Coefficient, ε ($M^{-1}cm^{-1}$)	Quantum Yield (□)
FDA approved ICG (**2**)	779	807	115,000	0.012
ICG bis-carboxylic acid (**9**)	754	778	211,000	0.066
2-Nitroimidazole-ethanolamine-ICG (**10a**)	756	779	205,222	0.066
4-Nitroimidazole-ethanolamine-ICG (**10b**)	755	779	207,519	0.054

Chapter 2.

SYNTHESIS, PHOTOPHYSICAL CHARACTERIZATION AND HYPOXIA EVALUATION OF FIRST GENERATION DYE CONJUGATES (NITROIMIDAZOLE-ETHANOLAMINE-ICG DYE CONJUGATES)

2.1 ICG biscarboxylic acid and its synthesis

The bioreduction of nitroimidazoles is responsible for selective cytotoxicity towards the cells in the hypoxic regions.[38] As a result of anaerobic enzymatic reduction, nitroimidazole containing compounds generate cytotoxic metabolites. In order to develop a hypoxia tumor probe that could be examined, it is very important to verify (i) a nitroimidazole moiety can be coupled to ICG bis-carboxylic acid and (ii) examine that the new dye-conjugate retains the useful photophysical properties for NIR fluorescence imaging. Commercially available ICG (**2**) has weak fluorescent properties, and it has no functional groups to couple nitroimidazole moiety to target hypoxia. Therefore, we chose ICG bis-carboxylic acid (**9**) as the prototype dye. A modified version of ICG was made with carboxylic acid groups, ICG bis-carboxylic acid. Photophysical properties of ICG bis-carboxylic acid are within the required range and better than commercial ICG (Table 1-1). The increase in quantum yield of ICG bis-carboxylic acid could be due to the suppression in the formation of fluorescence-quenched aggregates.[39,40] A straightforward synthesis of (**9**) was reported by Lindsey and co-workers (Scheme 2-1),[41] in which the reaction of *p*-hydrazinobenzoic acid (**11**) with 3-methyl-2-butanone gave a 68% yield of **12**, via a Fischer indole synthesis. Subsequent treatment with butanesultone gave a 32% yield of **13**. Ozinskas and co-workers prepared **12** by a similar route, in 98% yield.[41] In this later case, treatment of **12** with ethyl iodide at 120 °C in a sealed tube gave the corresponding alkylated product in

26% yield, and heating with butanesultone at 180 °C gave **13** in 88% yield.[42] Licha et al. prepared **9** by a similar route.[39] In all cases the dyes were assembled by condensation of **13** with the commercially available glutacondianil hydrochloride (**14**).[39,41,43]

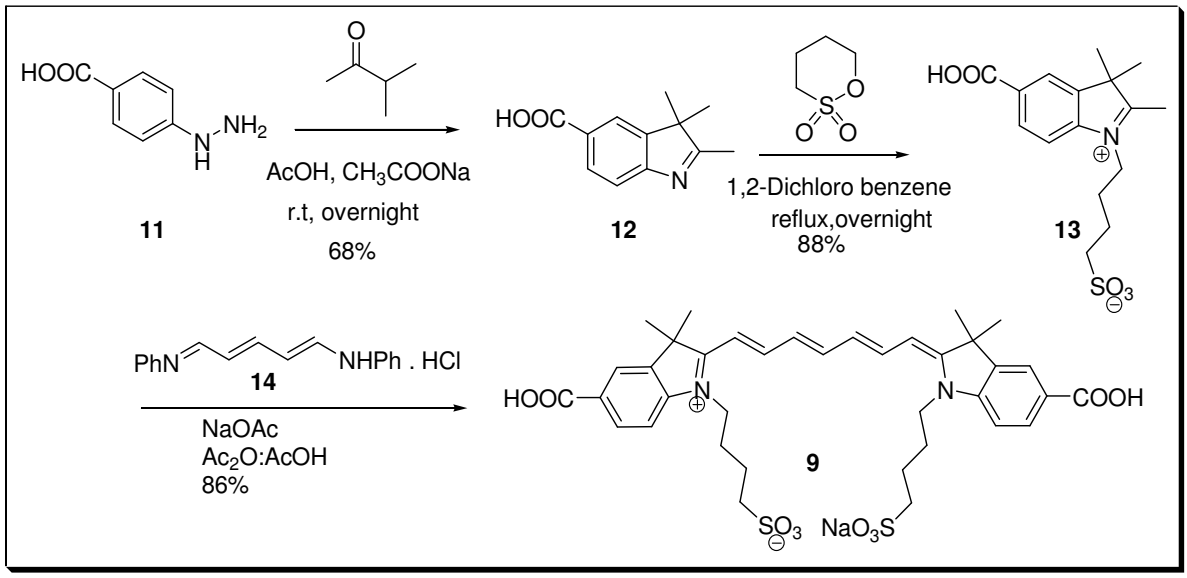

Scheme 2-1. Synthesis of ICG bis-carboxylic acid (**9**)

It is noted that the synthesis of **9** may lead to a mixture of stereoisomers due to rotation about each of the four C-C single bonds of the polyene unit. As seen in Figure 2.1, the HPLC trace for **2**, there is a clear indication that this compound is a mixture of stereoisomers. We can find no instance in the literature where a similar stereochemical analysis was reported in connection for a study. Our analysis of synthetic **9** in Figure 2.2, on the other hand, shows two peaks, indicating there are fewer stereoisomers when compared with the HPLC trace of **2**.

12/3/2012 15:17:26 1 / 1

==== Shimadzu LCsolution Analysis Report ====

C:\LabSolutions\Data\Project1\icg-std4.lcd

Acquired by	: Admin
Sample Name	:
Sample ID	:
Tray#	: 1
Vail #	: 3
Injection Volume	: 50 uL
Data File Name	: icg-std4.lcd
Method File Name	: OrganicSeparation.lcm
Batch File Name	:
Report File Name	: Default.lcr
Data Acquired	: 12/3/2012 11:33:42 AM
Data Processed	: 12/3/2012 12:03:45 PM

<Chromatogram>

C:\LabSolutions\Data\Project1\icg-std4.lcd

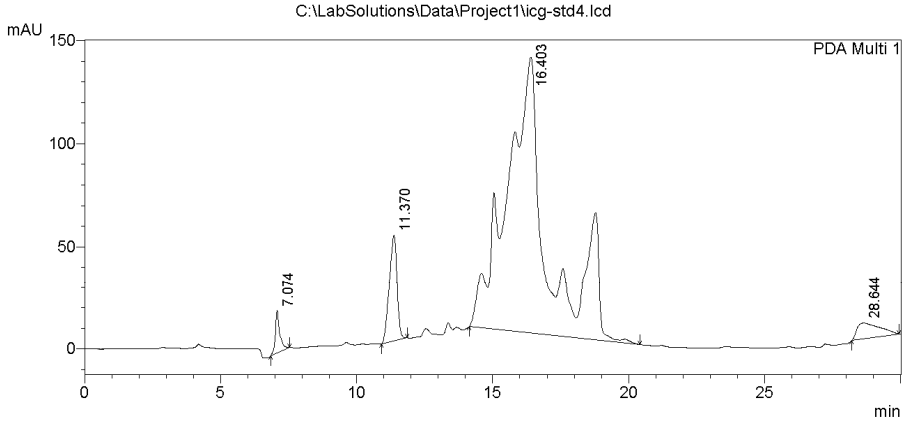

1 PDA Multi 1/254nm 4nm

PeakTable

PDA Ch1 254nm 4nm

Peak#	Ret. Time	Area	Height	Area %	Height %
1	7.074	231018	20497	1.497	9.574
2	11.370	1022011	51841	6.621	24.214
3	16.403	13736929	134118	88.998	62.645
4	28.644	445118	7636	2.884	3.567
Total		15435077	214092	100.000	100.000

C:\LabSolutions\Data\Project1\icg-std4.lcd

Figure 2.1. HPLC of commercial ICG **2**

11/16/2012 15:48:34 1 / 1

==== Shimadzu LCsolution Analysis Report ====

C:\LabSolutions\Data\Project1\MI-DYE-01-118-6.lcd

Acquired by	: Admin
Sample Name	:
Sample ID	:
Tray#	: 1
Vail #	: 1
Injection Volume	: 50 uL
Data File Name	: MI-DYE-01-118-6.lcd
Method File Name	: OrganicSeparation.lcm
Batch File Name	:
Report File Name	: Default.lcr
Data Acquired	: 11/16/2012 1:23:40 PM
Data Processed	: 11/16/2012 1:53:42 PM

<Chromatogram>

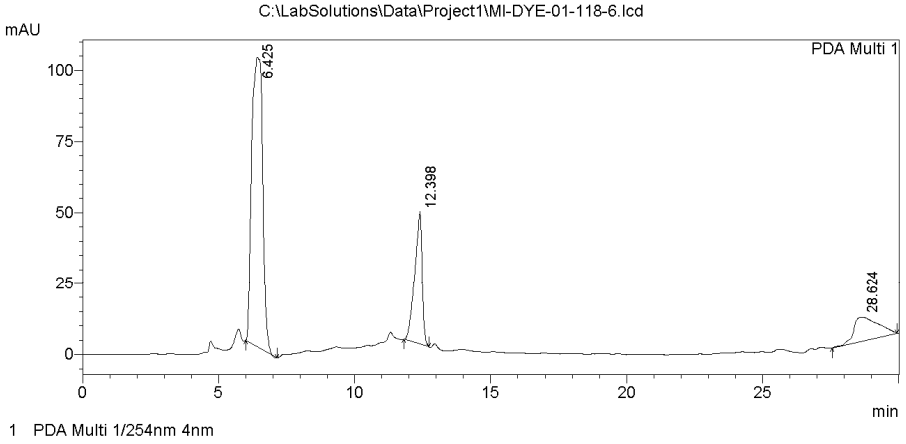

1 PDA Multi 1/254nm 4nm

PeakTable

PDA Ch1 254nm 4nm

Peak#	Ret. Time	Area	Height	Area %	Height %
1	6.425	2843675	101983	67.087	64.888
2	12.398	880680	46713	20.777	29.722
3	28.624	514457	8471	12.137	5.390
Total		4238812	157167	100.000	100.000

C:\LabSolutions\Data\Project1\MI-DYE-01-118-6.lcd

Figure 2.2. HPLC of ICG bis-carboxylic acid (**9**)

Many polyenes exist as the lower energy all-E isomer, but solvent effects as well as structural features of the molecule can stabilize other isomers, leading to mixtures.[44-46] The major stereoisomer of **9** may be the all-E isomer, but we have no evidence to absolutely rule out other isomers. It is clear, however, that ICG bis-carboxylic acid (**9**) is relatively pure when compared to compound commercial ICG (**2**). The dyes used in our study are bis-carboxylic acid derivatives, prepared in a manner identical to **9**, and we believe the stereochemistry of all dyes is similar to **9**. However, the compounds we have prepared, as well as those similar compounds reported in the literature, are probably not a single isomer, and isomers would arise from isomerization associated with the polyene linker. The interactions of the polar substituents incorporated into these dyes may lead to stabilization and the relatively small mixture of observed isomers.

2.2 Synthesis of first generation dye conjugates (nitroimidazole-ethanolamine-ICG)

Nitroimidazole moieties were prepared from the corresponding nitroimidazoles. Synthesis began by treating nitroimidazoles (**15**) with bromomethyl acetate to get the corresponding nitroimidazole acetates **16(a)**, **16(b)**, which were subsequently treated with ethanolamine to get the ethanolamine derivatives **17(a)**, **17(b)** (Scheme 2-2). Initial experiments attempted to couple the ethanolamine unit to the hydrazinobenzoic acid (**11**), but gave little or no yield of the desired coupled product. The targeted nitroimidazole-dye conjugates were prepared by combining the nitroimidazole fragments **17a**, **17b** with the ICG bis-carboxylic acid (**9**) in presence of PyBop, hydroxybenzotriazole (HOBt) and diisopropylethylamine (DIPEA). We prepared 4-nitro and 2-nitroimidazole ethanolamine fragments, **17(a)** in 60% yield, **17(b)** in 90% yield. Using PyBop as a coupling agent, ICG

bis-carboxylic acid was coupled to nitroimidazole ethanolamine fragments to get 2-nitroimidazole ethanolamine dye conjugate, **10a** in 25% yield and 4-nitroimidazole ethanolamine dye conjugate, **10b** in 20% yield.

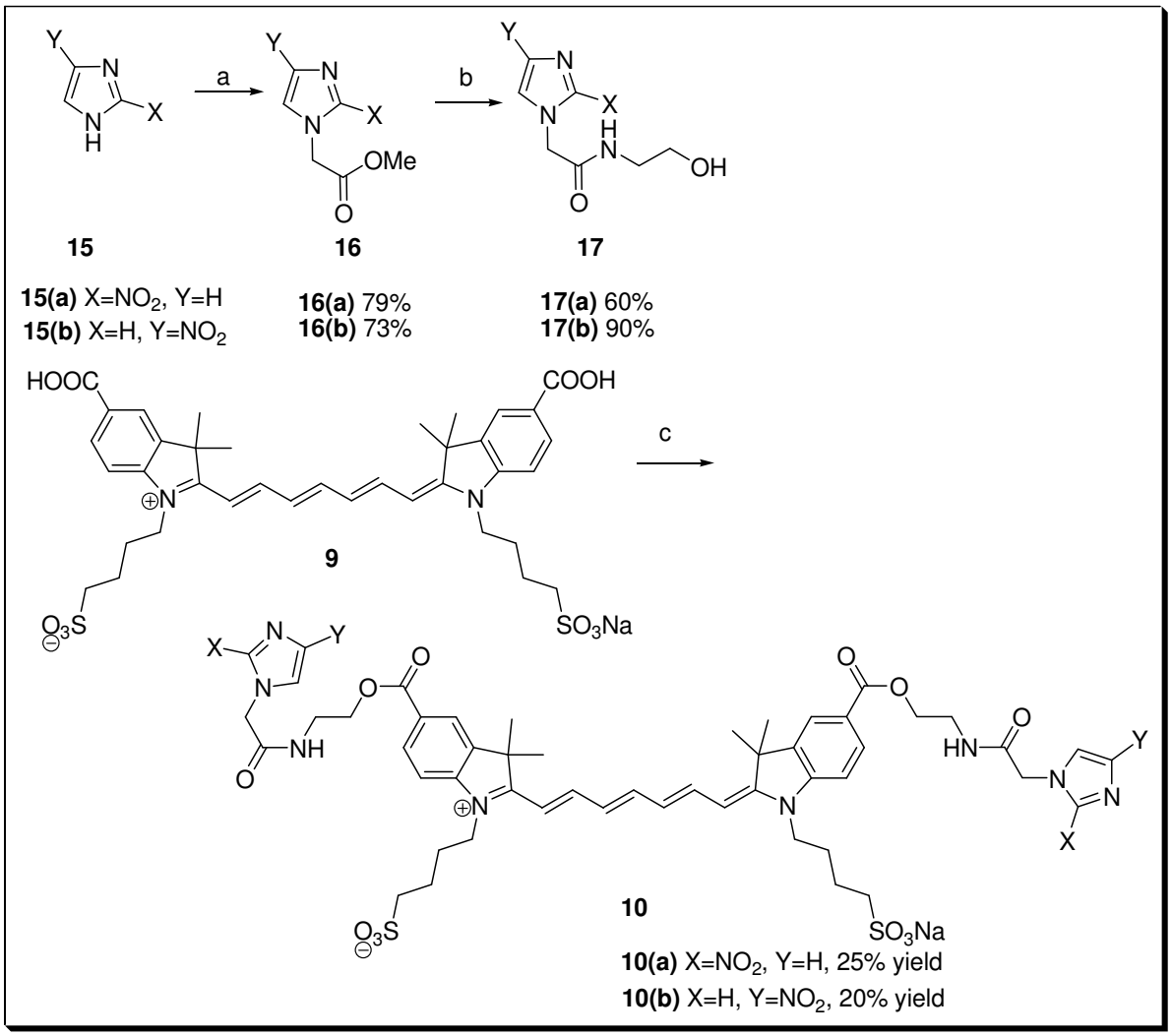

Scheme 2-2. Synthesis of nitroimidazole-ethanolamine-ICG dye conjugates.

Reaction Conditions: (a) bromomethyl acetate,TBAI, K_2CO_3, CH_3CN, 80 °C, 45 min (b) Methanol, ethanolamine, r.t., overnight (c) DMF, PyBOP, DIPEA, HOBt, **17a**, **17b**, 0 °C-r.t., 48 h.

2.3 Photophysical properties of first generation dye conjugates

Photophysical properties of indocyanine green bis-carboxylic acid (**9**), and ethanolamine linked nitroimidazole conjugates **10a, 10b** were measured using an UV-VIS spectrophotometer and a fluorescence spectrophotometer (Varian Analytical Instruments, Walnut Creek, CA). The wavelength range of both spectrophotometers is 250 nm-1100 nm. Dye solutions were made by dissolving dyes in Phosphate Buffer Saline (1×PBS) and the absorption and fluorescence spectra were recorded. The normalized absorption and fluorescence spectra of 1 mM solution of bis-carboxylic acid ICG (**9**) are shown in Figure 2.3.

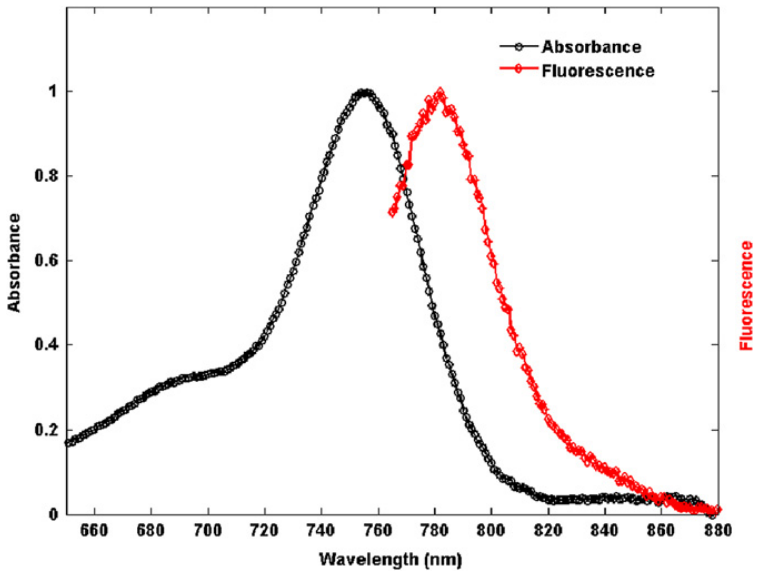

Figure 2.3. Absorption and fluorescence spectra of ICG bis-carboxylic acid

Table 2-1. Photophysical properties of nitroimidazole-ethanolamine-ICG dye conjugates

Dye	λ_{abs} (nm)	λ_{em} (nm)	Extinction Coefficient, ε ($M^{-1}cm^{-1}$)	Quantum Yield (□)
FDA approved ICG (**2**)	780	807	115,000	0.0120
ICG bis-carboxylic acid (**9**)	755	790	221,000	0.0728
2-Nitroimidazole-ethanolamine-ICG dye conjugate (**10a**)	760	790	159,000	0.0420
4-Nitroimidazole-ethanolamine-ICG dye conjugate (**10b**)	755	779	208,000	0.054

The results of photophysical characterization of **9**, **10a**, and **10b** in Phosphate Buffer Saline (PBS), are shown in Table 2-1, with absorbance peaks at 754-756 nm and fluorescence peaks at 778-779nm. Dye conjugates and ICG bis-carboxylic acid showed a blue shift of 25 nm in the absorption and 30 nm shifts in the fluorescence compared to FDA approved ICG (**2**). There is no significant change between the ICG bis-carboxylic acid (**9**) and the ethanolamine dye conjugates in the absorption and fluorescence spectral profiles. The extinction coefficients are 1.9 times higher than that of FDA approved ICG (**2**). The relative quantum yields are calculated using commercial ICG (**2**) as a standard.[39] The relative quantum yields of the new compounds are 4.5-6 times higher than that of FDA approved ICG (**2**). The fluorescence quantum yield of **9** (0.066) is slightly higher than the FDA approved ICG (0.012), probably due to the observation that formation of fluorescence-quenched aggregates is suppressed because dye-dye interaction and aggregation is reduced by hydrophilic, non-charged but sterically demanding substituents.[39,40]Among all the imidazole ethanolamine conjugates, 2-nitroimidazole ICG, **10a** has the highest quantum yield. The

ability of targeting hypoxic regions in cancer cells depends on the oxygen concentration at which bioreductive trapping happens and the enzyme activity in bioreductive activation.[47] As mentioned earlier, nitroimidazoles are selectively reduced by nitroreductase enzymes under hypoxic conditions to form reactive products that can bind to cellular nucleophiles.[48] Because **10a** has a higher reduction potential and a highest quantum yield, it was selected for the in-vivo hypoxia evaluation.

2.4 FDOT System and Tumor Imaging

The *in vivo* experiments were performed using a frequency domain fluorescence imaging system (Figure 2.4), developed by Prof. Quing Zhu in the engineering department at the University of Connecticut. The system consisted of 14 parallel detectors and 4 laser diodes of 690, 780, 808, and 830 nm. Each laser diode was sequentially switched to nine positions on a hand-held probe. The excitation wavelength used in this study was 690 nm. The 14-channel parallel detection system has two modes: fluorescence mode and absorption mode. The two modes can be easily switched by moving a mechanical handle. A stopper was designed in the system to ensure a precise optical collimation when switching between these two modes. Note that in the fluorescence mode, a bandpass filter was placed in the light path to remove the excitation and stray light; in the absorption mode, the bandpass filter was moved out of the light path. Fourteen photomultiplier tubes were used as detectors, and the received signals were amplified by preamplifiers, mixed by mixers, low pass filtered, and further amplified before analog to digital converters. Two National Instrument data acquisition cards of eight channels each were used to acquire FDOT data.

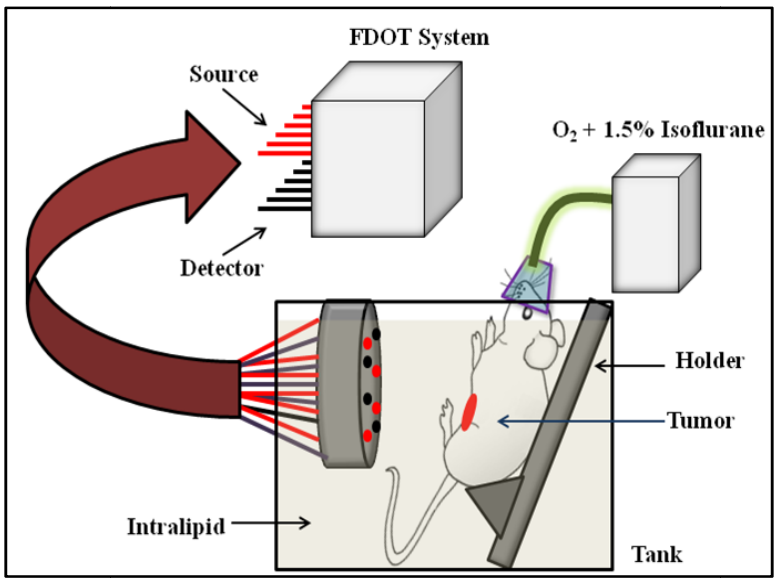

Figure 2.4. *In vivo* fluorescence tomography imaging set up[49]

The tumor was imaged for up to 1 min post injection and again at 15 min, 30 min, 1, 2, 3, 5, and 7 h. The center of the probe was aligned to the center of the tumor and the separation between the tumor center and the probe surface was defined as the imaging depth for fluorescence images. Several imaging data sets were collected to compare the in vivo imaging sensitivity of two hypoxia dye conjugates versus ICG bis-carboxylic acid (**9**) at different concentrations and tumors located at different depths.

To validate the in vivo FDOT imaging results, excised tumor samples were imaged using a commercially available Odyssey Imaging system (Li-COR Biosciences, Nebraska). Using this system, 10 μm tumor sample sections were dried and imaged at the highest scan resolution available (i.e., 21 μm). The excitation channel selected was 785 nm and emission was 820 nm with a bandwidth of 40 to 50 nm. The images were obtained using the analysis software provided by the company. The mean pixel value of the images including the entire tumor sample area was measured using Image *J* software. These *in vivo* experiments were done in Dr. Quing zhu's lab by her graduate students.

Figure 2.5, shows the fluorescence images obtained by FDOT of the mice mice injected with 25 μM ICG bis-carboxylic acid **9** and Figure 2.6, shows 25 μM 2-nitroimidazole-ethanolamine-ICG **10a**. These images are obtained over 5 to 7 h period. Each image is 9 cm × 9 cm in x and y spatial dimensions at the corresponding target depth and the color bar represents the reconstructed dye concentration in μM.

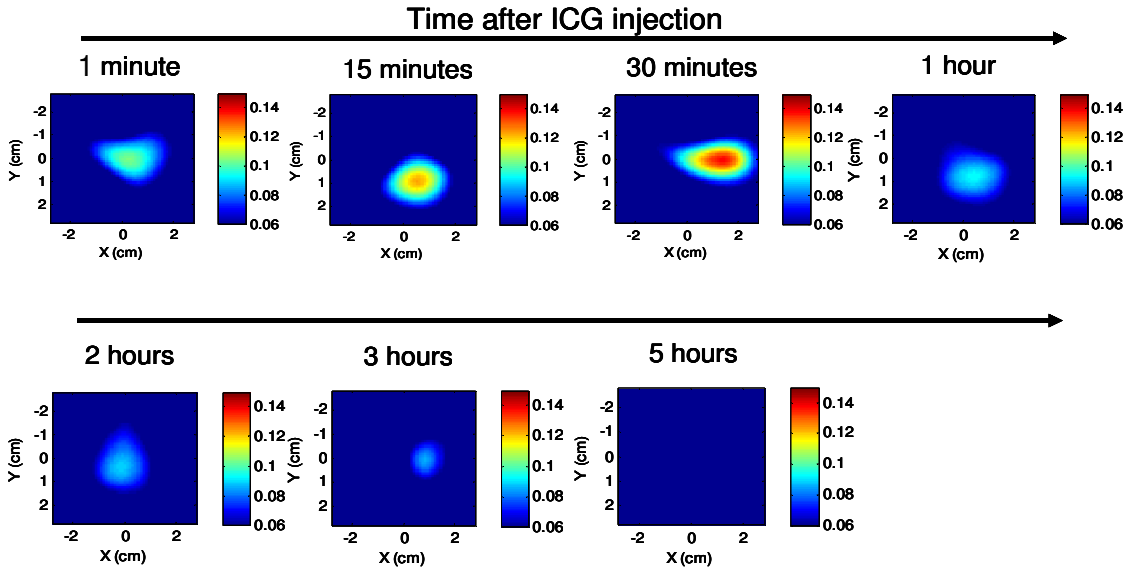

Figure 2.5. Tumor images of mice injected with 25 μM ICG bis-carboxylic acid (**9**)

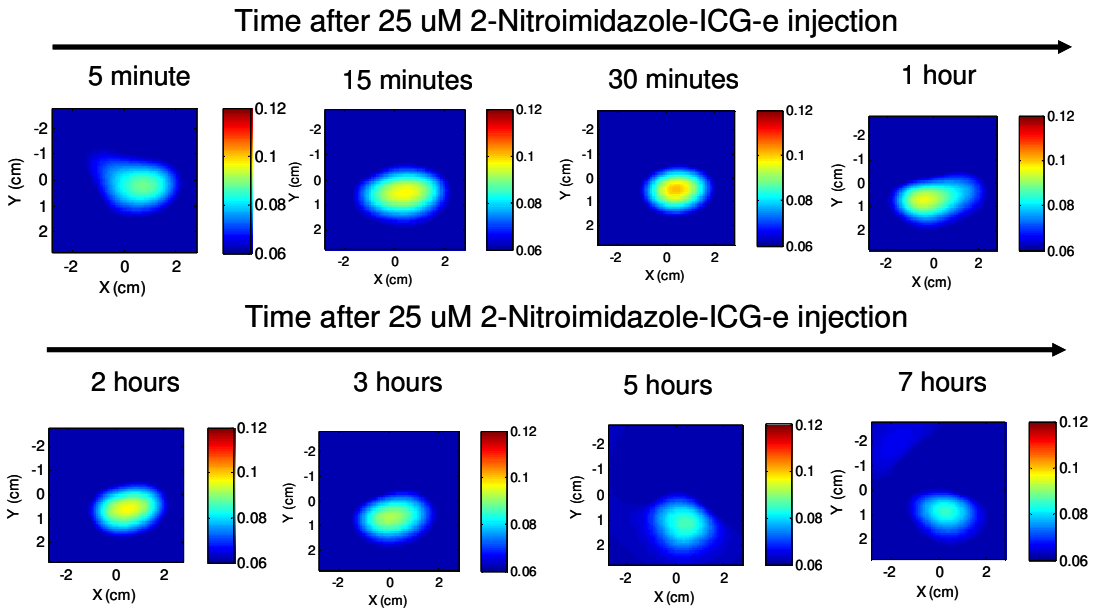

Figure 2.6. Tumor images of mice injected with 25 μM 2-nitroimidazole-ethanolamine-ICG dye conjugate (**10a**) [49]

ICG bis-carboxylic acid (**9**) was completely washed out after 3 h and the maximum fluorescence concentrations obtained from reconstructed images at 1, 15, 30, 60, 120, 180, and 300 min post injection were 0.044, 0.066, 0.078, 0.033, 0.029 0.025, and 0.000 μM, respectively, after subtraction of background value of 0.06 μM. However, for targeted conjugates, the maximum fluorescence concentrations measured post injection of 25 μM ethanolamine-2-nitroimidazole-ICG were 0.028, 0.037, 0.041, 0.037, 0.036, 0.032, 0.026, and 0.025 μM above the background. We are gratified to see that the 2-nitroethanolamine dye conjugate was retained up to 7 h, whereas ICG bis-carboxylic acid acid was washed out in 3 h.

Chapter 3.

SYNTHESIS, PHOTOPHYSICAL CHARACTERIZATION AND HYPOXIA EVALUATION OF SECOND GENERATION DYE CONJUGATES (NITROIMIDAZOLE-PIPERAZINE-ICG DYE CONJUGATES)

3.1 Synthesis of second generation dye conjugates

To further improve the retention time of the dye conjugate, the second generation dye conjugate was designed and synthesized. The ethanolamine linker was replaced with a piperazine linker in the second generation dye. This modification was based on two assumptions; (a) amide bonds are less susceptible to hydrolysis compared to ester bonds and (b) the bioavailability of the dye conjugate should increase by the presence of piperazine moiety. Since 2-nitroimidazole (**15a**) is very expensive chemical, 4-nitroimidazole was chosen to optimize the reaction conditions for the synthesis of nitroimidazole piperazine moiety (**25**).

4-Nitroimidazole acetate (**16b**) was prepared by treating 4-nitroimidazole (**15b**) with bromomethyl acetate, which was hydrolyzed to the corresponding acid (**18**) by simple refluxing in water (Scheme 3-1). In this reaction water acted as nucleophile to hydrolyze the methyl ester, we thought piperazine is a good nucleophile compared to water, so **16b** reflux with piperazine in water should provide the coupled product **19** (Scheme 3-2). Our attempt to couple 4-nitroimidazole methylacetate (**16b**) with piperazine gave a white solid. The melting point of the white solid was different than either of the starting materials, broad acid peak was absent in the IR spectrum. The HRMS was matched with the desired product mass, the ^{13}C showed the correct number of carbons, and proton NMR was consistent and matched with the proton count except the splitting pattern of piperazine protons. Based on the above

observations, we determined that we obtained the coupled product **19**, but the NMR splitting of piperazine protons peak was not convincing. Another possibility was formation of a salt of starting material. The solution to this puzzle lay in identifying the bond between piperazine and nitroimidazole fragment as covalent or ionic? We initiated 2D NMR experiments, and there was no correlation between the carbonyl and the piperazine carbon atoms in HMBC. This information along with the NMR splitting pattern showed that the product was not formed but rather a salt of starting material **20**. Careful examination of the starting material, suggests that salt formation is reasonable, because fragment **18** is a substituted acetic acid, and piperazine is a base containing a nitrogen atom (Scheme 3-1). Based on this experiment, we changed the synthetic route (Scheme 3-3). Piperazine was protected with Boc and treated with bromoacetyl bromide to give key intermediate **23**, which was coupled to nitroimidazole to give intermediate **24**. The boc group was removed by TFA and attempts to recover the product as a free base **19** were failed. And there were issues with the product going into aqueous layer during the work up. To overcome this issue, we bypassed the workup and obtained the product **25** as a TFA salt.

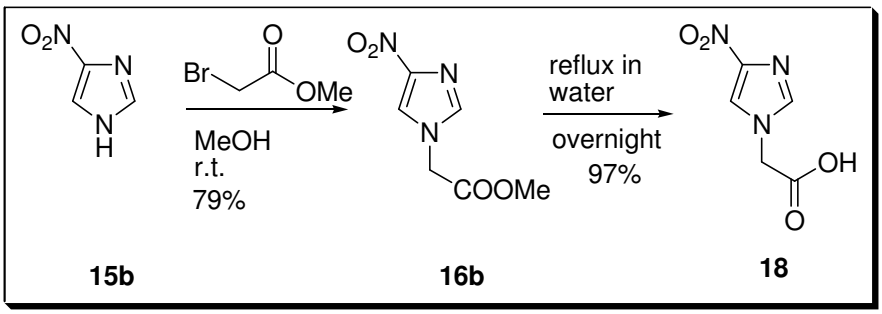

Scheme 3-1 Nitroimidazole methylacetate (**16b**) hydrolysis

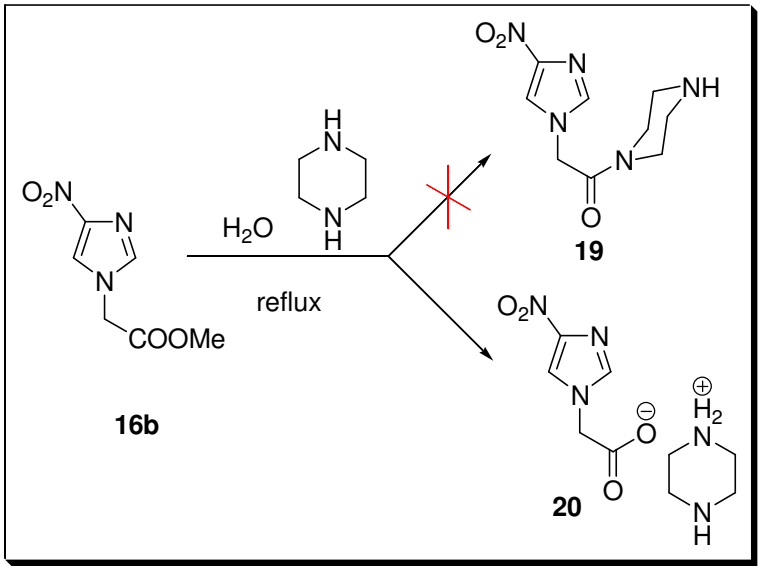

Scheme 3-2. Piperazine coupling to nitroimidazole methylacetate (**16b**)

The successful synthesis was began with piperazine, Boc protected piperazine **22** was prepared in 35% yield using a literature procedure.[50] Subsequent treatment of **22** with bromoacetyl bromide gave compound **23** in 81% yield, and subsequent coupling to 2-nitroimidazole gave compound **24a**, in 94% and **24b** in 90% yield (Scheme 3-3).

Removal of Boc group with trifluoroacetic acid gave trifluoroacetyl salt **25a** (76% yield) and **25b** (86% yield). These TFA salts were coupled to ICG bis-carboxylic acid (**9**) by the same coupling procedure used to prepare compound **10a** and **10b**,[51] giving 2-nitroimidazole-piperazine-ICG, **26a** in 20% yield, and 4-nitroimidazole-piperazine-ICG, **26b** in 25% yield (Scheme 3-4).

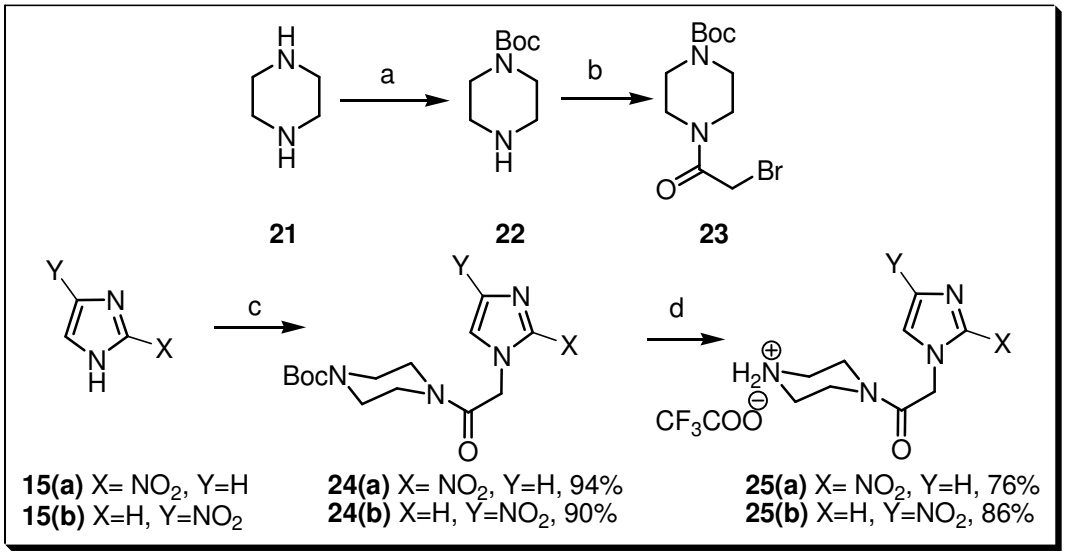

Scheme 3-3. Synthesis of nitroimidazole piperazine fragments.

Reaction Conditions: (a) CH_2Cl_2, $(Boc)_2$, 0 ^oC-r.t., 16 h, 35% (b) Et_3N, bromoacetyl bromide, r.t., overnight, 81% (c) NaH, DMF, 23, 0 ^oC-r.t., overnight (d) TFA, $CHCl_3$, overnight.

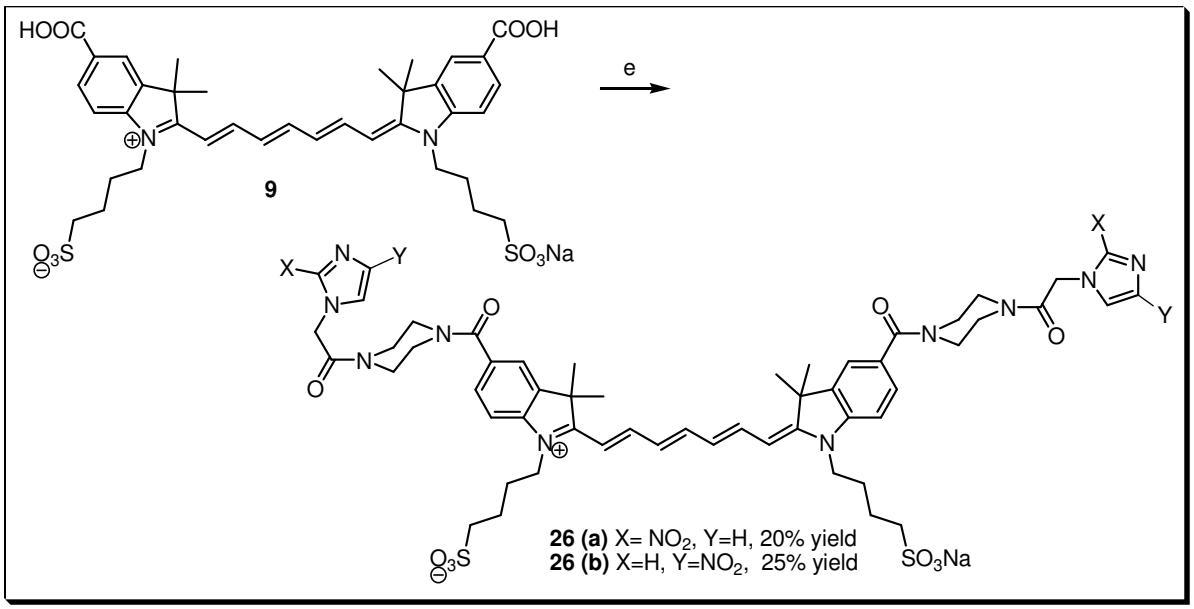

Scheme 3-4. Synthesis of nitroimidazole-piperazine-ICG dye conjugates.

Reaction Conditions: (e) DMF, PyBOP, DIPEA, HOBt, **25a** or **25b**, 0 °C-r.t., 48 h.

We considered ICG bis-carboxylic acid **9** as our standard in our first generation, however keeping in mind the structural features of second generation dye conjugates, imidazole-piperazine-ICG (**31**) would make the better standard rather than ICG bis-carboxylic acid (**9**). We wanted to synthesize imidazole-piperazine-ICG (**31**) and test against the second generation dyes. The synthesis of imidazole piperazine fragment **29** was not straightforward. Our initial attempt with NaH in DMF overnight, gave the 1,3-di-subustituted imidazolinium salt **28** (Scheme 3-5). Overnight stirring in DMF at room temperature also led to the di-substituted salt, **28**. We tried the reaction in acetonitrile with K_2CO_3 at 45 °C which gave the same di-substituted salt **28** as the product. The stoichiometric ratios of the reactants were modified but could not change the reaction outcome. It is conceivable that nitro groups on imidazole ring lower the nucleophilicity of the other nitrogen atom in the ring, thus allowing the mono substitution as favorable process in case of nitroimidazoles. We were able to get mono substituted product as a major product by stirring the reactants in acetone/K_2CO_3 at room temperature for 4 h or DMF/NaH at room temperature for 2 h.

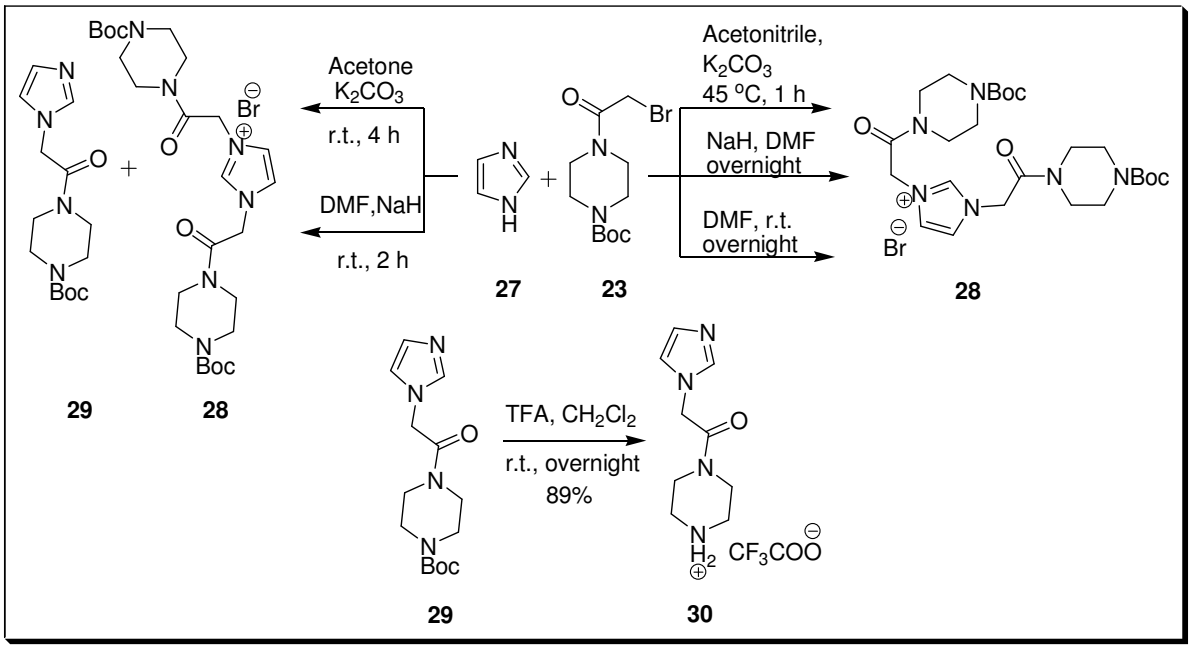

Scheme 3-5. Synthesis of imidazole piperazine fragment

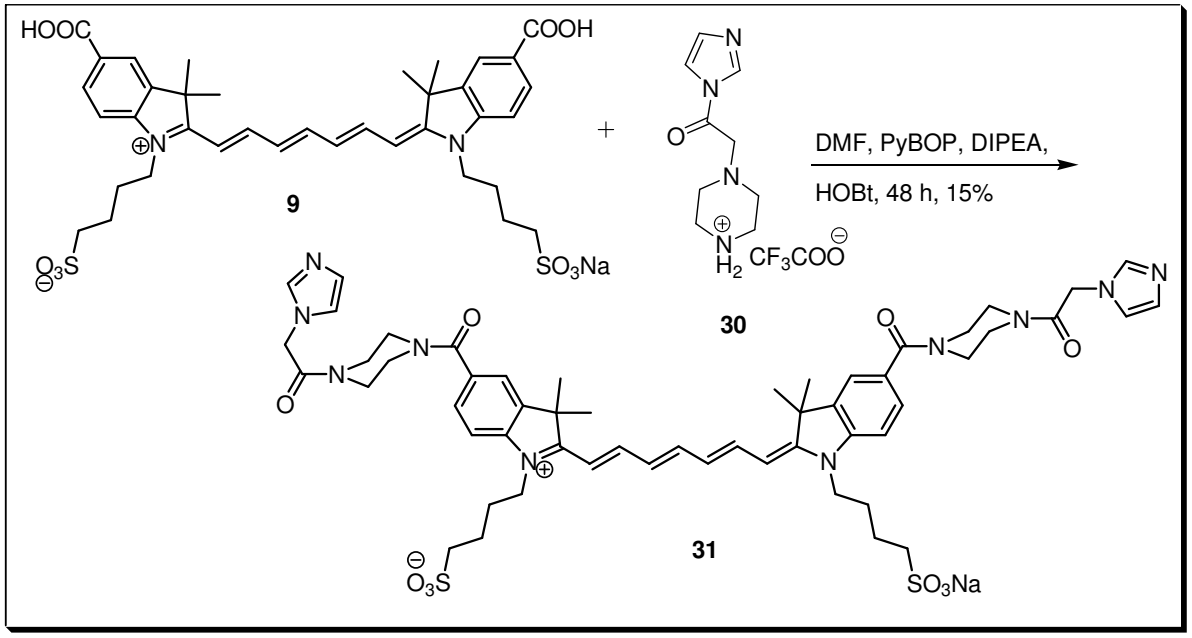

Scheme 3-6. Synthesis of imidazole-piperazine-ICG dye conjugate

The mixture of mono and disubstituted products was purified by column chromatography to obtain the pure imidazole piperazine fragment. Removal of boc and coupling with ICG bis-carboxylic acid proceeded smoothly to give the imidazole-piperazine-ICG dye conjugate (**31**) (Scheme 3-6).

3.2 Photophysical properties of second generation dye conjugates

The 2-nitroimidazole-piperazine-ICG (**26a**), 2-nitroimidazole-ethanolamine-ICG (**10a**), and ICG bis-carboxylic acid (**9**) were spectrally characterized by using a UV-Vis spectrophotometer and a fluorescence spectrophotometer (Table 3-1)(Varian Analytical Instruments, Walnut Creek, California). The wavelength range of both spectrophotometers is 250 nm to 1100 nm. The relative quantum yield of each dye was calculated according to the following equation.

$$_x = _{STD} \left\{\frac{Grad_x}{Grad_{STD}}\right\} \left(\frac{\eta_x}{\eta_{STD}}\right)^2$$

The term Grad was the gradient or slope from the plot of the integrated fluorescence intensity versus absorbance measured at different concentrations, x is any unknown dye, STD is the standard dye, and η is the refractive index of the solvent.

Table 3-1. The optical properties of ICG from Sigma-Aldrich, ICG bis-carboxylic acid, 2-nitroimidazole-ethanolamine-ICG, and 2-nitroimidazole-piperazine-ICG.

Dye	λ_{abs} (nm)[a]	λ_{em} (nm)	Extinction Coefficient, ε (M^{-1} cm^{-1})	Quantum Yield (□)
FDA approved ICG (Sigma Aldrich)	780	807	115,000	0.0120
ICG bis-carboxylic acid (**9**)	755	790	221,000	0.0728
2-Nitroimidazole-ethanolamine-ICG (**10a**)	760	790	159,000	0.0420
2-Nitroimidazole-piperazine-ICG (**26a**)	760	790	230,000	0.0825

[a] λ_{max} abs is the wavelength measured at the maximum absorption spectrum, and λ_{max} ems is the wavelength measured at the maximum emission spectrum.

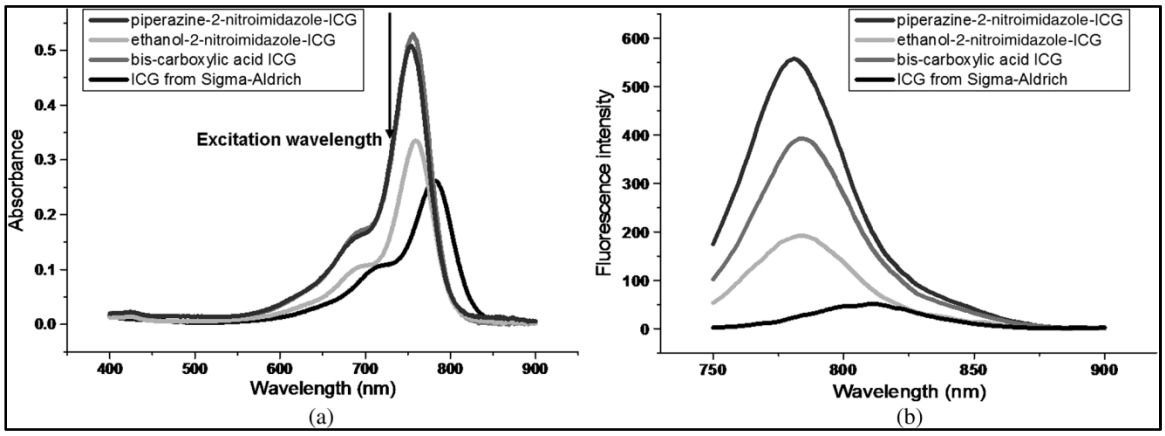

Figure 3.1. (a) Absorbance spectra of 2-nitroimidazole-piperazine-ICG (**26a**), 2-nitroimidazole-ethanolamine-ICG (**10a**), ICG bis-carboxylic acid (**9**), and FDA approved ICG (**2**). (b) Corresponding fluorescence emission intensity versus wavelength measured at the excitation wavelength of 730 nm. All the samples were in 2.35 μM concentration.

3.3 Hypoxia evaluation

After the synthesis was complete, the second-generation dye conjugate was tested in the mice. Fluorescence tomography images were collected over 5-7 h period. As expected the second-generation dye conjugate fluorescent signals were much more intense, when compared to the first-generation dye conjugates. As seen from the images (Figure 3.4), the signal intensity of second-generation piperazine dye conjugates improved 2.5 to 3 times during the first 3h post injection period and 1.8 times after 3 h post injection than the first generation ethanolamine dye conjugates (Figure 3.3). ICG was washed out with in the first 3 h (Figure 3.2). The signal intensity of both first-generation and second-generation dye conjugates **10a**, **26a** is strong compared to ICG bis-carboxylic acid (**9**), between the first and second generation, the sensitivity of the signal is substantially improved with the second generation dye, **26a**. The FDOT images of mouse tumor are shown in the following figures.

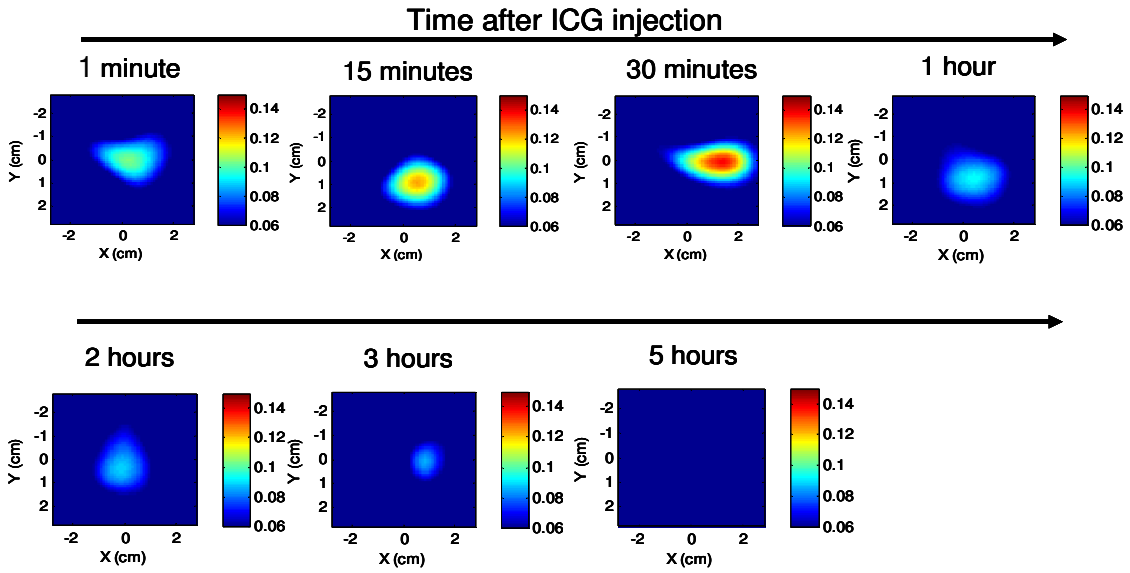

Figure 3.2. Mouse tumor images (~10 mm tumor size) injected with 25 μM ICG bis-carboxylic acid (**9**)

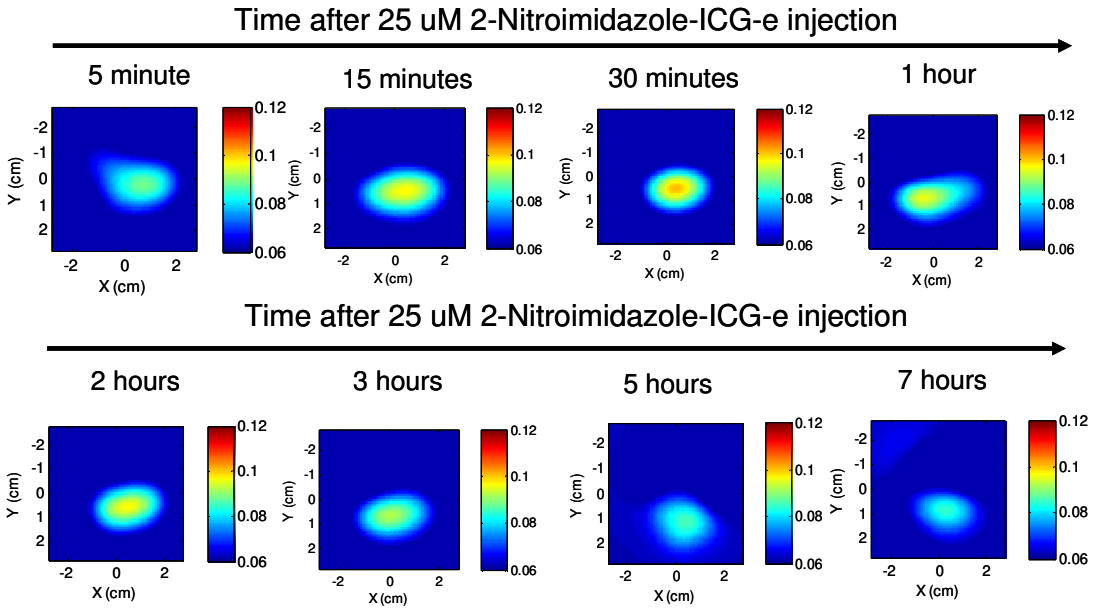

Figure 3.3. Mouse tumor images (~8 mm tumor) injected with 25 μM 2-nitroimidazole-ethanolamine-ICG (**10a**)

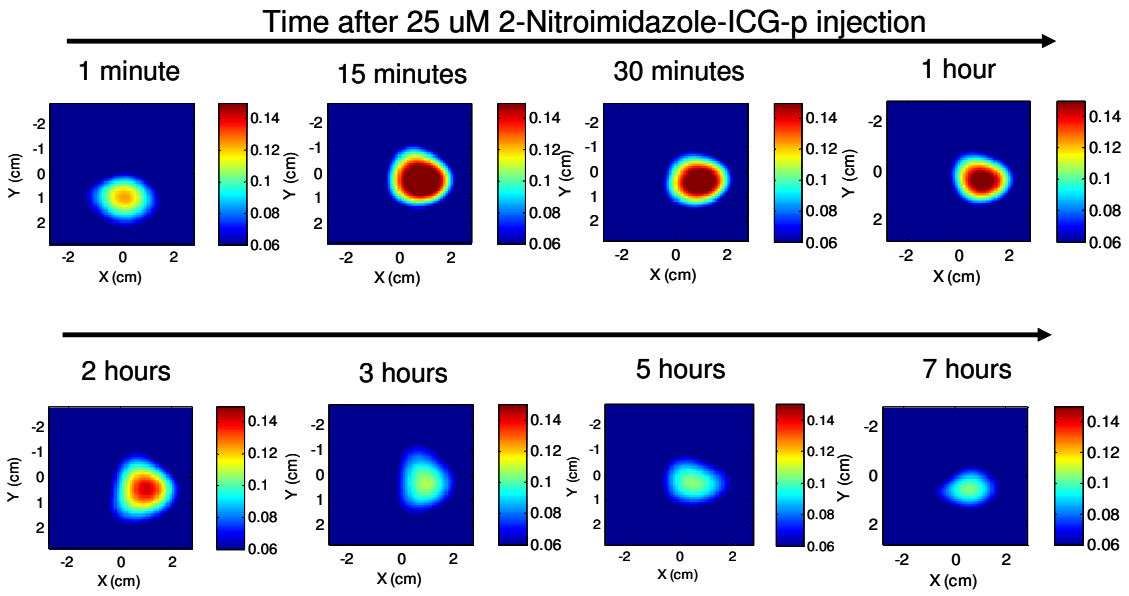

Figure 3.4. Images of a mouse tumor (~8 mm tumor) injected with 25 μM 2-nitroimidazole-piperazine-ICG (**26a**)

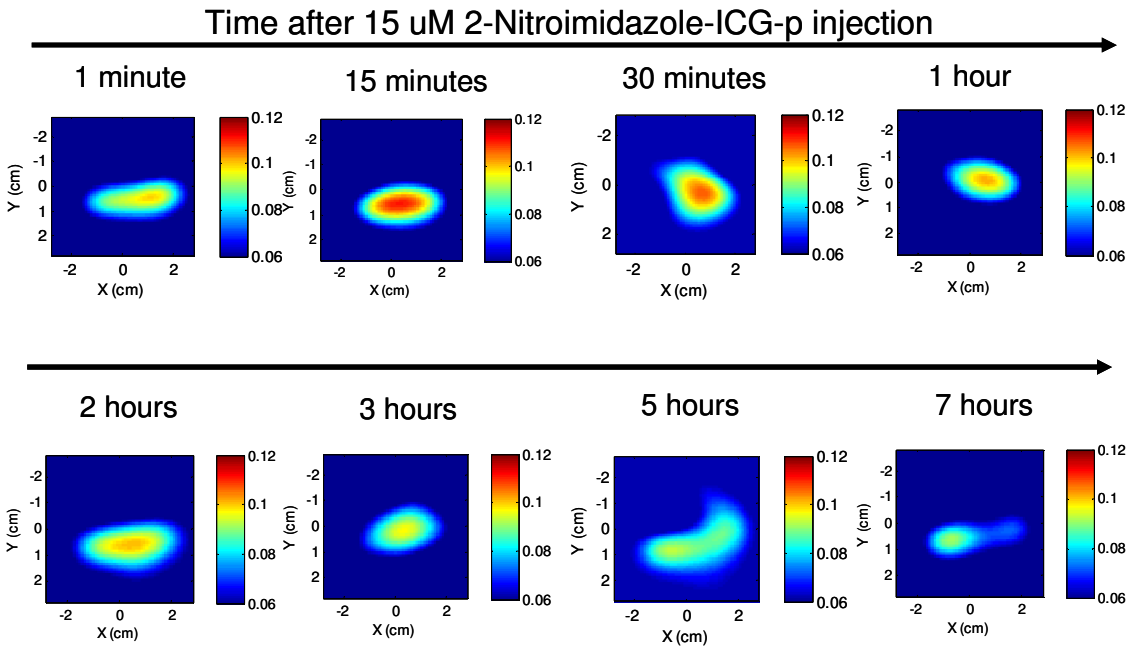

Figure 3.5. Images of a mouse tumor (~8 mm tumor) injected with 15 μM 2-nitroimidazole-piperazine-ICG (**26a**) [49]

The sensitivity of 2-nitroimidazole-piperazine-ICG-dye (**26a**) conjugate was further tested by using a 25 μM concentration for injection. A mouse with 10 mm size tumor was injected with 25 μM solution of piperazine dye conjugate and the fluorescence tomography images were collected over 24 h. This experiment showed the fluorescence signals even at 24 h.

One method to improve tumor imaging is to improve the bioavailability [52] of the dye conjugate. A piperazine unit is common in many drugs,[53] which was the reason we chose a piperazine linker, with the goal of increasing bioavailability[54] of the dye conjugate. We do not believe that the piperazine per se exhibits any influence on the hypoxia targeting. However, if the bioavailability of the dye conjugates leads to a greater concentration in the tumor, presumably, enzymatic reduction of the nitro group will lead to an increased concentration of the dye conjugate. We believe that the observed greater distribution of 2-nitroimidazole-piperazine-ICG in tissues may be due to the larger number of carbon atoms and slightly diminished polarity, which increases solubility in tissue when compared to the 2-nitroimidazole-ethanolamine-ICG. Increased solubility would lead to a greater percentage of dye reaching the tumor, along with other tissues; however, selective hypoxia binding of the dye should lead to a larger percentage of dye conjugate in the tumor relative to other tissues, which would be measured as greater long-lasting fluorescence intensity. Mice experiments were done by Saeid, a graduate student in Dr. Quing Zhu's group. Indeed, they have observed increased fluorescence intensity of excised mouse tissues, such as liver and kidney, injected with 2-nitromidazole-piperazine-ICG as compared with the tissues injected with 2-nitroimidazole- ethanolamine-ICG, as well as enhanced tumor imaging. 2-nitroimidazole compounds are reduced in hypoxic cells and irreversibly bind to macromolecules (protein,

nucleotides, etc). The bound compounds would remain until cell metabolism removed the macromolecules. It is well documented that the stability and half-life of the compound in the cells are dependent on cell type.[55] Different researchers have observed the turnover rates of hypoxic tumor cells with half-lives ranging from 17 to 49 h in various solid tumors. Due to animal study constraints, we did not image every mouse beyond 7 h, except for one. As shown in Figure 3.6, the fluorescence image obtained at 24 h is about the same level as that obtained at 3 h, which suggests that the optimal window to image hypoxia condition of the tumor is at least between 3 to 24 h.

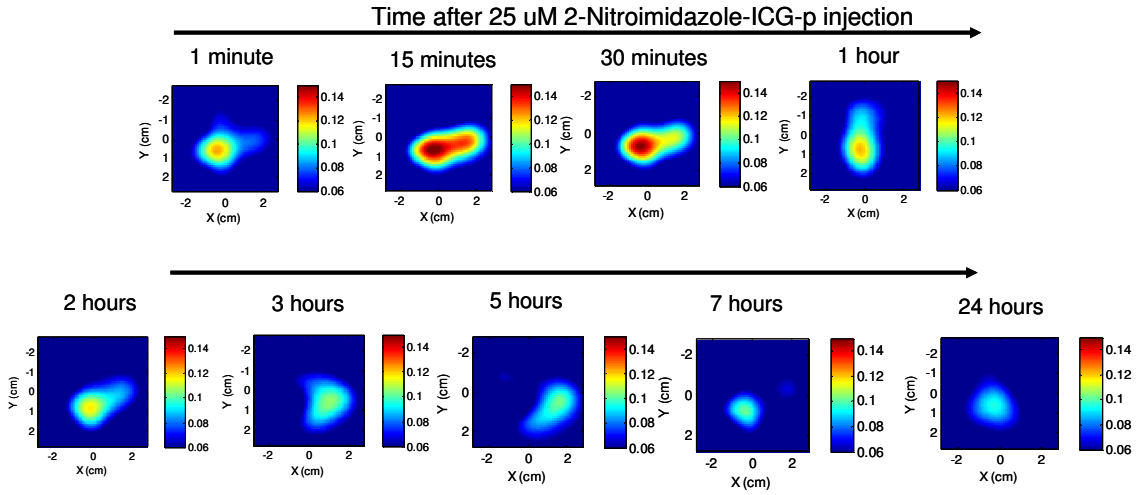

Figure 3.6. Tumor images injected with 25μM 2-nitroimidazole-piperazine-ICG dye conjugate **26a** [49]

Animals were sacrificed and immunohistochemistry (IHC) was performed on the tumor slices and the hypoxic regions were stained brown. All experiments involving animals were done by our collaborator, Dr. Quing Zhu.[49] Two areas of higher and lower fluorescence intensity in each Li-Cor images were selected to compare the corresponding hypoxic areas in IHC images. Within each image the higher and lower signal intensity areas correspond to higher (more brown stains) and lower (less brown stains) hypoxic areas.

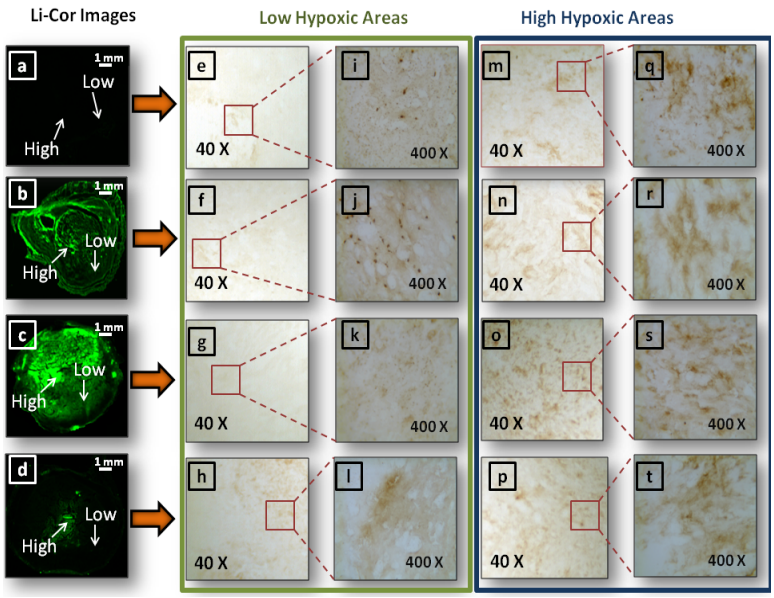

Figure 3.7. The corresponding ex vivo fluorescence images acquired from the Odyssey Imaging system of (a) mouse image injected with 25 μM ICG bis-carboxylic acid (**9**), (b) mouse image injected with 25 μM ethanolamine-2-nitroimidazole-ICG (**10a**), (c) and (d) corresponding images of two mice injected with 25 and 15 μM piperazine-2-nitroimidazole-ICG (**26a**) , respectively, (e) through (h) corresponding IHC stains (40×, brown) at low tumor hypoxic area as marked at corresponding images, (m) through (p) corresponding IHC stains (40×) at higher hypoxic area, (i) through (l) corresponding IHC stains at low hypoxic area (400×, brown), and (q) through (t) corresponding stains at higher hypoxic area.

A group of mice were injected with 25 μM solutions of ICG and 2-nitroimidazole-piperazine-ICG and fluorescence was measured in tumors located at different depths. Statistics of reconstructed fluorescence (concentration vs. time) of ICG and 2-nitroimidazole-piperazine-ICG were shown in Figure 3.8 and Figure 3.9. The horizontal axis is time in minutes and the vertical axis is the reconstructed maximum fluorescence concentration in μM. The dye concentration injected was 25 μM for all mice. (a) ICG (blue) and 2-nitroimidazole-piperazine-ICG (red) with tumor located at 1.5 cm and (b) 2 cm.

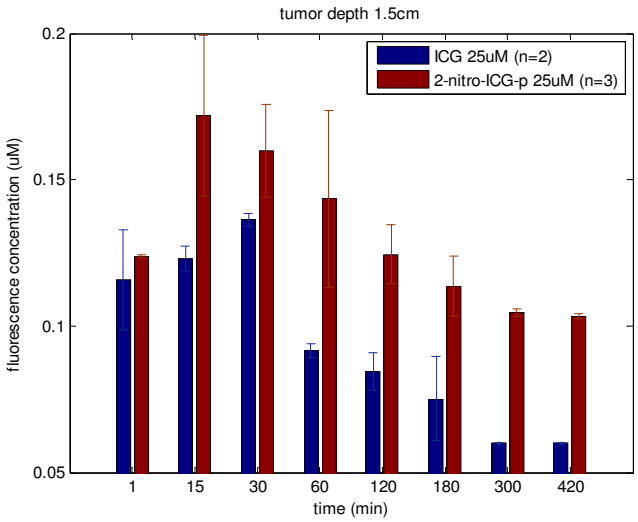

Figure 3.8. Statistics of reconstructed fluorescence of 25 μM ICG and 2-nitroimidazole-piperazine-ICG with tumors located at 1.5 cm depth

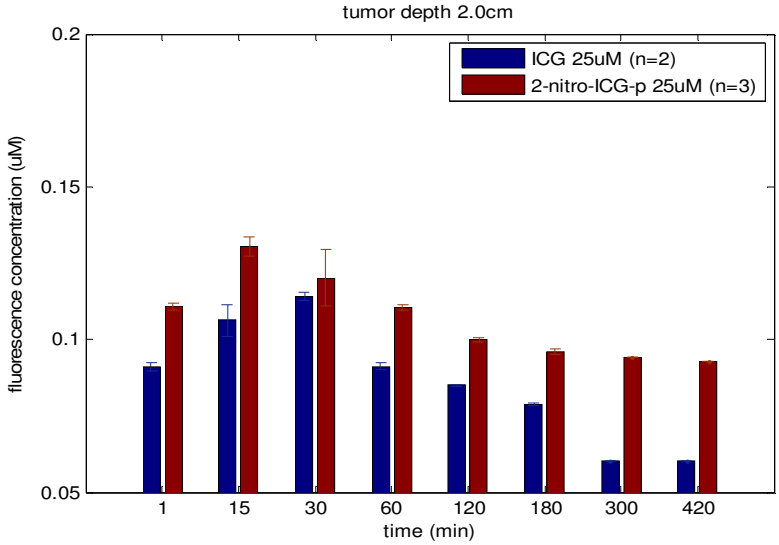

Figure 3.9. Statistics of reconstructed fluorescence of 25 μM ICG and 2-nitroimidazole-piperazine-ICG with tumors located at 2.0 cm depth

A group of two mice were injected with 50 μM solutions of ICG, 2-nitroimidazole-ethanolamine-ICG (**10a**) and 2-nitroimidazole-piperazine-ICG (**26a**) and the resconstructed fluorescence was plotted against time in minutes. The piperazine analog has a strong signal compared to ethanolamine analog; the statistical data is shown in Figure 3.10.

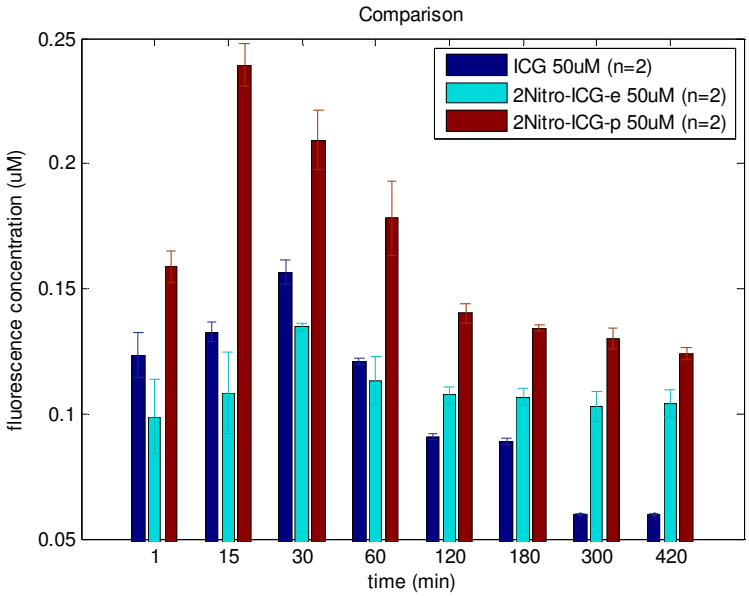

Figure 3.10.Comparison of reconstructed fluorescence concentration (maximum) vs. time (minutes) of 50 μM ICG (**9**), 2-nitroimidazole-ethanolamine-ICG (**10a**) and 2-nitroimidazole-piperazine-ICG (**26a**) with tumor center located at 1.5 cm.

Chapter 4.

SYNTHESIS, PHOTOPHYSICAL CHARACTERIZATION AND HYPOXIA EVALUATION OF THIRD GENERATION DYE CONJUGATES (NITROIMIDAZOLE-PIPERAZINE-RIGID ICG DYE CONJUGATES)

In an attempt to improve the targeting capability of the dye, as it affects NIR imaging of cancerous tumors, we attached a cancer targeting 2-nitroimidazole moiety to the fluorescent dye in order to improve detection of the tumor. We prepared bis-carboxylic acid ICG (**9**) using literature procedures, and used it to synthesize dye-conjugates **10a, 10b, 26** by linking 2-nitroimidazole acetate units to the dye via ethanolamine and piperazine linkers.[56,57] The purpose of this research was and is to develop a noninvasive probe for the detection of cancerous tumors using NIR fluorescent dyes that contain a nitroimidazole moiety which is known to target hypoxic tumors.[56,58] The quantum yield for the first and second generation dyes used in the study was about 0.06, which was sufficient for the NIR detection of hypoxic cancerous tumors in vivo.[56]

In our third generation, to further develop this work, we targeted the synthesis of dyes with a larger quantum yield with the goal of increasing the sensitivity of our tumor detection system. However, any structural changes should retain the emission/absorption wavelengths in the NIR region. Once the synthetic work was completed, the next step was to examine parameters that influence the fluorescent yield of the dye, without significant perturbation of the emission and absorption wavelengths. It is known that conversion of a non-planar molecule to a similar but more planar and rigid molecule often leads to an increase in the quantum yield of fluorescence.[59] Decreases in fluorescence may be associated with a higher collisional probability observed with molecules that have a high degree of flexibility. In other

words, molecules with more rigid structures have a lower probability of collision, which leads to a higher fluorescence potential, because the energy absorbed is not lost due to molecular vibration or collision. It has been shown, however, that rigidity (maintenance of a planar or near planar configuration) in the first excited S_1 excited state is more important than rigidity in the S_0 state.[60] One possible structural change that might lead to rigidity is incorporation of a ring into the polyene chain, which increases the rigidity and thereby the fluorescent quantum yield. Any structural modification of the polyene unit must produce a dye with absorption/emission in the NIR region because, our long term goal for any new dye is to eventually prepare derivatives for targeting hypoxia in cancerous tumors. In order to introduce the rigidity into the polyene chain, we targeted two new structural types: one, introducing a ring into the polyene unit and the second type of structurally modification shortened the polyene chain by two carbon atoms (pentamethine dye). The first step toward that goal requires synthesis of the dye and a study of the chemical and in vitro physical properties of the dye. Therefore, initial work involves the chemical synthesis, chemical properties, and in vitro stability studies in PBS and sucrose solution, as well as emission/absorbance data of the dyes. As part of initial work which, focuses on identifying a new dye with improved fluorescent properties, we have started the synthesis of five and six membered ring incorporated indocyanine dyes **32** and a pentamethine dye which has two carbon atoms less in the polyene chain **71**. (Figure 4.1)

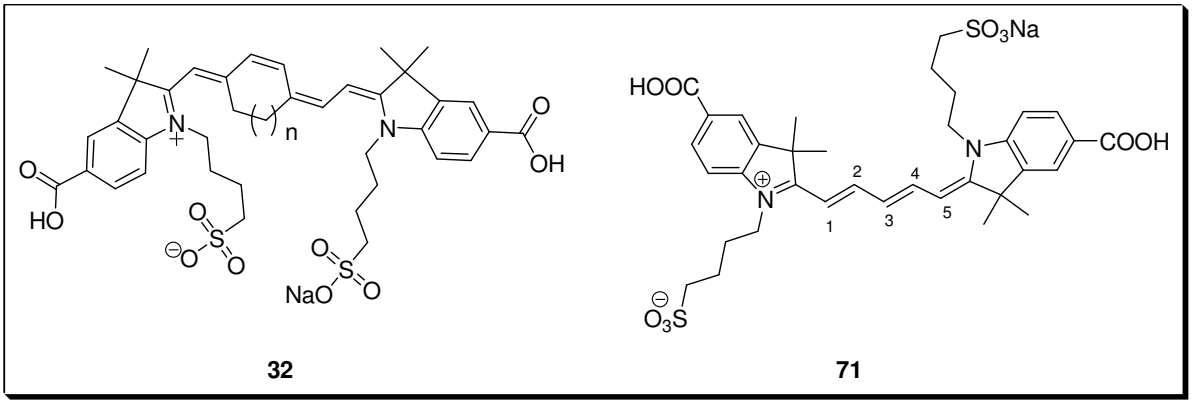

Figure 4.1.Structures of third generation dyes

4.1 Synthesis of third generation dye conjugates

4.1.1 Ring incorporation into the polyene chain of indocyanine green dye:

Our attempt to introduce a 1, 4 - substituted ring system in to the polyene chain was unsuccessful.

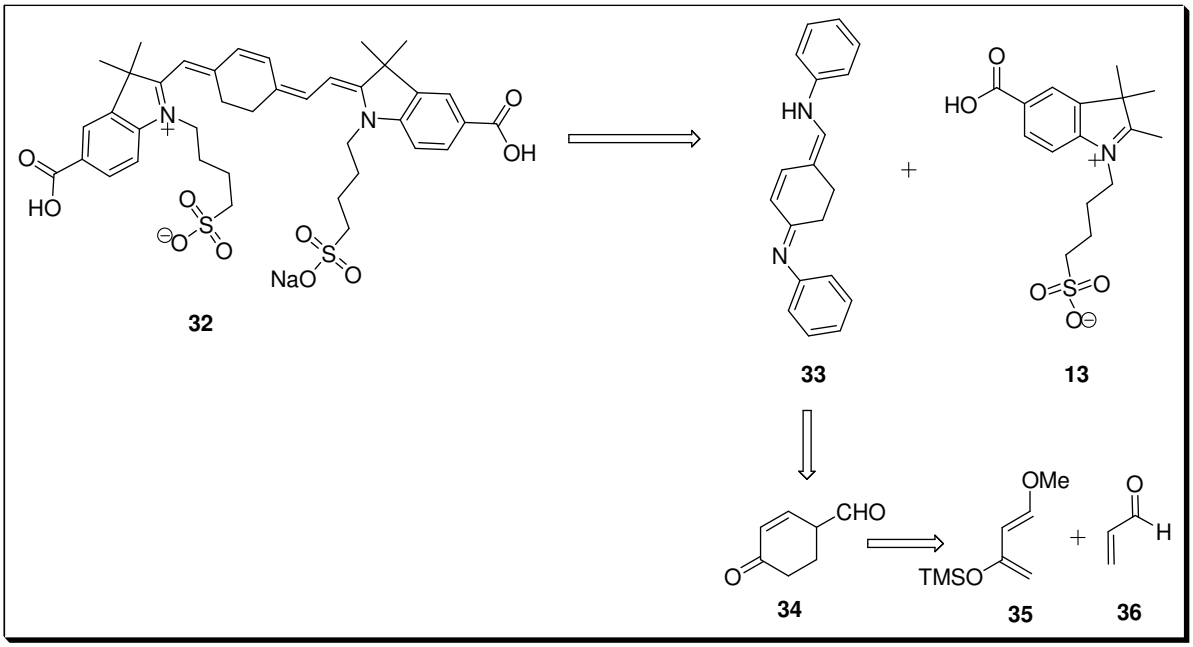

Scheme 4-1. Retrosynthesis of poly-ene modified indocyanine dye

Retrosynthesis for the synthesis of **32** was shown in Scheme 4-1, and the actual synthesis was started with a Diels-Alder reaction between Danishefsky's diene (**35**) and acryl aldehyde (**36**) shown in Scheme 4-2. The Diels-Alder reaction in toluene gave a black tar like product, whereas in dichloromethane at room temperature gave a clear reaction. The Diels-Alder adduct **37** was obtained in 38% yield after column chromatographic purification. We isolated a compound, that wasn't present in the crude originally, but eluted during the column purification. This explains the reason, for the low yield after purification. The isolated product was characterized as 2-methoxy-4-oxocyclohexanecarbaldehyde **39**. Since silica gel is acidic, we rationalize the observation as deprotection of TMS group by silica gel, followed by keto-enol tautomerization to provide the substituted cyclohexanone derivative **39** (Figure 4.2).

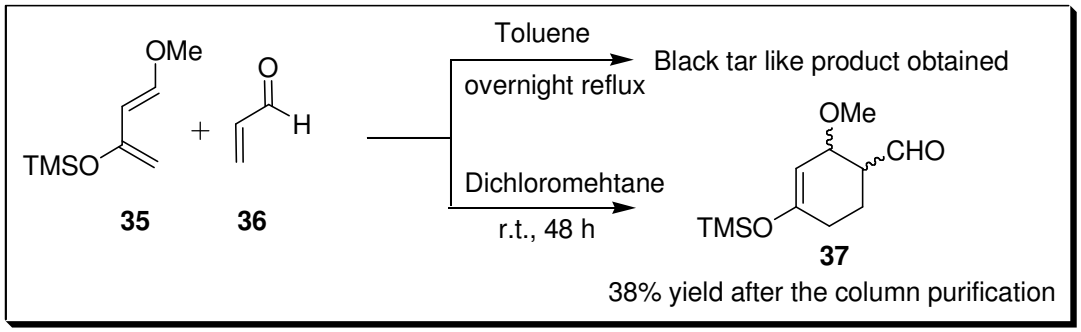

Scheme 4-2. Diels-Alder reaction of Danishefsky's diene with acrylaldehyde

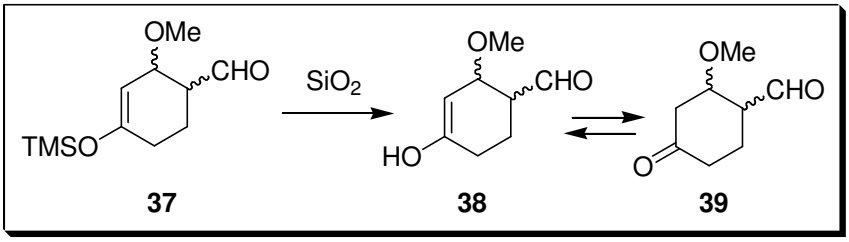

Figure 4.2. Rearrangement of Diels-Alder adduct (**37**) on silica gel

To avoid this issue, we bypassed the purification step and deprotected the Diels-Alder adduct to give oxocyclohexene carboxaldehyde **34** (Scheme 4-3). Treatment of the Diels-Adler adduct with 0.1N HCl in dichloromethane gave the oxo-cyclohexene carboxyaldehyde **34**, but upon loading on silica gel it rearranged to a new product **40**, which suggests that the product is unstable on silica gel.

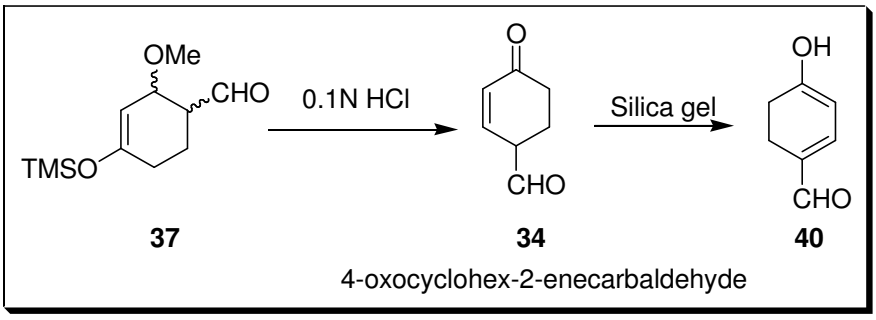

Scheme 4-3. Preparation of cyclohexenone carboxaldehyde **34** and its rearrangement

Therefore we treated the compound **37** with 0.1N HCl and aniline to get the bisanilide **33** directly, as shown in the following Scheme 4-4.

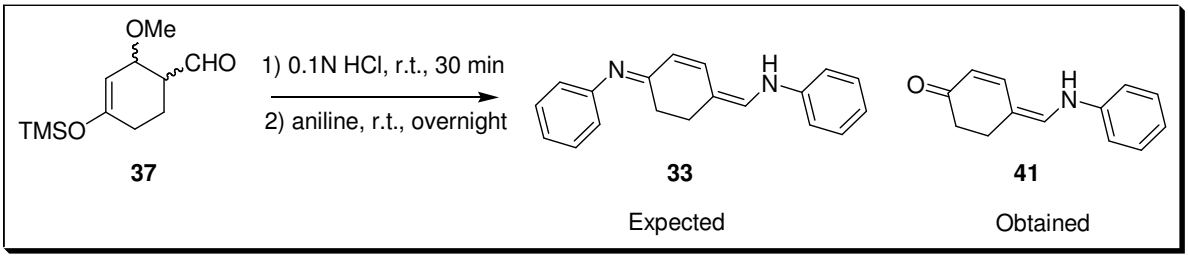

Scheme 4-4. Attempted synthesis of bisanilide, **33**

Compound **41** was obtained rather than the bisanilide **33**. Compound **41** appears to exhibits a vinylogous amide resonance (Figure 4.3) which explains why the reaction did not proceed further to get the bisanilide, **33**. Several reactions that used anilines substituted with electron withdrawing groups on them (4-nitro aniline, 2,4-di nitro aniline), and added Lewis

acids such as copper triflate, yetterbium triflate to activate the carbonyl group, did not solve the problem.

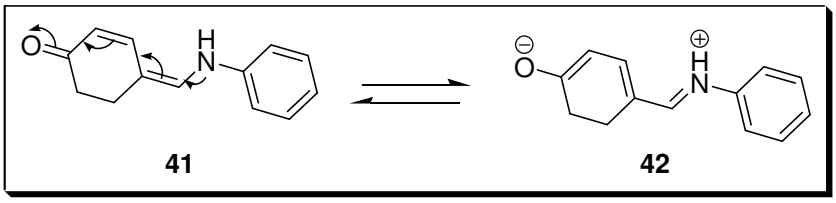

Figure 4.3. Vinylogous amide type resonance

To overcome this issue, we modified our synthetic route (Scheme 4-5), to replace acryl aldehyde with methyl acrylate. According to new synthetic route, the Diels-Alder adduct **44** of **35** and **43** could be treated with DIBAL-H to give the corresponding alcohol **45.** Subsequent deprotection of TMS group with yetterbium triflate could provide compound **46**. Treatment of **46** with aniline could provide compound **47**, which could be oxidized to aldehyde **48**. Finally treatment with 4-nitroaniline should provide the desired bisanilide **49**.

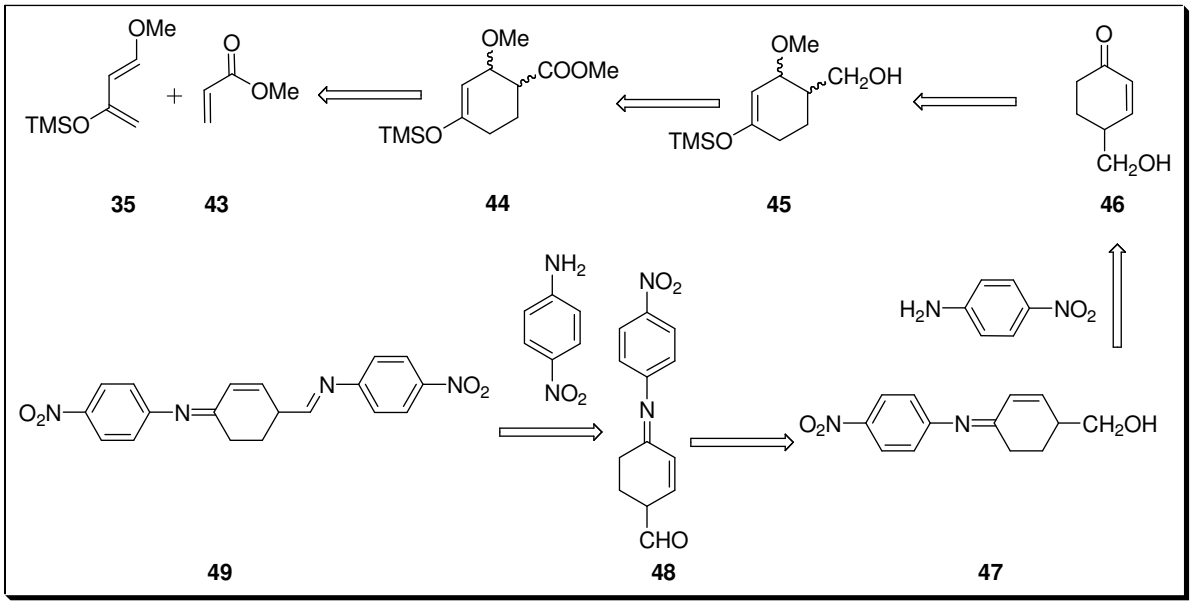

Scheme 4-5. Retrosynthesis of modified synthetic route to six-membered bisanilide **49**

During the DIBAL reduction step, elimination gave the product **50**, the TMS group was removed with yetterbium triflate to give compound **51**, which upon treatment with 4-nitroaniline gave compound **52**, which tautomerized to give the 1, 4- substituted diene **53** in 35% yield (Figure 4.4).

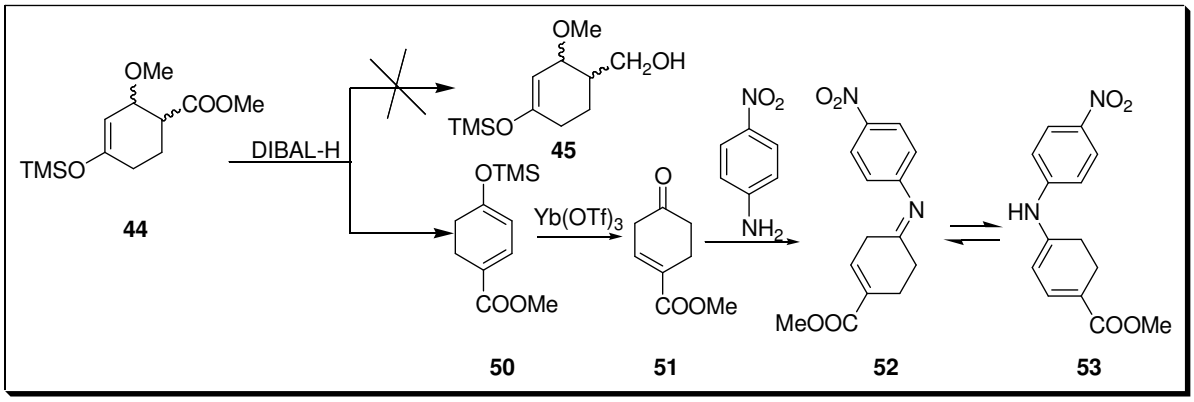

Figure 4.4. Formation of 1,4-substitued diene from diels-alder adduct **44**

We also attempted a condensation reaction between **13** and **40**, and the reaction yielded a highly hygroscopic solid (Scheme 4-6).

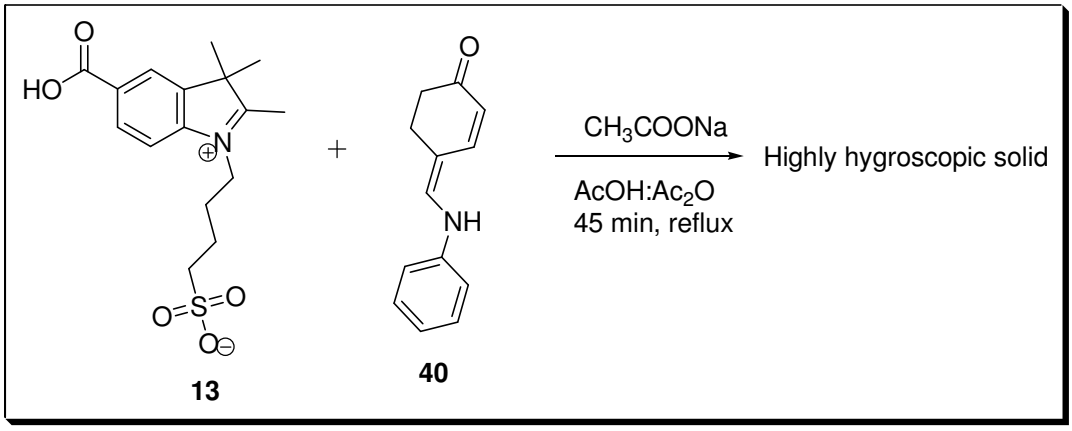

Scheme 4-6. Condesation of betaine indolium acid (**13**) and enone (**40**)

Despite all our efforts we did not obtain the desired product, although we found many unexpected transformations during the synthesis. Some of the transformations may be useful for making 1,4-disubstituted cyclic dienes for Diels-Alder reactions.

We attempted to incorporate an aromatic ring into the polyene chain (Figure 4.5); and the reactions yielded brick red solids. We were not able to characterize the outcomes of these reactions because of solubility issues.

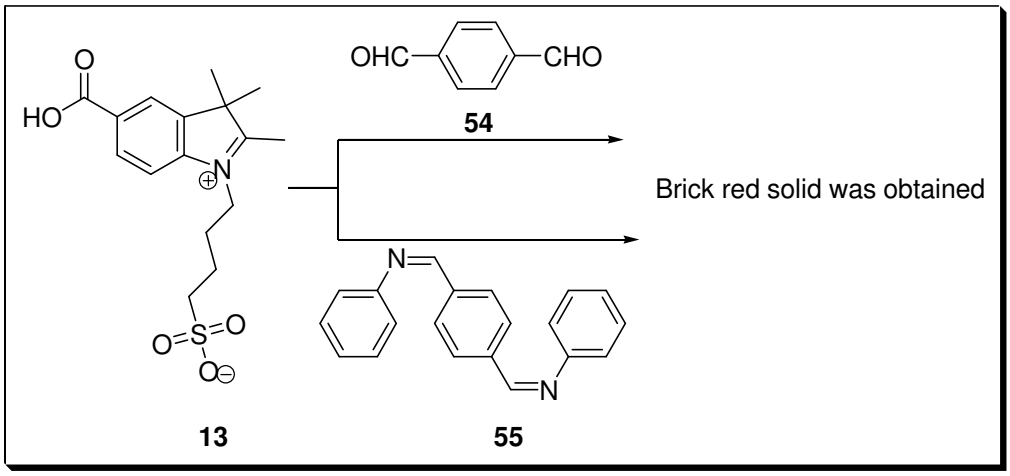

Figure 4.5.Condensation of betaine indolium acid (**13**) with *p*-phthalaldehyde (**54**) and phthalaldehyde imine

All our attempts to synthesize diimine **58** were unsuccessful (Figure 4.6), and all the reactions yielded the literature reported iminoisoindoline (**59**). The diimine **58** was never isolated as it is so reactive undergoing intramolecular cyclization to form the iminoisoindoline.[61]

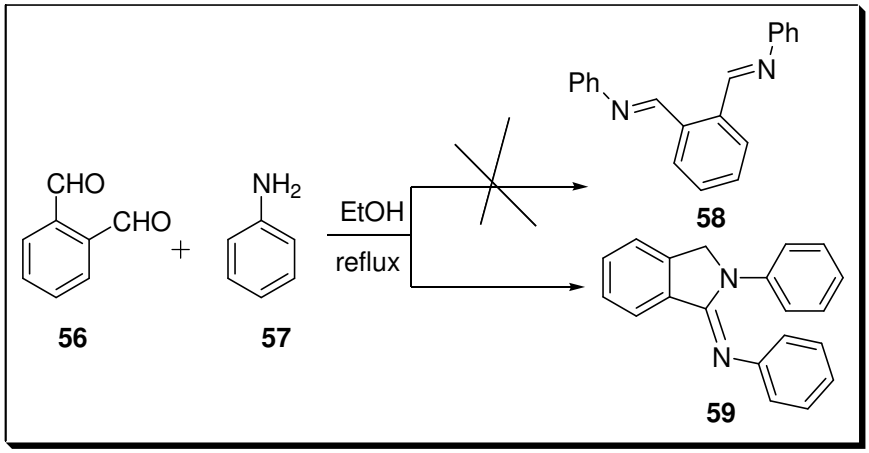

Figure 4.6. Formation of iminoisoindoline (**59**)

We slightly modified our target by changing the position at which the ring is incorporated in to the polyene chain. Instead of connecting the ring at 1,4 positions (**32**), we wanted to connect the ring at 1,3 positions (**32'**) (Figure 4.7).

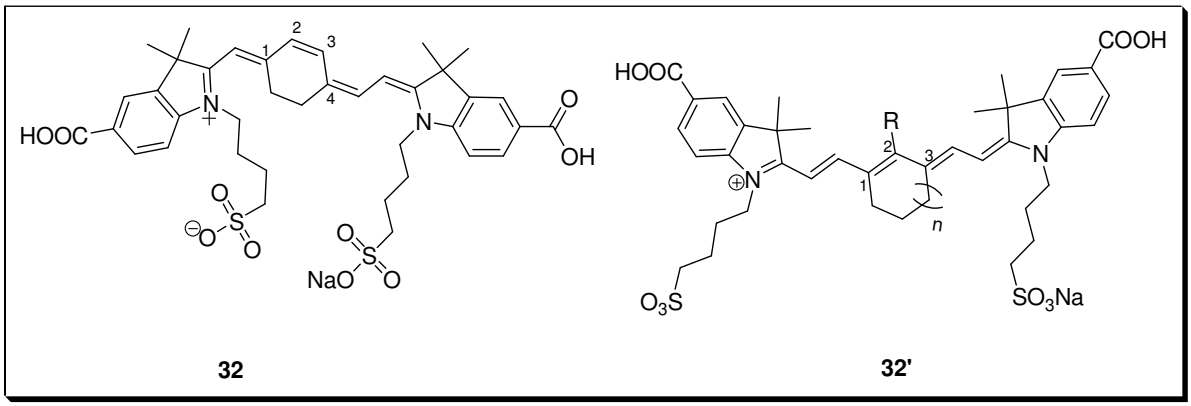

Figure 4.7. Incorporation of the ring at 1,3-positions

Tung and co-workers reported just such a molecule as a near infrared fluorochrome, in their synthesis of compound **67** (reported as compound NIR820).[62]

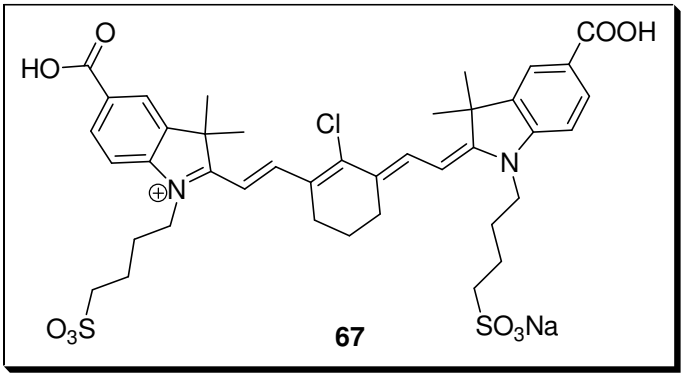

67

In earlier work, Reynolds and Drexhage had prepared heptamethine pyrylium dyes that contained a ring in the polyene moiety.[63] These dyes were relatively unstable and exhibited a bathochromic shift. Slominskii et al. prepared a series of dyes containing a polyene moiety (methine dyes), including examples with a cyclohexane ring.[64,65] It is noted that the reaction of **67** with amines produced a new class of NIR amine tricarbocyanine dyes with excellent photostability properties.[66] Similarly, reaction with amines followed by conversion to the corresponding amide produced NIR amide tricarbocyanine dyes that were further modified to include lipoic acid residues used for cancer imaging due their ability to serve as highly sensitive NIR SERS reporter molecules.[67] For our study, we prepared **67** as well as several related indocyanine dyes, first with a six- or a five-membered ring incorporated into the polyene system **65, 66** and **68**, and another derivative with a shorter polyene chain **71**.

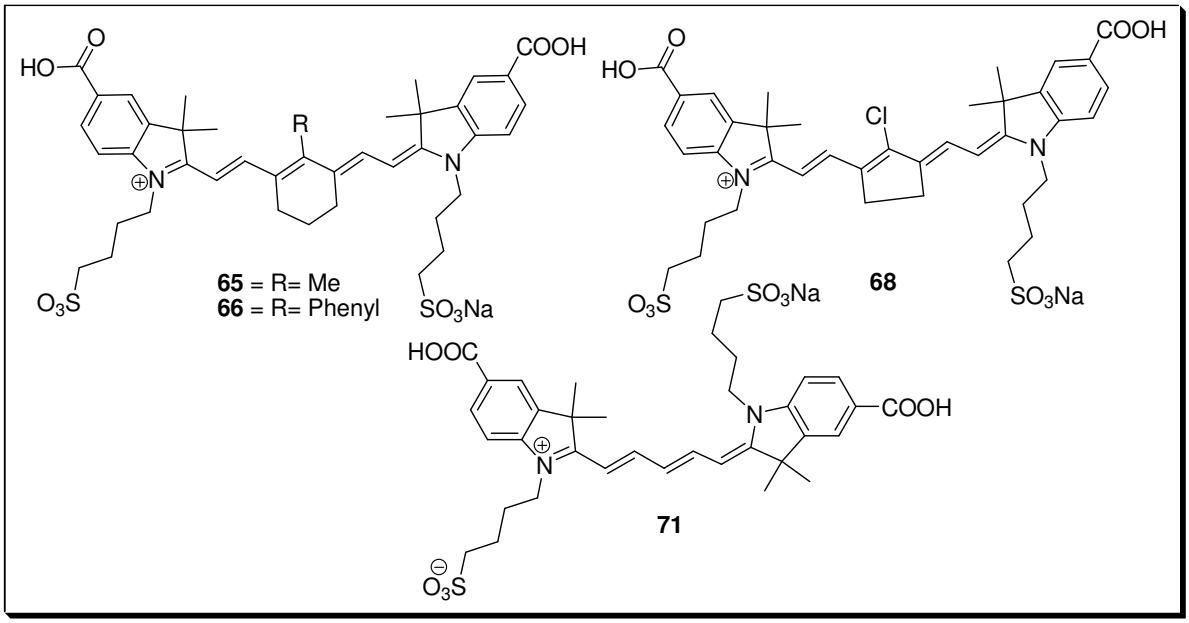

Figure 4.8. Polyene modified indocyanine green dyes

In Tung and coworker's work, **67** was used for protein labeling experiments and **67** was coupled to a peptide as an amino acid residue by initial conversion to the NHS activated ester.[62,68] Human transferrin (Tf) was used as a model protein and coupling of activated **67** with Tf gave a conjugate that facilitated florescence measurements in PBS solution as well as the protein binding studies. Our primary interest was the synthesis of these compounds and determination of changes in fluorescent yield as a function of structure, if any.

Synthesis of ring incorporated indocyanine dyes was begun by making the five- and six-membered bisanilides. Methyl and phenyl substituted bisanilides **61**, **62** were prepared from N-methylformanilide **60**, which was prepared by the reaction of N-methylaniline with formic acid and sodium formate.[69] As shown in (Scheme 4-7), N-methylformanilide was treated first with $POCl_3$ and then with methyl cyclohexene. Subsequent reaction with aniline hydrochloride gave six-membered methyl bisanilide **61** in 39% yield.[70] 1-Phenylcyclohexene was converted to **62** in 68% yield using an identical procedure.[70]

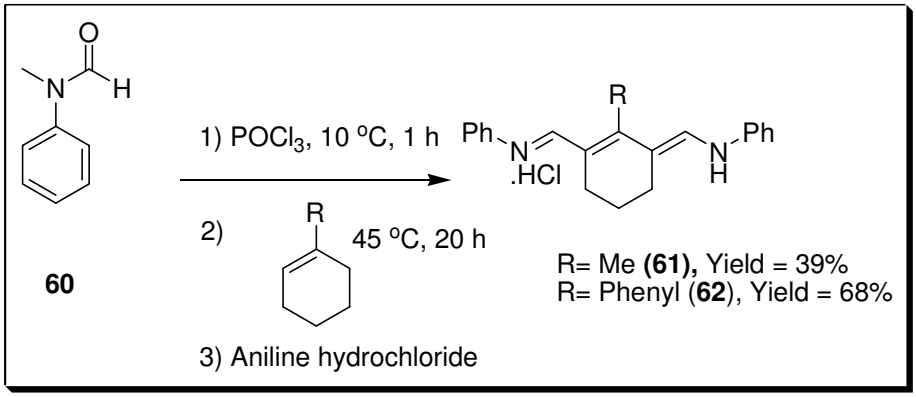

Scheme 4-7. Synthesis of six-membered methyl and phenyl bisanildes

The direct treatment of N-methylformanilide with $POCl_3$ in the presence of cyclohexanone and aniline hydrochloride led to a 79% yield of **63**.[70] The identical reaction with cyclopentanone led to **64** in 73% yield.[71]

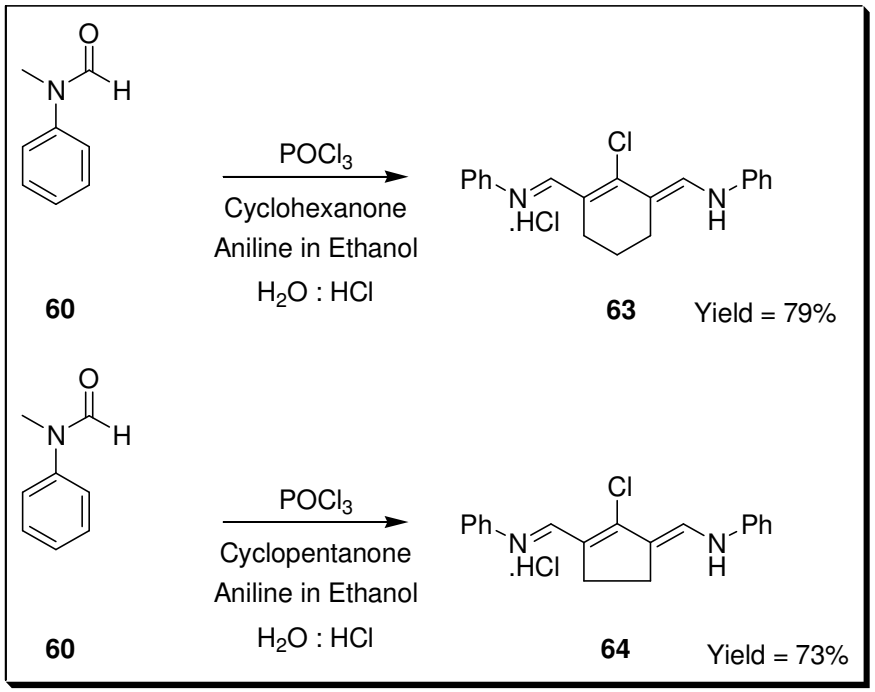

Scheme 4-8. Synthesis of five- and six-membered bisanilides

With these anilides in hand, coupling with indolenium sulfonate **13** was accomplished using the standard procedure from our previous work, as shown in(Scheme 4-9), anilide and indole heated to 120 °C in acetic acid-acetic anhydride, buffered with sodium acetate.[56] Using this procedure, **61** converted to **65** in 41% yield, **62** to **66** in 37% yield, **63** to **67** in 22% yield, and **64** to **68** in 41% yield. As noted earlier, Tung and co-workers prepared **67** in 67% yield by heating commercially available **63**, obtained from Aldrich, with **13** in ethanol at reflux for two hours in the presence of sodium acetate.[42]

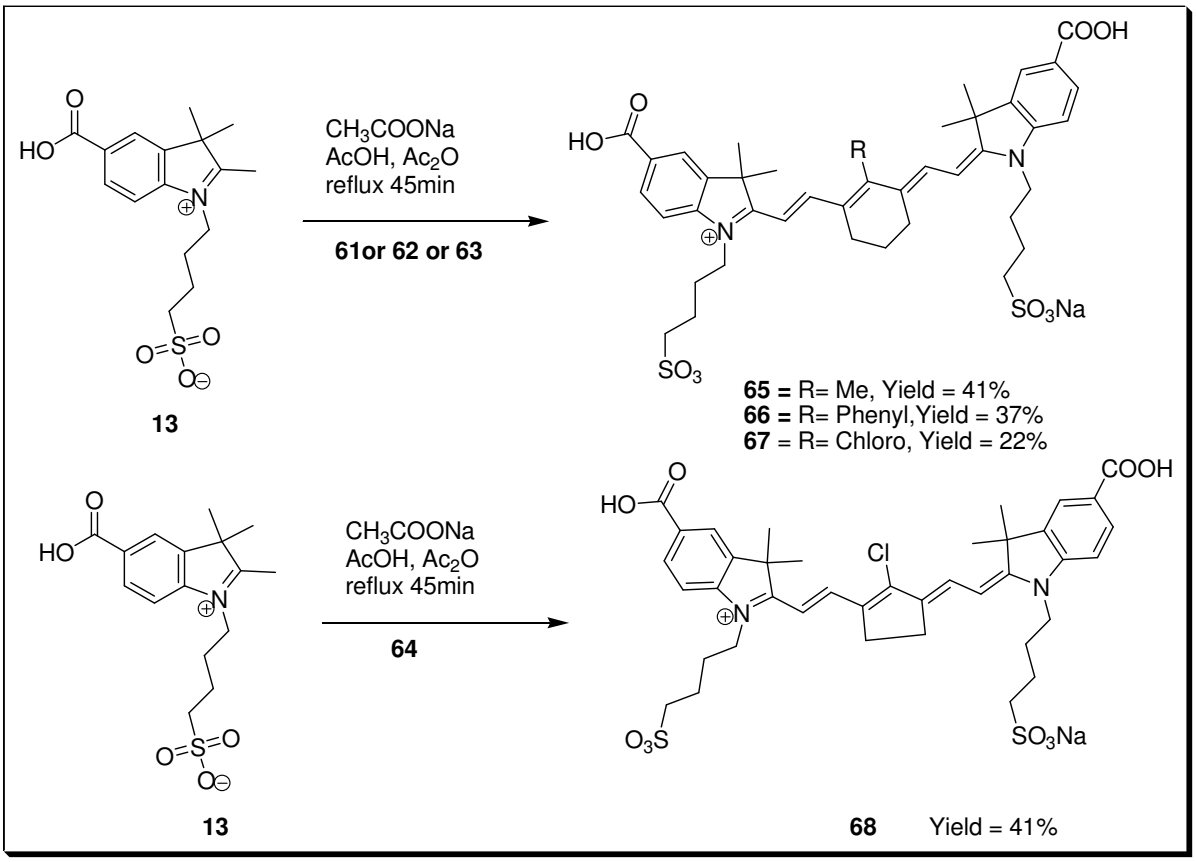

Scheme 4-9. Synthesis of ring incorporated indocyanine green dyes

We prepared a single example of the second target type (**71**, Scheme 4-10), with two carbons less in the polyene linker. Reaction of the bis(dimethyl acetal) of propanedial (**69**)

with aniline, in aqueous HCl led to anilide, **70** in 90% yield.[72] Subsequent reaction with indole **13** under the standard conditions gave a 30% yield of dye **71**.

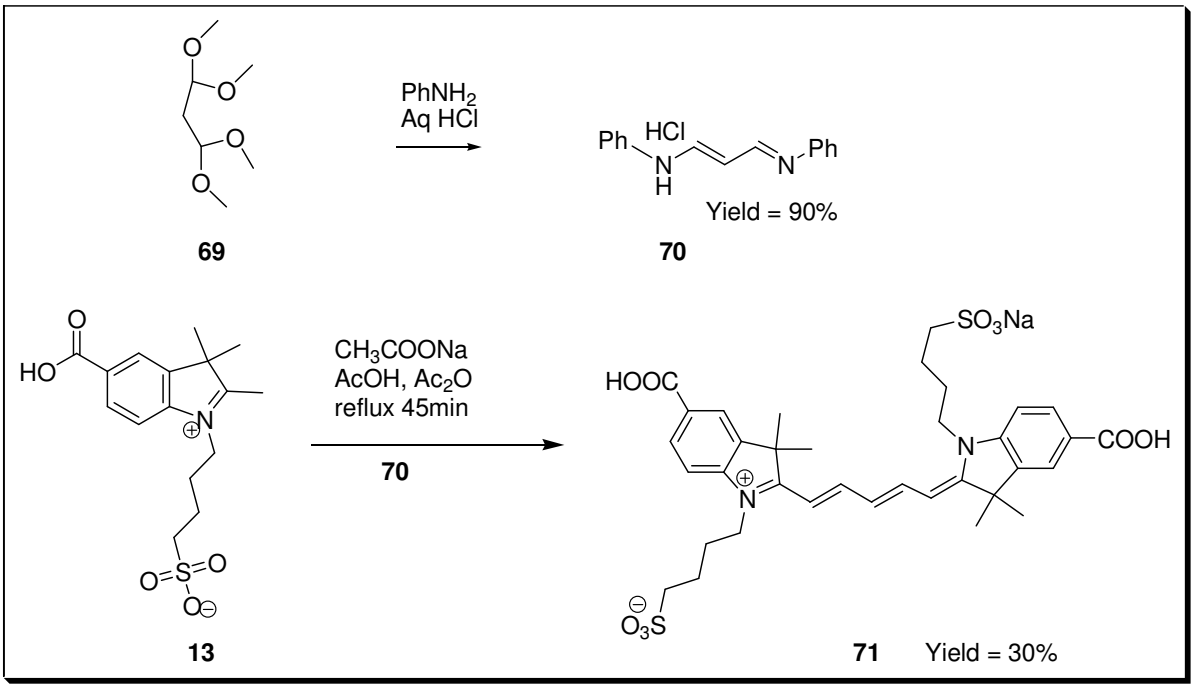

Scheme 4-10. Synthesis of pentamethine indocyanine dye

4.2 Absorption and fluorescence properties:

All derivatives were characterized using an UV-Vis spectrophotometer and a fluorescence spectrophotometer (Varian Analytical Instruments, Walnut Creek, CA). The wavelength range of both spectrophotometers is 250 nm to1100 nm. The dyes were suspended in either Phosphate Buffer Saline (PBS) or a 9.25% aqueous sucrose solution, and the absorption and fluorescence spectra were recorded. These two solvent systems were chosen to be compatible with our previously reported in vivo studies with **10, 26** and related compounds. Quantum yields were calculated relative to the standard samples that have a fixed fluorescence quantum yield value, according to the following equation

$$\Phi_x = \Phi_{STD} \left\{\frac{Grad_x}{Grad_{STD}}\right\} \left(\frac{\eta_x}{\eta_{STD}}\right)^2 \qquad \text{Eq. 1}$$

Where STD = standard and x = unknown, respectively, Φ is the fluorescence quantum yield, Grad is the gradient from the plot of integrated fluorescence intensity versus absorbance, and η is the refractive index of the solvent.

All UV-Vis spectra were recorded on Cary 50 spectrometer and fluorescence spectra on a Cary Eclipse. Fluorescence was measured in a 10 mm fluorescence cuvette and sample concentrations were maintained below 0.1 absorbance by diluting the stock solutions to the corresponding concentrations. All UV absorbance measurements were done with solvent background correction, at the concentrations listed in Table 4-1.

Table 4-1: Dye solutions used for UV-Vis analysis

Dye in PBS	Stock solution concentration in μM
65	542.7
66	428.5
67	354.3
68	734.1
71	420.7
Dye in Ethanol	Stock solution concentration in μM
65	636.5
66	417.1
67	728.5
68	307.7
71	144.8
Dye in 9.25% sucrose	Stock solution concentration in μM
65	681.4
66	731.9
67	700.2
68	1202.4
71	986.2

The florescence yield of **65**, **66**, **67**, **68** and **71** were measured in ethanol using Rh101 as the standard, in PBS and in a 9.25% sucrose solution using **9** as the standard. All results are shown in Table 4-2. It is clear that incorporating a ring into the polyene moiety as in **65**, **66**, **67** and **68** had little or no effect, or led to a slight decrease in the quantum yield. Although each of these derivatives should be more rigid in terms of rotation about the C-C bonds of the polyene, the increase in the number of atoms may mitigate any benefits. On the other hand, the chain-shortened derivative **71** showed a significant enhancement in the quantum yield, with quantum yields ranging from a low of 0.028 to a high of 0.34. Using Rh101 as the standard, the dye **71** absorbed at 657 nm and emission was measured at 676 nm. These values are in the useful range for NIR analysis, although a different filter would be required for a NIR analysis using any dye conjugate prepared from **71** that is structurally related to **10**, **26**. Using **9** as a standard, absorbance of **71** was at 655 nm and emission at 669 nm in PBS, and absorbance at 655 nm and emission at 672 nm in sucrose solution. The chloro and methyl derivatives **65** and **67** showed slight shifts in the absorption and emission peaks, relative to **9**, although **68** showed a peak past 800 nm. However, the emission peaks shifted to past 800 nm for **65**, **67**, and **68** using Rh101 as standard. Using **9** as standard emission peaks are past 800 nm for **67** and **68** (Table 4-2). Tung and coworkers reported data for **67** in methanol, and reported that **67** absorbs maximally at 790 nm and emits maximally at 820 nm in methanol with a molar extinction coefficient of 184,000, and a quantum yield of 0.08.[42] We found that **67** absorbs at 812 nm and emits at 826 nm, in ethanol, with a quantum yield of 0.025 and a molar extinction coefficient of 189,000. Our data was reported using Rh101 as a standard. Tung used the same method to determine relative fluorescence quantum yield, indicating the use of a standard, but that standard was not identified. As seen in Table

4-2, phenyl derivative **66** did not show the shifts observed for **67**. In all cases, the quantum yield was less than 2, although that of phenyl derivative **66** was close to **9**. It is clear from our results that incorporation of a ring in the polyene chain does not increase the florescence yield. While the ring may diminish the number of stereoisomers that arise due to rotation about the C-C bonds, any benefit may be offset by the increased number of atoms

Loss of two carbon atoms from the polyene chain led to a significant increase in fluorescent yield for **71**. It is not clear why this relatively minor structural change leads to such an increase, but one explanation is that the diminished number of C-C bonds leads to fewer isomers due to rotation. It is certainly possible that fewer structural isomers can account for the increase in florescence yield. It is also possible that bringing the two indole moieties closer together may restrict the rotation and lead to an increase in rigidity. At this time, our explanation remains speculative.

Table 4-2. Photophysical properties of rigid dyes

	In ethanol, Rh101 as a standard			
Dye	λ_{abs} (in nm)	λ_{em} (in nm)	Extinction Coefficient (ε) ($M^{-1}cm^{-1}$)	Φ
9	759	778	191,000	0.146
65	783	803	183,000	0.024
66	775	791	250,000	0.127
67	796	811	189,000	0.059
68	820	840	145,000	0.041
71	657	676	210,000	0.344

In 1× PBS, bis-carboxylic acid (**9**) as a standard				
Dye	λ_{abs} (in nm)	λ_{em} (in nm)	Extinction Coefficient (ε) ($M^{-1}cm^{-1}$)	Φ
9	756	778	237,000	0.066
65	774	791	184,000	0.024
66	766	779	210,000	0.055
67	789	802	210,000	0.028
68	812	826	255,000	0.025
71	655	669	220,000	0.289
In 9.25% Sucrose, bis-carboxylic acid (**9**) as a standard				
Dye	λ_{abs} (in nm)	λ_{em} (in nm)	Extinction Coefficient (ε) ($M^{-1}cm^{-1}$)	Φ
9	755	779	211,000	0.072
65	776	791	207,000	0.030
66	767	787	240,000	0.068
67	790	815	230,000	0.031
68	813	833	113,000	0.024
71	655	672	262,000	0.338

4.3 Optical stability of rigid dyes in solution

The photostabilities of all dyes prepared for this study were examined in both PBS solution and in 9.25% sucrose solution. The dyes were dissolved in PBS solution and 9.25% sucrose solution, and the absorbance of each solution was maintained at approximately 0.82. Each sample was irradiated under a 500 W halogen lamp, maintained at a distance of 300 mm, for 14 h. An aqueous solution of sodium nitrite (50.0 g/L) was placed between the samples and the lamp to filter the light to less than 400 nm, and also to mitigate heat from the lamp. The initial absorbance data was measured and then measurements were carried out each hour. As shown in Figure 4.10 (in PBS solution) and Figure 4.9 (in the sucrose solution), all dyes that contained a ring, **65**, **66**, **67**, and **68**, showed loss of absorbance over

the course of three hours. This data stands in sharp contrast to dye **71**, which showed significantly improved stability in both PBS and in sucrose. It is noted that we also examined the stability in ethanol, but unavoidable evaporation of ethanol over the course of the experiment led slight changes in concentration and we deemed the data unreliable. This experiment was repeated with the same result, so it is not included here.

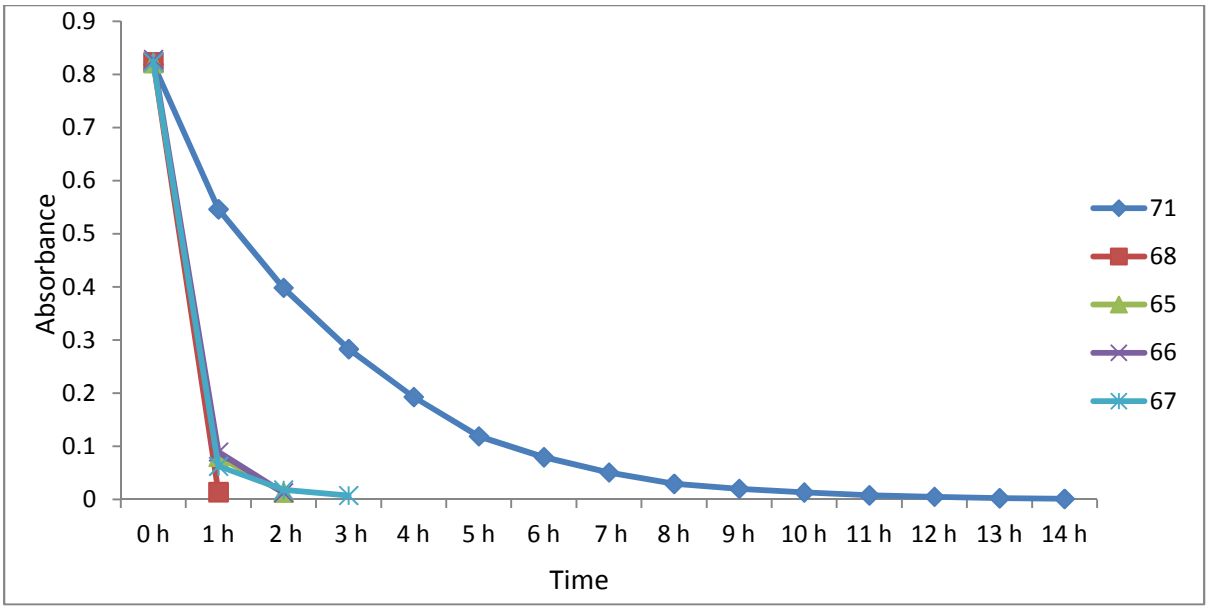

Figure 4.9. Photostability studies of rigid dyes in 9.25% sucrose solution

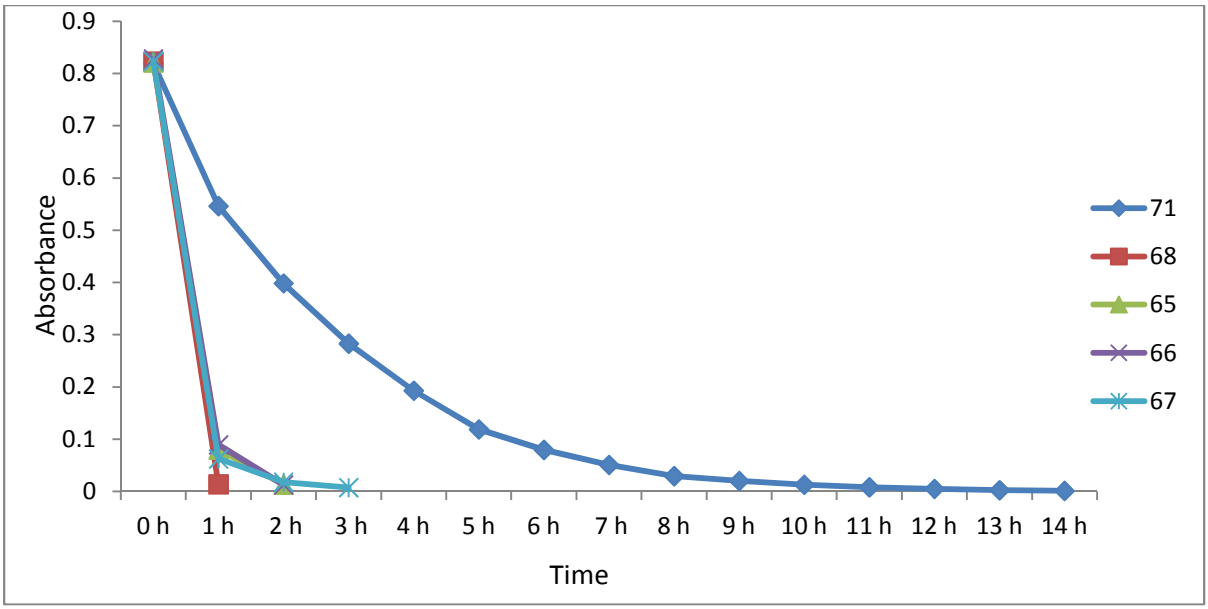

Figure 4.10. Photostability studies of rigid dyes in 1×PBS solution

4.4 2-nitroimidazole-piperazine-rigid ICG dye conjugate synthesis

Among all the polyene modified rigid dyes, pentamethine dye **71** has the highest quantum yield; therefore it was further coupled to ICG bis-carboxylic acid **9** to prepare 2-nitroimidazole-piperazine-rigid dye conjugate **72**. The same coupling procedure to make dye conjugates such as **10** and **26** was followed to couple the 2-nitroimidazole piperazine fragment **18a** to rigid dye **71** (Scheme 4-11). Pybop was used as a coupling agent, reaction was carried out in DMF and the reaction progress was monitored by TLC. After 48 h, the reaction mixture was dried up by blowing air. The crude mixture was washed couple of times with acetonitrile and ethyl acetate to remove soluble impurities. The crude solid was purified by C18 reversed phase automated flash column chromatography.

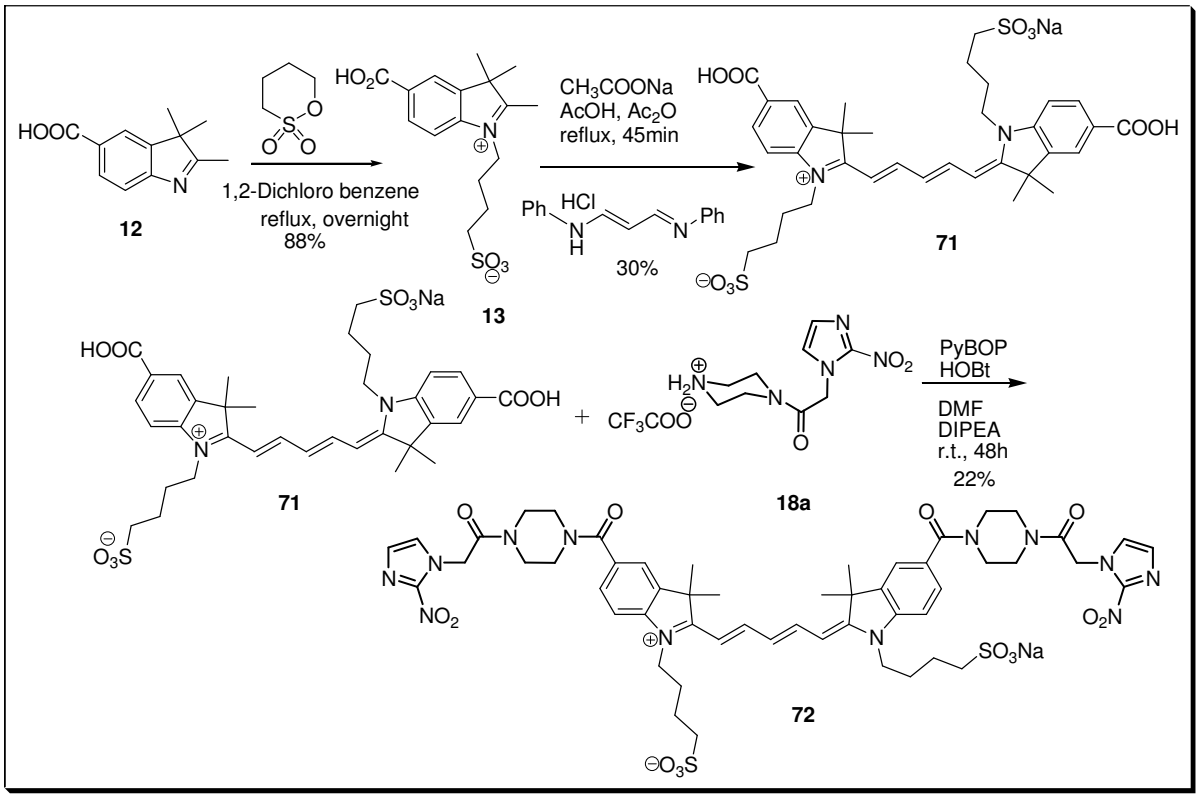

Scheme 4-11. Synthesis of 2-nitroimidazole-piperazine-rigid-ICG dye conjugate

Once we obtained the pure coupled product **72**, UV-Vis experiments were conducted to find out the extinction coefficient and quantum yield. The extinction coefficient of the coupled product was found to be 268,000 and the quantum yield in 9.25% sucrose solution was determined as 0.232.

Table 4-3. Photophysical studies of third generation dyes

S. No	Rigid dye	λ_{abs} (nm)	λ_{em} (nm)	Extinction Coefficient, ε ($M^{-1} cm^{-1}$)	Quantum Yield(□)
1	**71**	655	672	262,000	0.338
2	**72**	653	670	268,000	0.232

Both compounds **71** and **72** were submitted for *in vivo* studies in the mice. Since the emission wavelength for rigid dyes **71** and **72** is towards the low range, Li-Cor images were not collected. The signal strength of 2-nitroimidazole piperazine rigid dye conjugate is stronger compared to 2-nitroimidazole piperazine ICG dye conjugate. It stayed in the tumor for the same period of time. As the signal strength is very strong, it is possible to inject lower dye concentrations so that sensitivity would improve to a great extent.

4.5 Hypoxia evaluation of third generation dye conjugates

Preliminary hypoxia evaluation results are shown in Figure 4.11. The third generation dyes have higher quantum yield than the first and second generation dyes. The enhancement in the intensity of fluorescence signal could be because of higher quantum yield. Three dyes, rigid bis-carboxylic acid (nontargeted-rigid, **71**), 2-nitroimidazole-piperazine-rigid-ICG (targeted-rigid, **72**) and 2-nitroimidazole-piperazine-ICG (**26a**) were tested in the mouse as a preliminary evaluation.

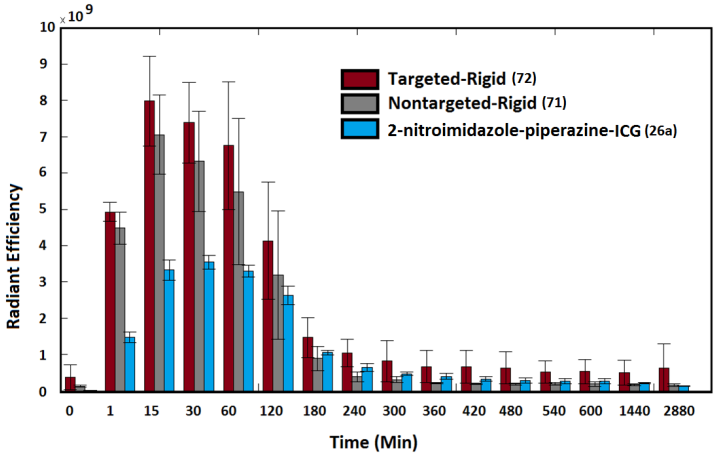

Figure 4.11. Fluorescence signal intensities of third generation dyes vs second generation

The rigid bis-carboxylic acid **71** and 2-nitroimidazole-piperazine-rigid ICG **72** have higher signal intensities than the 2-nitroimidazole-piperazine-ICG dye for the first 120 min time period. And then the rigid bis-carboxylic acid **71** signal intensity went down compared to the signal intensity of 2-nitroimidazole-piperazine-ICG **26a**, whereas the 2-nitroimidazole-rigid-ICG **72** signals remained as the higher intensity signals in this group of dyes. Though there is no 2-nitroimidazole is present in the rigid bis-carboxylic acid, it stayed as much time as the 2-nitroimidazole-piperazine-ICG does, the reason for this observation is not clear yet but it could be due to the higher quantum yield of the dye. Dyes with the higher the quantum yield can produce strong fluorescence signals even at lower concentrations. Further study is ongoing to validate the initial data obtained for the third generation dyes.

4.6 Future work

We would like to understand the key structural features in dye conjugates that are responsible for binding to hypoxic regions. We have designed few analogues to study the structure activity relationship. Compound **73** could provide information on role played by nitrogen atom in imidazole ring of the dye conjugates. As shown in Scheme 4-12, pyrrole methyl acetate **75** was prepared from tetrahydro-2,5-dimethoxy furan **74** and glycine methyl ester in 76% yield. Ethanolamine was coupled to pyrrole acetate **75** by simple overnight stirring in methanol at room temperature in 93% yield. Pyrrole ethanolamine fragment **76** will be coupled to ICG bis-carboxylic acid by the same method used to make our final dye conjugates to obtain **73**.

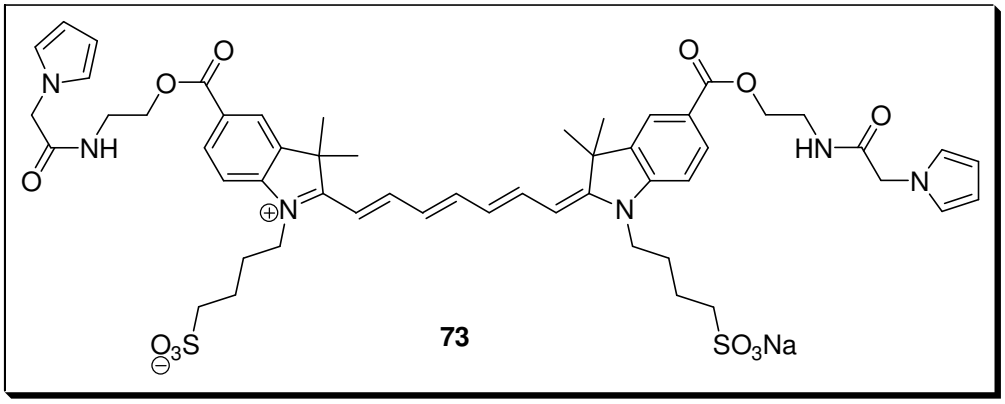

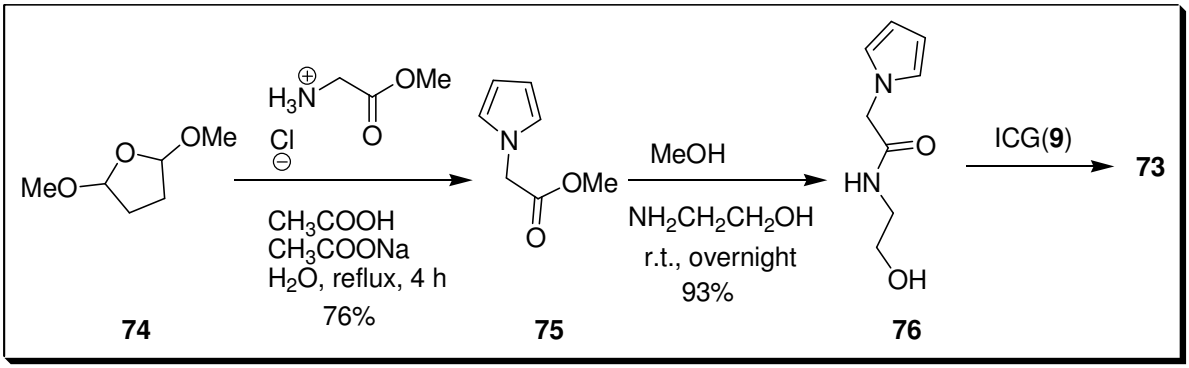

Scheme 4-12. Synthesis of pyrrole-ethanolamine-ICG dye conjugate **73**

Compound 77 could be useful to understand the effect of the group at the second position of imidazole ring in the dye conjugates. The 2-methylimidazole piperazine fragment **79** was prepared from 2-methylimidazole **78** and bromoacetyl piperazine **23** in 69% yield (Scheme 4-13). The boc group was removed by trifluoroacetic acid to give the TFA salt **80** in 91% yield. It will be coupled to ICG bis-carboxylic acid **9** to give 2-methylimidazole-piperazine-ICG dye conjugate **77**.

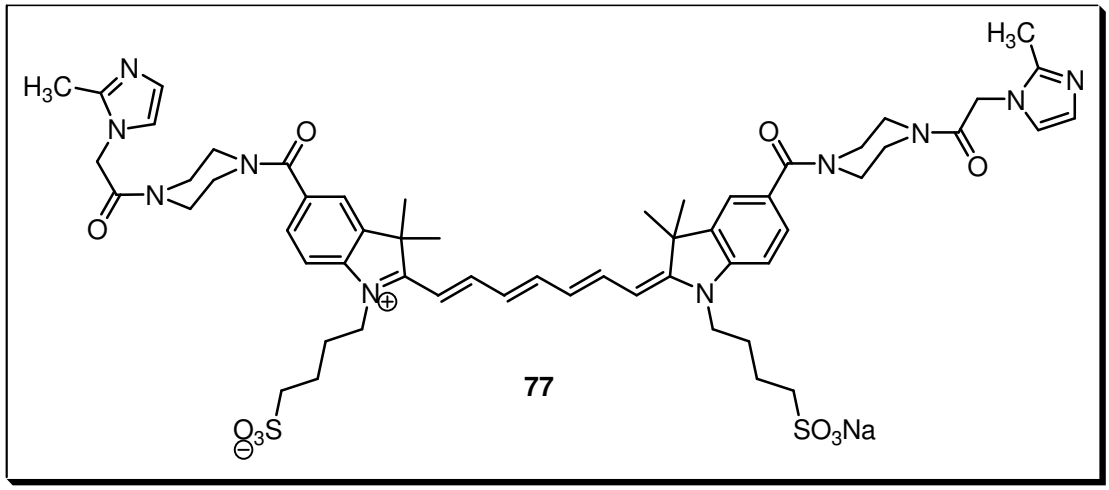

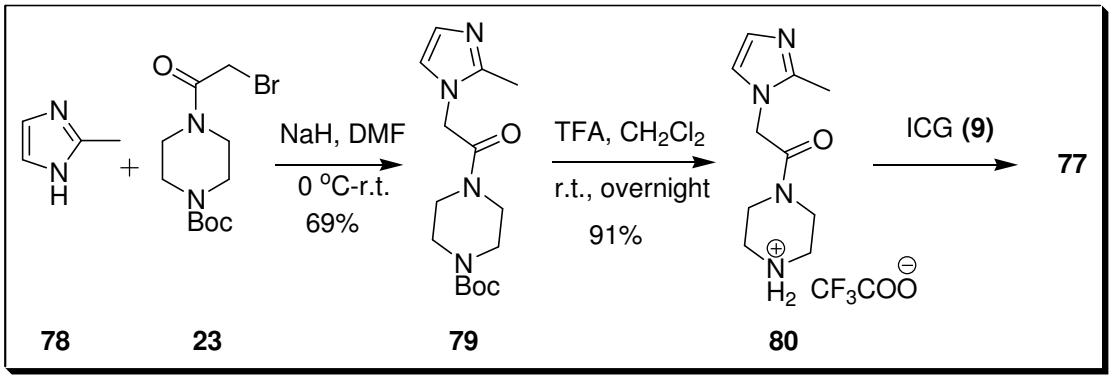

Scheme 4-13. Synthesis of 2-methylimidazole-piperazine-ICG dye conjugate **77**

Compound **81** could be useful for obtaining information about the role played by the carbonyl group linked to piperazine in dye conjugates. The carbonyl group of 2-nitroimidazole piperazine fragment **24a** could be reduced by lithium aluminium hydride (LAH) to give the reduced product **82**. The boc group can be removed by trifluoroacetic acid to give the TFA salt **83**, which can be coupled to ICG bis-carboxylic acid **9** to give the dye conjugate **81** (Scheme 4-14).

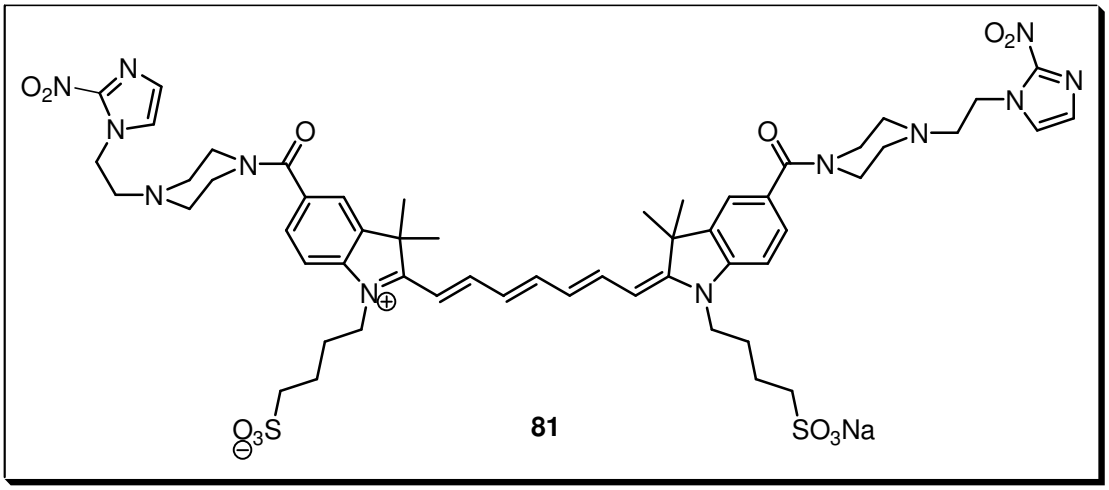

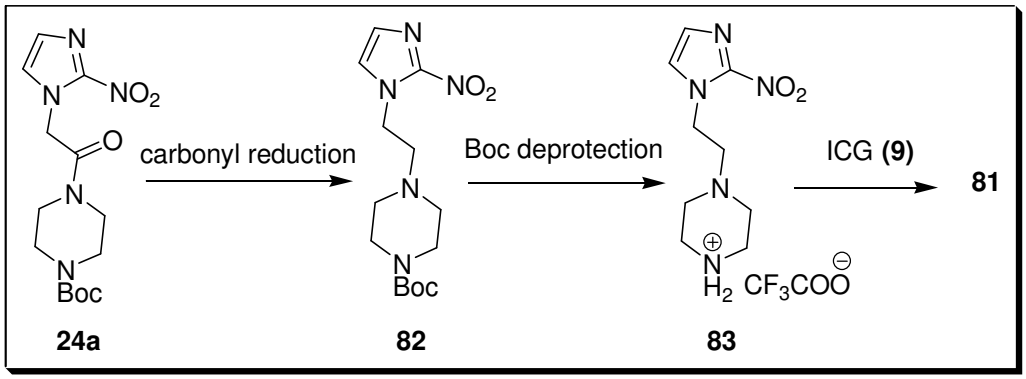

Scheme 4-14. Synthetic plan for the synthesis of dye **81**

To understand which protein is binding to nitroimidazole dye conjugate, it is important to make biotinlated dye conjugates **85**. Biotin **84** is very useful in this study because it binds to proteins and enables easy purification in order to study the protein. Biotin strongly binds to avidin and streptavidin.[73] If Biotin can attach to half loaded dye conjugate, (Figure 4.12) it would be possible to access the information about the protein that is binding with nitroimidazole moiety in the dye conjugate. With the help of avidin beads, biotin complexed protein of the hypoxic tumor cells can be separated from other proteins. The protein of interest sticks to the avidin beads while others wash through the column of avidin beads. If protein is isolated from the beads, it might provide useful information about how

and which part of the nitroimidazole piperazine dye conjugate is responsible for binding, which may allow to design more specific dye conjugates. The synthetic plan for the biotinlated dye conjugate is shown in Scheme 4-15, indolenium methyl ester **88** was made from indolinium betaine sulfate **13** or from hydrazine methylbenzoate.[74] From indolenium methyl ester **88**, mono-carboxylic acid ICG **89** (one of the carboxylic groups on ICG bis-carboxylic acid was protected as methyl ester) was prepared. The mono-carboxylic acid ICG **89** could be attached to nitroimidazole by reacting with 2-nitroimidazole piperazine fragment to give the half loaded ICG dye **90**, which could be coupled to biotin-piperazine fragment **87** to give the biotinlated dye conjugate, **85**.

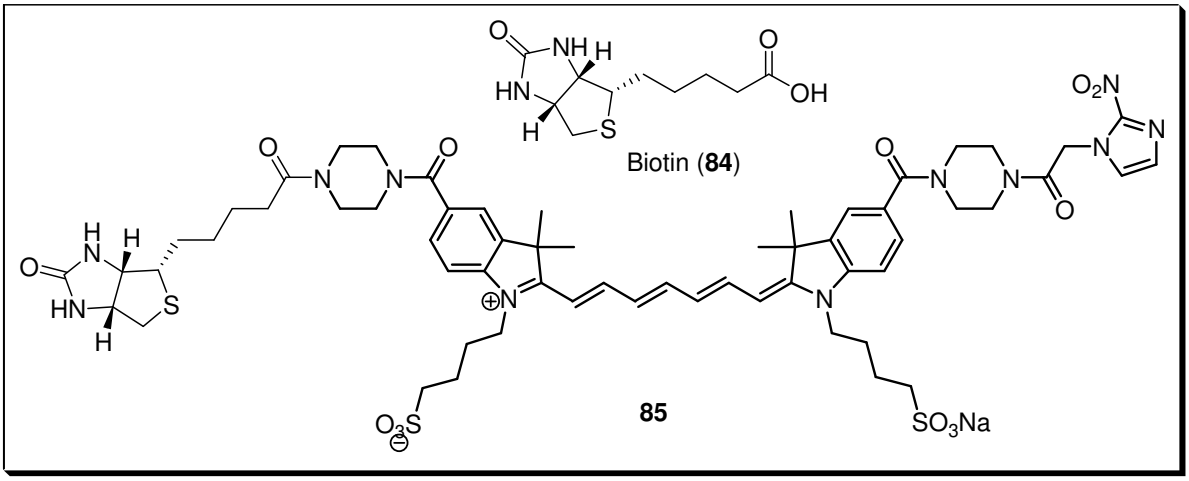

Figure 4.12: Biotinlated half loaded dye conjugate

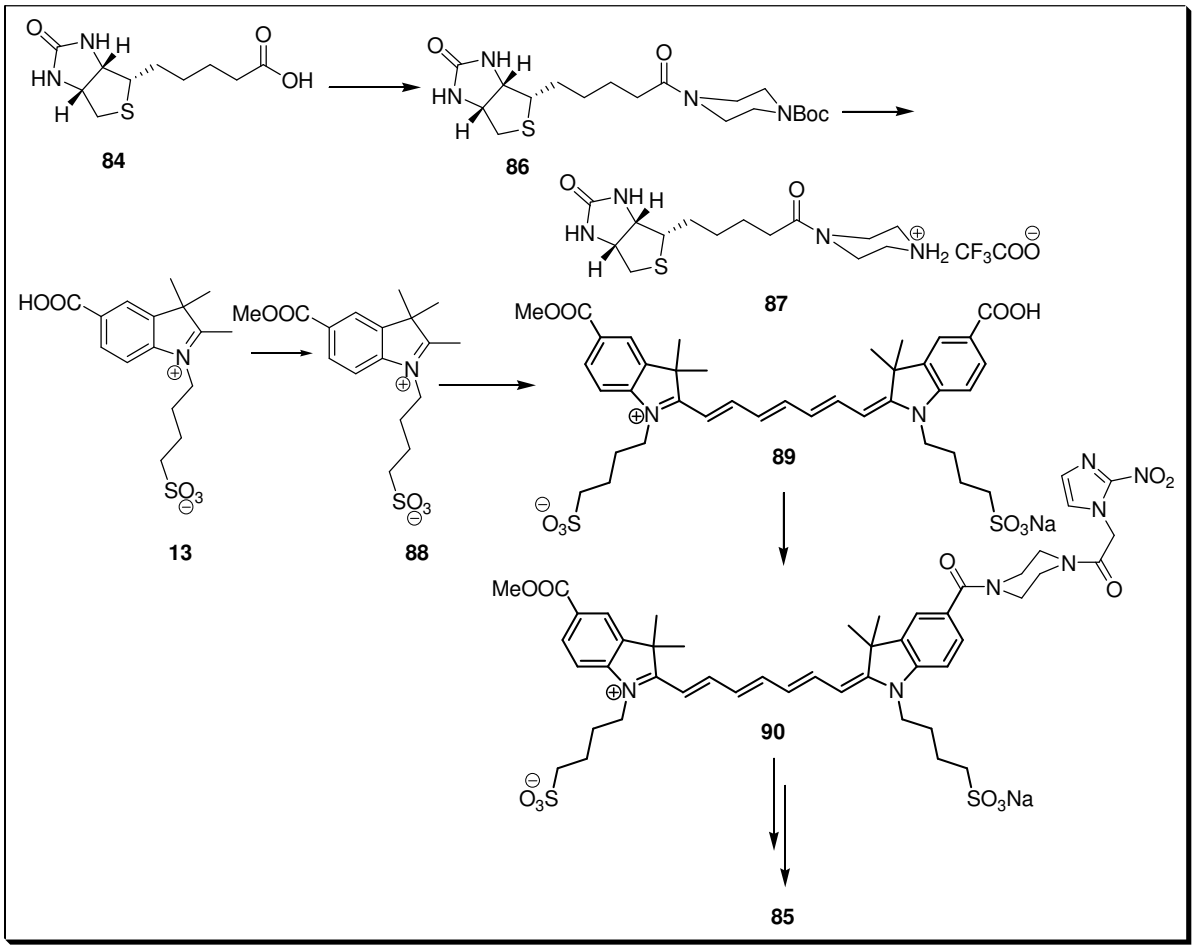

Scheme 4-15. Synthetic plan for biotinlated dye conjugate **85** synthesis

Chapter 5.

EXPERIMENTAL

General

All chemicals were used as received from Aldrich or Acros. All glassware was flame or oven dried, and all reactions in organic solvents were performed under a nitrogen atmosphere, unless otherwise noted. All solvents were dried according to standard procedures. THF was distilled from sodium benzophenone ketyl, methylene chloride was distilled from calcium hydride, and dimethylformamide was vacuum distilled from calcium hydride. Thin-layer chromatography was done on Sorbent Technologies aluminum-backed TLC plates with fluorescent indicator and 0.2 mm silica gel layer thickness, and *p*-anisaldehyde, Phosphomolybdic acid were used as developing agents. Column chromatography was done using 60 Å porosity, 32-63 µm silica gel. ^{1}H and ^{13}C NMR were collected on a Brüker Avance 300 (300.13 MHz ^{1}H, 75.48 MHz ^{13}C), Brüker DRX-400 (400.144 MHZ ^{1}H, 100.65 MHz ^{13}C) or a Brüker Avance 500 (500.13 MHz ^{1}H, 125.65 MHZ ^{13}C). Chemical shifts are given in ppm downfield from TMS in the following format chemical shift, multiplicity (s=singlet, d=doublet, t=triplet, q=quartet, m=multiplet) coupling constant in Hz and Integration. Photophysical properities of dyes were found on UV-Vis spectrophotometer and a fluorescence spectrophotometer (Varian Analytical Instruments Walnut Creek, California). Mass spectroscopy data was collected on a HP 5870B GC/MSD mass spectrometer with an HP-1 column, and high resolution mass spectrometry was done on a Micromass VB-QTOF tandem mass spectrometer. IR spectrums were taken on FT/IR-410/C031560585 JASCO and Nexus 670 FT-IR E.S.P under neat conditions unless and otherwise stated. Melting points were taken on a Uni-melt capillary melting point apparatus and Digimelt MPA160 and recorded to a maximum of 260 °C. For products described as waxy solid, melting points could not be obtained.

Methyl 2-(2-nitro-1H-imidazol-1-yl)acetate (16a)

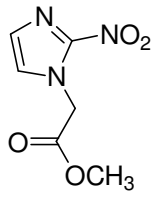

(16a)

Potassium carbonate (1.8 g, 13.0 mmol) and tetrabutylammonium iodide (0.070 g, 0.19 mmol) were added to a stirring solution of 2-nitroimidazole (1.0 g, 8.84 mmol) in 10 mL of dry acetonitrile. The reaction mixture was stirred at room temperature for 30 min and bromomethyl acetate (0.84 mL, 8.8 mmol) was added and heated to reflux for 45 min. After 45 min, the reaction mixture was cooled to room temperature and filtered to remove inorganic salts and then washed with acetonitrile. All the organic washings were combined and concentrated *in vacuo* to get viscous liquid. Evaporation under high vacuum gave a crude solid, which was purified by column chromatography to obtain pure methyl 2-(2-nitro-1H-imidazol-1-yl)acetate as light yellow solid (1.2 g, 6.5 mmol, 73%); mp: 95-96 °C; ^{1}H NMR (400 MHz, $CDCl_3$) δ 7.20 (d, J = 0.8 Hz, 1H), 7.08 (s, 1H), 5.13 (s, 2H), 3.80 (s, 3H); ^{13}C NMR (100 MHz, $CDCl_3$) δ 166.7, 144.8, 128.8, 126.7, 53.4, 51.0; HRMS (ESI, AccuTOF): [M+H]+ Calc'd for $C_6H_8N_3O_4$ *m/z* 186.0515. Found, *m/z* 186.0529.

Methyl 2-(4-nitro-1H-imidazol-1-yl)acetate (16b)

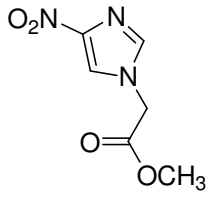

(16b)

Potassium carbonate (1.8 g, 13.0 mmol) and tetrabutylammonium iodide (TBAI) (0.070 g, 0.19 mmol) were added to a stirring solution of 4-nitroimidazole (1 g, 8.84 mmol) in 10 mL of dry acetonitrile. The mixture was stirred at room temperature for 30 min. After stirring 30 min at room temperature, bromomethyl acetate (0.84 mL, 8.8 mmol) was added and heated to reflux for 45 min. After 45 min, the reaction mixture was cooled to room temperature and filtered to remove inorganic salts and washed with acetonitrile. All the organic washings were combined and concentrated *in vacuo* to obtain a crude solid, which was recrystallized from ethyl acetate to yield pure white crystals of methyl 2-(4-nitro-1H-imidazol-1-yl)acetate (1.3 g, 7.0 mmol, 79%);[75] mp: 129-130 °C; ^{1}H NMR (400 MHz, $CDCl_3$) δ 7.83 (s, 1H), 7.47 (s, 1H), 4.79 (s, 2H), 3.84 (s, 3H); ^{13}C NMR (100 MHz, $CDCl_3$) δ 166.5, 148.6, 136.9, 120.4, 53.7, 48.9; HRMS (ESI, AccuTOF): [M + H]+ Calc'd for $C_6H_8N_3O_4$ *m/z* 186.0515. Found, *m/z* 186.0532.

N-(2-Hydroxyethyl)-2-(2-nitro-1H-imidazol-1-yl)acetamide (17a)

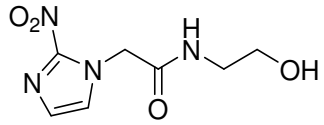

(**17a**)

Methyl-2-(2-nitro-1H-imidazol-1-yl)acetate **16a** (0.1 g, 0.54 mmol) was dissolved in methanol (2 mL), to this stirring solution 2-amino ethanol (0.31 g, 5.08 mmol) was added at room temperature and the resulting solution was stirred at room temperature overnight. The solvent was evaporated *in vacuo* to give a gummy viscous liquid, which was triturated with ethyl acetate to give a white solid which was filtered and dried under vacuum. This crude solid was purified by column chromatography (8% methanol in dichloromethane) to yield N-(2-hydroxyethyl)-2-(2-nitro-1H-imidazol-1-yl)acetamide as a white powder (0.07 g, 0.33 mmol, 60%);[75] mp: 163.5-164.5 °C; ^{1}H NMR (400 MHz, CD_3OD) δ 7.45 (d, J = 0.9 Hz, 1H), 7.18 (d, J = 1 Hz, 1H), 5.19 (s, 2H), 3.63 (t, J = 5.8 Hz, 2H), 3.36 (t, J = 5.8 Hz, 2H); ^{13}C NMR (100 MHz, CD_3OD) δ 168.3, 146.3, 129.3, 128.3, 61.4, 52.8, 43.1; HRMS (ESI-TOF): [M + H]+ Calc'd for $C_7H_{11}N_4O_4$ *m/z* 215.0780. Found, *m/z* 215.0800.

N-(2-Hydroxyethyl)-2-(4-nitro-1H-imidazol-1-yl)acetamide (17b)

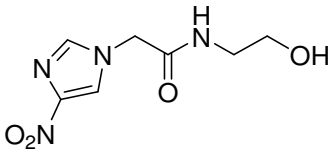

(**17b**)

2-(4-Nitro-1H-imidazol-1-yl)acetate **16b** (0.3 g, 1.62mmol) was dissolved in methanol (5 mL), to this stirring solution, 2-amino ethanol (0.31 g, 5.08 mmol) was added at room temperature and the solution was stirred at room temperature overnight. The resulting precipitate was filtered to give a white solid N-(2-hydroxyethyl)-2-(4-nitro-1H-imidazol-1-yl)acetamide (0.31 g, 1.45 mmol, 90%); mp: 136-137 °C; ^{1}H NMR (400 MHz, D_2O) δ 8.20 (d, *J* = 1.4 Hz, 1H), 7.77 (d, *J* = 1.4 Hz, 1H), 4.99 (s, 2H), 3.70-3.67 (m, 2H), 3.42-3.40 (m, 2H); ^{13}C NMR (100 MHz, D_2O) δ 168.6, 146.8, 138.8, 122.8, 60.0, 50.1, 41.9; HRMS (ESI-TOF): [M + H]+ Calc'd for $C_7H_{11}N_4O_4$ *m/z* 215.0780. Found, *m/z* 215.0824.

2,3,3-Trimethyl-3H-indole-5-carboxylic acid (12)

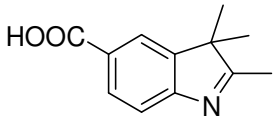

(**12**)

A 100 mL round-bottomed flask with was charged with 4-hydrazinobenzoic acid (4.5 g, 29.5 mmol), 3-methyl 2-butanone (4.6 mL, 43 mmol), sodium acetate (4.86 g, 59 mmol), and glacial acetic acid (55 mL). The reaction mixture was stirred for 1 h under a nitrogen atmosphere and then heated at reflux overnight. The solvent was evaporated *in vacuo* and 80 mL of 10% methanol in water was added. The resulting precipitate was vacuum filtered to yield a tan powder (4.07 g, 20.0 mmol, 68%);[75] mp: 205-208 °C decomposed; ^{1}H NMR (400

MHz, $CDCl_3$) δ 8.14 (d, *J* = 8.2 Hz, 1H), 8.05 (s, 1H), 7.64 (d, *J* = 8.1 Hz, 1H), 2.36 (s, 3H), 1.36 (s, 6H); ^{13}C NMR (100 MHz, $CDCl_3$) δ 192.7, 171.4, 157.9, 145.9, 131.1, 126.9, 123.5, 119.9, 54.2, 23.1, 15.8. GC-MS *m/z* (% relative intensity, ion): 203 [M]+, 188 [M-CO_2]+, 158 [M-2CH_3];[76] MS(ESI^+): *m/z* 268 (50), 245 (45), 224 (90), 203.9 (100).[77]

5-Carboxy-1-(δ-sulfobutyl)-2,3,3-trimethyl-3H-indolium (13)

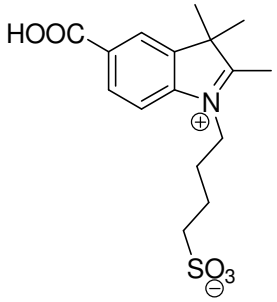

(**13**)

1,4-Butane sultone (2.95 mL, 28.8 mmol) was added to a stirring solution of 2,3,3-trimethyl-3H-indole-5-carboxylic acid **12** (1.0 g, 4.9 mmol) in 20 mL of 1,2 - dichlorobenzene. The solution was heated at reflux overnight under a nitrogen atmosphere. The reaction mixture was cooled to room temperature and the resulting precipitate was filtered and washed with acetone and dried under vacuum to obtain 5-carboxy-1-(δ-sulfobutyl)-2,3,3-trimethyl-3H-indolium as a pale pink powder (1.46 g, 4.3 mmol, 88%);[75] mp: 230-232 °C decomposed; ^1H NMR (400 MHz, CD_3OD) δ 8.40 (d, *J* = 1.3 Hz, 1H), 8.34 (dd, *J* = 8.4, 1.6 Hz, 1H), 8.07 (d, *J* = 8.4 HZ, 1H), 4.61 (t, *J* = 7.8 Hz, 2H), 2.93 (t, *J* = 7.1 Hz, 2H), 2.24-2.16 (m, 2H), 2.02-1.95 (m, 2H), 1.68 (s, 6H);[78] ^{13}C NMR(100MHz, CD_3OD) δ 201.1, 167.9, 145.6, 143.6, 133.7, 132.3, 125.6, 116.8, 56.2, 51.0, 27.3, 23.2, 22.6; MS (ESI^+): *m/z* 403.0 (30), 203.9 (100), 296 (20), 268.1 (25).[79]

tert-Butyl piperazine-1-carboxylate (22)

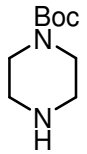

(**22**)

A solution of di-*tert*-butyl dicarbonate (2.54 g, 11.6 mmol) in 30 mL of CH_2Cl_2 was added to a stirring solution of piperazine (2.0 g, 23.2 mmol) in 60 mL of CH_2Cl_2 at room temperature. The solution was stirred for 16 h at room temperature. The solvent was removed under reduced pressure and the residue was dissolved in water (50 mL). Aqueous solution was extracted with methylene chloride (4 × 60 mL). All the organic extracts were combined, dried over anhydrous magnesium sulfate and concentrated *in vacuo* to give a crude oil, which was purified by column chromatography to give tert-butyl piperazine-1-carboxylate as white solid (1.5 g, 8.05 mmol, 69%); mp: 46-47 °C; ^{1}H NMR (400 MHz, $CDCl_3$) δ 3.39-3.36 (m, 2H), 2.81-2.78 (m, 2H), 1.57 (bs, 1H), 1.44 (s, 9H); ^{13}CNMR (100 MHz, $CDCl_3$) δ 154.3, 79.8, 45.6, 44.5, 28.8; HRMS (ESI-TOF): [M + H]+ Calc'd for $C_9H_{19}N_2O_2$ *m/z* 187.1447. Found, *m/z* 187.0532.

tert-Butyl-4-(2-bromoacetyl)piperazine-1-carboxylate (23)

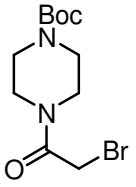

(**23**)

Triethylamine (0.5 mL, 3.5 mmol) was added to a stirring solution of tert-butyl piperazine-1-carboxylate **22** (0.60 g, 3.22 mmol) in 25 mL of dry dichloromethane at 0 °C. After stirring for 15 min at 0 °C, bromoacetyl bromide (0.3 mL, 3.5 mmol) was added dropwise. The

resulting reaction mixture was stirred at room temperature (c.a 48 h). The reaction progress was monitored by TLC. After the reaction completed, the mixture was concentrated *in vacuo* to give a crude solid which was purified by column chromatography (petroleum ether: ethyl acetate 15-20%) to give tert-butyl-4-(2-bromoacetyl)piperazine-1-carboxylate as a white solid (0.8 g, 2.6 mmol, 81%): mp: 95-97 °C; ^{1}H NMR (400 MHz, $CDCl_3$) δ 3.87 (d, J = 3.1 Hz, 2H), 3.61-3.59 (m, 2H), 3.51-3.50 (m, 4H), 3.45-3.42 (m, 2H), 1.47 (s, 9H); ^{13}C NMR (100 MHz, $CDCl_3$) δ 165.7, 154.7, 80.7, 46.8, 42.2, 28.6, 25.8; HRMS (ESI-TOF): [M + H]+ Calc'd for $C_{11}H_{19}BrN_2O_3$ *m/z* 307.0657. Found, *m/z* 307.0652.

tert-Butyl-4-(2-(2-nitro-1H-imidazol-1-yl)acetyl)piperazine-1-carboxylate (24a)

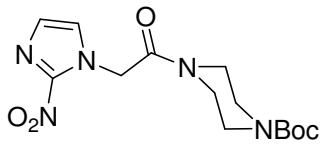

(**24a**)

Sodium hydride (0.025 g, 1.06 mmol) was added to a stirring solution of 2-nitroimidazole (0.1 g, 0.88 mmol) in 1 mL of dry DMF under a N_2 atmosphere at 0 °C. The mixture was stirred at 0 °C temperature for 30 min, at that time, tert-butyl 4-(2-bromoacetyl) piperazine-1-carboxylate (0.272 g, 0.88 mmol) was added slowly and the reaction mixture was stirred at room temperature overnight. The DMF was evaporated *in vacuo* and 5 mL of water was added to give a white precipitate, which was filtered and dried under vacuum to obtain tert-butyl 4-(2-(2-nitro-1H-imidazol-1-yl)acetyl)piperazine-1-carboxylate as a white powder (0.28 g, 0.83 mmol, 93%); mp: 149-151 °C; ^{1}H NMR (400 MHz, $CDCl_3$) δ 7.21(d, J = 0.9 Hz, 1H), 7.07 (s, 1H) 5.23 (bs, 2H), 3.62-3.59 (m, 4H), 3.52-3.47 (m, 4H), 1.48 (s, 9H); ^{13}C NMR (100 MHz, $CDCl_3$) δ 163.5, 154.5, 145.3, 128.4, 127.3, 80.8, 51.0, 45.1, 43.5, 42.5,

28.5; HRMS (ESI-TOF): [M + H]+ Calc'd for $C_{14}H_{22}N_5O_5$ *m/z* 340.1621. Found, *m/z* 340.1608.

tert-Butyl-4-(2-(4-nitro-1H-imidazol-1-yl)acetyl)piperazine-1-carboxylate (24b)

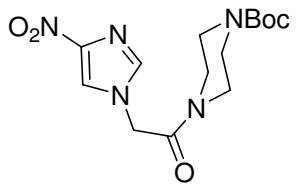

(**24b**)

Sodium hydride (0.025 g, 1.06 mmol) was added to a stirring solution of 4-nitroimidazole (0.1 g, 0.88 mmol) in 1 mL of dry DMF under a N_2 atmosphere at 0 °C. The mixture was stirred at 0 °C temperature for 30 min, at that time, tert-butyl 4-(2-bromoacetyl) piperazine-1-carboxylate (0.272 g, 0.88 mmol) was added portionwise and the reaction mixture was stirred at room temperature overnight. The DMF was evaporated *in vacuo* and 5 mL of water was added to give a white precipitate, which was filtered and dried under vacuum to obtain tert-butyl 4-(2-(4-nitro-1H-imidazol-1-yl)acetyl)piperazine-1-carboxylate as a white powder (0.25 g, 0.74 mmol, 83%);[80] mp: 197-199 °C; ^{1}H NMR (400 MHz, D_2O) δ 7.58 (s, 1H), 7.41 (s, 1H), 5.69 (s, 2H), 4.10-4.08 (m, 2H), 4.03-4.01 (m, 2H), 3.61-3.59 (m, 2H), 3.50-3.48 (m, 2H); ^{1}H NMR (400 MHz, $CDCl_3$) δ 7.81 (s, 1H), 7.44 (d, *J* = 1.1 Hz, 1H), 4.87 (s, 2H), 3.65-3.63 (m, 2H), 3.55-3.54 (m, 2H), 3.49-3.47 (m, 4H); 1.48 (s, 9H); ^{13}C NMR (100 MHz, $CDCl_3$) δ 163.4, 154.6, 148.2, 137.4, 121.5, 81.0, 49.0, 45.0, 42.5, 28.6; HRMS (ESI-TOF): [M + H]+ Calc'd for $C_{14}H_{22}N_5O_5$ *m/z* 340.1621. Found, *m/z* 340.1607.

2-(4-Nitro-1H-imidazol-1-yl)-1-(piperazin-1-yl)ethanone.trifluoroaceticacid salt (25b)

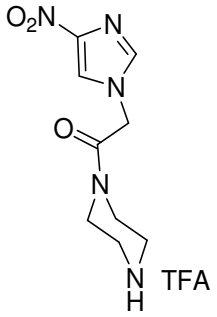

(**25b**)

Trifluoroacetic acid (1 mL) was added dropwise to a stirring solution of tert-butyl 4-(2-(4-nitro-1H-imidazol-1-yl)acetyl)piperazine-1-carboxylate **24b** (0.28 g, 0.83 mmol) in 10 mL of dry chloroform. The solution was stirred at room temperature overnight. The reaction mixture was concentrated *in vacuo* to give a crude solid. The crude solid was triturated with ethyl acetate to give 2-(4-nitro-1H-imidazol-1-yl)-1-(piperazin-1-yl)ethanone TFA as a white solid, which was filtered and dried under vacuum (0.22 g, 0.62 mmol, 76%);[81] mp: 228-229 °C; ^{1}H NMR (300 MHz, D_2O) δ 8.14 (d, *J* = 1.2 Hz, 1H), 7.72 (d, *J* = 1.2 Hz, 1H), 5.31 (s, 2H), 3.90-3.87 (m, 4H), 3.44-3.41 (m, 2H), 3.37-3.33 (m, 2H); ^{13}C NMR (75 MHz, D_2O) δ 166.6, 163.4, 163.0, 162.5, 162.0, 146.7, 138.7, 123.5, 118.7, 49.0, 42.9, 42.9, 41.7, 39.2; HRMS (ESI-TOF): [M + H]+ Calc'd for $C_{10}H_{14}F_3N_5O_5$ *m/z* 240.1096. Found, *m/z* 240.1100.

2-(2-Nitro-1H-imidazol-1-yl)-1-(piperazin-1-yl)ethanone .TFA salt (25a)

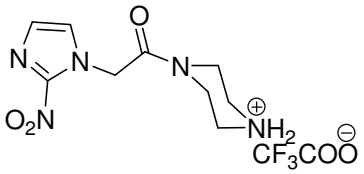

(**25a**)

Trifluoroacetic acid (1 mL) was added dropwise to a stirring solution of tert-butyl 4-(2-(2-nitro-1H-imidazol-1-yl)acetyl)piperazine-1-carboxylate **24a** (0.28 g, 0.83 mmol) in dry

chloroform (10 mL). The solution was stirred overnight at room temperature. The reaction mixture was concentrated to give a crude solid. The crude solid was triturated with ethyl acetate to give 2-(2-nitro-1H-imidazol-1-yl)-1-(piperazin-1-yl)ethanone TFA as a white solid, which was filtered and dried under vacuum (0.25 g, 0.71 mmol, 86%); mp: 120-122 °C; ^{1}H NMR (400 MHz, D_2O) δ 7.58 (s, 1H), 7.40 (s, 1H), 5.68 (s, 2H), 4.08 (t, *J* = 4 Hz, 2H), 4.03-4.00 (m, 2H), 3.59 (t, *J* = 4 Hz, 2H), 3.50-3.47 (m, 2H); ^{1}H NMR (400 MHz, CD_3OD) δ 7.45 (s, 1H), 7.22 (s, 1H), 5.54 (s, 2H), 3.89 (d, *J* = 13 Hz, 4H), 3.40-3.28 (m, 4H); ^{13}C NMR (100 MHz, CD_3OD) δ 166.5, 162.4, 14.7, 129.3, 128.5, 52.0, 44.4, 42.9, 40.2; HRMS (ESI-TOF): [M-CF_3COO+H]+ Calc'd for $C_9H_{14}F_3N_5O_3$ *m/z* 240.1091. Found, *m/z* 240.1149.

tert-Butyl 4-(2-(1H-imidazol-1-yl)-2-oxoethyl)piperazine-1-carboxylate (29)

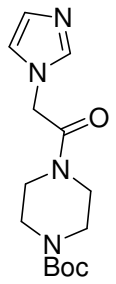

(**29**)

Method A:

Sodium hydride (0.070 g, 2.93 mmol) was added to a stirring solution of imidazole (0.066 g, 0.977 mmol) in 5 mL of dry THF under a N_2 atmosphere at 0 °C. The mixture was stirred at the same temperature for 30 min. At that time, tert-butyl 4-(2-bromoacetyl) piperazine-1-carboxylate (0.300 g, 0.977 mmol) was added portionwise and the reaction mixture was stirred at room temperature for 2 h. The reaction mixture was quenched with 15 mL of water and extracted with ethyl acetate (2 × 10 mL). The organic extracts were combined, dried

over anhyd. $MgSO_4$ and concentrated *in vacuo* to give a crude solid, which was purified by column chromatography to give tert-butyl 4-(2-(1H-imidazol-1-yl)-2-oxoethyl)piperazine-1-carboxylate as a white solid (0.22 g, 0.75 mmol, 77%);[80] mp: 147-149 °C; ^{1}H NMR (400 MHz, $CDCl_3$) δ 7.53 (s, 1H), 7.11 (s, 1H), 6.96 (s, 1H), 4.80 (s, 2H), 3.62 (bs, 2H), 3.48 (bs, 6H), 1.47 (s, 9H); ^{13}C NMR (100 MHz, $CDCl_3$) δ 165.0, 154.5, 138.1, 129.7, 120.2, 80.8, 48.2, 45.1, 43.5, 42.2, 28.5; HRMS (ESI+TOF): [M+H]+ Calc'd for $C_{14}H_{23}N_4O_3$ *m/z* 295.1770. Found, *m/z* 295.1751.

Method B:

Potassium carbonate (0.180 g, 1.30 mmol) was added to a stirring solution of imidazole (0.057 g, 0.847 mmol) in 3 mL of acetone, and then tert-butyl 4-(2-bromoacetyl) piperazine-1-carboxylate (0.200 g, 0.651 mmol) was added portionwise. The reaction mixture was stirred at room temperature under a N_2 gas for 4 h. The reaction mixture was filtered to separate the 1,3-disubstituted imidazolinium salt, and the mother liquor was concentrated *in vacuo* to give a crude solid, which was purified by column chromatography to give tert-butyl 4-(2-(1H-imidazol-1-yl)-2-oxoethyl)piperazine-1-carboxylate (0.18 g, 0.612 mmol, 73%); mp: 147-149 °C; ^{1}H NMR (400 MHz, $CDCl_3$) δ 7.53 (s, 1H), 7.11 (s, 1H), 6.96 (s, 1H), 4.80 (s, 2H), 3.62 (bs, 2H), 3.48 (bs, 6H), 1.47 (s, 9H); ^{13}C NMR (100 MHz, $CDCl_3$) δ 165.0, 154.5, 138.1, 129.7, 120.2, 80.8, 48.2, 45.1, 43.5, 42.2, 28.5; HRMS (ESI+TOF): [M+H]+ Calc'd for $C_{14}H_{23}N_4O_3$ *m/z* 295.1770. Found, *m/z* 295.1751.

tert-Butyl 4-(2-(1H-imidazol-1-yl)-2-oxoethyl)piperazine-1-carboxylate. TFA salt (30)

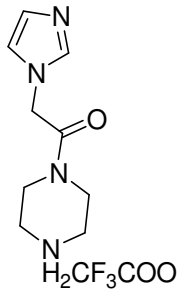

(**30**)

Trifluoroacetic acid (1 mL) was added dropwise to a stirring solution of tert-butyl 4-(2-(1H-imidazol-1-yl)-2-oxoethyl)piperazine-1-carboxylate **29** (0.3 g, 1.02 mmol) in 10 mL of dry chloroform at room temperature. The solution was stirred at room temperature overnight. The reaction mixture was concentrated *in vacuo* to give a crude solid, which was triturated with ethyl acetate to give 2-(1H-imidazol-1-yl)-1-(piperazin-1-yl)ethanone.TFA as a white solid, which was filtered and dried under vacuum (0.28 g, 0.91 mmol, 89%); mp: 129-130 °C ^{1}H NMR (400 MHz, D_2O) δ 8.76 (s, 1H), 7.53 (s, 1H), 7.46 (s, 1H), 5.43 (s, 2 H), 3.90-3.87 (m, 4H), 3.44-3.41 (m, 2H), 3.36-3.34 (m, 2H); ^{13}C NMR (100 MHz, D_2O) δ 166.0, 163.4, 163.0, 136.5, 123.6, 119.8, 118.0, 115.1, 50.1, 42.9, 41.8, 39.3; HRMS(ESI+TOF): [M-CF_3COO^-+H] Calc'd for $C_9H_{15}N_4O$ *m/z* 195.1246. Found, *m/z* 195.1231.

Monosodium(II)mono(4-((Z)-2-((2E,4E,6E)-7-(3,3-dimethyl-5-(4-(2-(2-nitro-1H-imidazol-1-yl)acetyl)piperazine-1-carbonyl)-1-(4-sulfonatobutyl)-3H-indolium-2-l)hepta-2,4,6-trienylidene)-3,3-dimethyl-5-(4-(2-(2-nitro-1H-imidazol-1-yl)acetyl)piperazine-1-carbonyl)indolin-1-yl)butane-1-sulfonate) (26a)

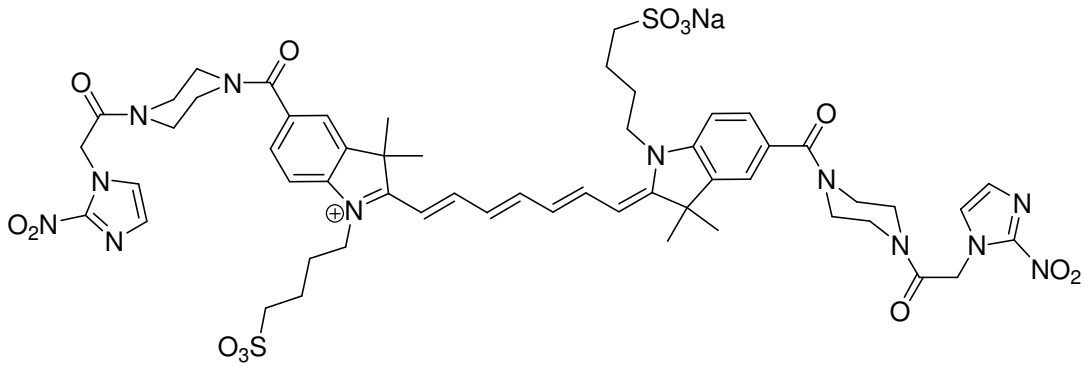

(**26a**)

To a stirring solution of ICG bis-carboxylic acid **9** (0.2 g, 0.26 mmol) in dry DMF (2 mL) at 0 °C was added pyBop (0.30 g, 0.57 mmol), HOBt (0.08 g, 0.57 mmol), DIPEA (220 µL, 0.57 mmol) respectively. The mixture was stirred at 0 °C for 15 min. The 2-nitroimidazole piperazine fragment (**25a**) (0.204 g, 0.57 mmol) was added and stirred at room temperature for 48 h. The DMF was removed by air drying and the resulting crude reaction mixture was washed with acetonitrile (2×5 mL) and ethyl acetate (2×5 mL) to remove the soluble impurities. The crude solid was purified by C18 reverse phase column chromatography to yield **26a** as a green solid (0.065 g, 0.055mmol, 20%); mp: decomposed to black residue > 250 °C; ^{1}H NMR (400 MHz, D_2O) δ 7.84 (t, *J* = 12 Hz, 2H), 7.57 (bs, 2H), 7.44 (bs, 5H), 7.35-7.33 (bs, 2H), 7.26 (m, 2H), 6.56 (t, *J* = 12.4 Hz, 2H), 6.29 (d, *J* = 13.2 Hz, 2H), 5.57-5.49 (m, 4H), 4.15 (bs, 4H), 3.85-3.51 (m, 16H), 2.96 (t, *J* = 7.3 Hz, 4H), 1.98-1.96 (m, 4H), 1.90-1.87 (m, 4H), 1.60 (bs, 12H); ^{13}C NMR;[82] HRMS (ESI-TOF): [M + 2H-Na]+ Calc'd for *m/z* $C_{55}H_{67}N_{12}O_{14}S_2$ 1183.4341. Found, *m/z* 1183.4399.

Monosodium(II)mono(4-((Z)-2-((2E,4E,6E)-7-(3,3-dimethyl-5-(4-(2-(4-nitro-1H-imidazol-1-yl)acetyl)piperazine-1-carbonyl)-1-(4-sulfonatobutyl)-3H-indolium-2-l)hepta-2,4,6-trienylidene)-3,3-dimethyl-5-(4-(2-(4-nitro-1H-imidazol-1-yl)acetyl)piperazine-1-carbonyl)indolin-1-yl)butane-1-sulfonate) (26b)

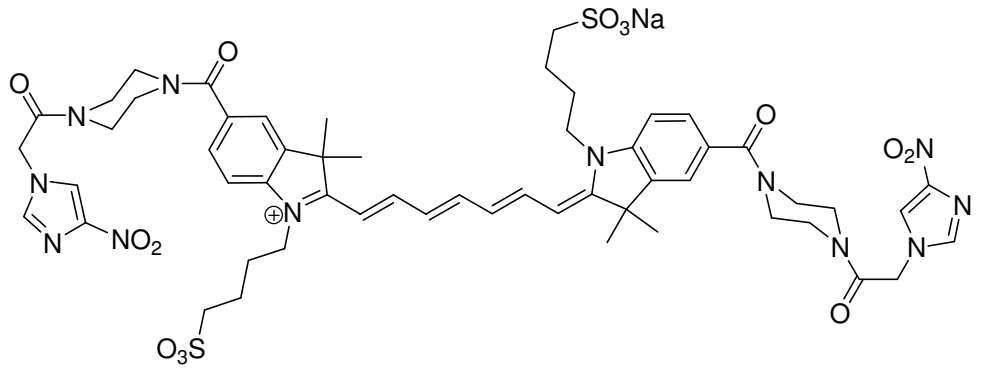

(**26b**)

To a stirring solution of ICG bis-carboxylic acid **9** (0.09 g, 0.12 mmol) in dry DMF (2.5 mL) at 0 °C was added pyBop (0.135 g, 0.26 mmol), HOBt (0.035 g, 0.26 mmol), DIPEA (5 µL, 0.29 mmol) respectively. The mixture was stirred at 0 °C and stirred for 15 min. The 4-nitroimidazole piperazine fragment (0.107 g, 0.26 mmol) was added and stirred at room temperature for 48 h. The DMF was removed by air drying and the resulting crude reaction mixture was washed with acetonitrile (2×5 mL) and ethyl acetate (2×5 mL) to remove soluble impurities. The crude mixture was purified by C18 reverse phase column chromatography to yield **26b** as a green solid (0.036 g, 0.030 mmol, 25%); mp: decomposed to a black residue > 250 °C; ^{1}H NMR (400 MHz, DMSO-d^6) δ 8.26 (s, 2H), 7.92 (t, J = 12 Hz, 2H), 7.81 (s, 2H), 7.75 (s, 2H), 7.69 (s, 2H), 7.52-7.48 (m, 4H), 6.65-6.59 (m, 2H), 6.51 (d, J = 8 Hz, 2H), 5.21 (bs, 4H), 4.11 (m, 4H), 3.58 (m, 16H), 1.80-1.71(m, 8H), 1.68 (s, 12H); HRMS (ESI-TOF): [M-Na+H]+ Calc'd for $C_{55}H_{65}N_{12}O_{14}S_2$ *m/z* 1181.4190. Found, m/z 1181.4174.

N-(2-Hydroxyethyl)-2-(4-nitro-1H-imidazol-1-yl)acetamido-ICG (10b)

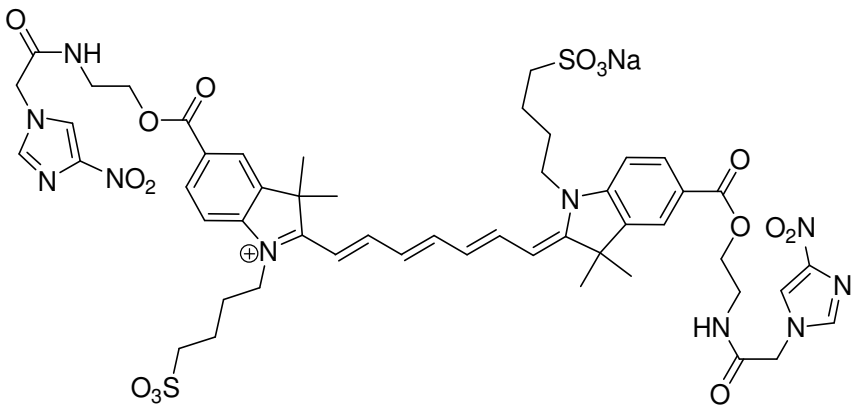

(**10b**)

To a stirring solution of ICG bis carboxylic acid (0.2 g, 0.26 mmol) in dry DMF (2 mL) at 0 °C was added pyBop (0.30 g, 0.57 mmol), HOBt (0.078 g, 0.57 mmol), DIPEA (260 µL, 1.57 mmol) respectively. The mixture was stirred at 0 °C for 15 mn. The 4-nitroimidazole ethanolamine fragment (0.124 g, 0.57 mmol) was added and stirred at room temperature for 48 h. The DMF was removed by air drying and the resulting crude reaction mixture was washed with acetonitrile (2×5 mL) and ethyl acetate (2×5 mL) to remove soluble impurities. The crude mixture was purified by C18 reverse phase column chromatography to yield **10b** as a green solid (0.060 g, 0.052 mmols, 20%); mp: decomposed to black residue > 250 °C; ^{1}H NMR (400 MHz, DMSO-d^6) δ 8.60-8.57 (m, 2H), 8.31 (s, 2H), 8.12 (s, 2H), 8.05 (d, J = 16 Hz, 2H), 8.00-7.94 (m, 2H), 7.80 (s, 2H), 7.54 (d, J = 8 Hz, 2H), 6.68 (t, J = 12 Hz, 2H), 6.56 (d, J = 12 Hz, 2H), 4.88 (s, 4H), 4.33-4.30 (m, 4H), 4.14 (bs, 4H), 3.54-3.52 (m, 4H), 1.80-1.79 (m, 4H), 1.73 (t, J = 8 Hz, 4H), 1.67 (s, 12H); HRMS (ESI-TOF): [M+H]+ Calc'd for $C_{51}H_{60}NaN_{10}O_{16}S_2$ *m/z* 1155.3528. Found, *m/z* 1155.3490.

N-(2-Hydroxyethyl)-2-(1H-imidazol-1-yl)acetamido-ICG (10a)

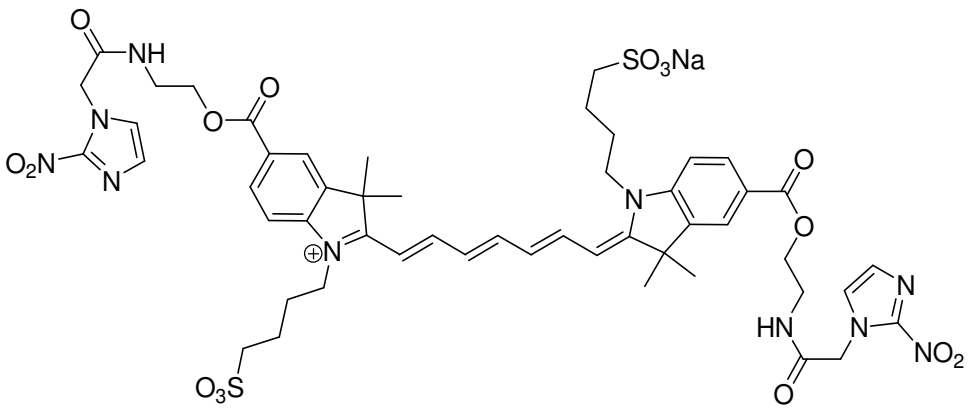

(**10a**)

To a stirring solution of ICG bis carboxylic acid **9** (0.2 g, 0.26 mmol) in dry DMF (2 mL) at 0 °C was added pyBop (0.30 g, 0.57 mmol), HOBt (0.078 g, 0.57 mmol), DIPEA (260 µL, 1.57 mmol) respectively. The mixture was stirred at 0 °C for 15 min. The 2-nitroimidazole ethanolamine fragment (0.124 g, 0.57 mmol) was added and stirred at room temperature for 48 h. The DMF was by air drying and the resulting crude reaction mixture was washed with acetonitrile (2×5 mL) and ethyl acetate (2×5 mL) to remove soluble impurities. The crude mixture was purified by C18 reverse phase column chromatography to yield **10a** as a green solid (0.105 g, 0.0091mmols, 35%); mp; decomposed to black residue > 250 °C; ^{1}H NMR (400 MHz, DMSO-d^{6}) δ 8.64-8.61 (m, 2H), 8.12 (s, 2H), 8.05 (d, J = 8 Hz, 2H), 8.00-7.88 (m, 3H), 7.63 (s, 2H), 7.54 (d, J = 8 Hz, 2H), 7.20 (s, 2H), 6.67 (t, J = 12 Hz, 2H), 6.56 (d, J = 8 Hz, 2H), 5.14 (s, 4H), 4.29-4.28 (m, 4H), 4.14 (bs, 4H), 3.53-3.52 (m, 4H), 1.80-1.72 (m, 8H), 1.67 (bs, 12H); ^{13}C NMR (DMSO-d^{6}) δ 166.5, 165.8, 146.7, 145.4, 141.6, 131.2, 129.3, 127.9, 125.8, 123.7, 111.5, 64.0, 52.1, 51.2, 48.9, 44.2, 38.5, 27.6, 26.5, 22.9; HRMS (ESI-TOF): [M+2H]+ Calc'd for $C_{51}H_{61}N_{10}O_{16}S_2$ *m/z* 1133.3708. Found, *m/z* 1133.3765.

Monosodium(II)mono(4-((Z)-2-((2E,4E,6E)-7-(3,3-dimethyl-5-(4-(2-(1H-imidazol-1-yl)acetyl)piperazine-1-carbonyl)-1-(4-sulfonatobutyl)-3H-indolium-2-l)hepta-2,4,6-trienylidene)-3,3-dimethyl-5-(4-(2-(1H-imidazol-1-yl)acetyl)piperazine-1-carbonyl)indolin-1-yl)butane-1-sulfonate) (31)

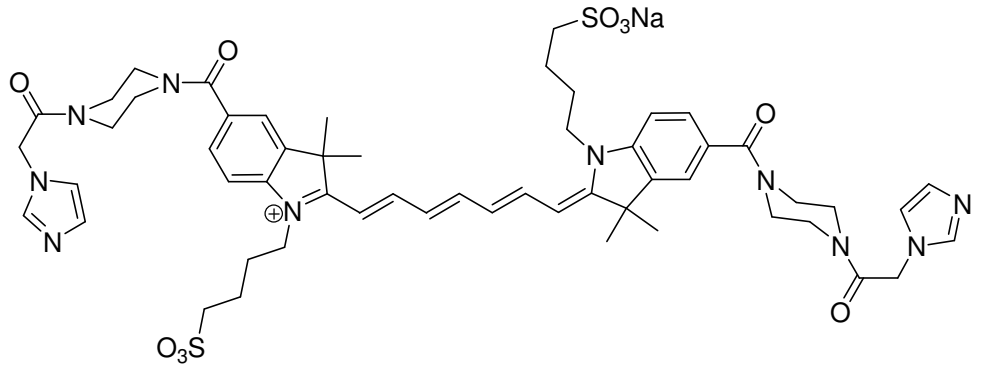

(**31**)

To a stirring solution of ICG bis carboxylic acid **9** (0.3 g, 0.39 mmol) in dry DMF (3 mL) at 0 °C was added pyBop (0.45 g, 0.86 mmol), HOBt (0.117 g, 0.86 mmol), DIPEA (200 µL, 1.18 mmol) respectively. The mixture was stirred at 0 °C for 15 min. The imidazole piperazine fragment (0.266 g, 0.86 mmol) was added and stirred at room temperature for 48 h. The DMF was evaporated and the resulting solid was purified by C18 reverse phase column chromatography to yield **31** as a green solid (0.065 g, 0.0058 mmol, 15%); mp: decomposed to black residue >250 °C; ^{1}H NMR (400 MHz, DMSO-d^6) δ 7.92 (t, J = 12 Hz, 2H), 7.69 (s, 2H), 7.51 (d, J = 16 Hz, 6H), 7.06 (s, 2H), 7.0-6.95 (m, 1H), 6.87 (s, 2H), 6.62 (t, J = 12 Hz, 2H), 6.50 (d, J = 12 Hz, 2H), 5.06 (s, 4H), 4.10 (bs, 4H), 3.57 (bs, 16H), 1.77 (m, 8H), 1.67 (s, 12H); HRMS (ESI-TOF): [M-Na]- Calc'd for $C_{55}H_{67}N_{10}O_{10}S_2$ *m/z* 1091.4483. Found, *m/z* 1091.4456.

N-((E)-(2-Chloro-3-((E)-(phenylimino)methyl)cyclohex-2-enylidene)methyl)aniline (63)

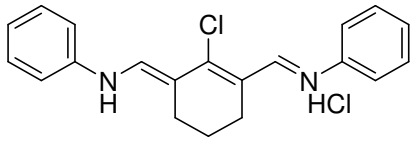

(63)

Phosphorus oxychloride (22 mL, 0.12 mol) was added dropwise to dimethylformamide (26 mL, 0.17 mol) at 0 ºC, and the resulting solution was stirred for 30 min. Cyclohexanone (11 mL, 0.053 mol), was added and the reaction mixture was heated at reflux for 1 h. The solution was cooled to ambient temperature, 36 mL of aniline/ethanol (1:1 (v/v)) mixture was added dropwise and the solution stirred for 30 min. The reaction mixture was poured into 220 mL of ice cold water/concentrated HCl (10:1) and cooled for 2 h in an ice bath. Subsequent filtration gave a solid that was washed with cold water, diethyl ether and then acetone to give **63** as a brick red solid (15.3 g, 42.7 mmol, 40%);[71] mp: 190- 193 °C; ^{1}H NMR (400 MHz, DMSO-*d6*) δ 11.35 (s, 2H), 8.29 (s, 2H), 7.44-7.42 (m, 4H), 7.25-7.18 (m, 6H), 7.05-7.02 (m, 2H), 2.57-2.54 (m, 4H), 1.50-1.46 (m, 2H); ^{13}C NMR (100 MHz, CD_3OD) δ 173.7, 168.6, 151.0, 146.0, 145.1, 141.5, 131.2, 128.8, 123.5, 110.9, 102.6, 50.5, 49.3, 44.2, 27.3, 27.1, 26.2, 26.1, 22.4, 20.9.

N-((E)-(2-Chloro-3-((E)-(phenylimino)methyl)cyclopent-2-enylidene)methyl)aniline hydrochloride (64)

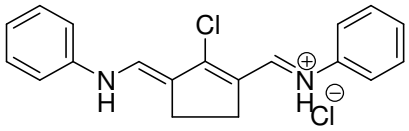

(64)

A stirred solution of N, N-dimethylformamide (13.5 g, 99.9 mmol) in chloroform (13 mL) was treated with phosphorous oxychloride (14 mL, 153 mmol) at 10 °C and stirred at ambient temperature for 1 h. Cyclopentanone (3.36 g, 39.9 mmol) was added and the solution was stirred at 50 °C for 4 h, cooled to ambient temperature and potassium carbonate (10 g, 72.5 mmol) was added, followed by aniline (8.4 g, 90.2 mmol), concentrated HCl (7.5 mL) and water (50 mL) in that order. Subsequent stirring at ambient temperature for 1 h was followed by addition of CH_2Cl_2, A solid precipitated, which was filtered and washed with acetone (5×10 mL) and water (5×20 mL) to obtain **64** as a brick red colored powder (10 g, 29.0 mmol, 73%); mp: 195-198 °C;[83] ^{1}H NMR (400 MHz, DMSO-*d6*) δ 11.40 (bs, 2H), 8.30 (s, 2H), 7.62-7.60 (m, 4H), 7.46 (t, *J* = 8 Hz, 4H), 7.27-7.24 (m, 2H), 3.02 (s, 4H); ^{13}C NMR (100 MHz, DMSO-*d6*) δ 142.8, 140.5, 139.6, 139.3, 138.1, 130.2, 129.7, 129.5, 126.0, 122.9, 118.5, 116.3, 114.9, 110.6, 26.1.

N-((E)-(2-Methyl-3-((E)-(phenylimino)methyl)cyclohex-2-enylidene)methyl)aniline (61)

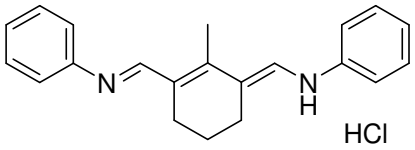

(61)

A stirred solution of N-formyl-N-methylaniline (2.11 g, 15.6 mmol) in chloroform (2 mL) at -5 °C was treated with phosphorous oxychloride (1.5 mL, 15.6 mmol), dropwise, and stirred for 1 h at 10 °C. Methylcyclohexene (0.6 mL, 5.2 mmol) was added dropwise and the solution stirred at 45 °C for 20 h. The reaction mixture was poured into a beaker containing vigorously stirred water (20 mL). Solid potassium carbonate (2 g, 14.5 mmol) was added carefully. A solution of aniline hydrochloride salt (1.52 g, 11.7 mmol) in water (3 mL) was added and the mixture stirred at ambient temperature for 30 min. At this time, potassium carbonate (2 g, 14.5 mmol) was added portionwise and the resulting solution cooled to give a precipitate that was filtered, washed several times with cold water and stirred vigorously with acetone (2×3 mL) filtered and dried *in vacuo* to afford **61** (0.68 g, 2.0 mmol, 39%);[84] mp: 207-210 °C; ^{1}H NMR (400 MHz, CD_3OD) δ 8.51 (s, 2H), 7.53-7.32 (m, 8H), 7.31-7.29 (m, 2H), 2.64-2.61(m, 7H), 2.02-1.96 (m, 2H); ^{13}C NMR (100 MHz, DMSO-*d6*) δ 165.9, 147.7, 139.8, 129.6, 129.5, 129.3, 125.6, 118.8, 117.5, 115.1, 29.1, 23.5, 19.8, 14.3.

N-[5-Anilino-3-phenyl-2,4-(propane-1',3'-diyl)-2,4-pentadien-1-ylidene]anilinium Chloride (**62**)

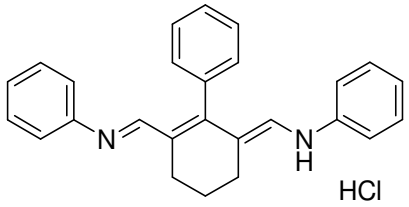

(62)

A stirred solution of *N*-formyl-*N*-methylaniline (1.28 g, 9.5 mmol) in chloroform (2 mL) at -5 °C was treated with phosphorous oxychloride (0.9 mL, 9.5 mmol), dropwise, and stirred for 1 h at 10 °C. Phenylcyclohexene (0.5 g, 3.2 mmol) was added dropwise and then stirred at 45 °C for 20 h. The reaction mixture was poured into a beaker of vigorous stirred water (20 mL), and potassium carbonate (2 g, 14.5 mmol) was carefully added. A solution of aniline hydrochloride salt (0.92 g, 7.11 mmol) in water (3 mL) was added and the mixture stirred at ambient temperature for 30 min. After then potassium carbonate (2 g, 14.5 mmol) was added portionwise. The mixture was cooled and the resulting precipitate was filtered, washed several times with cold water, stirred vigorously with acetone (2×10 mL), filtered and dried *in vacuo* to afford **62** as a dark red powder (0.85 g, 2.12 mmol, 67%);[84] mp: 246-250 °C; ^{1}H NMR (400 MHz, DMSO-*d*^{6}) δ 11.00 (s, 2H), 7.57-7.53 (m, 3H), 7.41-7.39 (m, 2H), 7.36-7.32 (m, 4H), 7.24 (bs, 2H), 7.14 (t, *J* = 7.4 Hz, 2H), 7.06 (d, *J* = 7.9 Hz, 4H); ^{13}C (100 MHz, DMSO-*d6*) δ 157.8, 150.5, 142.0, 139.8, 136.2, 135.3, 134.7, 130.6, 130.2, 129.8, 129.5, 128.3, 128.0, 125.8, 121.2, 118.7, 118.2, 114.6, 113.6, 23.9,23.3, 21.9, 20.5, 19.8.

N-((1E,3E)-3-(Phenylimino)prop-1-enyl)benzenamine hydrochloride (70)

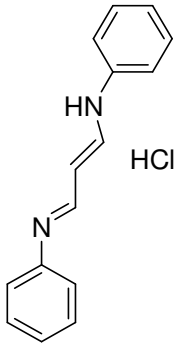

(**70**)

A solution of distilled water (70 mL), HCl (5 mL) and aniline (3.7 mL, 0.04 mol) was added dropwise to a solution of propanedial bis(dimethyl acetal) (5.25 mL, 0.03 mol) and HCl (4.25 mL) in distilled water (90 mL) at 50 °C. The resulting solution was stirred at 50 °C for 30 min. The reaction mixture was cooled, and the resulting precipitate was isolated by vacuum filtration and dried *in vacuo* to give **70** as an orange solid (6.35 g, 24.5 mmol, 82%);[85] mp: charring at 150 °C; ^{1}H NMR (400 MHz, $CDCl_3$) δ 8.75 (dd, *J* = 11.6, 6.1 Hz, 2H), 7.46-7.39 (m, 9H), 7.24 (t, *J* = 7.1 Hz, 2H), 6.29 (t, *J* = 11.6 Hz, 1H); ^{13}C NMR (100 MHz, DMSO-d^6) δ 159.6, 139.8, 131.1, 131.0, 127.6, 118.8, 118.7, 99.5, 99.4.

Sodium-2-((*E*)-2-((*E*)-3-((*Z*)-2-(5-carboxy-3,3-dimethyl-3-(4-sulfonatobutyl)Indolin-2-ylidene)ethylidene)-2-chlorocyclopent-1-enyl)vinyl)-3,3-dimethylindole-1-sulfonate-5-carboxylic acid (68)

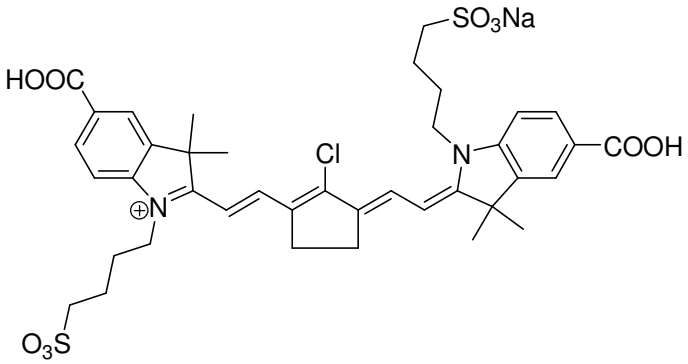

(**68**)

A vigorously stirred solution of 3-(5-carboxy-2,3,3-trimethyl-3*H*-indolium-1-yl)propane-1-sulfonate (0.197 g, 0.58 mmol) and **64** (0.1 g, 2.9 mmol) in acetic anhydride (1.5 mL) and acetic acid (1 mL) was treated with sodium acetate (0.084 g, 1.02 mmol) and heated at reflux (120 °C) for 45 min. The reaction mixture was cooled to ambient temperature and anhydrous diethyl ether (10 mL) was added. The resulting filtrate was isolated by vacuum filtration to give a crude solid that was recrystallized (methanol: water) to give **68** as a green solid (0.06 g, 0.07 mmol, 25%); mp: charring at 145-150 °C; ^{1}H NMR (400 MHz, CD_3OD) δ 8.13-8.11 (m, 4H), 8.00 (d, *J* = 14.2 Hz, 2H), 7.43 (d, *J* = 8.2 Hz, 2H), 6.28 (d, *J* = 14.2 Hz, 2H), 4.26 (t, *J* = 7.3 Hz, 4H), 3.06 (bs, 4H), 2.92 (t, *J* = 7.3 Hz, 4H), 2.05-1.97(m, 8H), 1.77 (s, 12H); ^{13}C NMR (100 MHz, DMSO-*d6*) δ 167.8, 167.0, 153.9, 148.6, 145.9, 141.2, 138.4, 137.3, 130.8, 123.4, 122.6, 103.9, 99.4, 53.8, 51.3, 51.1, 50.7, 48.8, 44.5, 28.2, 27.7, 27.4, 26.1, 23.0, 22.7, 22.5, 20.1; HRMS (ESI-TOF): [M + H]+ Calc'd for $C_{39}H_{45}ClN_2O_{10}S_2$ *m/z* 801.2282. Found, *m/z* 801.2367.

Sodium-2-((*E*)-2-((*E*)-3-((*Z*)-2-(5-carboxy-3,3-dimethyl-3-(4-sulfonatobutyl)Indolin-2-ylidene)ethylidene)-2-chlorocyclohex-1-enyl)vinyl)-3,3-dimethylindole-1-sulfonate-5-carboxylic acid (67)

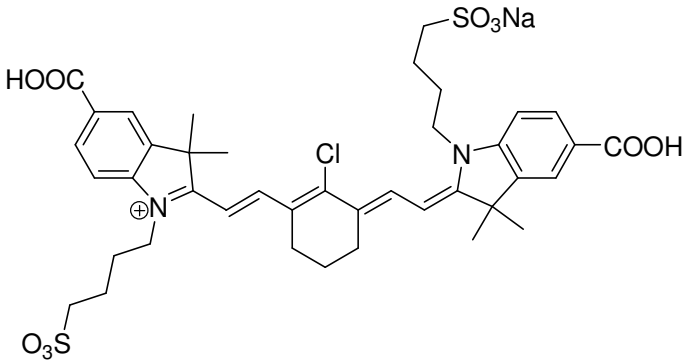

(**67**)

A vigorously stirred solution of 3-(5-carboxy-2,3,3-trimethyl-3*H*-indolium-1-yl)propane-1-sulfonate (**13**, 0.1 g, 0.29 mmol) and **63** (0.05 g, 0.14 mmol) in acetic anhydride (1 mL) and acetic acid (0.5 mL) was treated with sodium acetate (0.039 g, 0.47 mmol) and heated at reflux (120 °C) for 45 min. The reaction mixture was cooled to ambient temperature and anhydrous diethyl ether (5 mL) was added. The resulting precipitate was isolated by vacuum filtration to give a crude solid that was recrystallized (methanol: water) to give **67** as a green solid (0.055 g, 0.07 mmol, 47%); mp: charring at 130-140 °C; ^{1}H NMR (400 MHz, CD_3OD) δ 8.51 (d, *J* = 13.9 Hz, 2H), 8.15-8.11 (m, 4H), 7.46 (d, *J* = 8.7 Hz, 2H), 6.46 (d, *J* = 14.2 Hz, 2H), 4.28-4.25 (m, 4H), 2.95-2.90 (m, 4H), 2.81-2.77 (m, 4H), 2.05-1.99 (m, 10H), 1.80 (s, 12H); ^{13}C NMR (100 MHz, CD_3OD) δ 174.9, 169.8, 152.1, 147.2, 146.3, 142.7, 132.4, 130.0, 124.7, 112.1, 103.7, 45.3, 28.5, 28.3, 27.4, 27.2, 23.6, 22.1; HRMS (ESI-TOF): [M+H]+ Calc'd for $C_{40}H_{48}N_2O_{10}S$ *m/z* 815.2439. Found, *m/z* 815.2451.

Sodium-2-((*E*)-2-((*E*)-3-((*Z*)-2-(5-carboxy-3,3-dimethyl-3-(4-sulfonatobutyl)Indolin-2-ylidene)ethylidene)-2-methylcyclohex-1-enyl)vinyl)-3,3-dimethylindole-1-sulfonate-5-carboxylic acid (65)

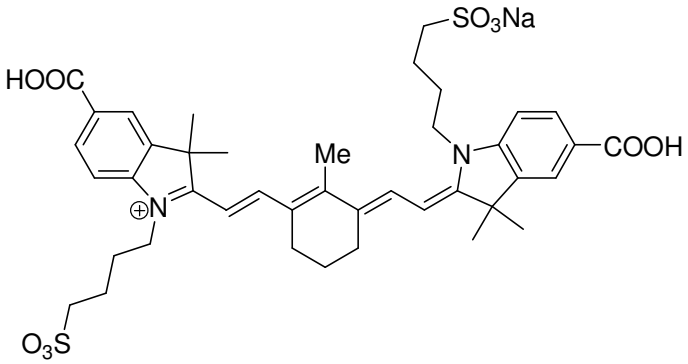

(**65**)

A vigorously stirred solution of 3-(5-carboxy-2,3,3-trimethyl-3*H*-indolium-1-yl)propane-1-sulfonate (**13**, 0.107 g, 0.32 mmol) and **61** (0.05 g, 0.15 mmol) in acetic anhydride (1 mL) and acetic acid (0.5 mL) was treated with sodium acetate (0.041 g, 0.5 mmol) and heated at reflux (120 °C) for 45 min. The reaction mixture was cooled to ambient temperature and anhydrous diethyl ether (5 mL) was added. The resulting precipitate was isolated by vacuum filtration to give a crude solid that was recrystallized (methanol: water) to give **65** as a green solid (0.030 g, 0.04 mmol, 25%); mp: charring at 255-260 °C; ^{1}H NMR (400 MHz, CD_3OD) δ 8.23 (d, *J* = 13.6 Hz, 2H), 8.11 (d, *J* = 1.4 Hz, 1H), 8.09 (s, 2H), 7.37 (d, *J* = 8.4 Hz, 2H), 6.37 (d, *J* = 13.8 Hz, 2H), 4.24-4.20 (m, 4H), 2.94-2.90 (m, 4H), 2.68-2.66 (m, 4H), 2.51 (s, 3H), 2.03-1.93 (m, 10H), 1.79 (s, 12H); ^{13}C NMR (100 MHz, CD_3OD) δ 173.4, 158.4, 146.8, 142.3, 134.1, 124.6, 111.4, 102.6, 52.0, 45.2, 28.7, 27.4, 26.6, 23.8, 15.4; HRMS (ESI-TOF): [M+H]+ Calc'd for $C_{41}H_{51}N_2O_{10}S_2$ m/z 795.2985. Found, m/z 795.2964.

Sodium-2-((*E*)-2-((*E*)-3-((*Z*)-2-(5-carboxy-3,3-dimethyl-3-(4-sulfonatobutyl)Indolin-2-ylidene)ethylidene)-2-phenylcyclohex-1-enyl)vinyl)-3,3-dimethylindole-1-sulfonate-5-carboxylic acid (66)

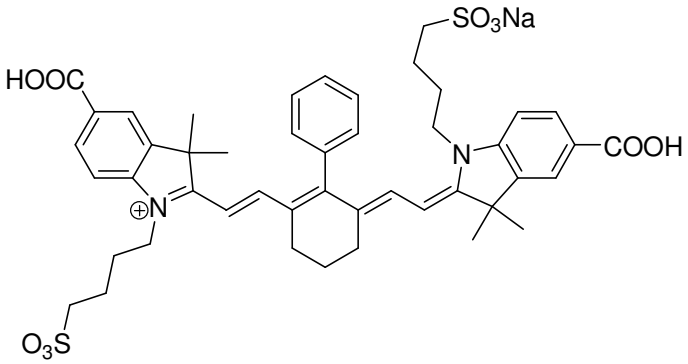

(**66**)

A vigorously stirred solution of 3-(5-carboxy-2,3,3-trimethyl-3*H*-indolium-1-yl)propane-1-sulfonate (**13**, 0.36 g, 1.06 mmol) and **62** (0.2 g, 0.5 mmol) in acetic anhydride (1.5 mL) and acetic acid (1 mL) was treated with sodium acetate (0.139 g, 1.7 mmol) and heated at reflux (120 °C) for 45 min. The reaction mixture was cooled to ambient temperature and anhydrous diethyl ether (15 mL) was added. The resulting precipitate was isolated by vacuum filtration to give a crude solid that was recrystallized (methanol:water) to give **66** as a green solid (0.025 g, 0.03 mmol, 57%); mp: charring at 255-260 °C; ^{1}H NMR (400 MHz, CD_3OD) δ 8.08 (d, *J* = 8.6 Hz, 2H), 7.94 (s, 2H), 7.68-7.64 (m, 3H), 7.39-7.35 (m, 4H), 7.30 (d, *J* = 6.6 Hz, 2H), 6.36 (d, *J* = 13.9 Hz, 2H), 4.18 (bs, 4H), 2.93-2.90 (m, 4H), 2.80 (bs, 4H), 2.10 (bs, 2H), 1.96 (bs, 8H), 1.25 (s, 12H); ^{13}C NMR (100 MHz, CD_3OD) δ 175.6, 169.2, 156.8, 147.4, 142.8, 132.3, 128.7, 128.6, 124.6, 112.0, 106.0, 51.7, 50.4, 45.1, 27.9,27.2, 23.5; HRMS (ESI-TOF): [M+H]+ Calc'd for $C_{46}H_{53}N_2O_{10}S_2$ *m/z* 857.3142. Found, *m/z* 857.3097.

Sodium 4-[2-[(1*E*,3*E*,5*Z*)-7-[1,1-dimethyl-3-(4-sulfonatobutyl)indol-2-ylidene]penta-1,3-dienyl]-1,1-dimethylindol-3-ium-3-yl]butane-1-sulfonate (71)

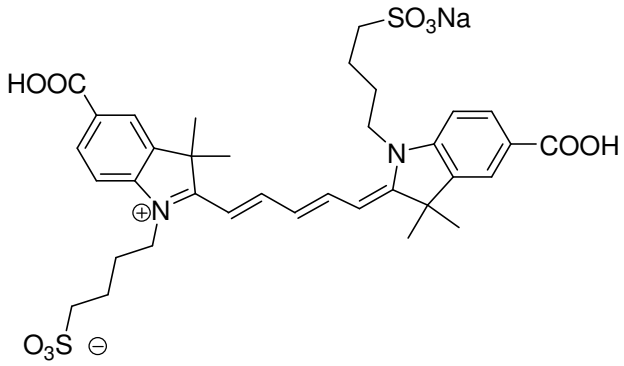

(**71**)

A vigorously stirred solution of 3-(5-carboxy-2,3,3-trimethyl-3*H*-indolium-1-yl)propane-1-sulfonate (**13**, 0.14 g, 0.41 mmol) and **70** (0.05 g, 0.19 mmol) in acetic anhydride (1 mL) and acetic acid (0.5 mL) was treated with sodium acetate (0.054 g, 0.66 mmol) and heated at reflux (120 °C) for 45 min. The reaction mixture was cooled to ambient temperature and anhydrous diethyl ether (5 mL) was added. The resulting precipitate was isolated by vacuum filtration to give a crude solid that was recrystallized (methanol: water) to give **71** as a blue solid (0.09 g, 0.12 mmol, 63%); mp: decomposition at 287 °C; ^{1}H NMR (400 MHz, CD_3OD) δ 12.92 (bs, 2H), 8.43 (t, *J* = 13 Hz, 2H), 8.17 (s, 2H), 8.00 (d, *J* = 8.4 Hz, 2H), 7.53 (d, *J* = 8.4 Hz, 2H), 6.71 (t, *J* = 12.4 Hz, 1H), 6.50 (d, *J* = 13.7 Hz, 2H), 4.15 (bs, 4H), 1.18-1.76 (m, 8H), 1.73 (s, 12H); ^{13}C NMR (100 MHz, CD_3OD) δ 175.7, 169.2, 156.8, 147.4, 142.8, 132.3, 128.7,128.6, 124.6, 112.0, 106.0, 51.7, 50.4, 45.1, 27.9, 27.2, 23.5; HRMS (TOF): [M+H]+ Calc'd for $C_{35}H_{43}N_2O_{10}S_2$ *m/z* 715.2359. Found, *m/z* 715.2321.

4-Trimethylsilyloxy-2-methoxycyclohex-3-enecarbaldehyde (37)

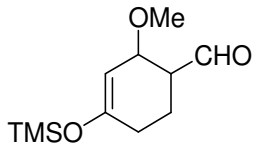

(**37**)

A mixture of trans-l-methoxy-3-trimethylsilyloxy-1,3-butadiene (0.5 g, 29 mmol) and acrylaldehyde (0.325 g, 5.8 mmol) in dry dichloromethane (10 mL) was heated to reflux at 50 °C under a nitrogen atmosphere for overnight. The reaction mixture was concentrated *in vacuo* to give a crude oil, which was purified by column chromatography to obtain 4-trimethylsilyloxy-2-methoxycyclohex-3-enecarbaldehyde as a clear oil (0.25 g, 1.09 mmol, 38%); ^{1}H NMR (400 MHz, $CDCl_3$) δ 9.79 (s, 1H), 5.19 (d, *J* = 8 Hz, 1H), 4.28 (t, *J* = 4 Hz, 1H), 3.33 (s, 3H), 2.45-2.41 (m, 1H), 2.18-2.08 (m, 2H), 2.05-1.97 (m, 1H), 1.95-1.88 (m, 1H); ^{13}C NMR (100 MHz, $CDCl_3$) δ 203.4, 156.3, 102.1, 73.4, 56.0, 50.6, 29.1, 18.2, 0.4.

Methyl-2-methoxy-4-trimethylsilyloxycyclohex-3-ene-1-carboxylate (44)

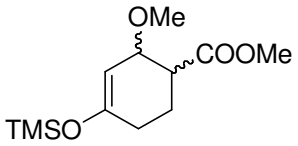

(**44**)

To a stirred solution of trans-1-methoxy-3-trimethylsilyloxybutadiene **16** (0.2 g, 1.16 mmol) in benzene (10 mL) was added methyl acrylate (0.21 mL, 24.0 mmol). The reaction mixture was heated at reflux for 48 h. The solution was concentrated to give **44** as an oil consisting of 45:55 mixture of cis and trans isomers, which was used in the next step without further purification (0.28 g, 1.08 mmol, 94%); cis-isomer: ^{1}H NMR (400 MHz, $CDCl_3$) δ 4.98 (d, *J*

= 5.3, 1H), 4.10 (t, *J* = 4 Hz, 1H), 3.69 (s, 3H), 3.28 (s, 3H), 2.59 (dt, *J* = 12.2, 3.6, 1H), 1.96-1.83 (m, 4H); ^{13}C NMR (100 MHz, $CDCl_3$) δ 173.1, 155.5, 101.5, 73.6, 55.9, 51.3, 44.5, 29.4, 19.0, 0.3; tras-isomer: ^{1}H NMR (400 MHz, $CDCl_3$) δ 4.24 (bs, 1H), 5.13 (d, *J* = 4 Hz, 1H), 3.70 (s, 3H), 3.31 (s, 3H), 1.96-1.83 (m, 5H), 0.20 (s, 9H); ^{13}C NMR(100 MHz, $CDCl_3$) δ 0.2, 22.7, 28.4, 44.2, 51.6, 55.4, 76.6, 102.9, 153.3, 174.2.[86,87]

Methyl-4-oxocyclohex-1-enecarboxylate (51)

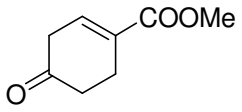

(**51**)

A solution of methyl-2-methoxy-4-trimethylsilyloxycyclohex-3-ene-1-carboxylate, **44** (0.27 g, 1.05 mmol) in toluene (5 mL) was cooled to 0 °C, yetterbium triflate (0.013 g, 2 mol%) was added and stirred for 45 min. The reaction mixture was evaporated *in vacuo* to give methyl-4-oxocyclohex-1-enecarboxylate as a crude oil which was purified by column chromatography (0.08 g, 0.52 mmol, 50%). Analytical characterization of the enone has been previously reported by Jung et al.[88] ^{1}H NMR (300 MHz, $CDCl_3$) δ 7.01 (m, 1H), 378 (s, 3H), 3.04 (m, 2H), 2.81-2.76 (m, 2H), 2.56 (t, *J* = 8 Hz, 2H).

4-hydroxycyclohexa-1,3-dienecarbaldehyde (40)

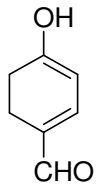

(**40**)

A solution of 0.1N HCl in tetrahydrofuran (1 mL) was added to a stirring solution of **37** in dichloromethane (0.1 g, 0.44 mmol) and the resulting solution was stirred overnight at room temperature. The solvent was removed *in vacuo* to get a crude oil. In an attempt to purify the crude, the desired product rearranged to a 4-hydroxycyclohexa-1,3-dienecarbaldehyde; ^{1}H NMR (400 MHz, $CDCl_3$) δ 9.42 (s, 1H), 6.89 (d, *J* = 4 Hz, 1H), 5.28 (d, *J* = 4 Hz, 1H), 2.57 (t, *J* = 8 Hz, 2H), 2.42 (t, *J* = 8 Hz, 2H).

(4Z)-4-((Phenyl lamino)methylene)cyclohex-2-enone (41)

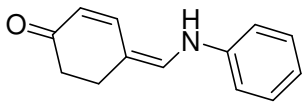

(**41**)

Yetterbium triflate (0.006 g, 2 mol%) was added to a stirring solution of **37** (0.1 g, 0.44 mmol) in toluene (2 mL) at 0 °C and stirred at room temperature for 40 min. The reaction progress was monitored by TLC. After stirring at room temperature for 40 min, aniline (0.15 g, 1.61 mmol) was added to the same reaction pot and the resulting solution was stirred for overnight. Toluene was removed *in vacuo* to give the crude, which was purified by column chromatography to obtain (4Z)-4-((phenyllamino)methylene)cyclohex-2-enone

(0.026 g, 0.13 mmol, 29%); ^{1}H NMR (400 MHz, $CDCl_3$) δ 7.31 (s, 2H), 7.10-6.98 (m, 4H), 6.98 (s, 1H), 5.70 (d, *J* = 4 Hz, 1H), 2.73 (bs, 2H), 2.55 (bs, 2H); ^{13}C NMR (100 MHz, $CDCl_3$) δ 199.2, 150.0, 141.3, 133.5, 129.9, 122.1, 119.3, 115.1, 109.4, 36.0, 21.8.

Methyl 4-(4-nitrophenylamino)cyclohexa-1,3-dienecarboxylate (53)

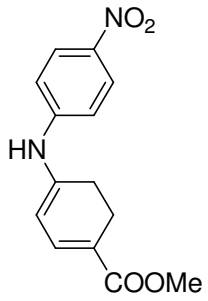

(**53**)

A mixture of trans-l-methoxy-3-trimethylsilyloxy-1,3-butadiene (0.2 g, 1.16 mmol) and methyl acrylate (0.2 g, 2.32 mmol) in benzene (10 mL) was heated to reflux under a nitrogen atmosphere for 48 h. The reaction mixture was cooled to 0 °C, diisobutyl aluminium hydride (0.31g, 2.2 mmol) was added and the resulting solution was slowly warmed to room temperature and stirred for 2 h. The reaction progress was monitored by TLC. After the complete consumption of the Diels-Alder adduct, yetterbium triflate was added to the same reaction pot and stirred at room temperature for 2 h. The reaction progress was monitored by TLC. After the starting material consumption, 4-nitroaniline (0.07 g, 0.51 mmol) was added and the resulting solution was stirred at room temperature for overnight. The reaction mixture was concentrated *in vacuo* to give a crude, which was purified by column chromatography to obtain methyl 4-(4-nitrophenylamino)cyclohexa-1,3-dienecarboxylate (0.11 g, 0.40 mmol, 35%); ^{1}H NMR (300 MHz, $CDCl_3$) δ 8.21 (d, *J* = 3 Hz, 2H), 7.20-7.15 (m, 3H), 5.93 (bs,

1H), 5.86 (d, *J* = 9 Hz, 1H), 3.79 (s, 3H), 2.68 (t, *J* = 9 Hz, 2H), 2.49 (t, *J* = 9 Hz, 2H); ^{13}C NMR (75 MHz, $CDCl_3$) δ 167.3, 153.4, 139, 131.8, 129.0, 121.6, 118.1, 69.8, 47.0, 41.5.$C_{17}H_{24}NO_5S$ *m/z* 354.1375. Found, *m/z* 354.1375.

Methyl 2-(1H-pyrrol-1-yl)acetate (75)

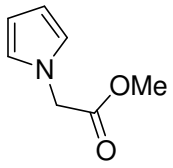

(**75**)

Glycine methyl ester hydrochloride (3.0 g, 21.5 mmol) and sodium acetate (2.9 g, 12 mmol) were dissolved in water (15 mL). Acetic acid (30 mL) was then added. The solution was heated to reflux and 2,5-dimethoxytetrahydrofuran (2.9 mL, 22 mmol) was added. The mixture was heated at reflux for 4 hours before being allowed to cool to room temperature. The dark brown solution was diluted with water (120 mL), neutralised with solid $NaHCO_3$ (25 g) and extracted with CH_2Cl_2 (3×80 mL). The organic layers were dried (MgSO4), filtered, concentrated *in vacuo* to give a dark brown liquid. The material was purified by flash chromatography to give light brown oil (2.19 g, 15.7 mmol, 69%); ^{1}HNMR (300 MHz, $CDCl_3$) δ 6.63-6.62 (m, 2H), 6.17-6.16 (m, 2H), 4.62 (s, 2H), 3.72 (s, 3H); ^{13}C NMR (75 MHz, CDCl3) δ 169.7, 121.7, 108.9, 52.4; HRMS (ESI, AccuTOF): Calc'd for $C_7H_{10}NO_2$ [M+H]+ *m/z* 140.0712. Found, *m/z* 140.0693.

N-(2-Hydroxyethyl)-2-(1H-pyrrol-1-yl)acetamide (76)

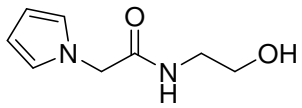

(**76**)

Ethanolamine (12.6 g, 20.7 mmol) was added to a solution of Methyl 2-(1H-pyrrol-1-yl)acetate (7.5 g, 54 mmol) in 50 mL of methanol and the resulting solution was stirred at room temperature for overnight. The reaction mixture was concentrated *in vacuo* to give a crude solid which was purified by column chromatography to give N-(2-Hydroxyethyl)-2-(1H-pyrrol-1-yl)acetamide as an off white solid (6.5 g, 38.7 mmol, 72%); mp: 89-90 °C; ^{1}HNMR (300 MHz, $CDCl_3$) δ 6.64 (d, *J* = 1.68 Hz, 2H), 6.22 (d, *J* = 1.68 Hz, 2H), 5.79 (bs, 1H), 4.57 (bs, 2H), 3.61-3.58 (m, 2H), 3.35-3.30 (m, 2H), 2.52 (bs, 1H); ^{13}C NMR (75 MHz, $CDCl_3$) δ 170.1, 121.8, 110.1, 61.4, 52.9, 41.2; HRMS (ESI, accuTOF): $[M+NH_3]+$ Calc'd for $C_7H_{12}N_2O_2$ *m/z* 156.0899. Found, *m/z* 156.0655.

2-(4-nitro-1H-imidazol-1-yl)acetic acid (18)

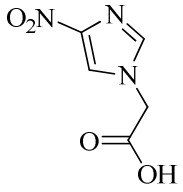

(**18**)

A 50 mL round-bottomed flask with a magnetic stirbar was charged with methyl 2-(4-nitro-1H-imidazol-1-yl)acetate **16b** (1.0 g, 5.40 mmol), and 30 mL of water. The system was heated under reflux for 24 hours. Then, the solution was cooled, and any remaining solid

was filtered off. The water was removed *in vacuo*, and solid was placed in drying pistol with phosphorus pentoxide for 24 h, to give a white solid (0.88 g, 5.14 mmol, 97%); mp: 151-152 °C; ^{1}H NMR (400 MHz, DMSO-d_6): δ 8.12 (d, J = 0.84 Hz, 1H), 7.59 (d, J = 1.12 Hz, 1H), 4.74 (s, 2H); ^{13}C NMR (100 MHz, CD_3OD): δ 170.0, 148.4, 139.2, 122.8, 53.3; HRMS(ESI-TOF): [M+H]+ Calc'd for $C_5H_6N_3O_4$: *m/z* 172.0358. Found, *m/z* 172.0369.

5-Carboxylate-1-(δ-sulfobutyl)-2,3,3-trimethyl-3H-indolium (88)

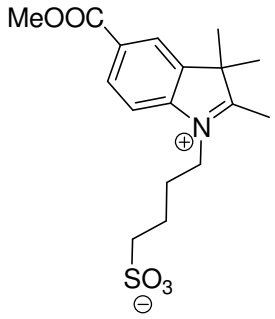

(**88**)

A 50 mL round-bottomed flask with a magnetic stirbar was charged with the carboxylic acid indolium salt **13** (1.01 g, 2.97 mmol), and absolute methanol (15 mL). The mixture was stirred at room temperature under nitrogen as oxalyl chloride (1.0 mL, 11.9 mmol) was added dropwise. Then the mixture was stirred for 24 h. The mixture was reduced *in vacuo* to give a red paste. The crude product was stirred in ether until it became a suspension, about 24 h. The solid was filtered and washed with ether to yield a red powder (1.02 g, 2.89 mmol, 97%); mp: decompose at 159 °C; ^{1}H NMR (400 MHz, CD_3OD): δ 8.34 (d, J = 1.1 Hz, 1H), 8.28 (dd, J = 8.5, 1.5 Hz, 1H), 8.05 (d, J = 8.5 Hz, 1H), 4.57 (t, J = 7.8 Hz, 2H), 3.95 (s, 3H), 2.89 (t, J = 7.1 Hz, 2H), 2.18-2.11 (m, 2H), 1.97-1.91 (s, 2H), 1.63 (s, 6H); ^{13}C NMR (100 MHz, CD_3OD) δ 22.6, 23.3, 27.3, 53.1, 56.3, 116.9, 125.5, 132.1, 133.0, 143.7, 145.8, 166.9,

201.3. HRMS (ESI, accuTOF): [M+H]+ Calc'd for $C_{17}H_{24}NO_5S$ *m/z* 354.1375. Found: *m/z* 354.1375.

Bis-1-1′-(4-sulfobutyl)indoletricarbocyanine-5-carboxy-5′-carboxylate sodium salt (89)

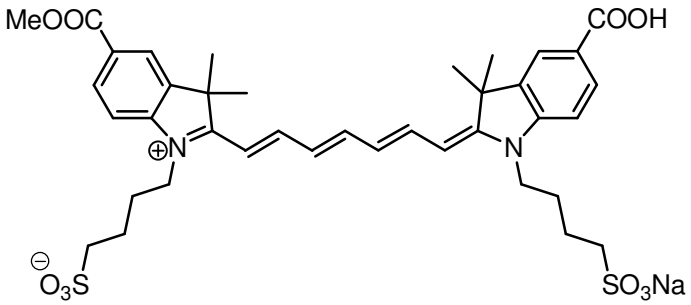

(**89**)

A 100 mL round-bottomed flask with a magnetic stirrbar was charged with the carboxylic acid indolium salt **13** (0.50 g, 1.47 mmol) and *N*-[5-(Phenylamino)-2,4-pentadienylidene]aniline monohydrochloride (0.37 g, 1.49 mmol). Then acetic anhydride (19 mL) and glacial acetic acid (12 mL) were added to flask. The mixture was stirred as sodium acetate (0.48 g, 5.84 mmol) was added. The solution was heated at reflux under a nitrogen atmosphere for 30 min. Next, the methyl ester indolium salt **88** (0.54 g, 1.52 mmol) was added to the flask, and the mixture continued to reflux for an additional 45 minutes. The mixture was cooled to room temperature, and then poured into 150 mL of hot anhydrous ether. The solution was cooled at 5 °C overnight, and then the precipitate was filtered and washed with ether. The collected solid was recrystallized in a 1:4 mixture of water and propanol. The crystals were filtered and dried for two days under vacuum to yield a blue green powder (0.96 g, 1.24 mmol, 83%); mp: decomposed at 238-239 °C; ^{1}H NMR (400 MHz, DMSO-*d6*) δ 12.96 (bs, 1H), 8.08 (d, *J* = 7.34 Hz, 2H), 7.97 (d, *J* = 7.34 Hz, 2H), 7.84

(m, 2H), 7.52 (d, *J* = 9.05 Hz, 2H), 7.47 (s, 1H), 6.48 (m, 4H), 4.15-4.06 (m, 4H), 3.86 (s, 3H), 1.73 (s, 8H), 1.63 (s, 12H); ^{13}C NMR (100 MHz, DMSO-*d6*) δ 167.7, 166.6, 147.1, 142.0, 131.3, 125.6, 124.0, 123.8, 52.8, 51.4, 49.4, 41.8, 27.7, 26.8, 23.2; HRMS (ESI-TOF): [M+Na]+ Calc'd for $C_{38}H_{45}N_2NaO_{10}S_2$ *m/z* 755.2736. Found, *m/z* 777.2540.

tert-Butyl 4-(2-(2-methyl-1H-imidazol-1-yl)acetyl)piperazine-1-carboxylate (79)

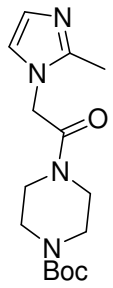

(**79**)

Sodium hydride (0.0235 g, 1.46 mmol) was added to a stirring solution of 2-methylimidazole (0.1 g, 1.22 mmol) in 1 mL of dry DMF under a N_2 atmosphere at 0 °C. The mixture was stirred at 0 °C temperature for 30 min, at that time, tert-butyl 4-(2-bromoacetyl) piperazine-1-carboxylate (0.374 g, 1.22 mmol) was added slowly and the reaction mixture was stirred at room temperature overnight. The DMF was evaporated *in vacuo* and the resulting crude reaction mixture was purified by column chromatography to give tert-butyl 4-(2-(2-methyl-1H-imidazol-1-yl)acetyl)piperazine-1-carboxylate as a colorless oil (0.263 g, 0.85 mmol, 69%); mp: 147-149 °C; ^{1}H NMR (400 MHz, $CDCl_3$) δ 6.81 (s, 1H), 7.70 (s, 1H) 4.58 (s, 2H), 3.50 (m, 2H), 3.35 (m, 6H), 2.20 (s,3H), 1.38 (s, 9H); ^{13}C NMR (100 MHz, $CDCl_3$) δ 164.9, 154.3, 145.4, 127.1, 120.3, 80.5, 53.5, 47.2, 44.6, 43.3, 43.1, 41.9, 28.3, 12.9.[80]

2-(2-methyl-1H-imidazol-1-yl)-1-(piperazin-1-yl)ethanone.TFA salt (80)

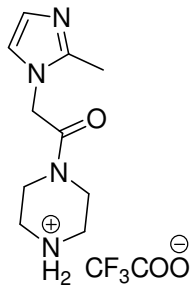

(**80**)

Trifluoroacetic acid (1 mL) was added dropwise to a stirring solution of tert-butyl 4-(2-(4-nitro-1H-imidazol-1-yl)acetyl)piperazine-1-carboxylate **79** (0.26 g, 0.85 mmol) in 10 mL of dry chloroform. The solution was stirred at room temperature overnight. The reaction mixture was concentrated *in vacuo* to give a crude solid. The crude solid was triturated with ethyl acetate to give 2-(2-methyl-1H-imidazol-1-yl)-1-(piperazin-1-yl)ethanone TFA as a white solid, which was filtered and dried under vacuum (0.24 g, 0.75 mmol, 88%); mp:150-152 °C; ^{1}H NMR (300 MHz, DMSO-d_6) δ 7.32-7.27 (m, 2H), 5.41 (s, 3H), 5.28 (s, 2H), 3.78 (d, J = 4 Hz, 4H), 3.32-3.31 (m, 2H), 3.25-3.20 (m, 2H); ^{13}C NMR (75 MHz,CD_3OD) δ 165.5, 162.5, 162.0, 161.5, 161.0, 147.7, 124.7, 119.4,118.9,115.6, 44.2, 43.0, 40.3, 10.7; HRMS(ESI-TOF): (submitted for HRMS)

1,3-bis-tert-Butyl-4-(2-(1H-imidazol-1-yl)acetyl)piperazine-1-carboxylate bromide (28)

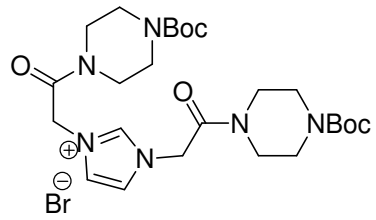

(**28**)

tert-Butyl 4-(2-bromoacetyl)piperazine-1-carboxylate (0.9 g, 29.4 mmol) was added to a stirring solution of imidazole (0.2 g, 29.4 mmol) in dry DMF (2 mL) and the resulting solution was stirred overnight at room temperature. The solvent was evaporated *in vacuo* and the resulted solid was washed with water (5 mL) to remove inorganic salts and then the solid was filtered to obtain 1,3-bis-tert-butyl-4-(2-(1H-imidazol-1-yl)acetyl)piperazine-1-carboxylate bromide (1.3 g, 2.16 mmol, 74%); mp: decomposed to black residue at >270 °C; ^{1}H NMR (400 MHz, $CDCl_3$) δ 9.82 (s, 1H), 7.45 (s, 1H), 5.53 (bs, 4H), 3.61-3.58 (m, 4H), 3.56-3.54 (m, 4H), 3.52-3.51 (m, 4H), 3.46-3.44 (m, 4H), 1.57 (bs, 2H), 1.45 (s, 18H); ^{13}C NMR (100 MHz, CD_3OD) δ 165.4, 156.2, 124.7, 81.8, 45.7, 44.1, 43.3, 28.6;

1,3-bis-tert-Butyl-4-(2-(2-methyl-1H-imidazol-1-yl)acetyl)piperazine-1-carboxylate bromide (92)

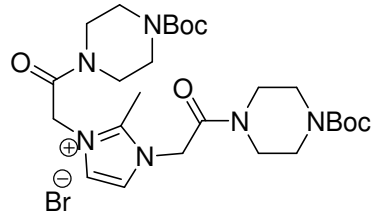

(**92**)

Followed the same procedure as in the preparation of **28**; ^{1}H NMR (400 MHz, $CDCl_3$) δ 7.62 (s, 2H), 5.60 (bs, 4H), 3.64(m, 8H), 3.59-3.56 (m, 6H), 3.48-3.45 (m, 6H), 1.47 (s, 18H); ^{13}C NMR (100 MHz, CD_3OD) δ 170.4, 165.1, 156.2, 149.3, 123.5, 81.7, 45.8, 43.2, 28.6, 22.4; mp: 241-242 °C

(Z)-N-(2-Phenylisoindolin-1-ylidene)benzenamine (59)

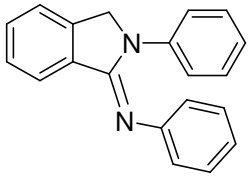

(**59**)

Aniline was added to a solution of phthalaldehyde (1 g, 7.45 mmol) in ethanol (20 mL) and the resulting solution was heated to reflux overnight. The solid precipitated in the reaction mixture was filtered and dried under vacuum to obtain (Z)-N-(2-phenylisoindolin-1-ylidene)benzenamine (1.9 g, 6.68 mmol, 90%); mp: 140-142 °C; ^{1}H NMR (400 MHz, $CDCl_3$) δ 8.01 (d, *J* = 7 Hz, 2H), 7.47-7.33 (m, 5H), 7.11-7.00 (m, 5H),6.68 (d, *J* = 7.4 Hz,

2H), 4.96 (s, 2H); ^{13}C NMR (100 MHz, $CDCl_3$) δ 153.4, 150.7, 141.6, 140.4, 131.5, 130.4, 129.2, 129.0, 127.3, 126.5, 123.1, 122.8, 122.3, 121.3, 119.9, 53.0.

2-(4-nitro-1H-imidazol-1-yl)acetic acid.piperazine salt (20)

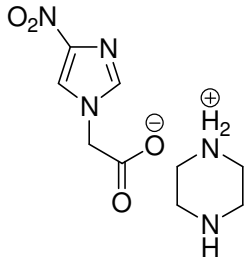

(**20**)

A 50 mL round bottom flask was charged with 2-(4-nitro-1H-imidazol-1-yl)acetic acid **18** (0.050 g, 29.2 mmol) and piperazine (0.025 g, 29.2 mmol) in CH_2Cl_2 (3 mL). EDC hydrochloride salt (0.056 g, 29.2 mmol) was added at 0 °C and the resulting solution was slowly warmed up to room temperature and stirred for overnight. The resulted solid was filtered and dried under vacuum (0.06 g, 86%); ^{1}H NMR (300 MHz, CD_3OD) δ 7.78 (d, J = 0.75 Hz, 1H), 7.25 (s, 1H), 3.31-3.29 (s, 10H); ^{13}C NMR (75 MHz, CD_3OD) δ 170.0, 148.9, 146.3, 131.4, 49.8, 53.3.

5.1 Appendix (Part I NMR spectrums)

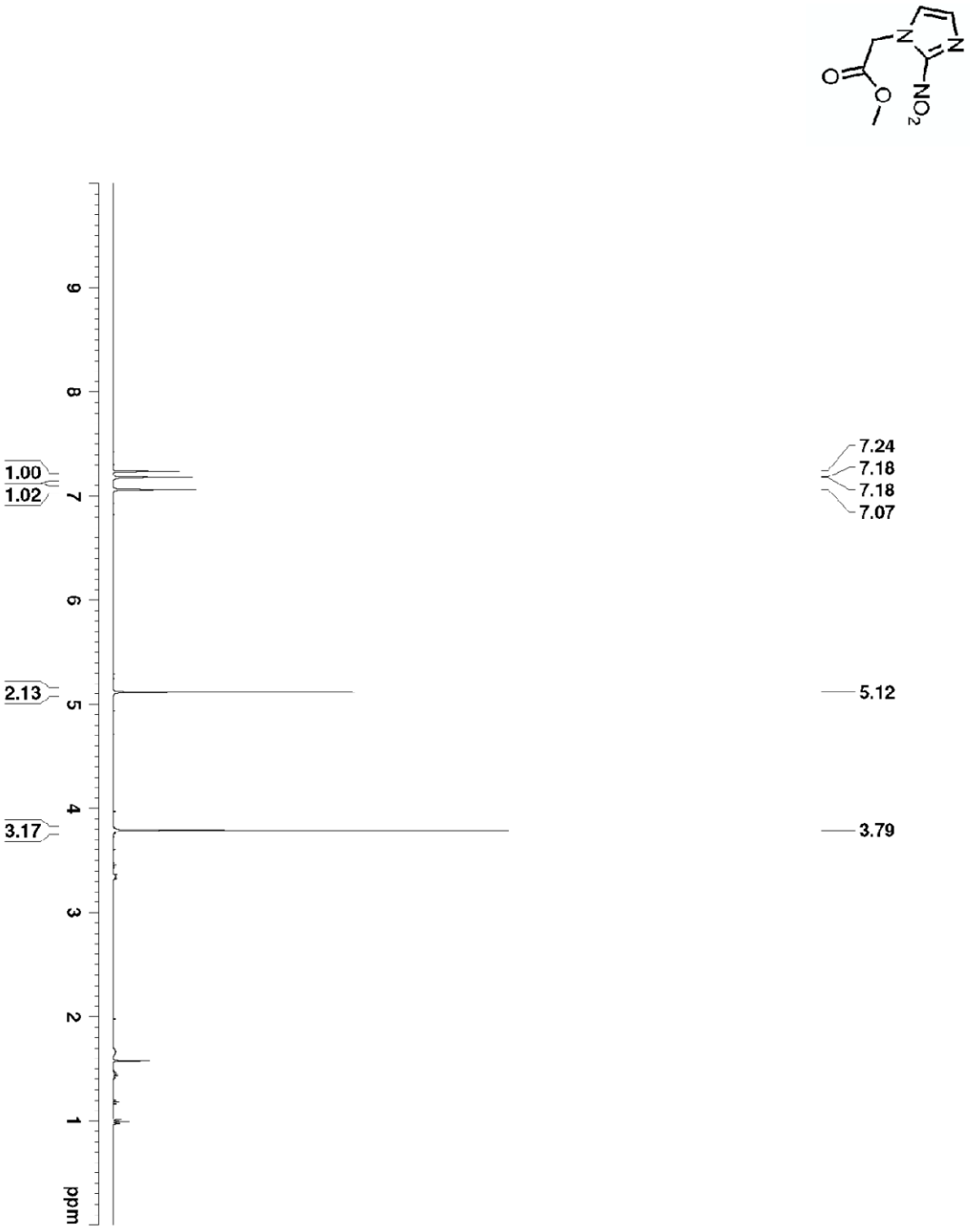
1.00
1.02
2.13
3.17
ppm
7.24
7.18
7.18
7.07
5.12
3.79

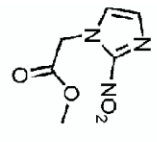

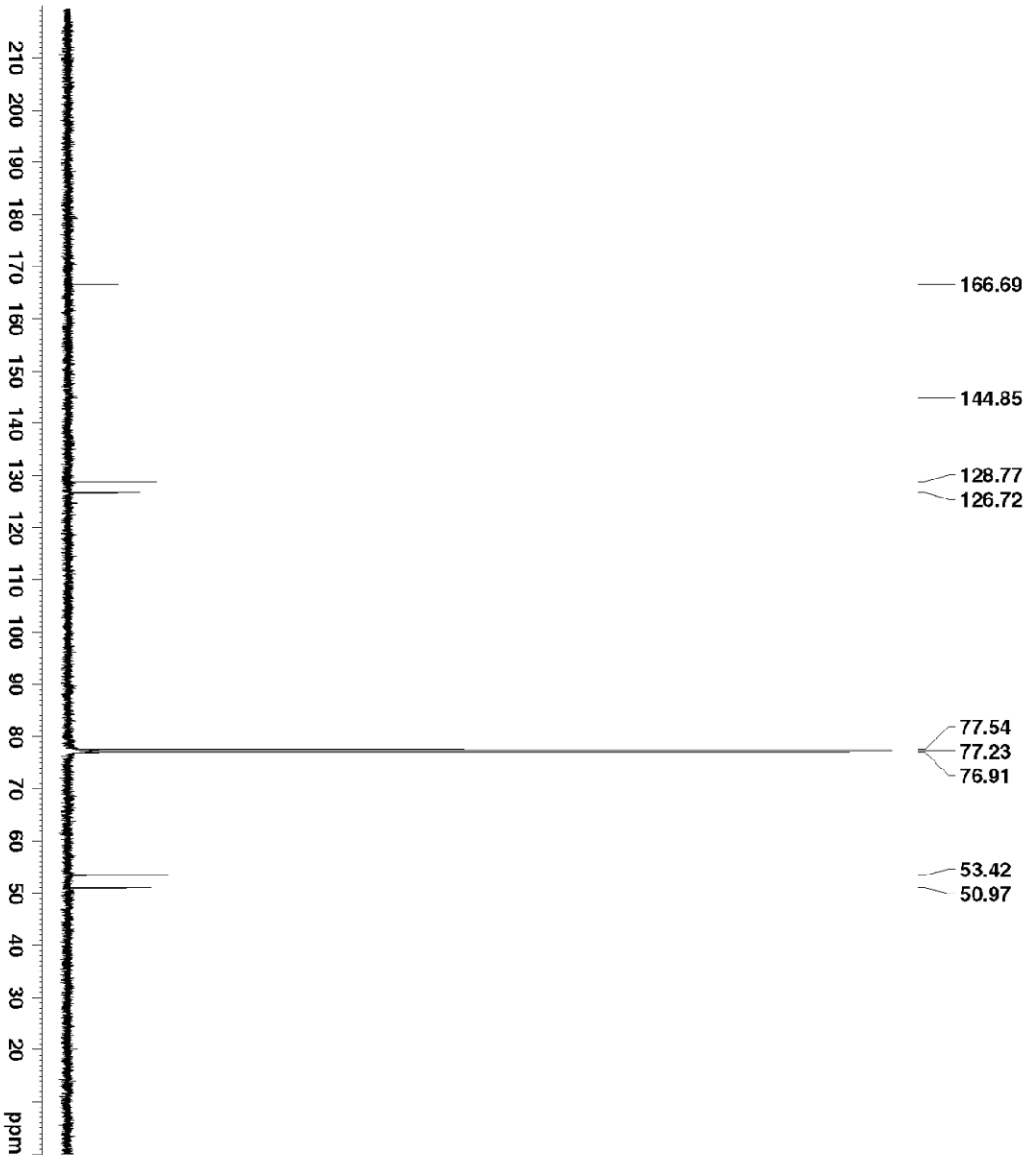
166.69
144.85
128.77
126.72
77.54
77.23
76.91
53.42
50.97
ppm

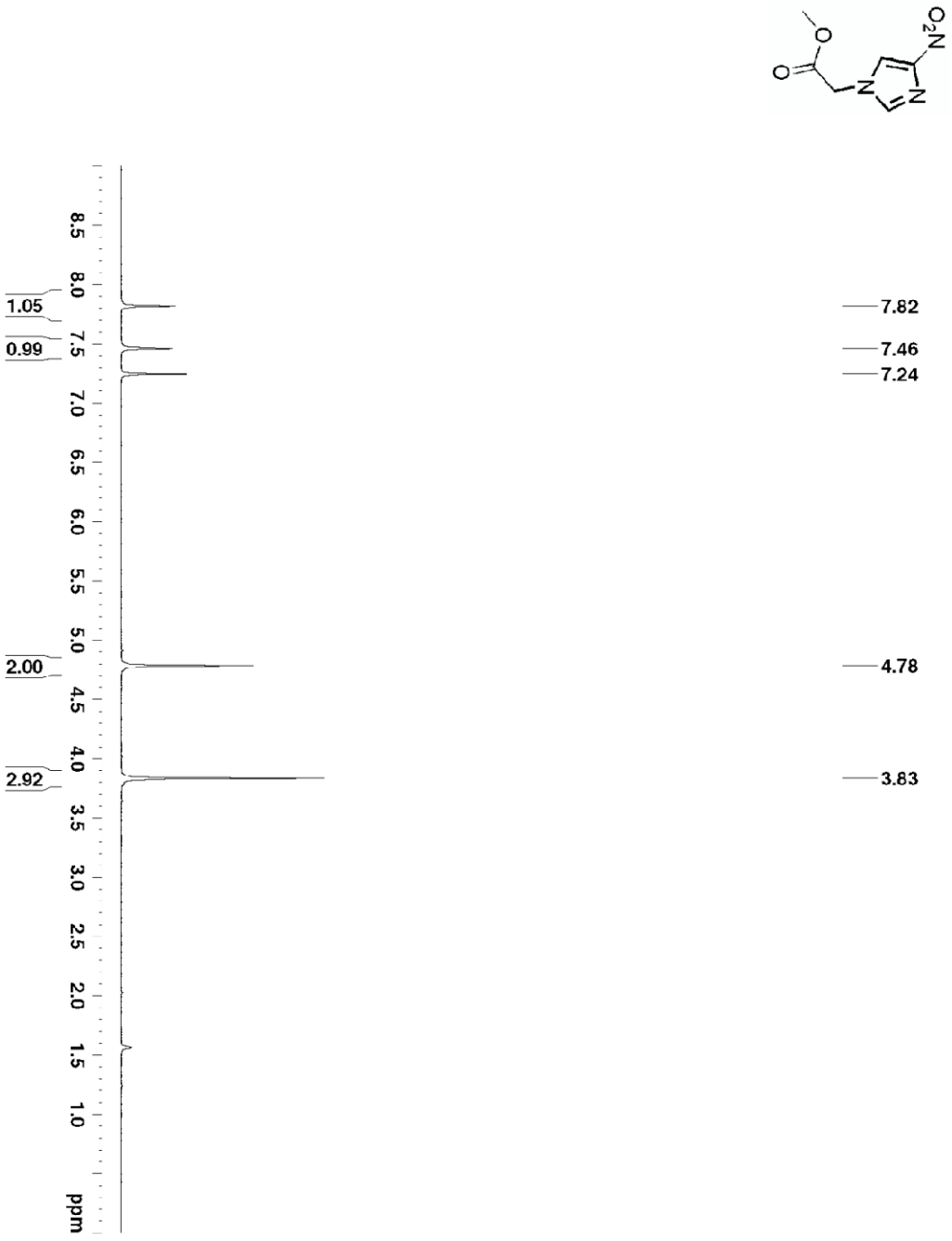
O2N
O
O
1.05
0.99
2.00
2.92
7.82
7.46
7.24
4.78
3.83
8.5
8.0
7.5
7.0
6.5
6.0
5.5
5.0
4.5
4.0
3.5
3.0
2.5
2.0
1.5
1.0
ppm

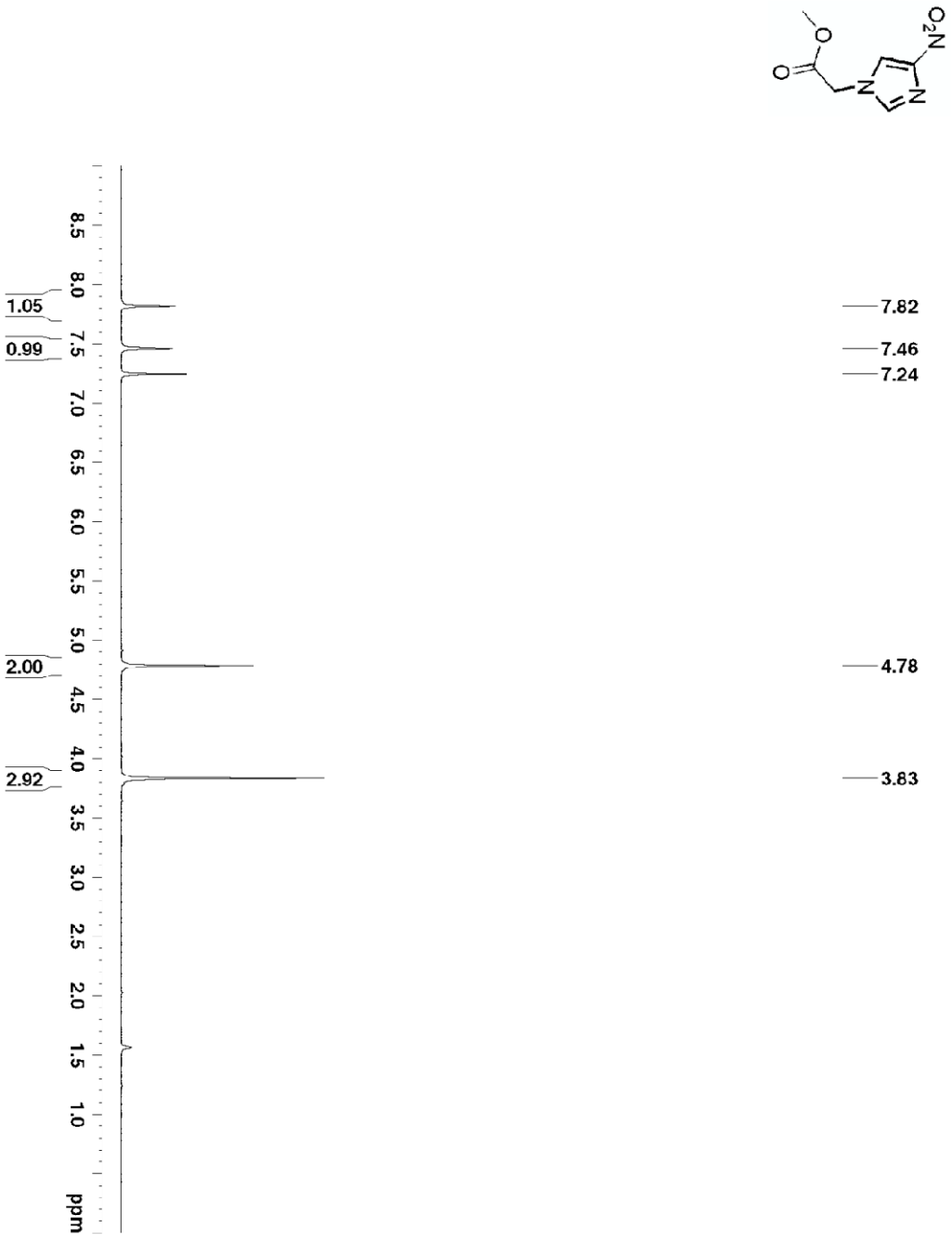
O2N
O
O
1.05
0.99
2.00
2.92
7.82
7.46
7.24
4.78
3.83
8.5
8.0
7.5
7.0
6.5
6.0
5.5
5.0
4.5
4.0
3.5
3.0
2.5
2.0
1.5
1.0
ppm

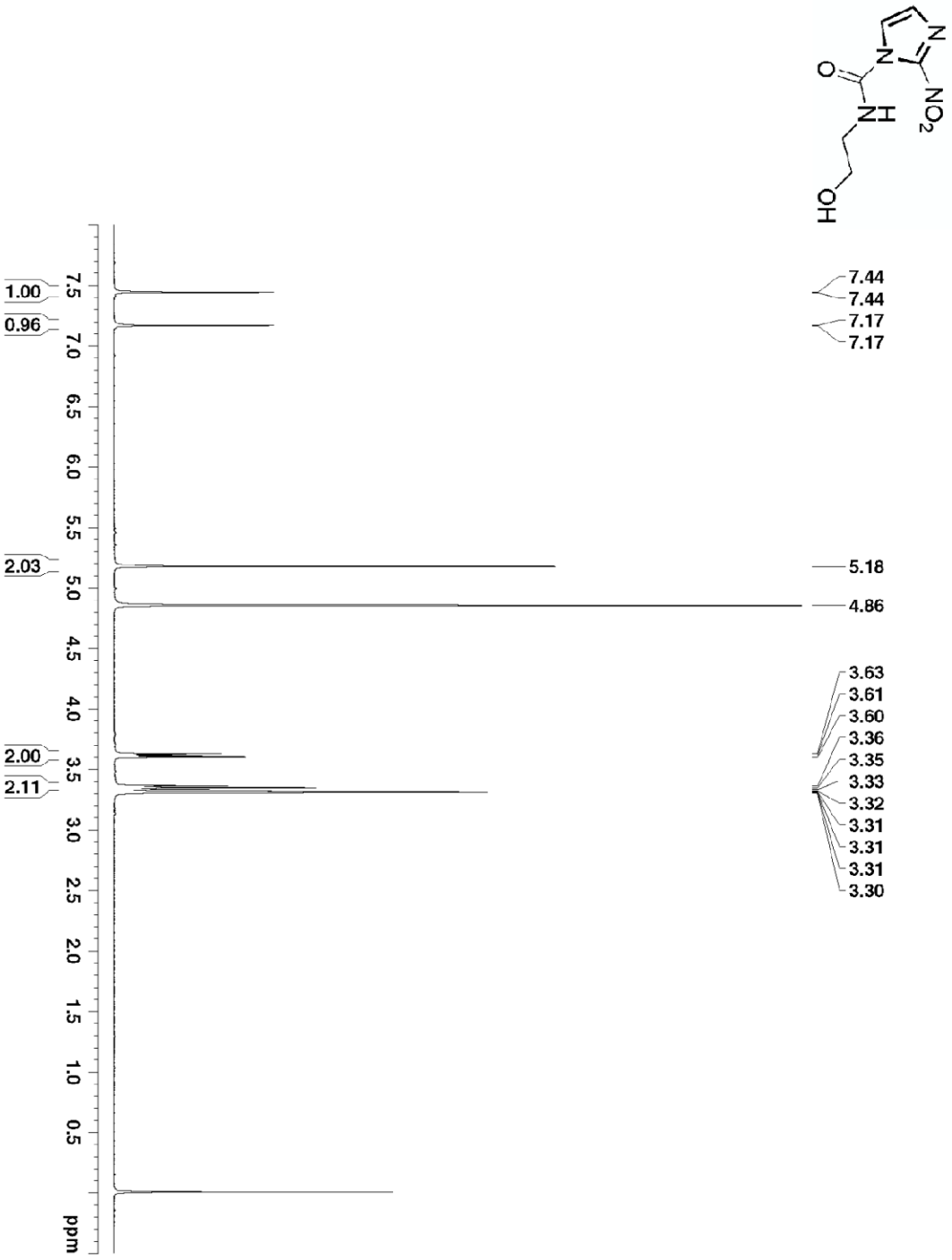
1.00
0.96
2.03
2.00
2.11
7.5
7.0
6.5
6.0
5.5
5.0
4.5
4.0
3.5
3.0
2.5
2.0
1.5
1.0
0.5
ppm
7.44
7.44
7.17
7.17
5.18
4.86
3.63
3.61
3.60
3.36
3.35
3.33
3.32
3.31
3.31
3.31
3.30
O
N
N
NH
NO2
HO

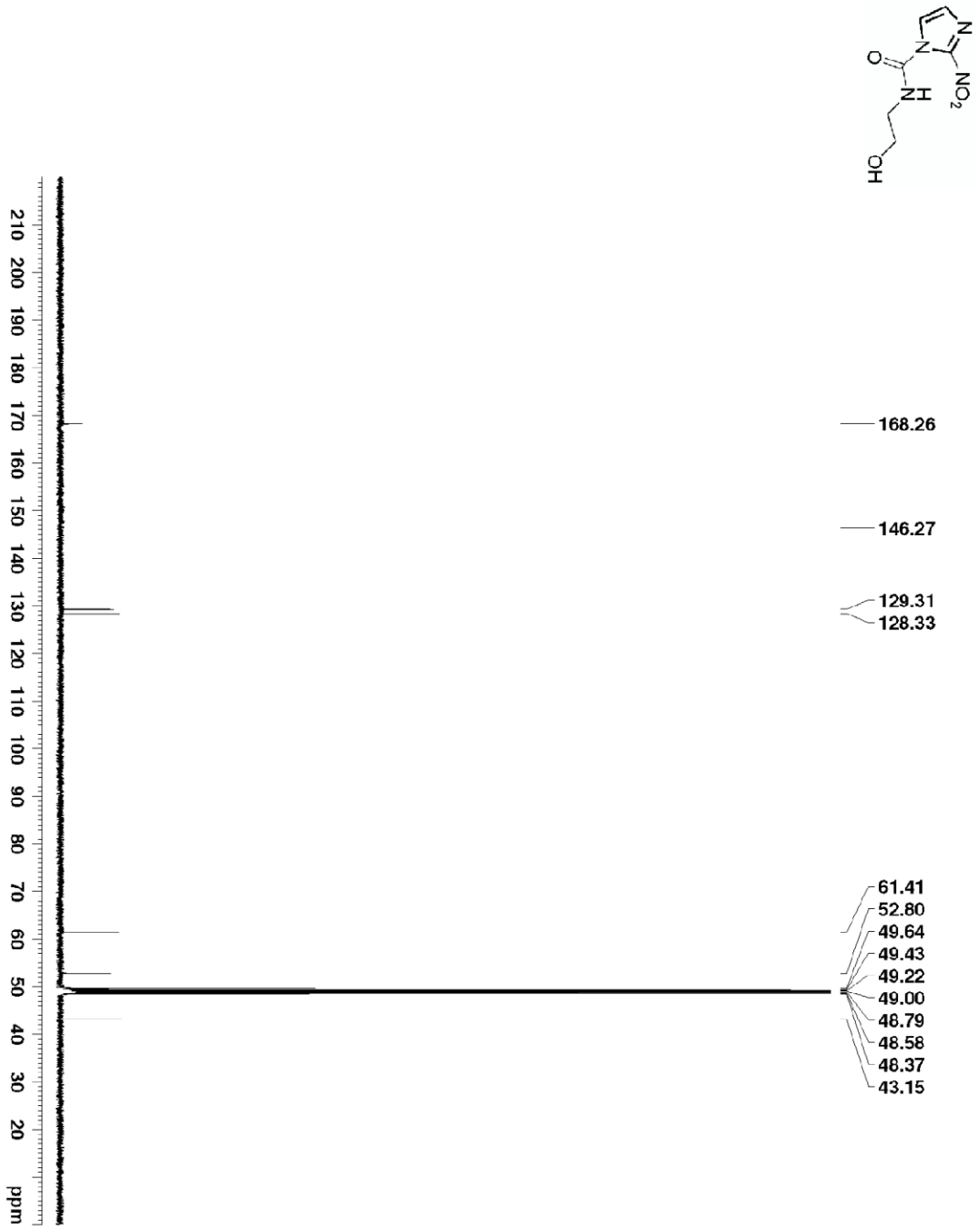
168.26
146.27
129.31
128.33
61.41
52.80
49.64
49.43
49.22
49.00
48.79
48.58
48.37
43.15
ppm

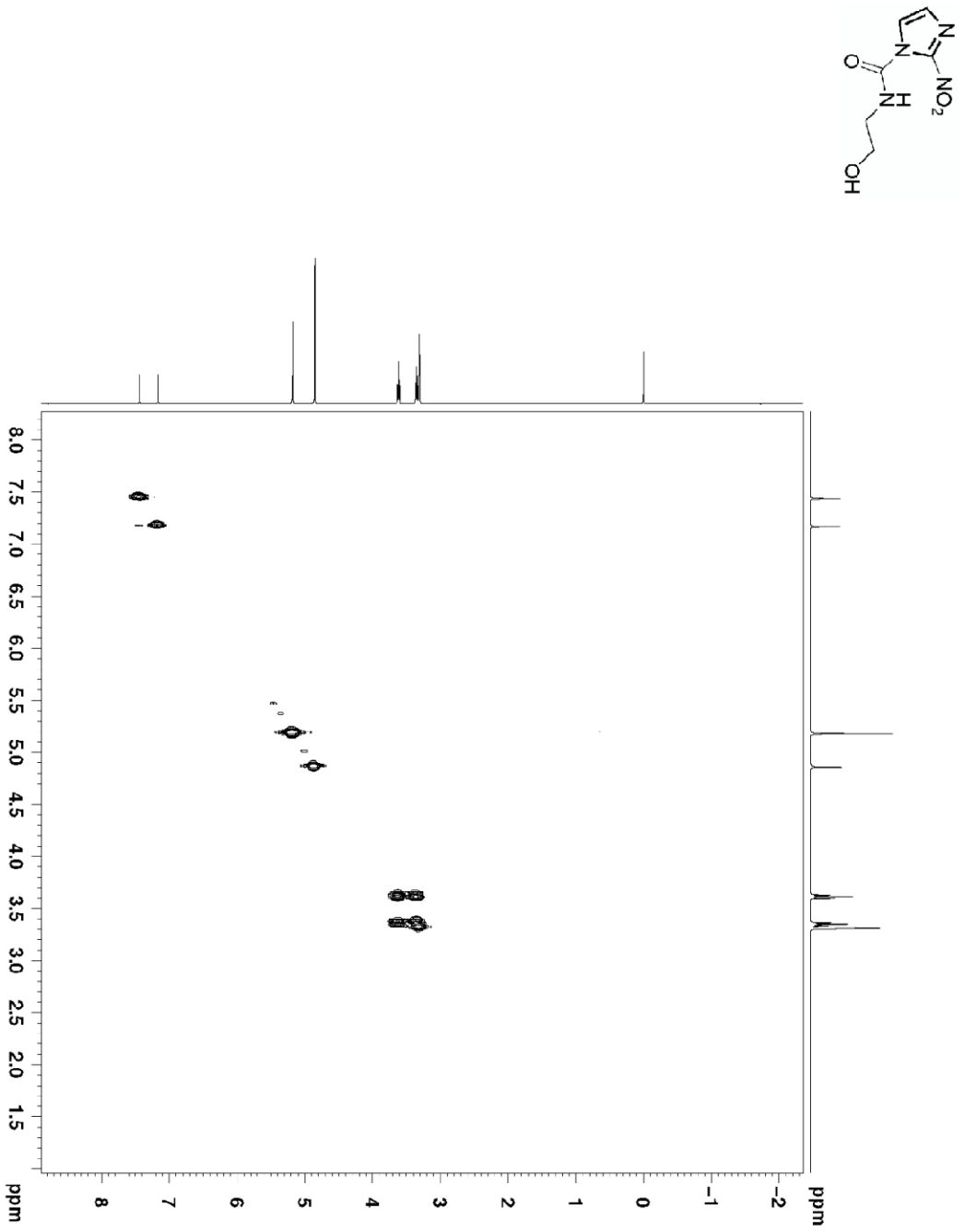
N
N
O
H
N
NO2
OH
8.0 7.5 7.0 6.5 6.0 5.5 5.0 4.5 4.0 3.5 3.0 2.5 2.0 1.5
ppm
8 7 6 5 4 3 2 1 0 −1 −2
ppm

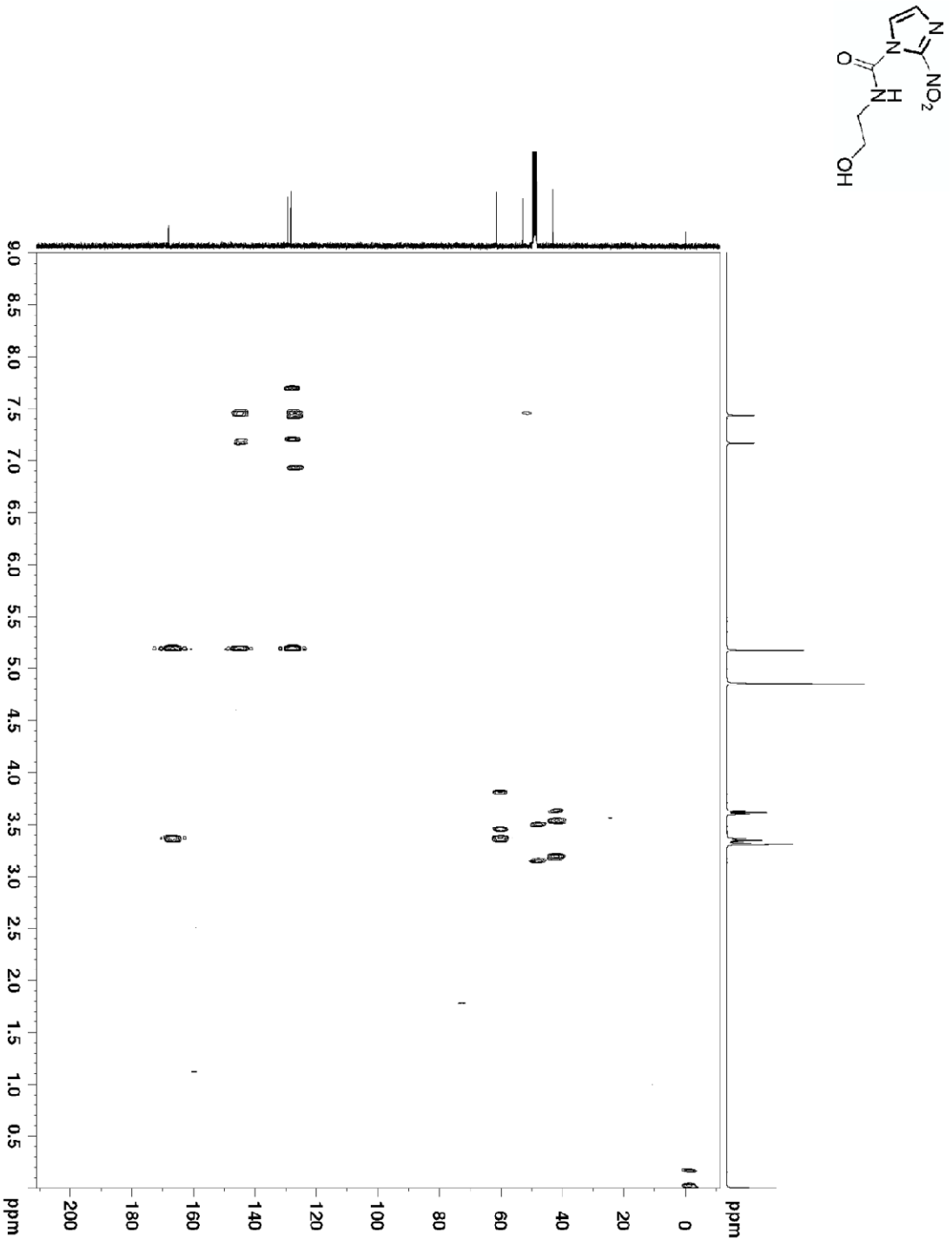
N
N
O
H
N
NO2
OH
9.0
8.5
8.0
7.5
7.0
6.5
6.0
5.5
5.0
4.5
4.0
3.5
3.0
2.5
2.0
1.5
1.0
0.5
ppm
200
180
160
140
120
100
80
60
40
20
0
ppm

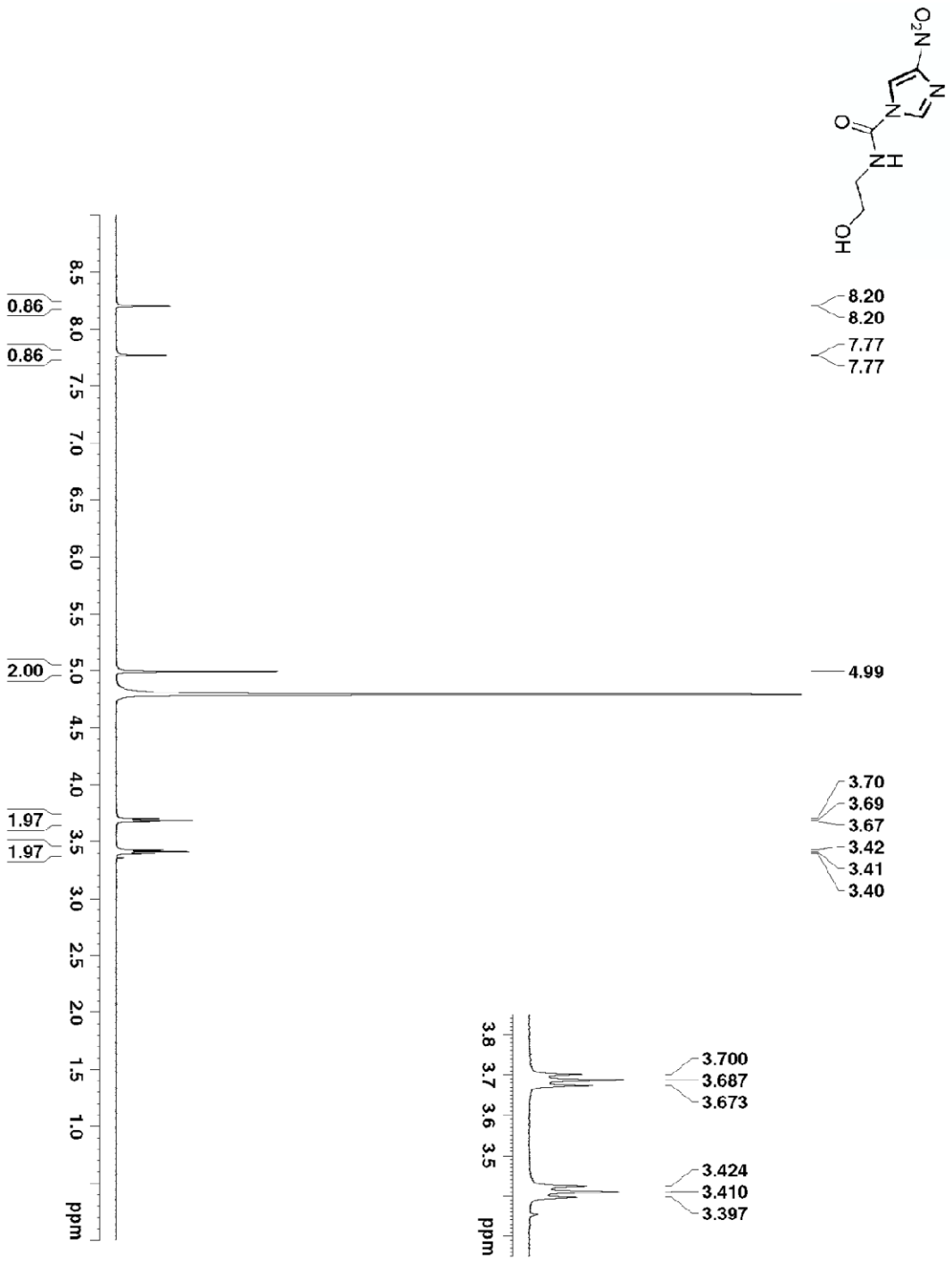
O2N
N
N
O
NH
OH
8.20
8.20
7.77
7.77
4.99
3.70
3.69
3.67
3.42
3.41
3.40
0.86
0.86
2.00
1.97
1.97
8.5 8.0 7.5 7.0 6.5 6.0 5.5 5.0 4.5 4.0 3.5 3.0 2.5 2.0 1.5 1.0 ppm
3.700
3.687
3.673
3.424
3.410
3.397
3.8 3.7 3.6 3.5 ppm

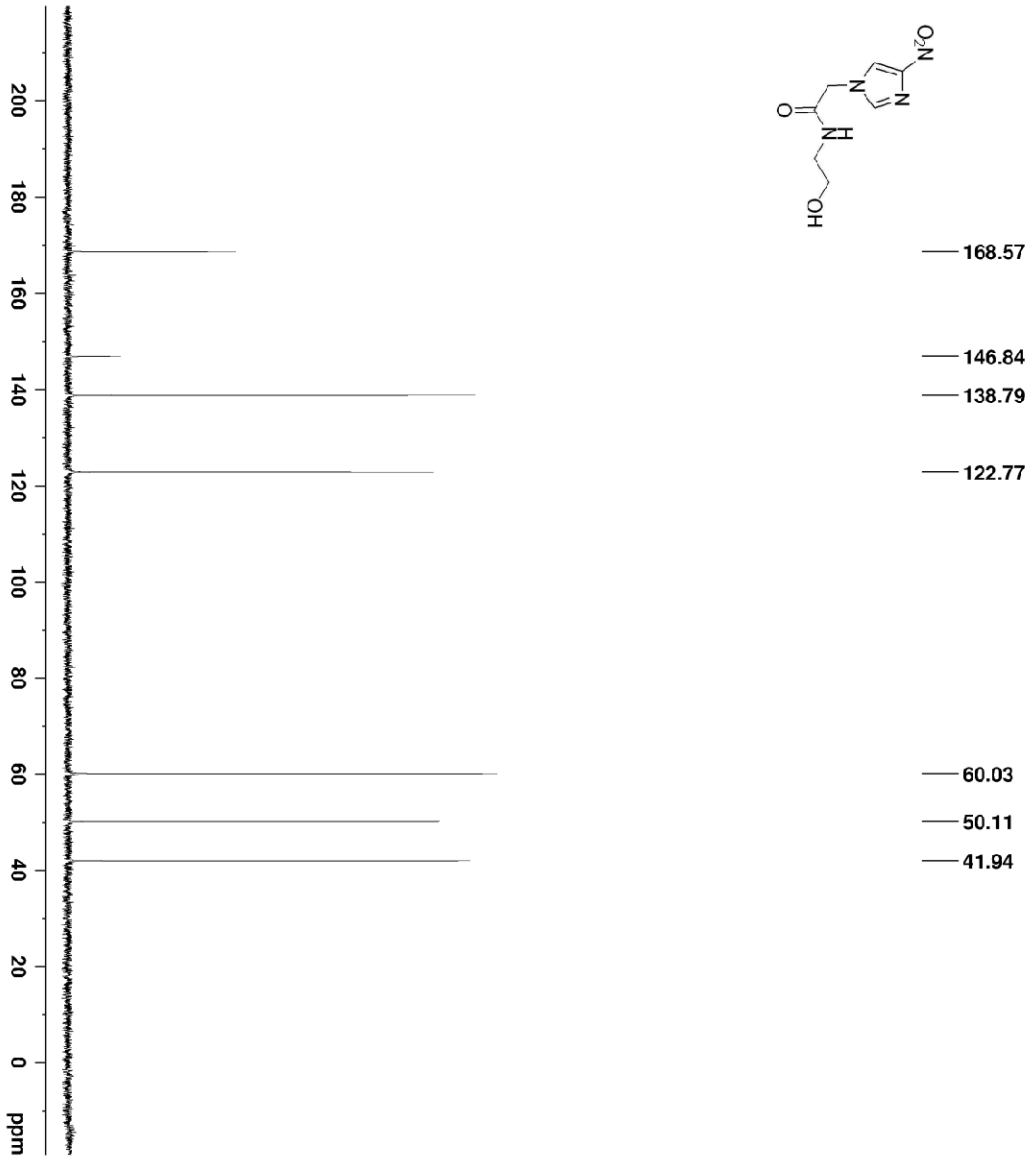
200
180
160
140
120
100
80
60
40
20
0
ppm
O2N
N
N
O
N
H
HO
168.57
146.84
138.79
122.77
60.03
50.11
41.94

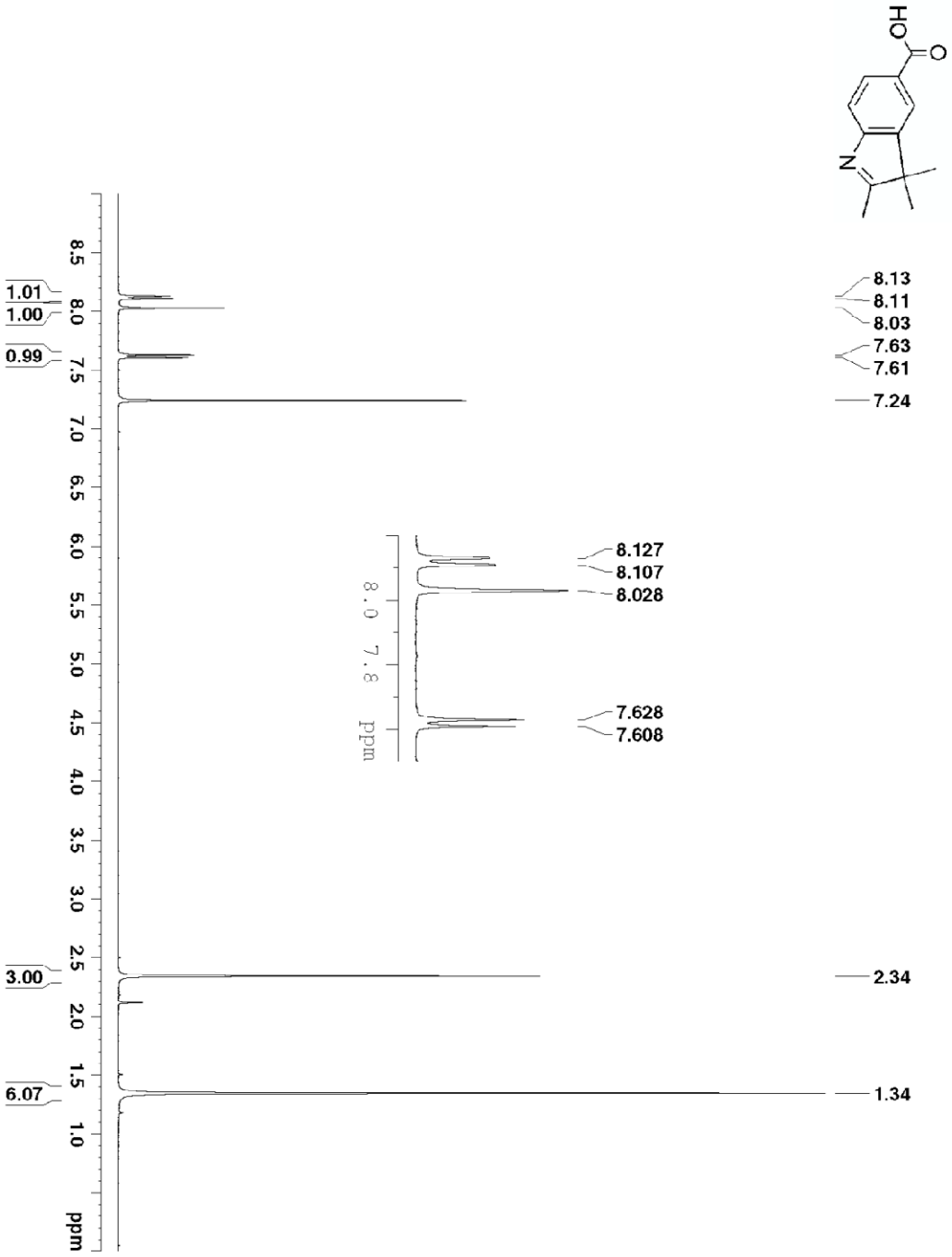
HO
O
N
8.13
8.11
8.03
7.63
7.61
7.24
8.127
8.107
8.028
7.628
7.608
8.0 7.8 ppm
2.34
1.34
1.01
1.00
0.99
3.00
6.07
ppm

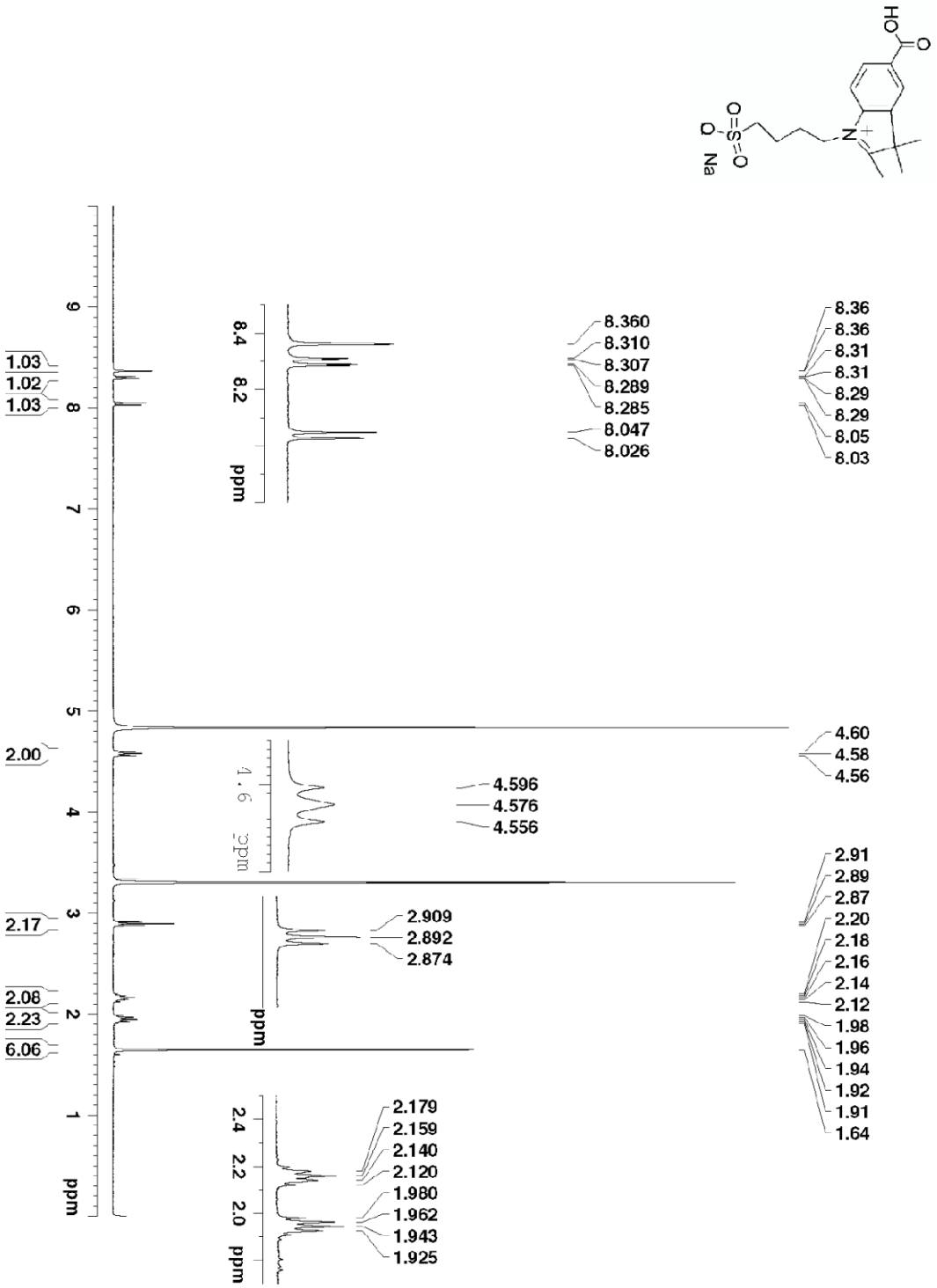
HO
O
O
S
O
O
Na
N+
1.03
1.02
1.03
2.00
2.17
2.08
2.23
6.06
ppm
8.4
8.2
8.360
8.310
8.307
8.289
8.285
8.047
8.026
8.36
8.36
8.31
8.31
8.29
8.29
8.05
8.03
4.60
4.58
4.56
4.596
4.576
4.556
2.91
2.89
2.87
2.20
2.18
2.16
2.14
2.12
1.98
1.96
1.94
1.92
1.91
1.64
2.909
2.892
2.874
2.179
2.159
2.140
2.120
1.980
1.962
1.943
1.925
2.4
2.2
2.0

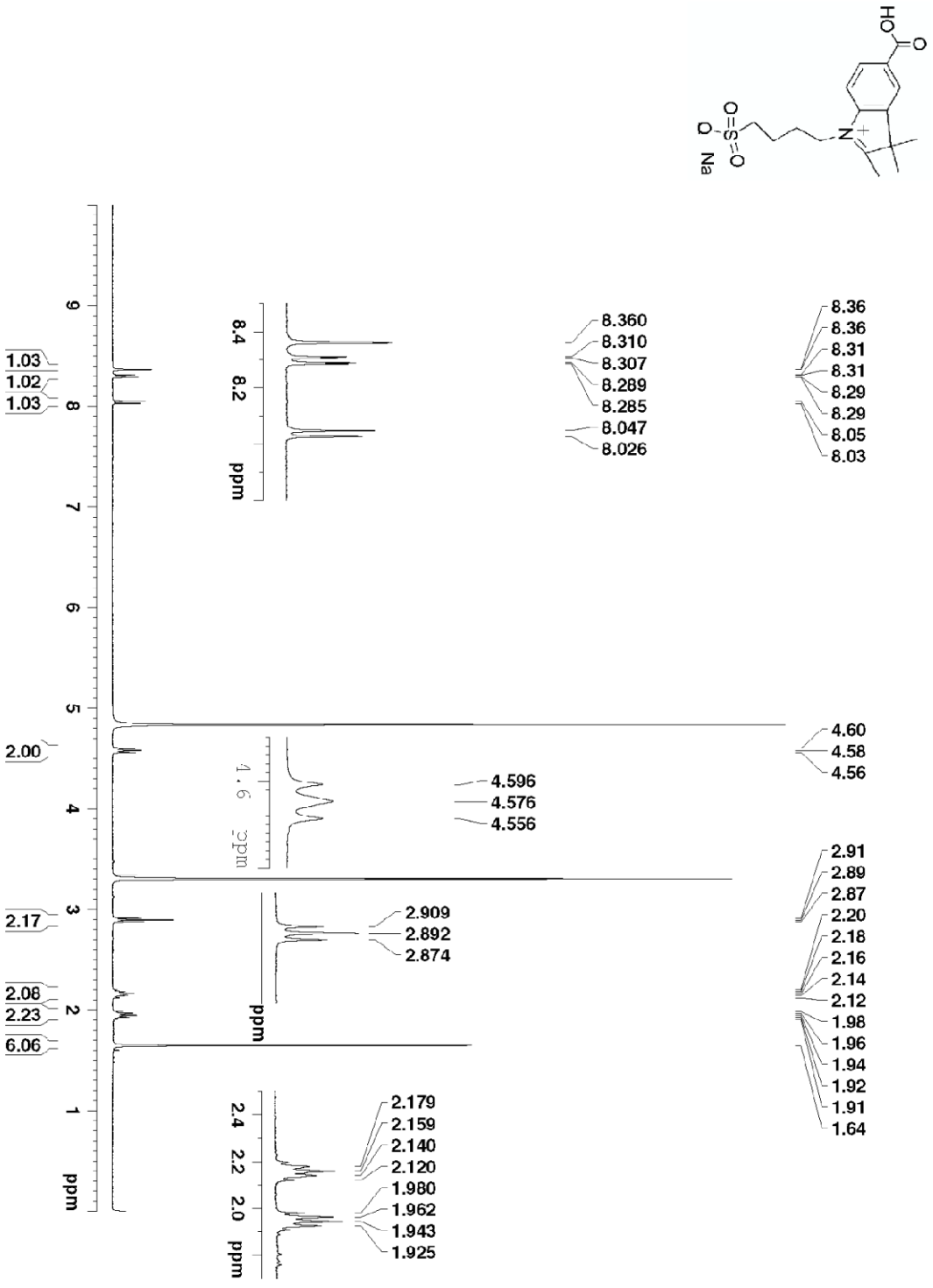
HO
O
O
O
S
O
O
Na
N+
1.03
1.02
1.03
2.00
2.17
2.08
2.23
6.06
8.360
8.310
8.307
8.289
8.285
8.047
8.026
8.36
8.36
8.31
8.31
8.29
8.29
8.05
8.03
4.596
4.576
4.556
4.60
4.58
4.56
2.909
2.892
2.874
2.91
2.89
2.87
2.20
2.18
2.16
2.14
2.12
1.98
1.96
1.94
1.92
1.91
1.64
2.179
2.159
2.140
2.120
1.980
1.962
1.943
1.925
ppm

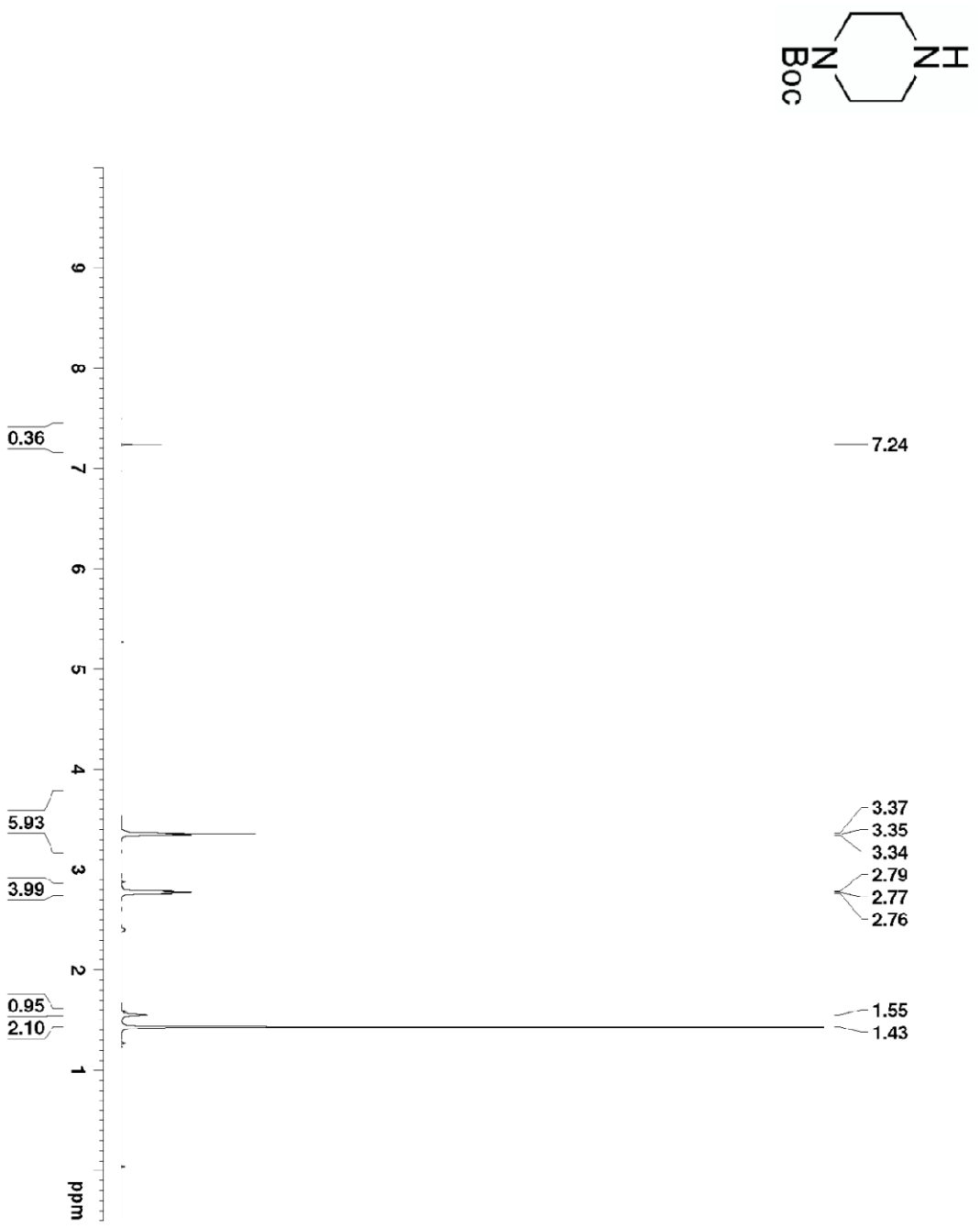
Boc
N
NH
0.36
5.93
3.99
0.95
2.10
7.24
3.37
3.35
3.34
2.79
2.77
2.76
1.55
1.43
ppm

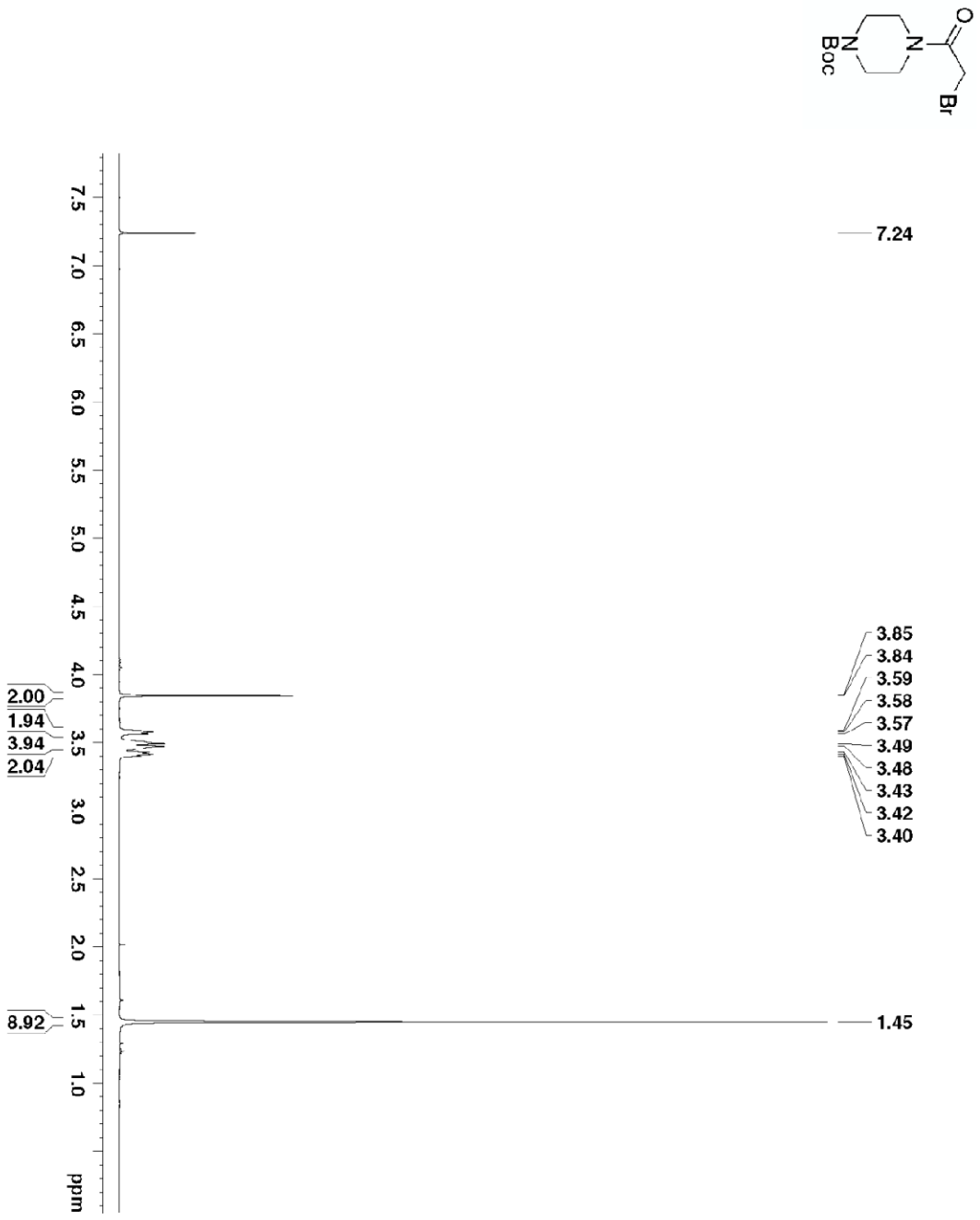
Boc
N
N
O
Br
7.24
3.85
3.84
3.59
3.58
3.57
3.49
3.48
3.43
3.42
3.40
1.45
2.00
1.94
3.94
2.04
8.92
7.5
7.0
6.5
6.0
5.5
5.0
4.5
4.0
3.5
3.0
2.5
2.0
1.5
1.0
ppm

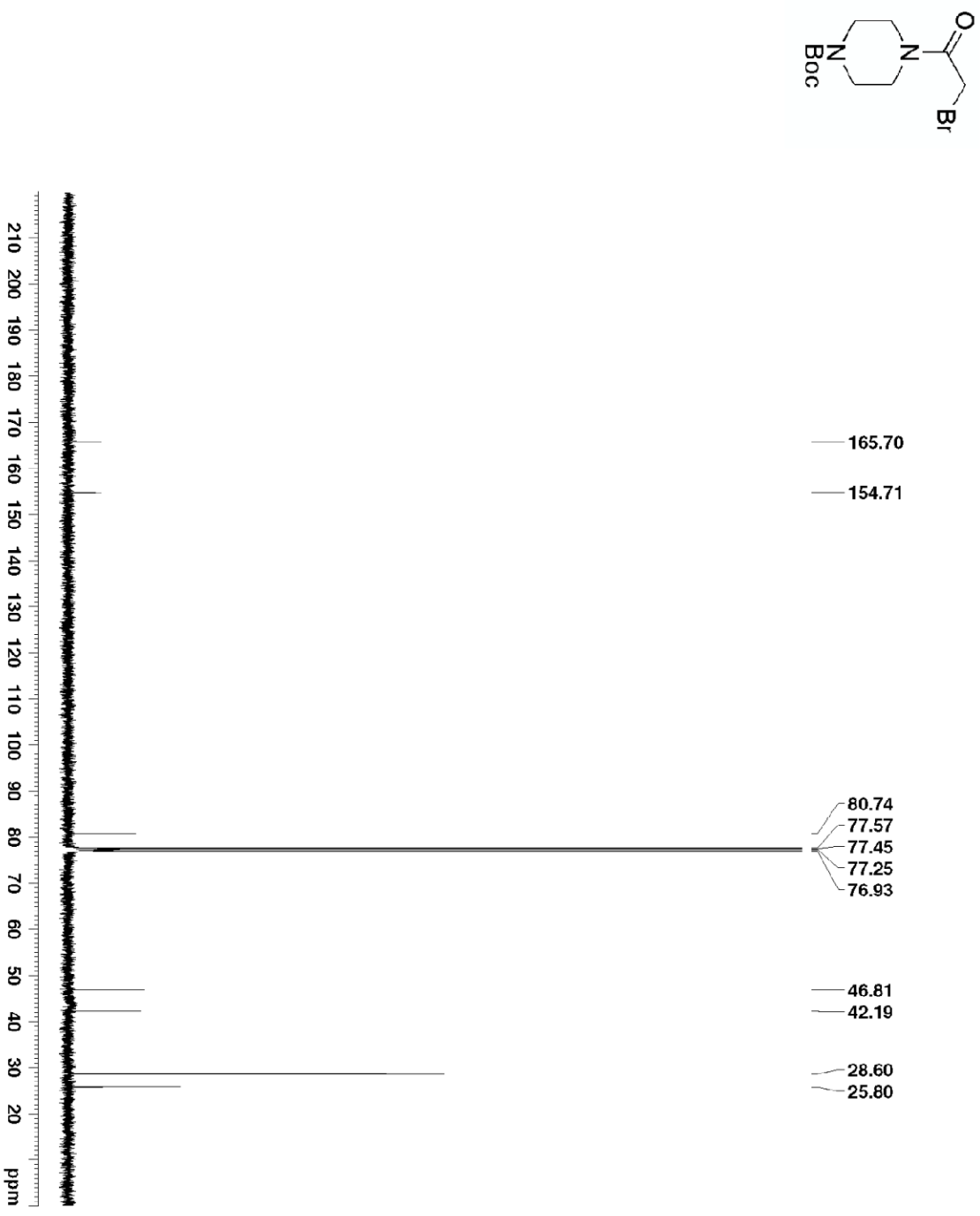
Boc
N
N
O
Br
165.70
154.71
80.74
77.57
77.45
77.25
76.93
46.81
42.19
28.60
25.80
210 200 190 180 170 160 150 140 130 120 110 100 90 80 70 60 50 40 30 20 ppm

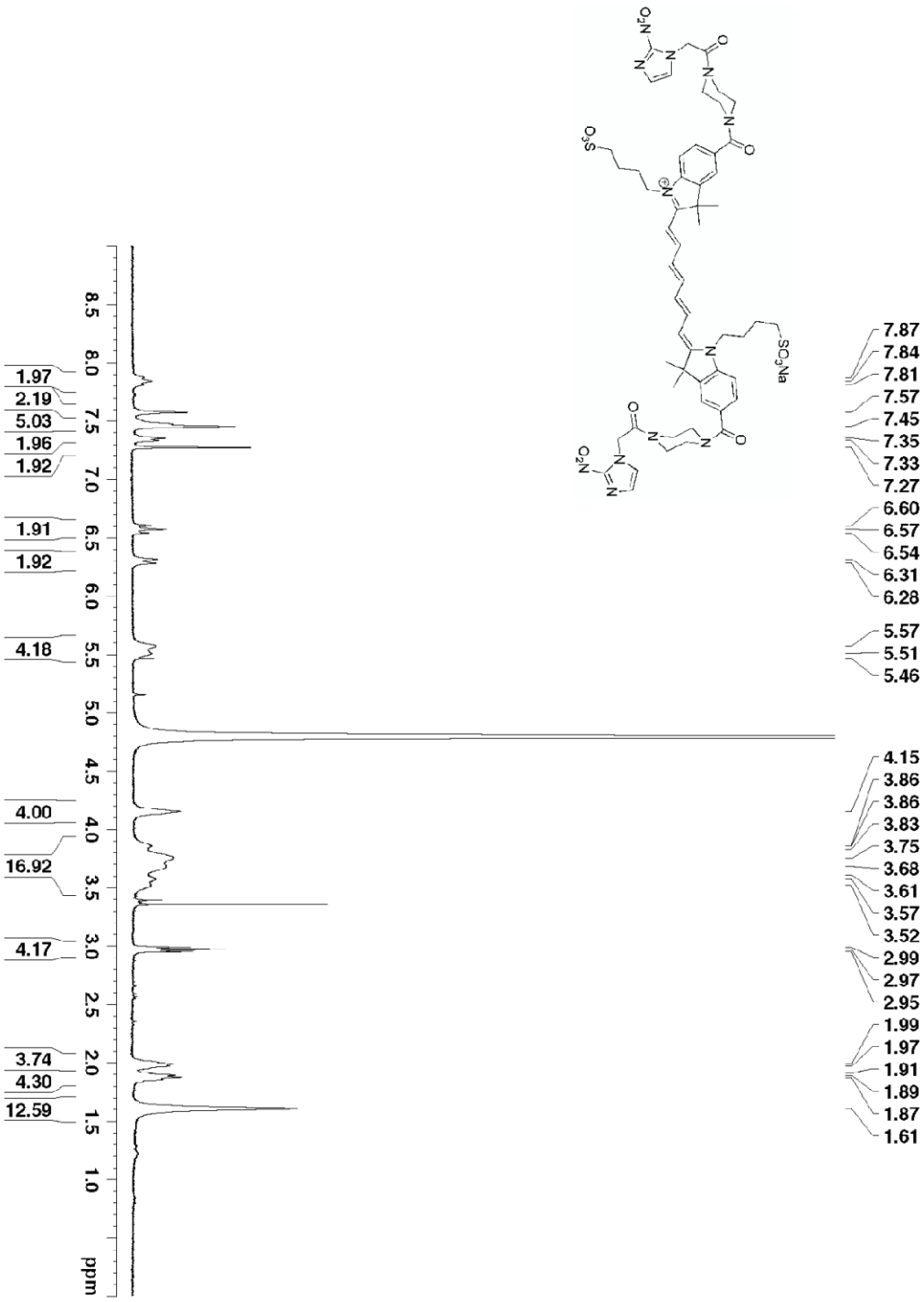
1.97
2.19
5.03
1.96
1.92
1.91
1.92
4.18
4.00
16.92
4.17
3.74
4.30
12.59
7.87
7.84
7.81
7.57
7.45
7.35
7.33
7.27
6.60
6.57
6.54
6.31
6.28
5.57
5.51
5.46
4.15
3.86
3.86
3.83
3.75
3.68
3.61
3.57
3.52
2.99
2.97
2.95
1.99
1.97
1.91
1.89
1.87
1.61
ppm

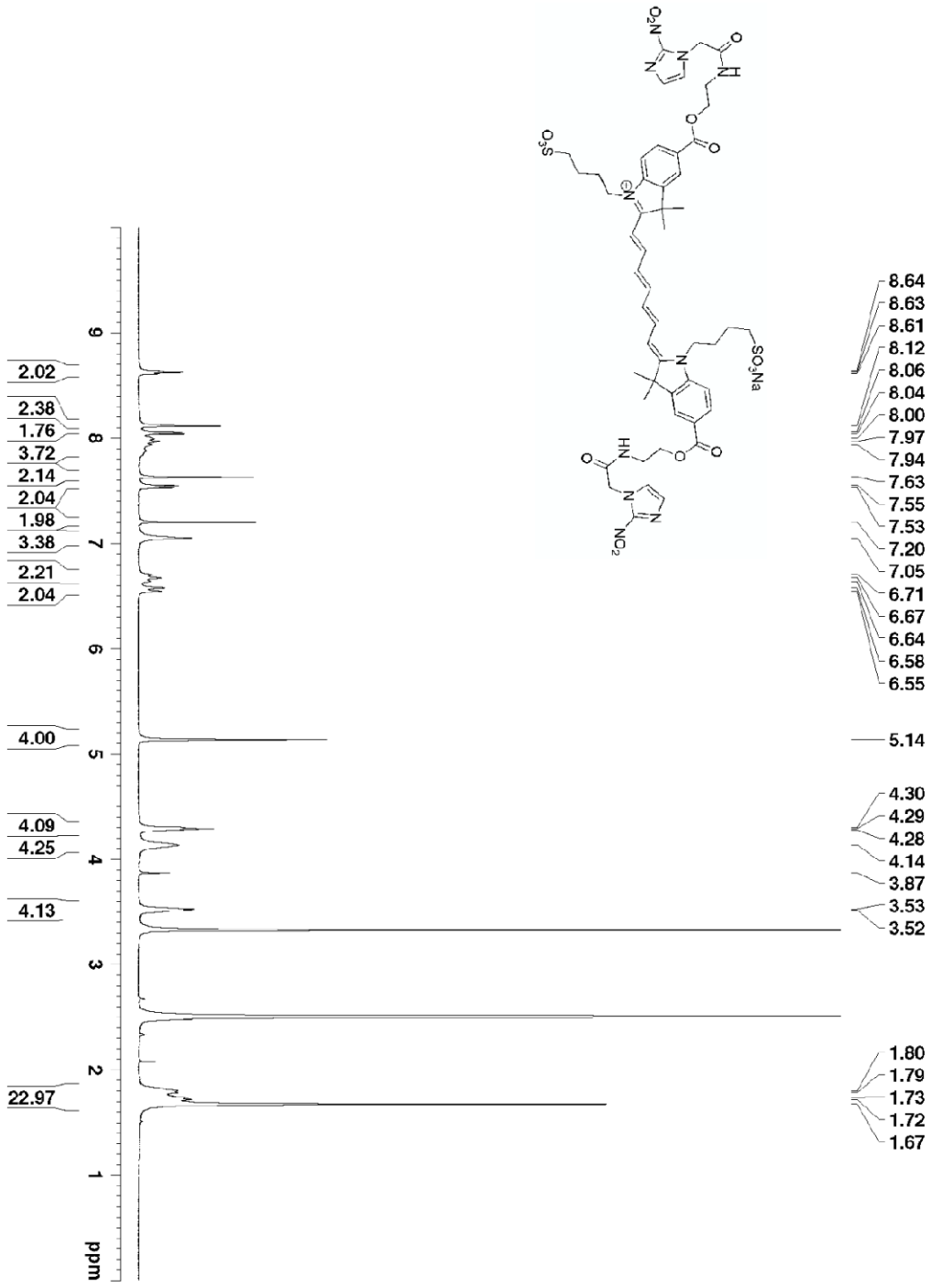
2.02
2.38
1.76
3.72
2.14
2.04
1.98
3.38
2.21
2.04
4.00
4.09
4.25
4.13
22.97
ppm
8.64
8.63
8.61
8.12
8.06
8.04
8.00
7.97
7.94
7.63
7.55
7.53
7.20
7.05
6.71
6.67
6.64
6.58
6.55
5.14
4.30
4.29
4.28
4.14
3.87
3.53
3.52
1.80
1.79
1.73
1.72
1.67

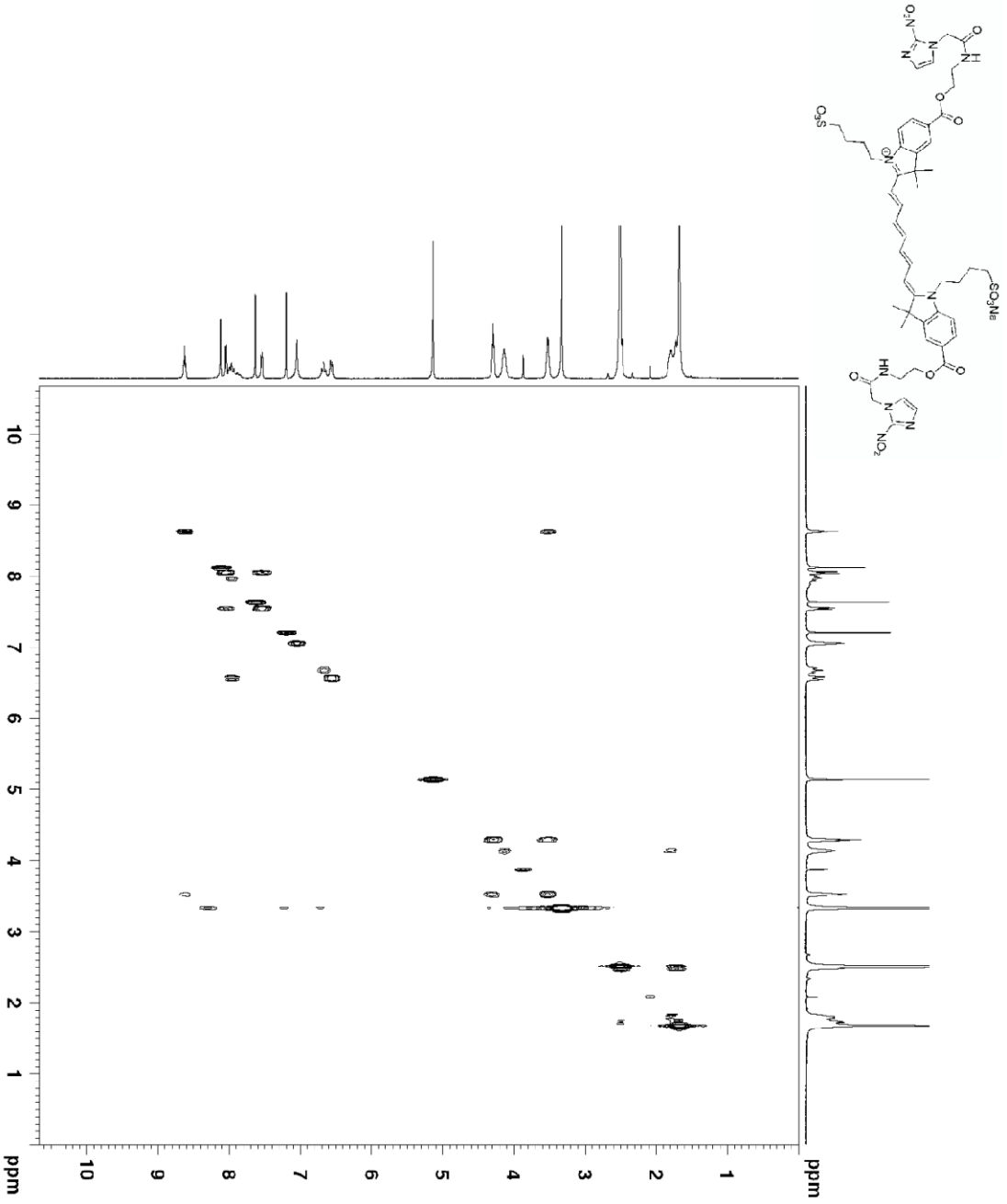
ppm
ppm

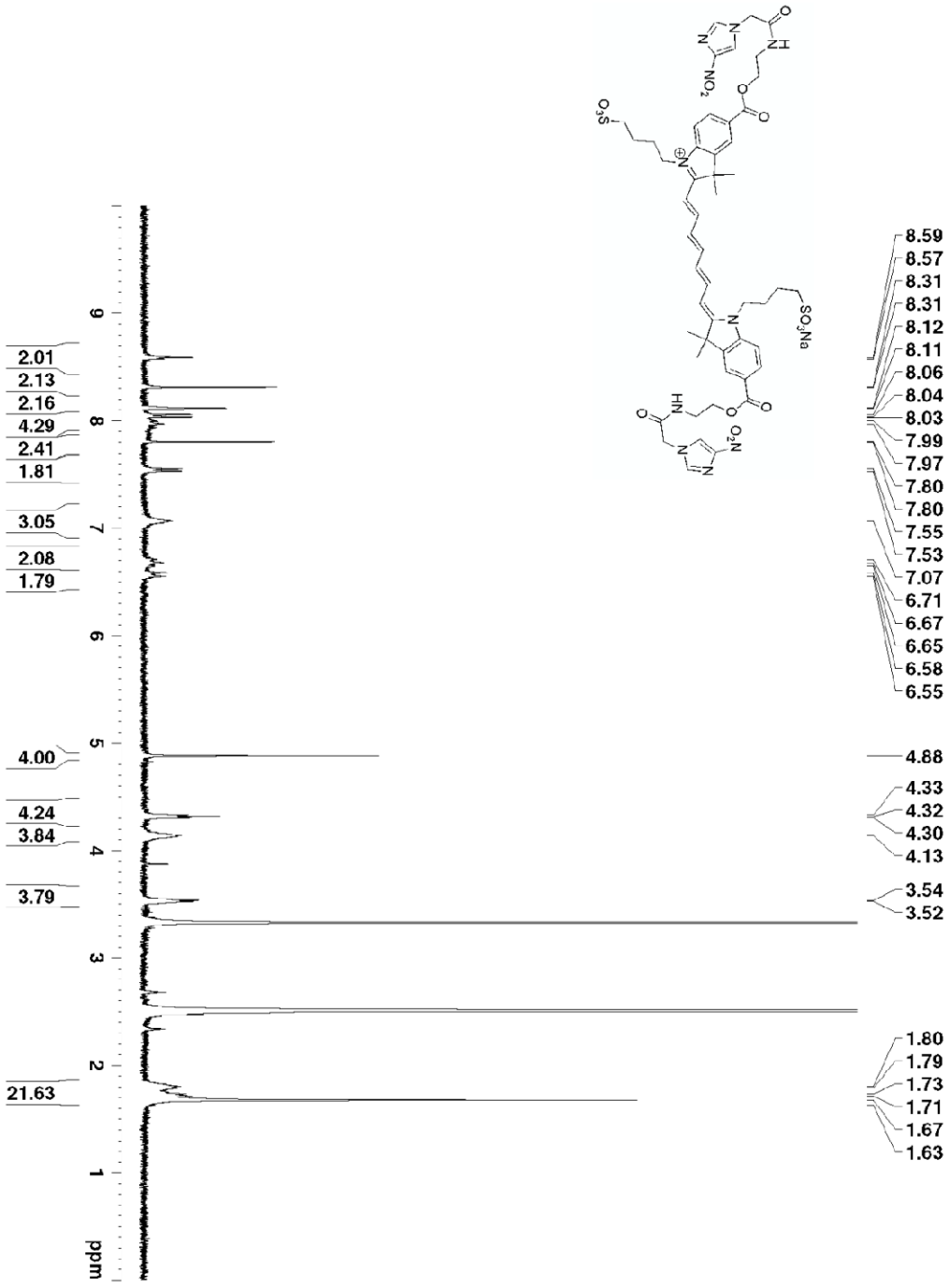
8.59
8.57
8.31
8.31
8.12
8.11
8.06
8.04
8.03
7.99
7.97
7.80
7.80
7.55
7.53
7.07
6.71
6.67
6.65
6.58
6.55
4.88
4.33
4.32
4.30
4.13
3.54
3.52
1.80
1.79
1.73
1.71
1.67
1.63
2.01
2.13
2.16
4.29
2.41
1.81
3.05
2.08
1.79
4.00
4.24
3.84
3.79
21.63
ppm

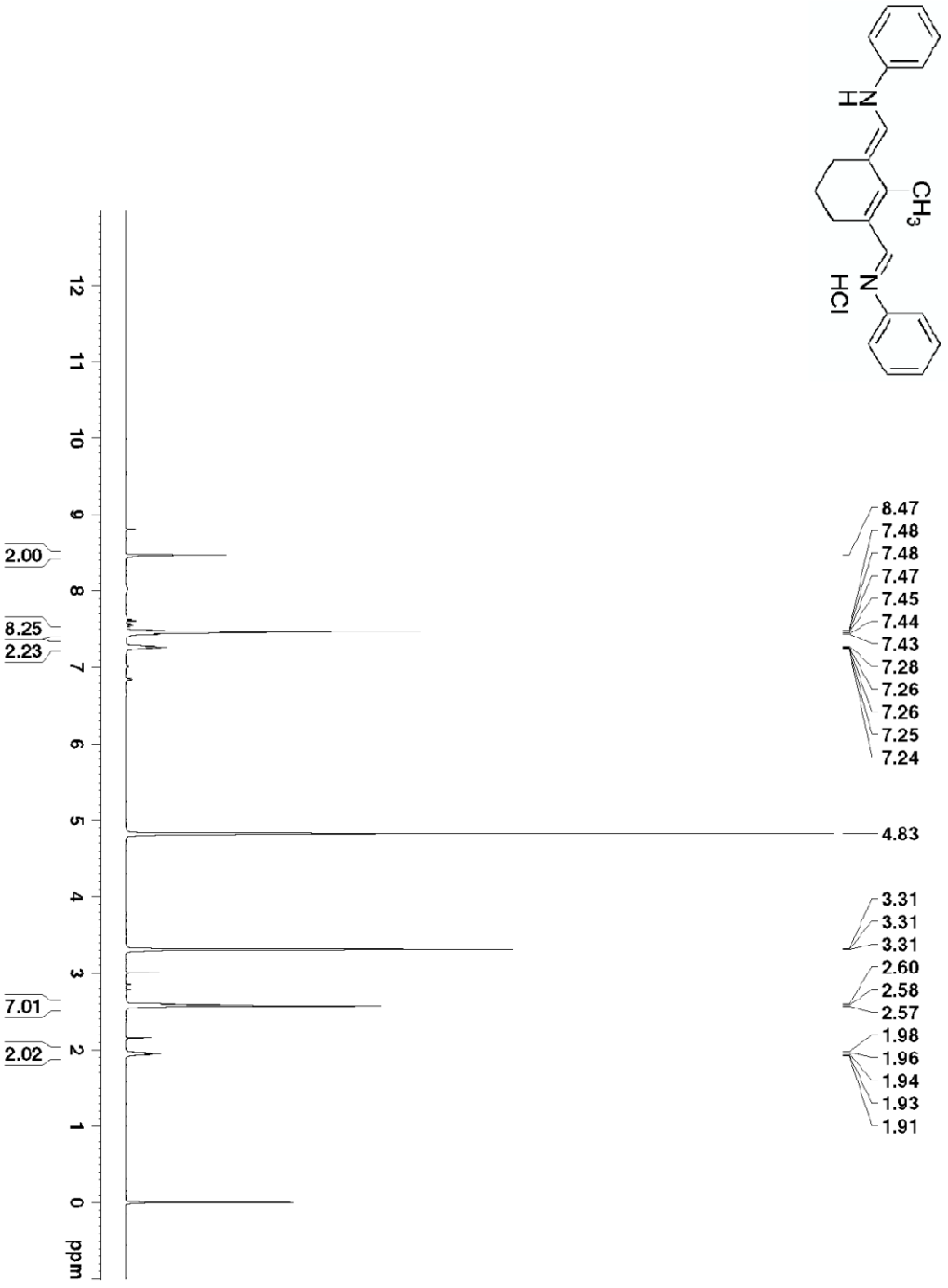
HCl
N
N
CH3
8.47
7.48
7.48
7.47
7.45
7.44
7.43
7.28
7.26
7.26
7.25
7.24
4.83
3.31
3.31
3.31
2.60
2.58
2.57
1.98
1.96
1.94
1.93
1.91
2.00
8.25
2.23
7.01
2.02
ppm

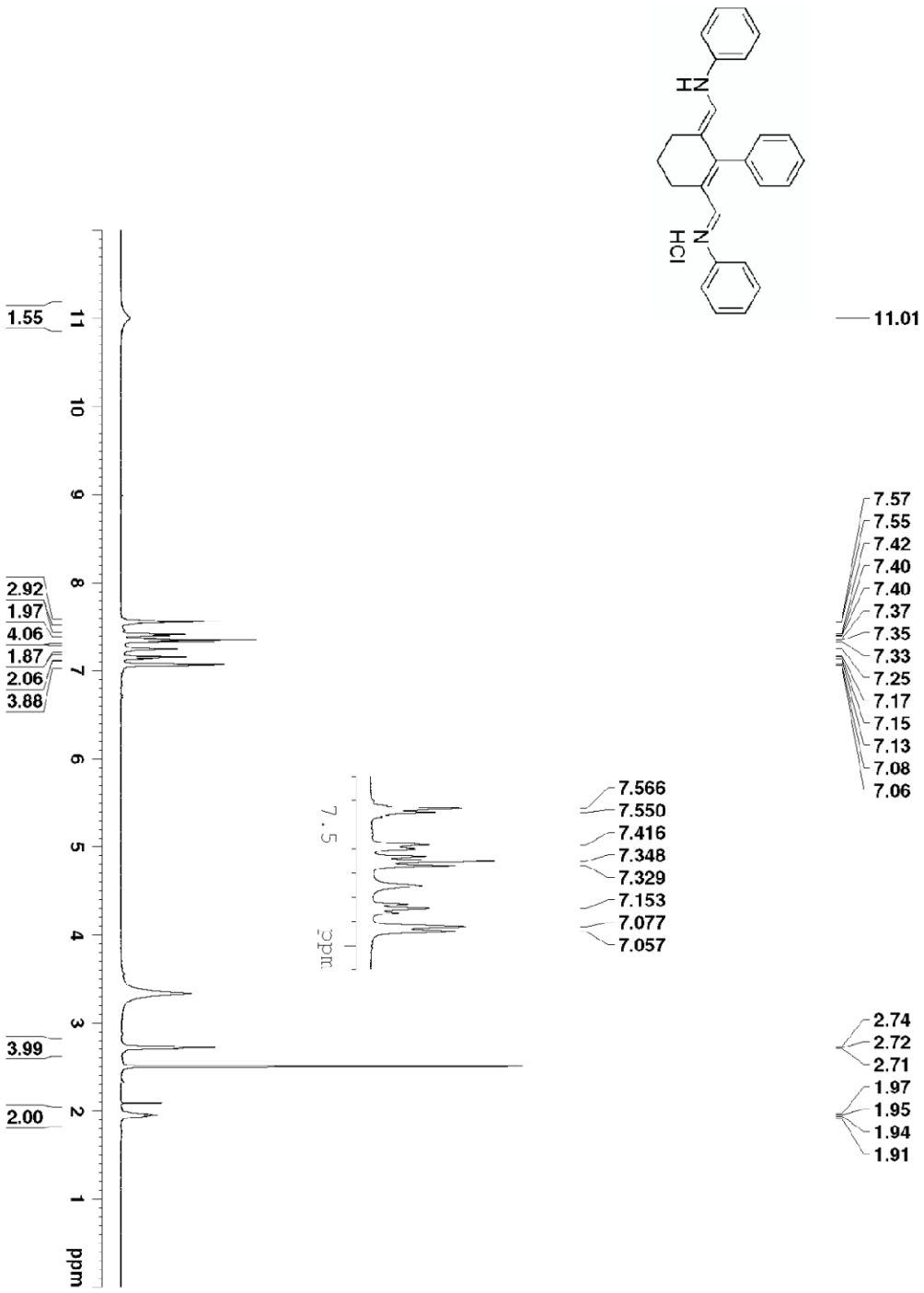
HN
HCl
N
11.01
1.55
2.92
1.97
4.06
1.87
2.06
3.88
3.99
2.00
7.57
7.55
7.42
7.40
7.40
7.37
7.35
7.33
7.25
7.17
7.15
7.13
7.08
7.06
7.566
7.550
7.416
7.348
7.329
7.153
7.077
7.057
2.74
2.72
2.71
1.97
1.95
1.94
1.91
7.5
ppm
ppm

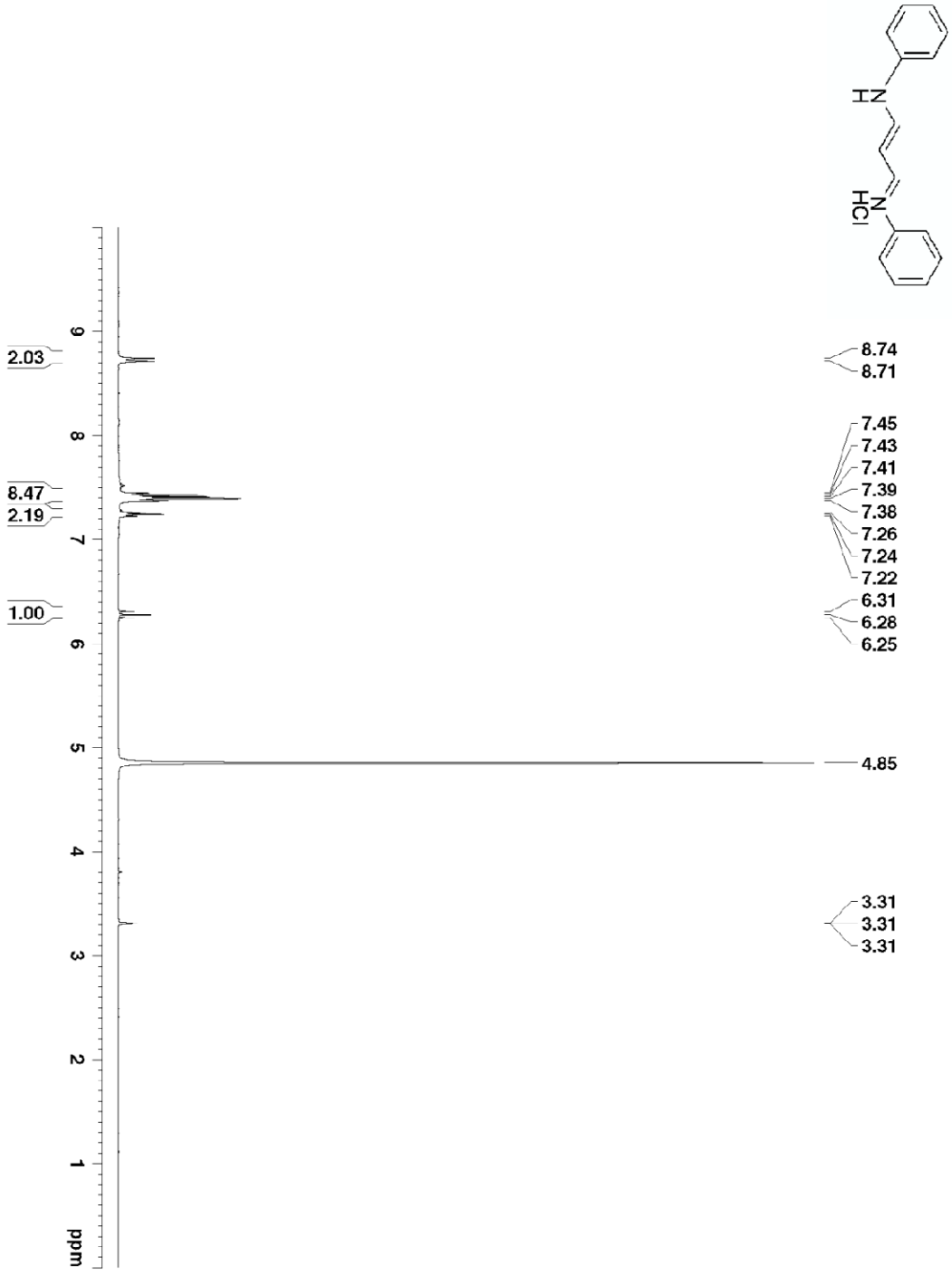
2.03
8.47
2.19
1.00
9
8
7
6
5
4
3
2
1
ppm
8.74
8.71
7.45
7.43
7.41
7.39
7.38
7.26
7.24
7.22
6.31
6.28
6.25
4.85
3.31
3.31
3.31
HN
HCl

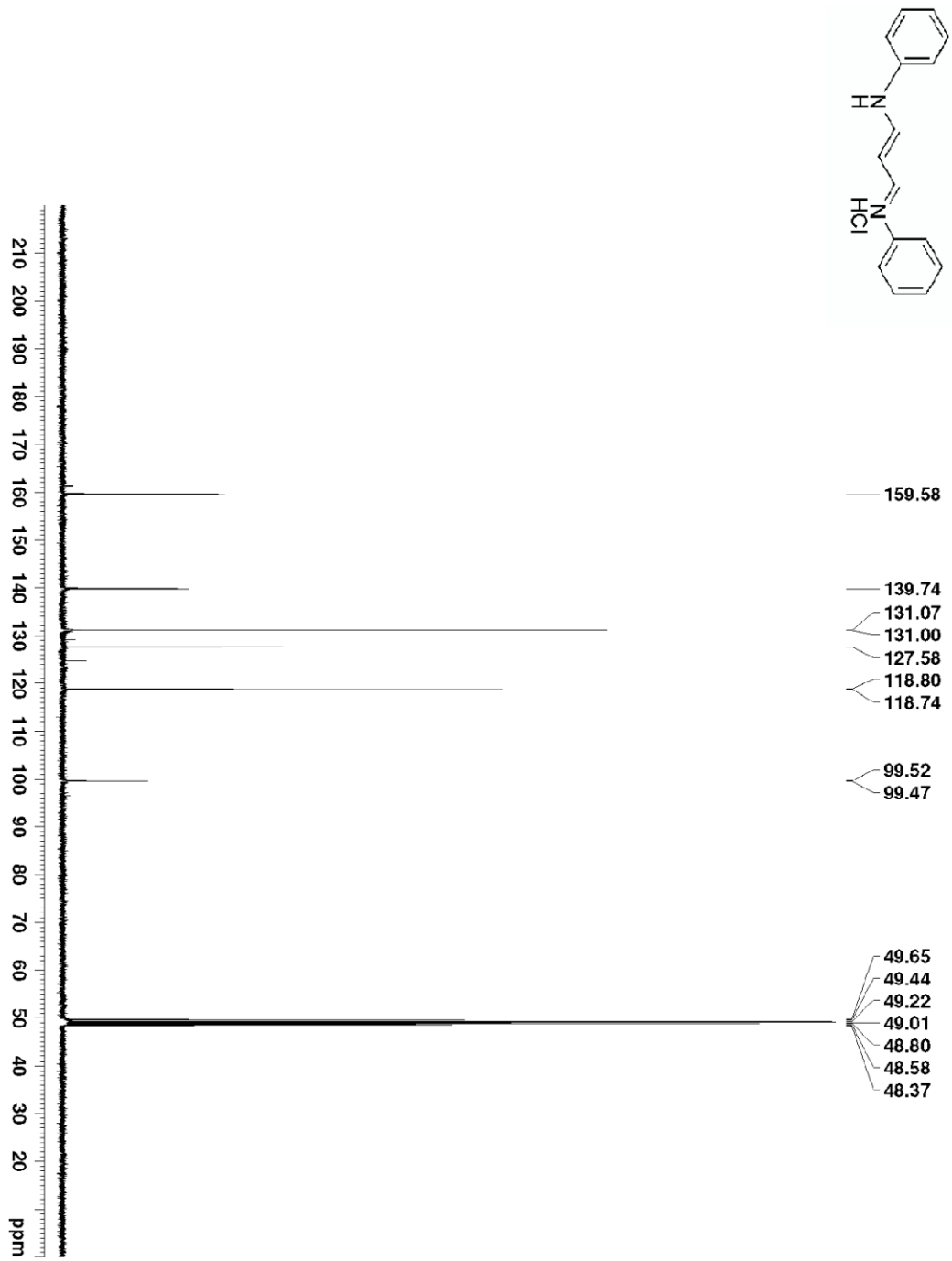
HN
HCl
N
159.58
139.74
131.07
131.00
127.58
118.80
118.74
99.52
99.47
49.65
49.44
49.22
49.01
48.80
48.58
48.37
210 200 190 180 170 160 150 140 130 120 110 100 90 80 70 60 50 40 30 20
ppm

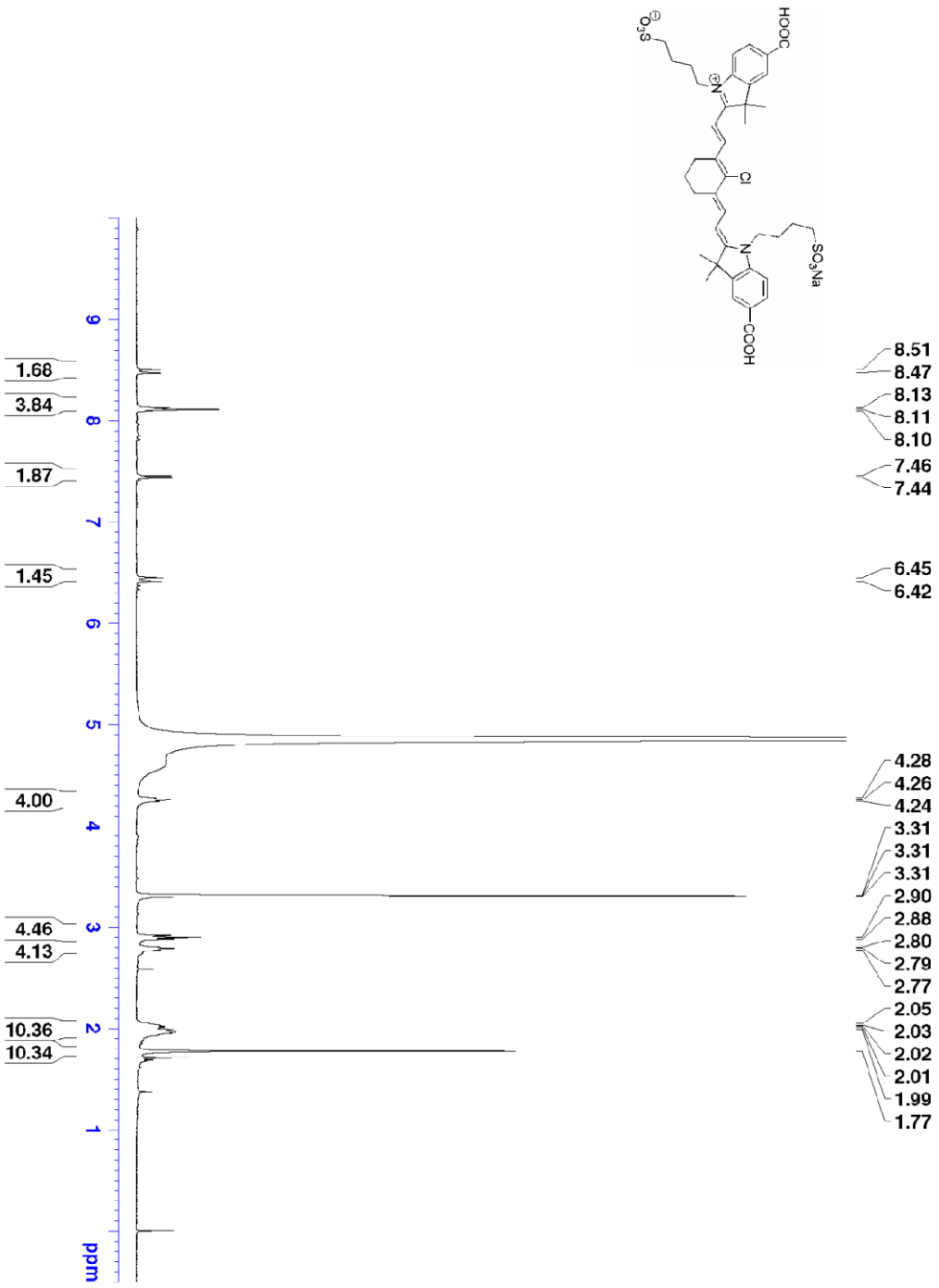
HOOC
Cl
SO3Na
COOH
1.68
3.84
1.87
1.45
4.00
4.46
4.13
10.36
10.34
8.51
8.47
8.13
8.11
8.10
7.46
7.44
6.45
6.42
4.28
4.26
4.24
3.31
3.31
3.31
2.90
2.88
2.80
2.79
2.77
2.05
2.03
2.02
2.01
1.99
1.77
ppm

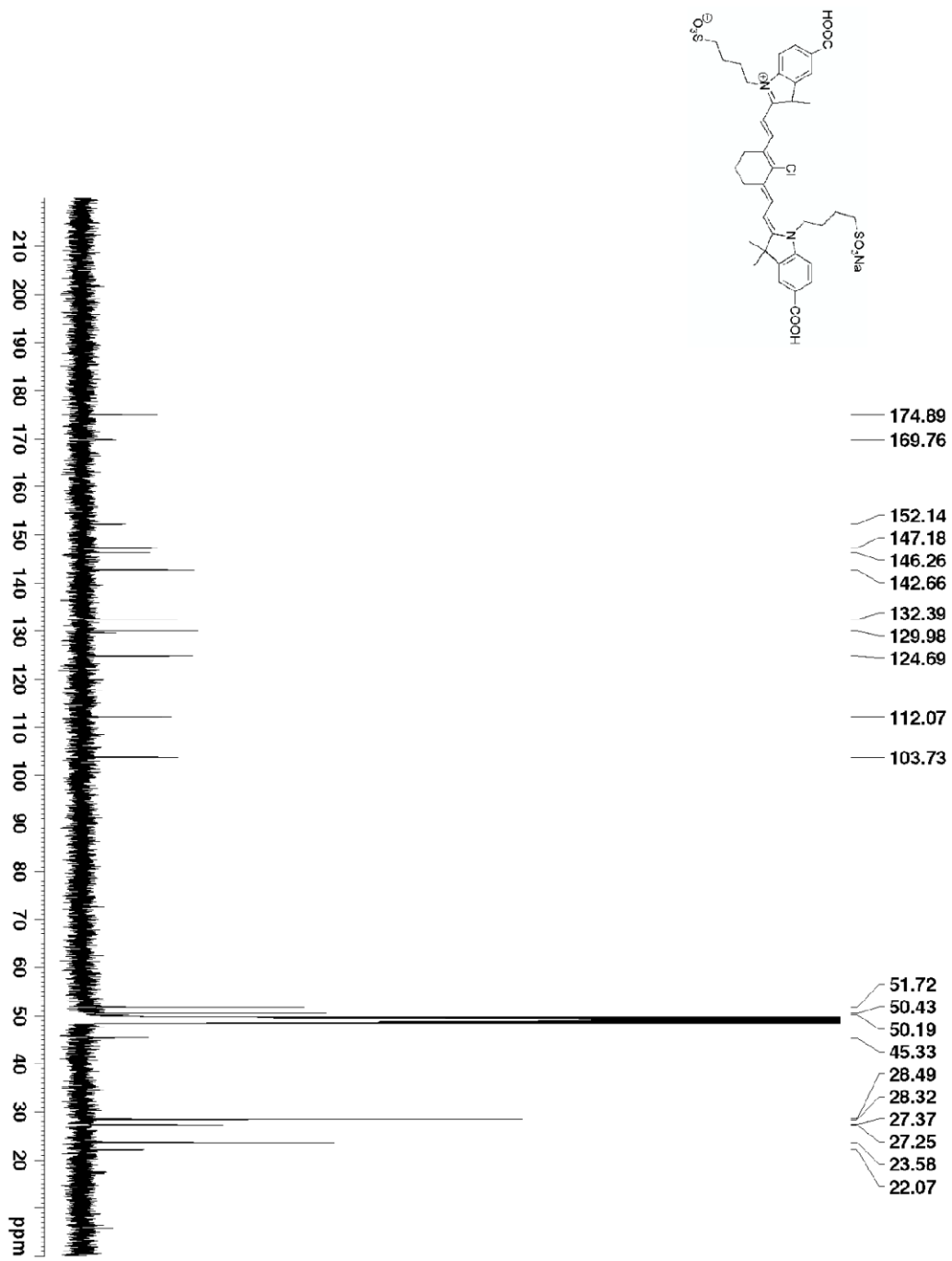
HOOC
Cl
N
SO3Na
COOH
174.89
169.76
152.14
147.18
146.26
142.66
132.39
129.98
124.69
112.07
103.73
51.72
50.43
50.19
45.33
28.49
28.32
27.37
27.25
23.58
22.07
ppm

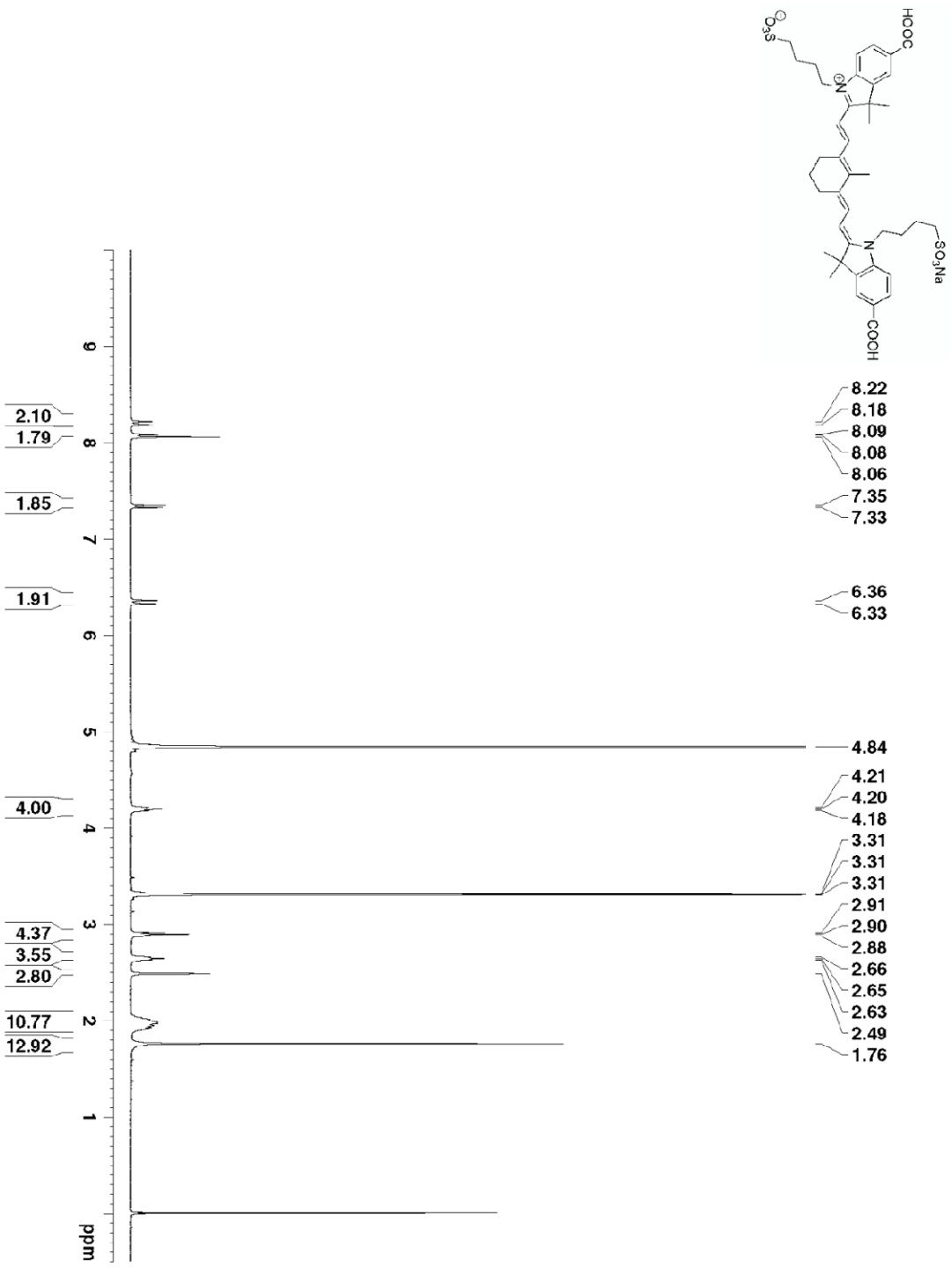
HOOC
$^{-}O_3S$
N
SO_3Na
COOH
8.22
8.18
8.09
8.08
8.06
7.35
7.33
6.36
6.33
4.84
4.21
4.20
4.18
3.31
3.31
3.31
2.91
2.90
2.88
2.66
2.65
2.63
2.49
1.76
2.10
1.79
1.85
1.91
4.00
4.37
3.55
2.80
10.77
12.92
ppm

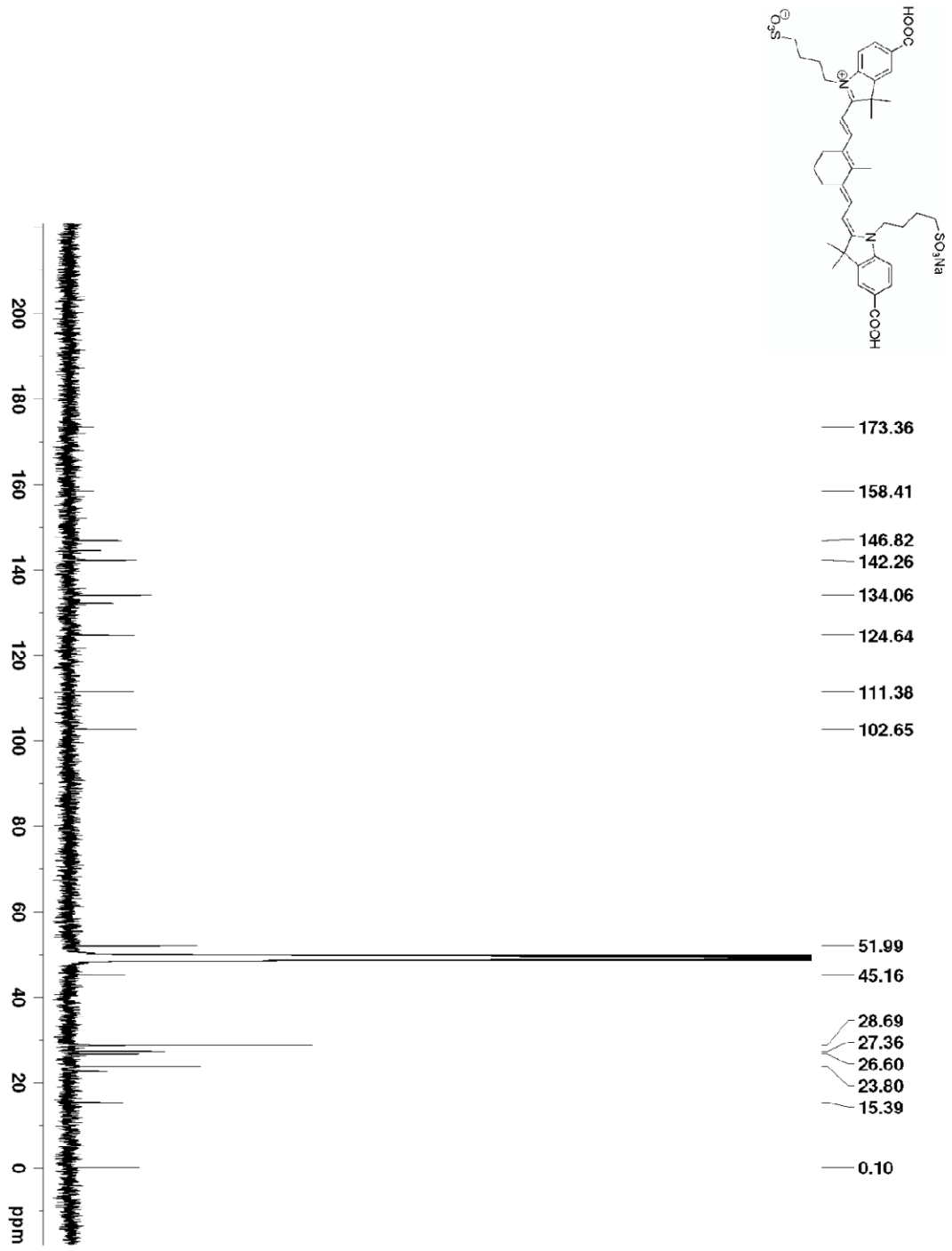
HOOC
SO3Na
COOH
173.36
158.41
146.82
142.26
134.06
124.64
111.38
102.65
51.99
45.16
28.69
27.36
26.60
23.80
15.39
0.10
200
180
160
140
120
100
80
60
40
20
0
ppm

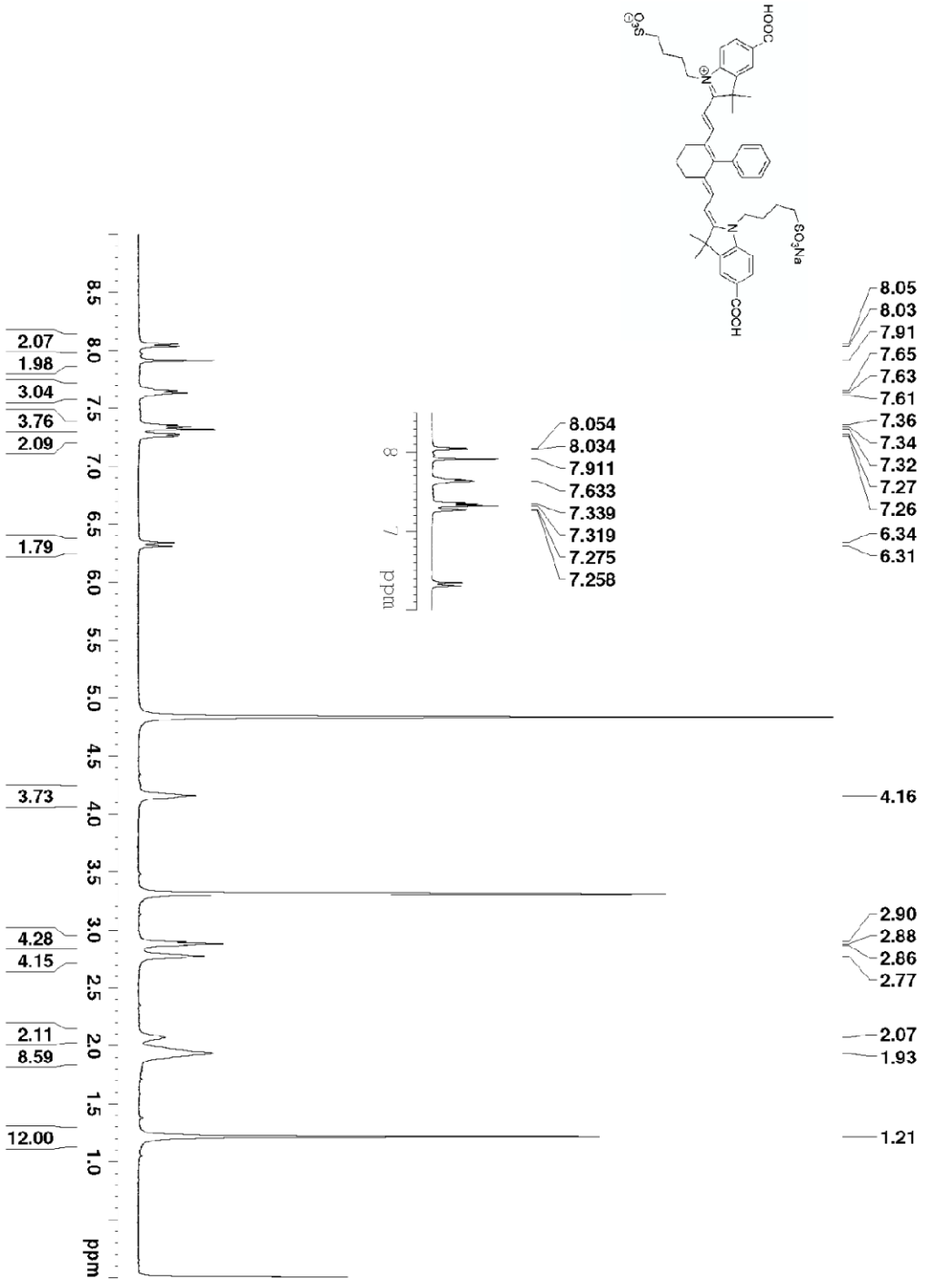
HOOC
SO3Na
SO3
COOH
8.05
8.03
7.91
7.65
7.63
7.61
7.36
7.34
7.32
7.27
7.26
6.34
6.31
8.054
8.034
7.911
7.633
7.339
7.319
7.275
7.258
4.16
2.90
2.88
2.86
2.77
2.07
1.93
1.21
2.07
1.98
3.04
3.76
2.09
1.79
3.73
4.28
4.15
2.11
8.59
12.00
ppm

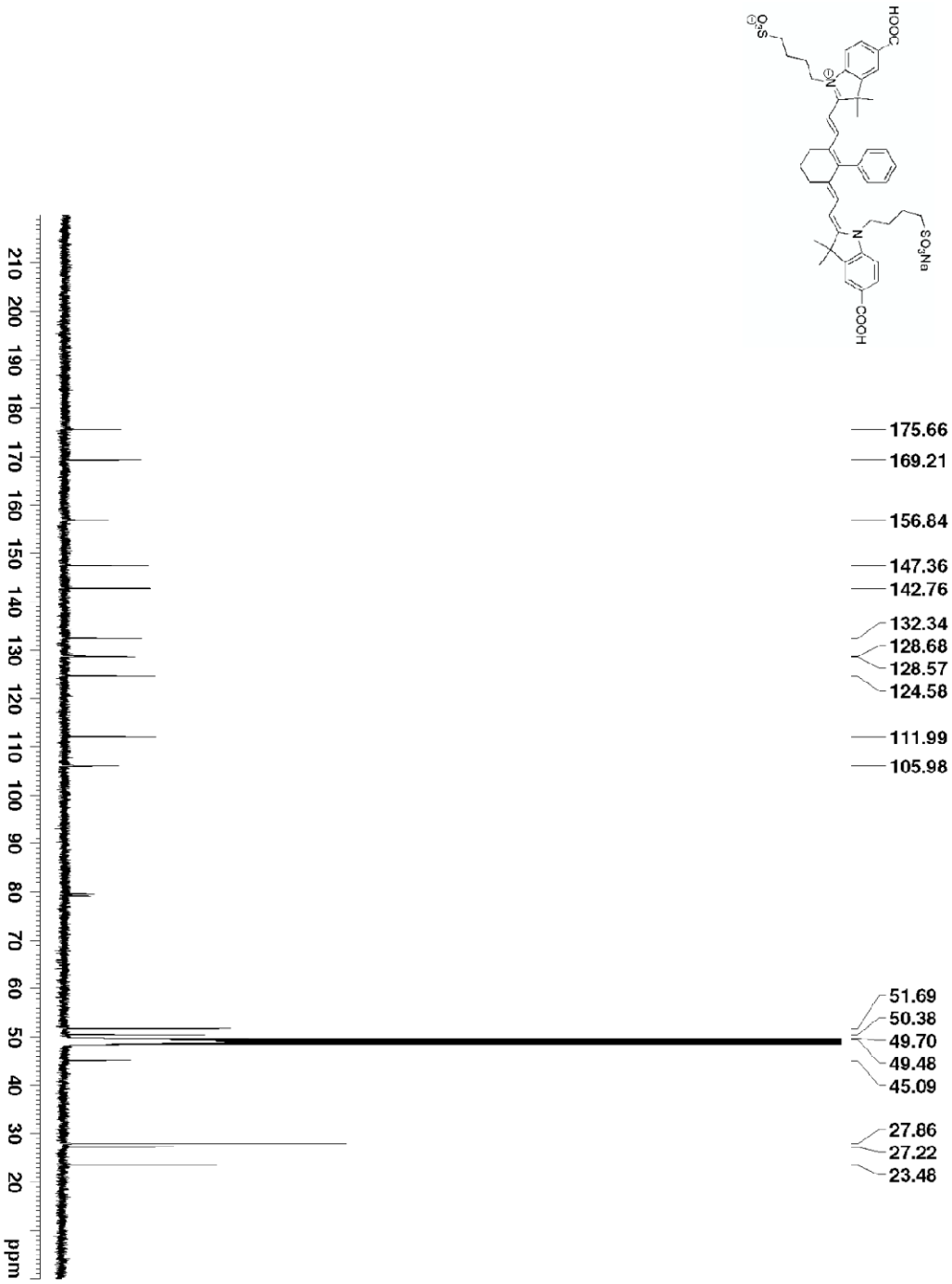
HOOC
COOH
175.66
169.21
156.84
147.36
142.76
132.34
128.68
128.57
124.58
111.99
105.98
51.69
50.38
49.70
49.48
45.09
27.86
27.22
23.48
ppm

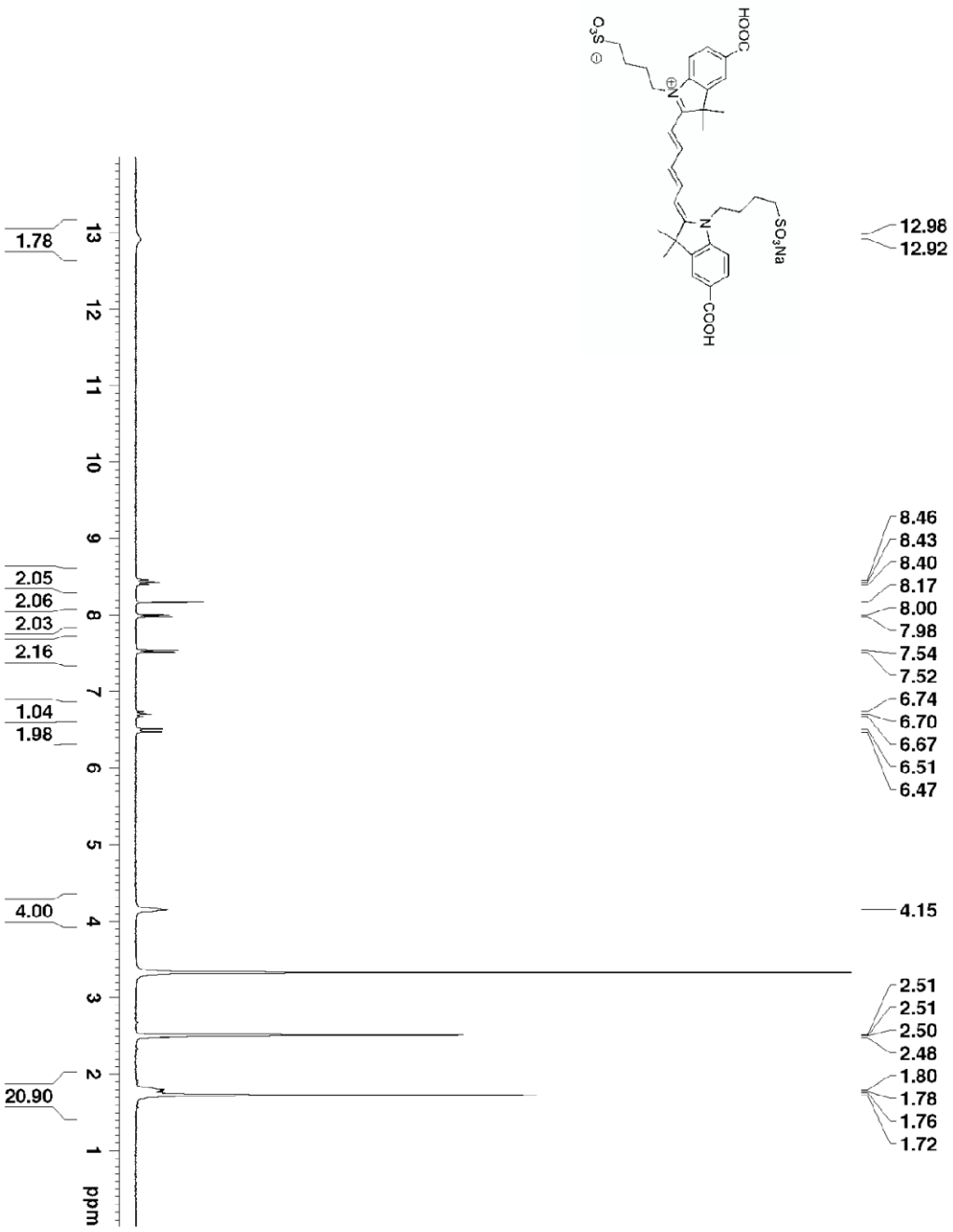
HOOC
O3S
SO3Na
COOH
12.98
12.92
8.46
8.43
8.40
8.17
8.00
7.98
7.54
7.52
6.74
6.70
6.67
6.51
6.47
4.15
2.51
2.51
2.50
2.48
1.80
1.78
1.76
1.72
1.78
2.05
2.06
2.03
2.16
1.04
1.98
4.00
20.90
ppm

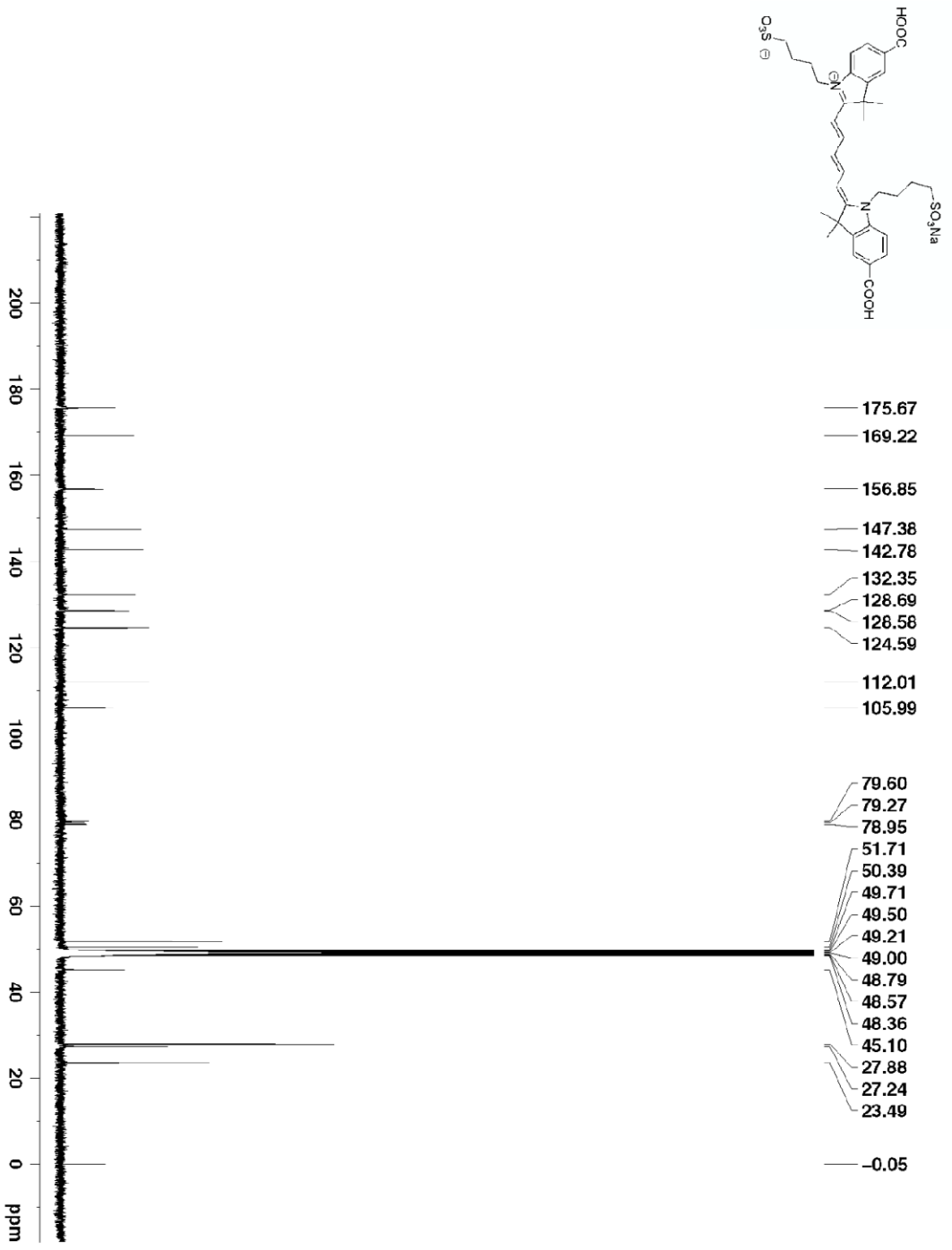
HOOC
O3S
N
SO3Na
COOH
175.67
169.22
156.85
147.38
142.78
132.35
128.69
128.58
124.59
112.01
105.99
79.60
79.27
78.95
51.71
50.39
49.71
49.50
49.21
49.00
48.79
48.57
48.36
45.10
27.88
27.24
23.49
-0.05
200
180
160
140
120
100
80
60
40
20
0
ppm

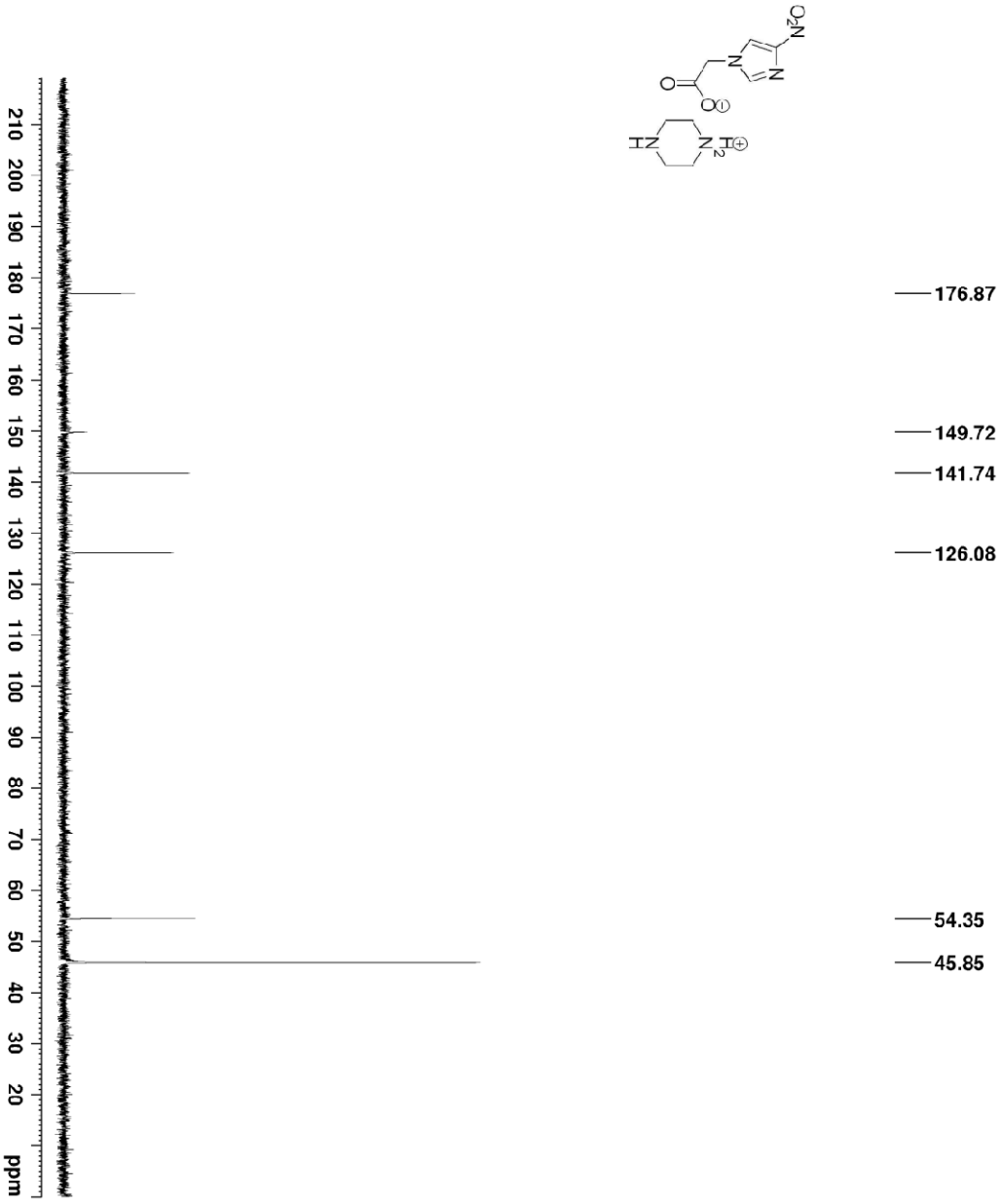
176.87
149.72
141.74
126.08
54.35
45.85
ppm

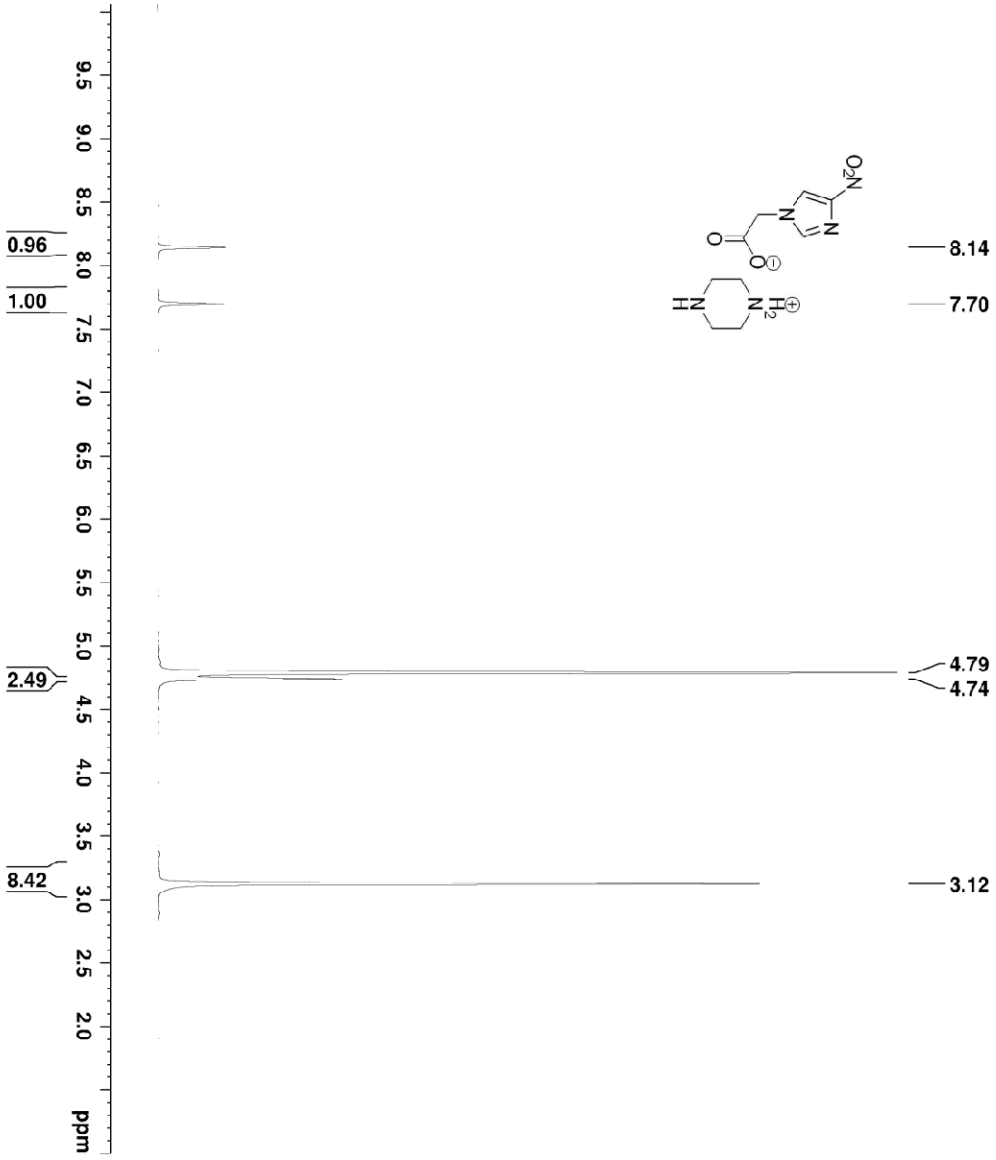
0.96
1.00
2.49
8.42
8.14
7.70
4.79
4.74
3.12
ppm

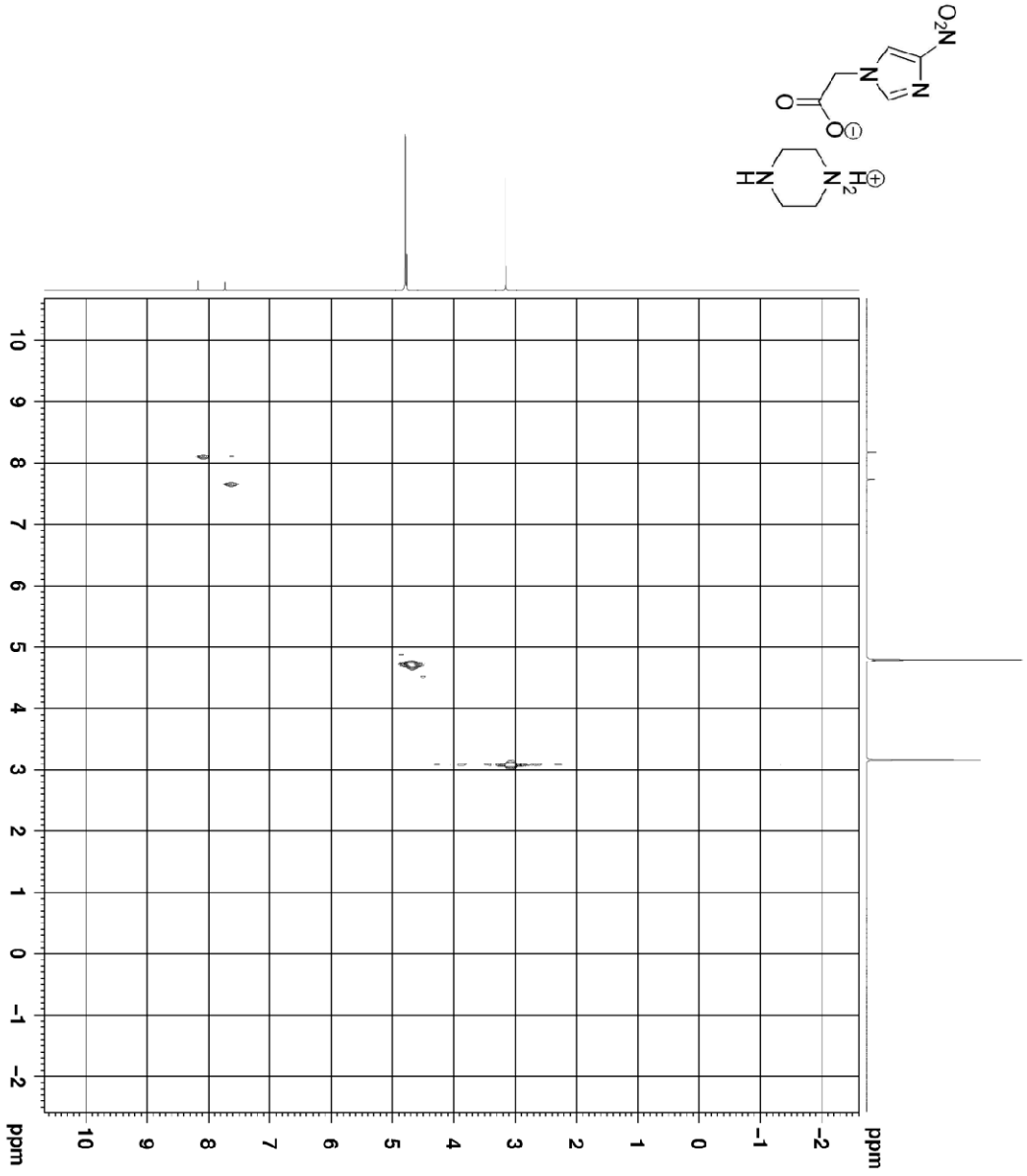
O2N
N
N
O
O
H
N
N
H2
ppm
10
9
8
7
6
5
4
3
2
1
0
−1
−2

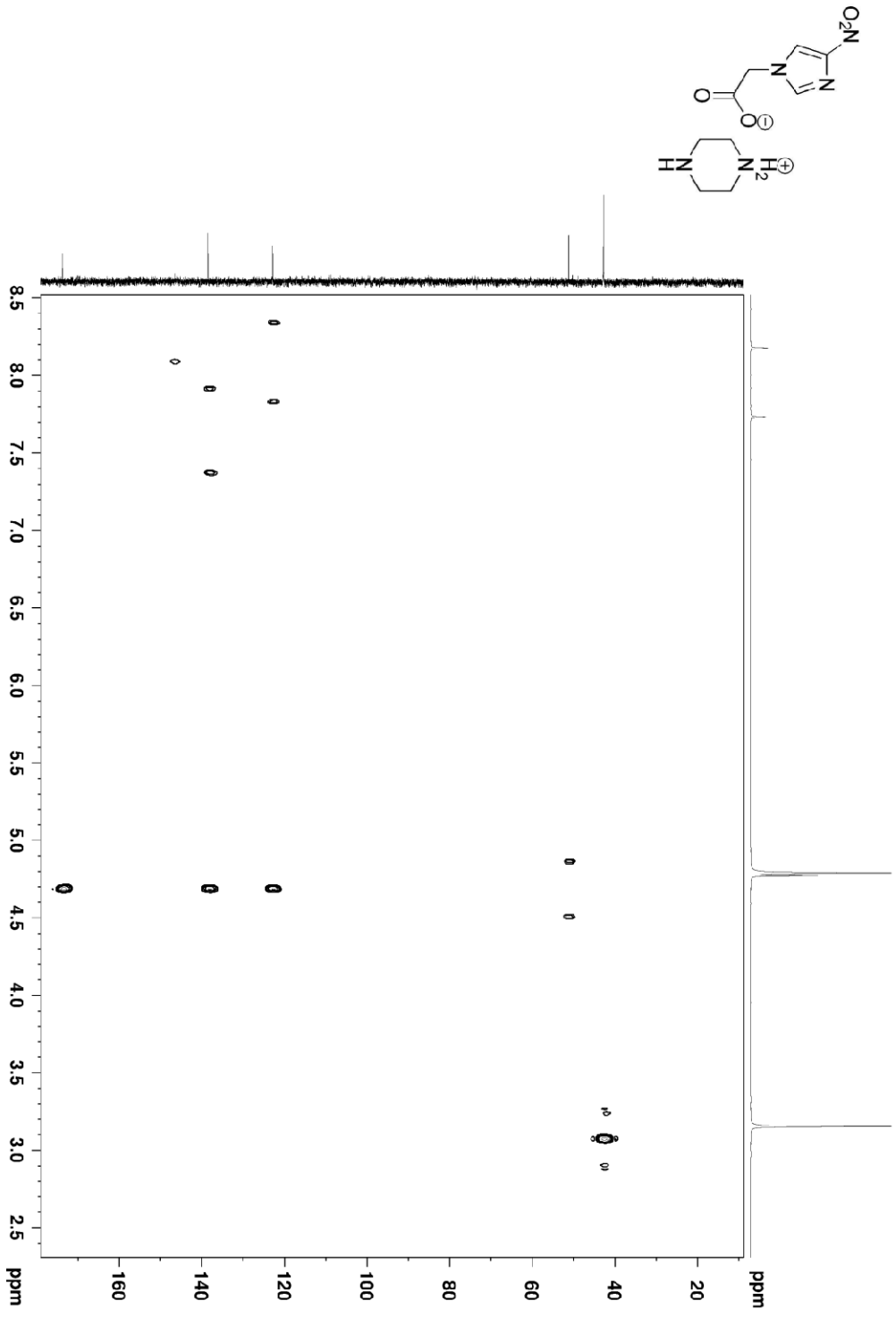
O2N
N
N
O
O
N
H
N
H2
ppm
8.5
8.0
7.5
7.0
6.5
6.0
5.5
5.0
4.5
4.0
3.5
3.0
2.5
ppm
160
140
120
100
80
60
40
20

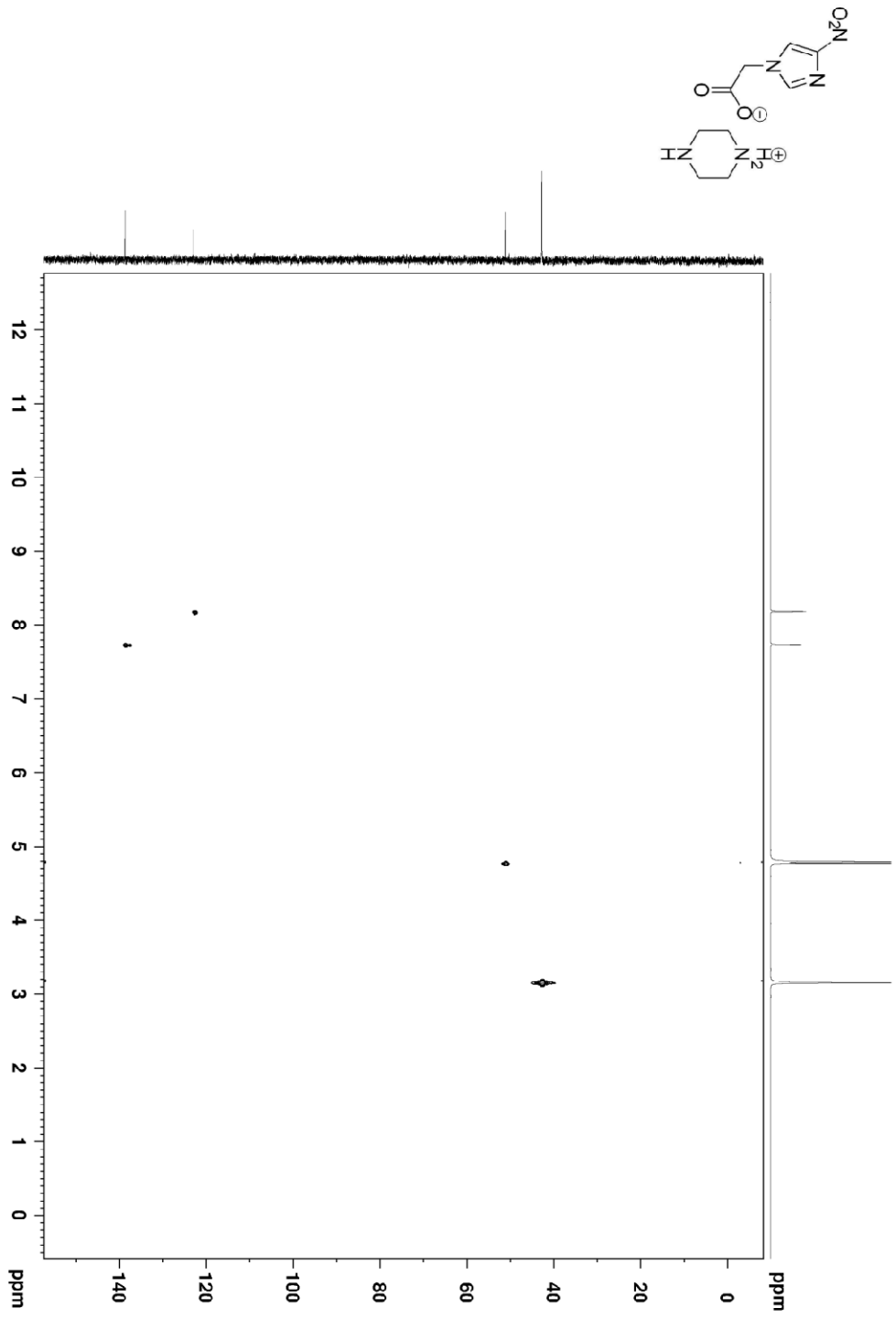
O2N
N
N
O
O
H
N
N
H2
ppm
0
20
40
60
80
100
120
140
ppm
0
1
2
3
4
5
6
7
8
9
10
11
12

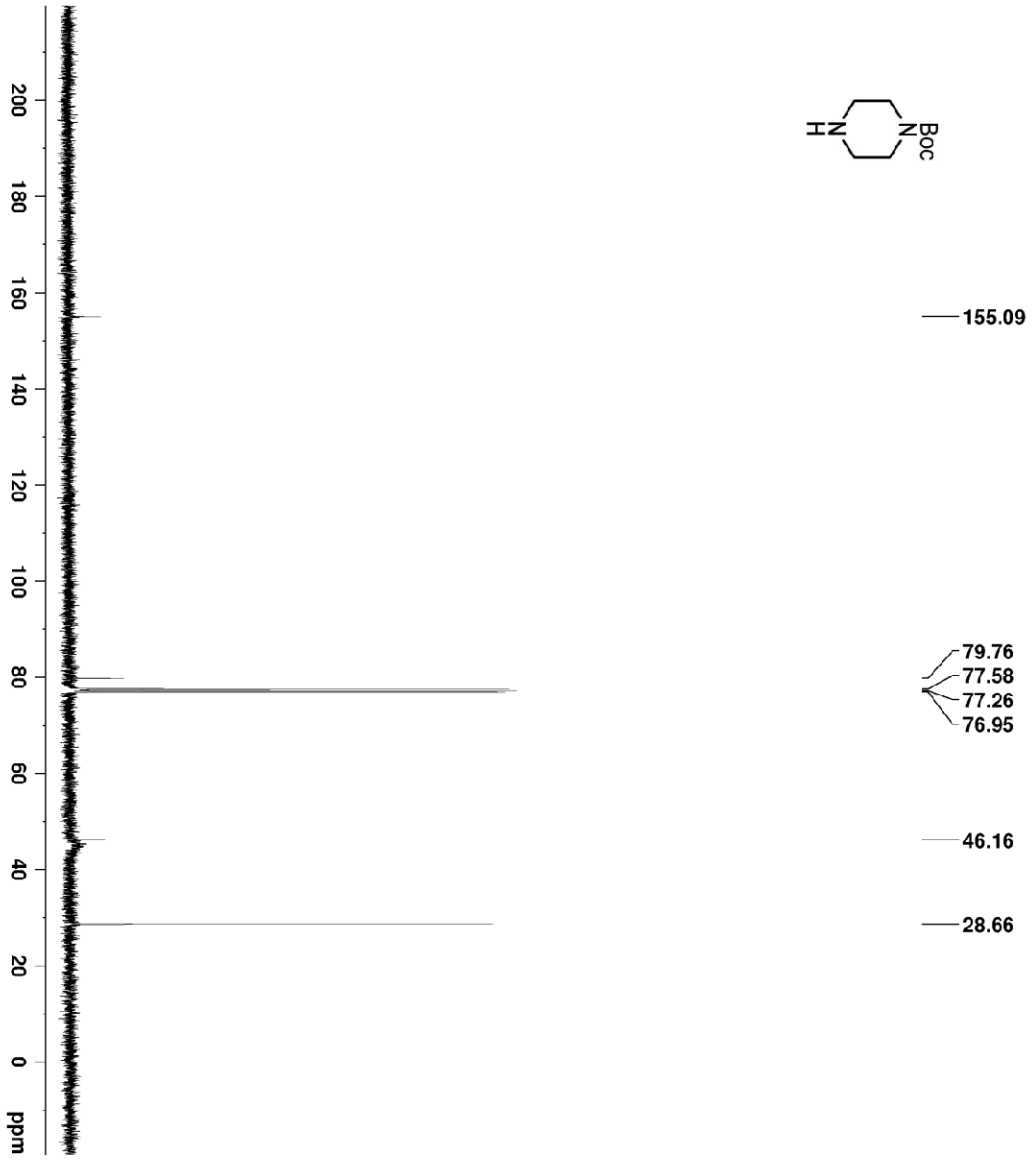
200
180
160
140
120
100
80
60
40
20
0
ppm
Boc
N
H
155.09
79.76
77.58
77.26
76.95
46.16
28.66

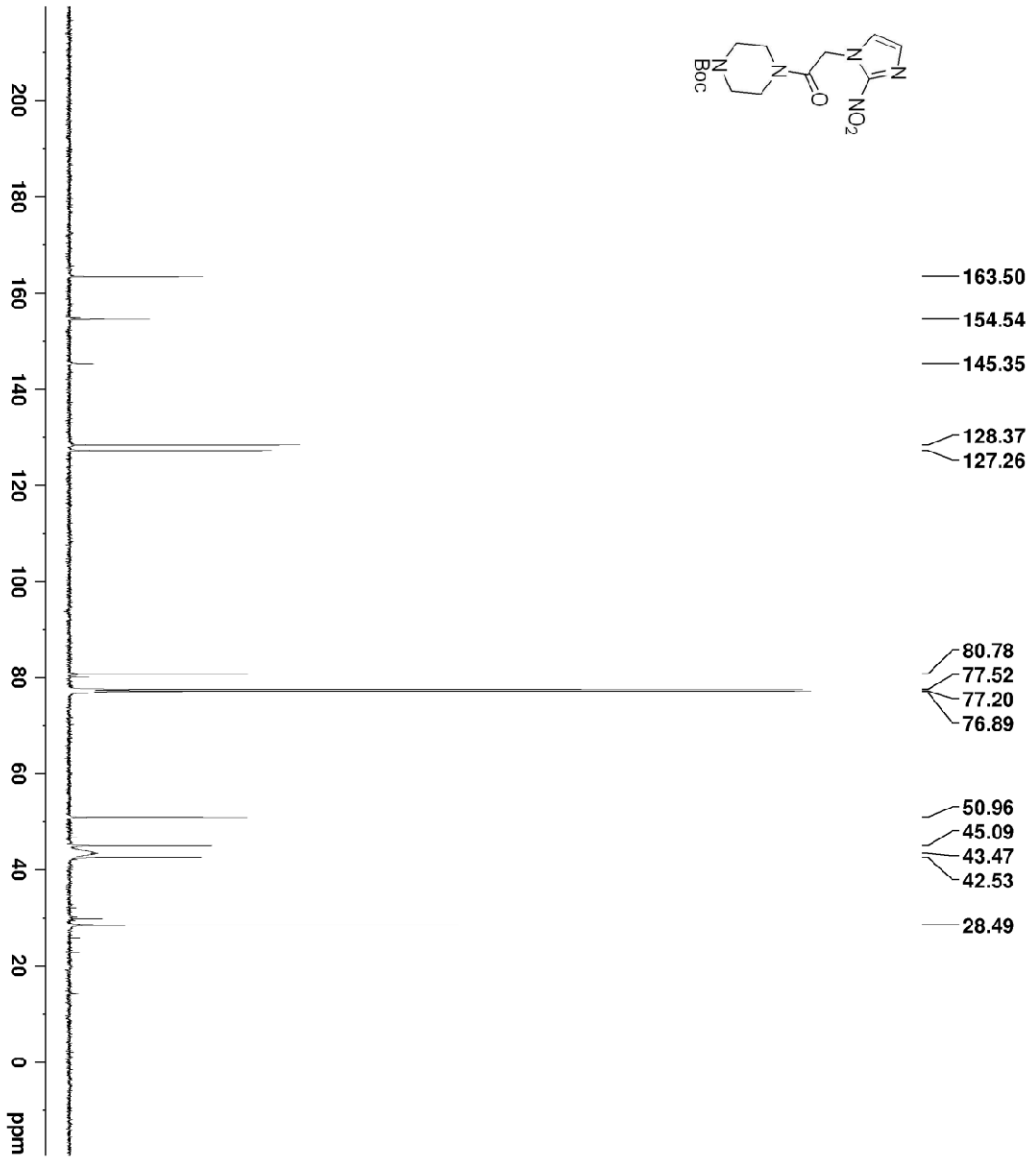
Boc
N
O
N
N
NO2
163.50
154.54
145.35
128.37
127.26
80.78
77.52
77.20
76.89
50.96
45.09
43.47
42.53
28.49
200
180
160
140
120
100
80
60
40
20
0
ppm

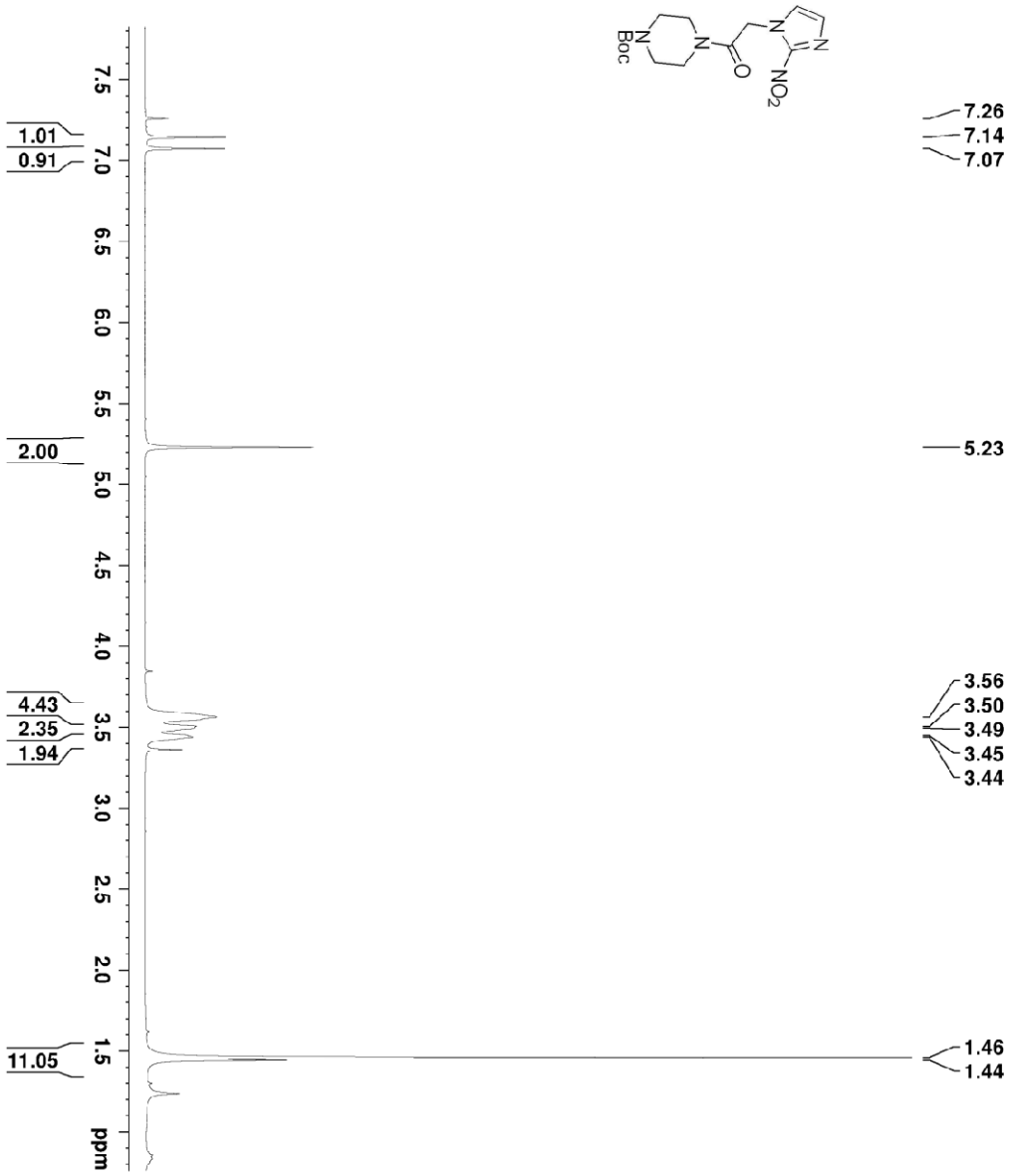
Boc
N
O
NO2
7.26
7.14
7.07
5.23
3.56
3.50
3.49
3.45
3.44
1.46
1.44
1.01
0.91
2.00
4.43
2.35
1.94
11.05
ppm

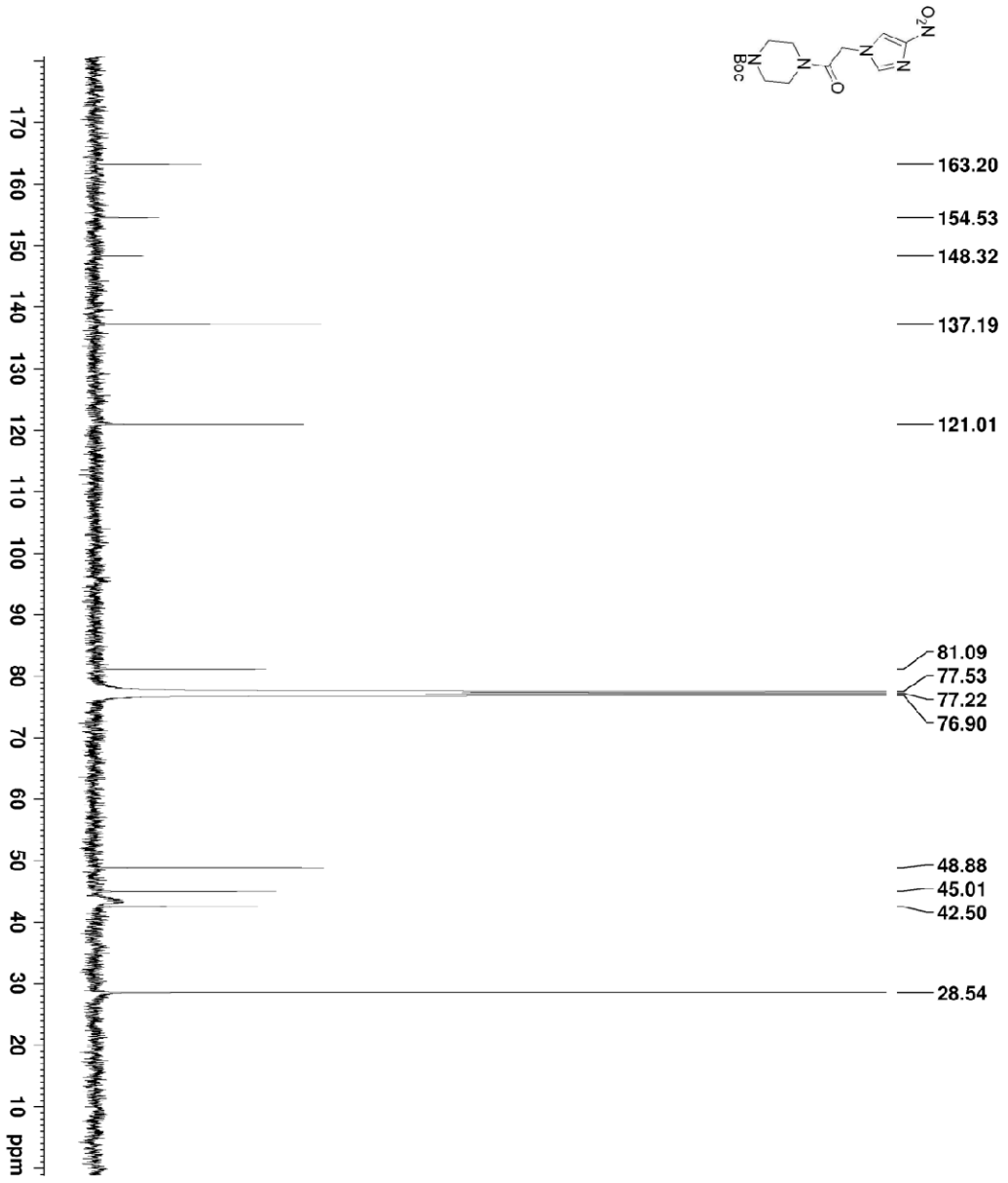
Boc
O
O2N
163.20
154.53
148.32
137.19
121.01
81.09
77.53
77.22
76.90
48.88
45.01
42.50
28.54
170
160
150
140
130
120
110
100
90
80
70
60
50
40
30
20
10
ppm

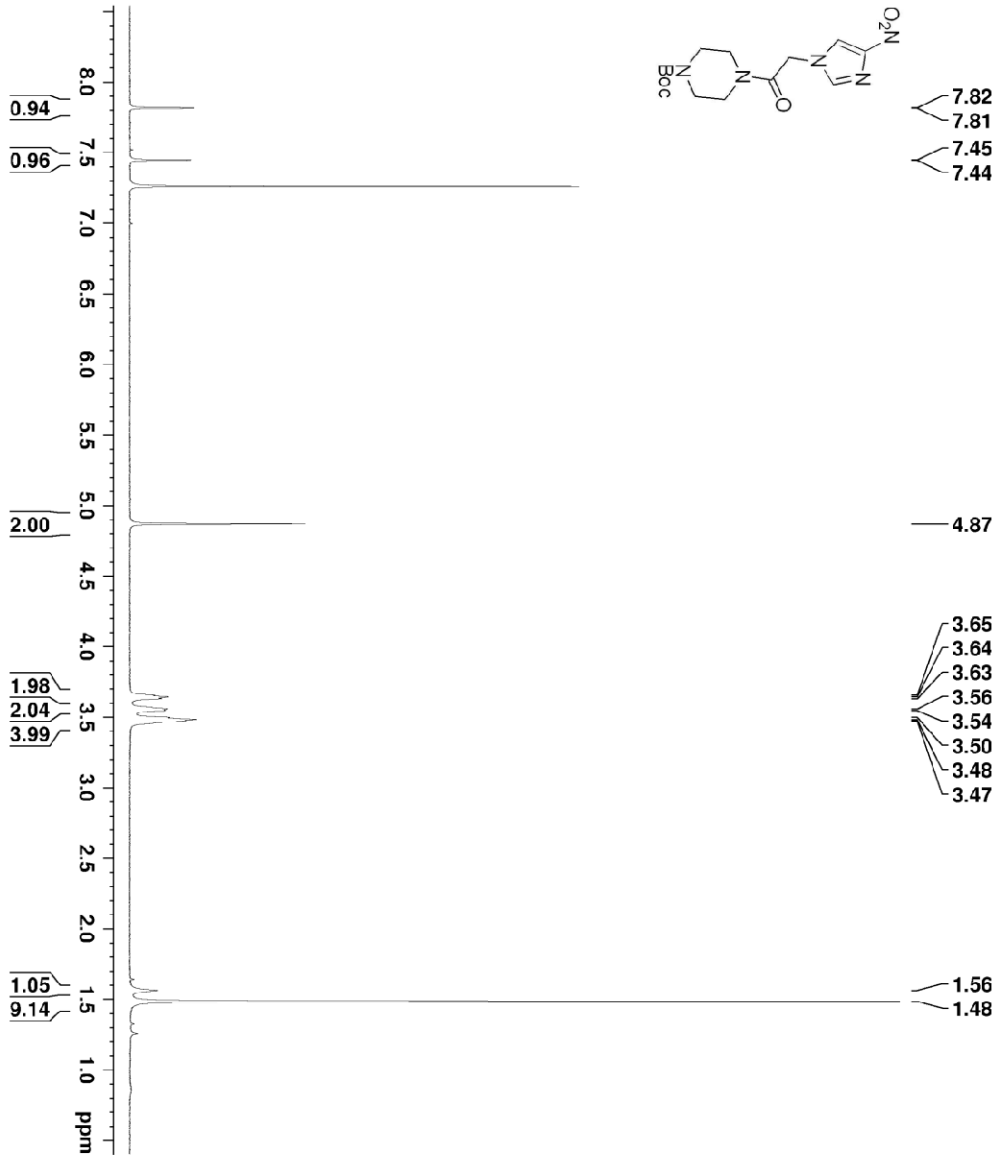
O2N
N
Boc
N
O
N
N
7.82
7.81
7.45
7.44
4.87
3.65
3.64
3.63
3.56
3.54
3.50
3.48
3.47
1.56
1.48
0.94
0.96
2.00
1.98
2.04
3.99
1.05
9.14
8.0
7.5
7.0
6.5
6.0
5.5
5.0
4.5
4.0
3.5
3.0
2.5
2.0
1.5
1.0
ppm

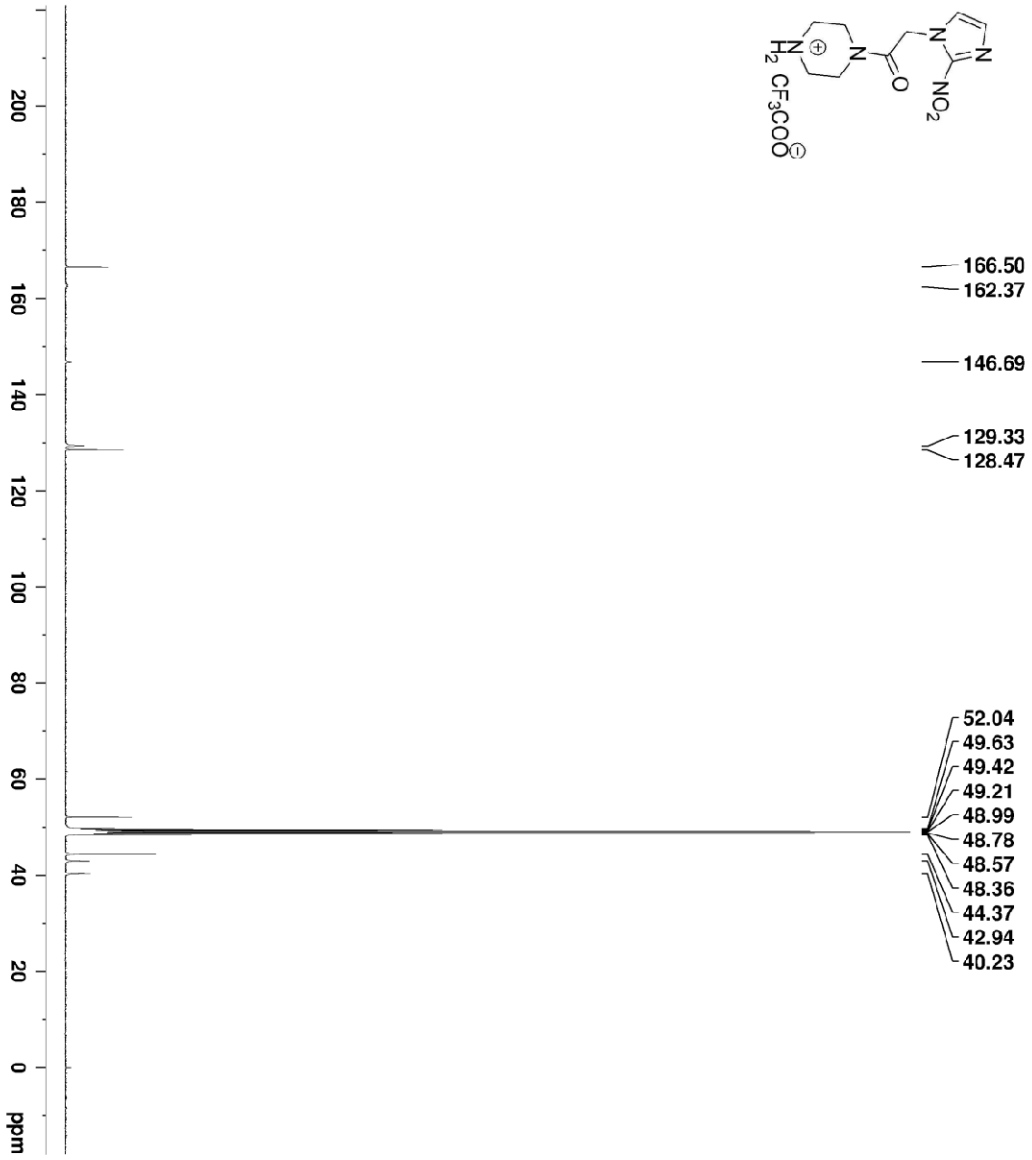
166.50
162.37
146.69
129.33
128.47
52.04
49.63
49.42
49.21
48.99
48.78
48.57
48.36
44.37
42.94
40.23
200
180
160
140
120
100
80
60
40
20
0
ppm

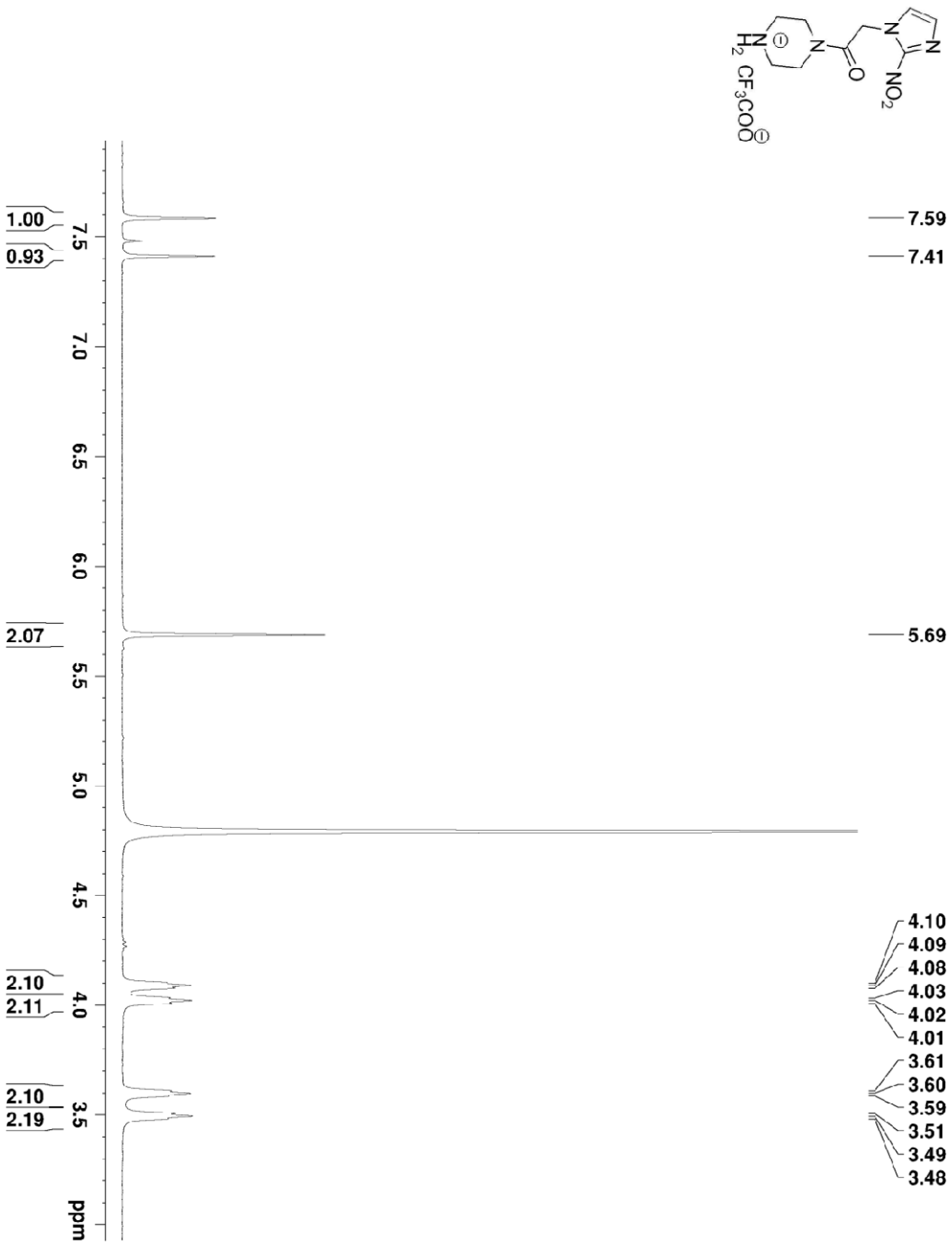
1.00
0.93
2.07
2.10
2.11
2.10
2.19
7.5
7.0
6.5
6.0
5.5
5.0
4.5
4.0
3.5
ppm
7.59
7.41
5.69
4.10
4.09
4.08
4.03
4.02
4.01
3.61
3.60
3.59
3.51
3.49
3.48

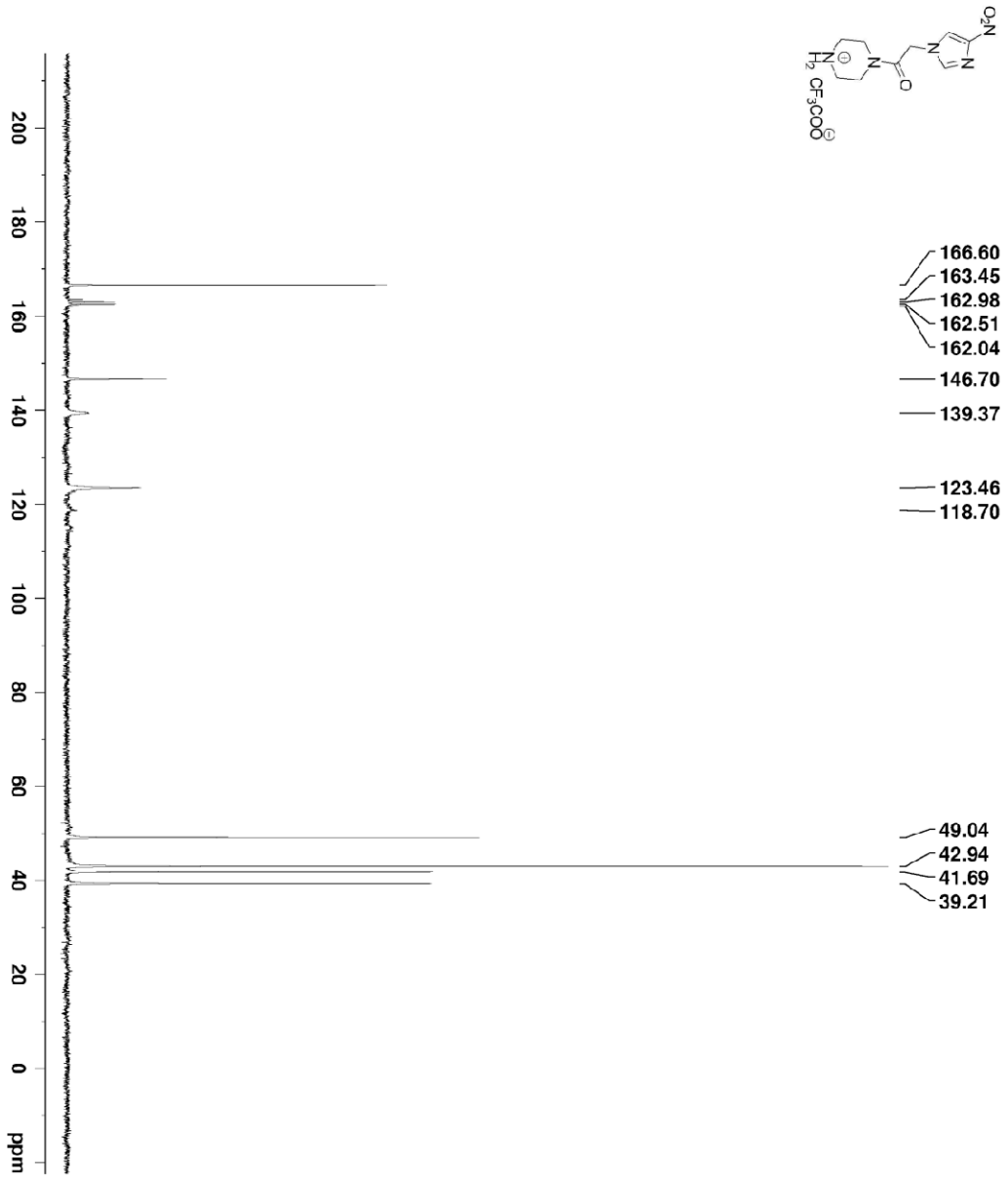
166.60
163.45
162.98
162.51
162.04
146.70
139.37
123.46
118.70
49.04
42.94
41.69
39.21
200
180
160
140
120
100
80
60
40
20
0
ppm

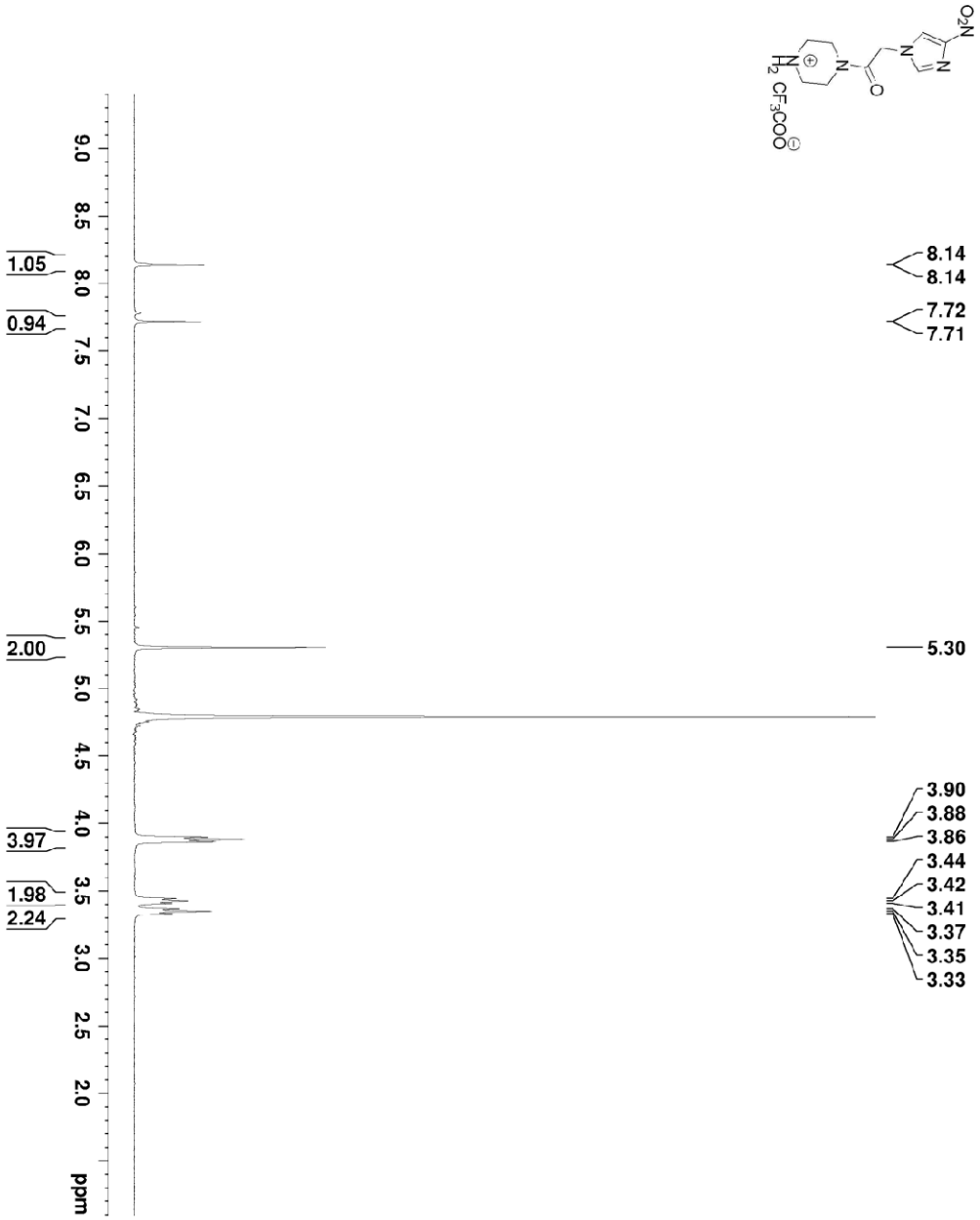
8.14
8.14
7.72
7.71
5.30
3.90
3.88
3.86
3.44
3.42
3.41
3.37
3.35
3.33
1.05
0.94
2.00
3.97
1.98
2.24
ppm

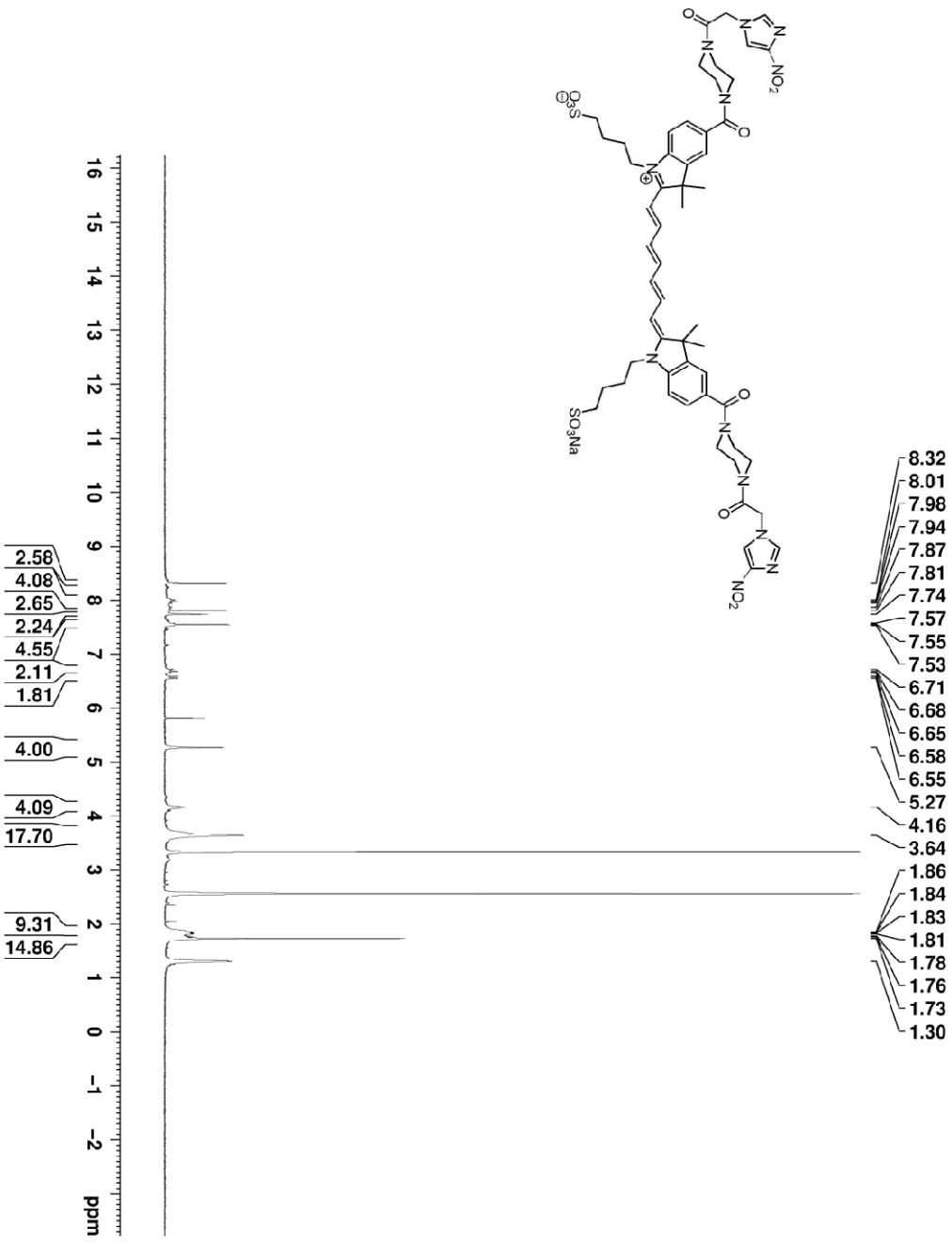
8.32
8.01
7.98
7.94
7.87
7.81
7.74
7.57
7.55
7.53
6.71
6.68
6.65
6.58
6.55
5.27
4.16
3.64
1.86
1.84
1.83
1.81
1.78
1.76
1.73
1.30
2.58
4.08
2.65
2.24
4.55
2.11
1.81
4.00
4.09
17.70
9.31
14.86
ppm

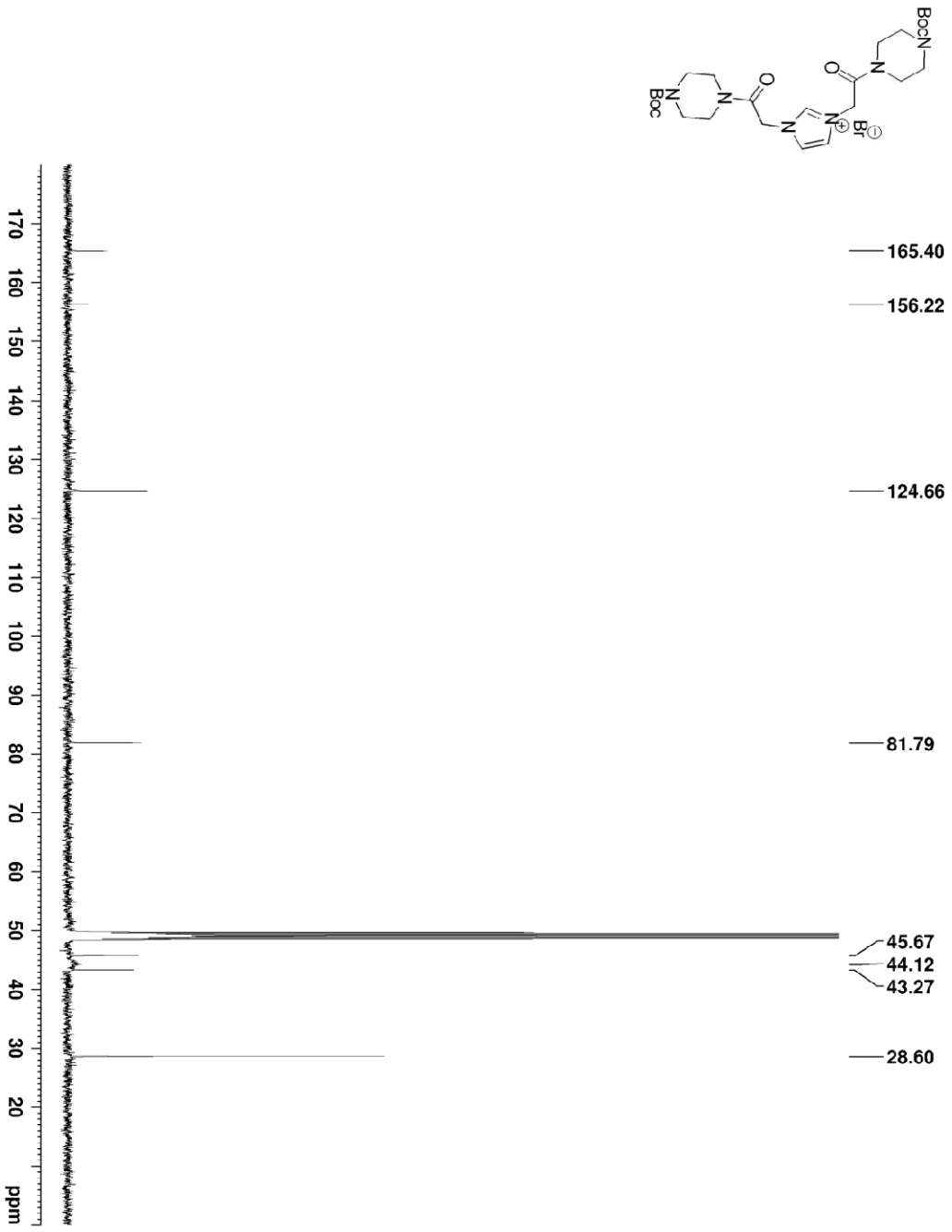
BocN
N
O
N
N
N
Boc
Br
165.40
156.22
124.66
81.79
45.67
44.12
43.27
28.60
170
160
150
140
130
120
110
100
90
80
70
60
50
40
30
20
ppm

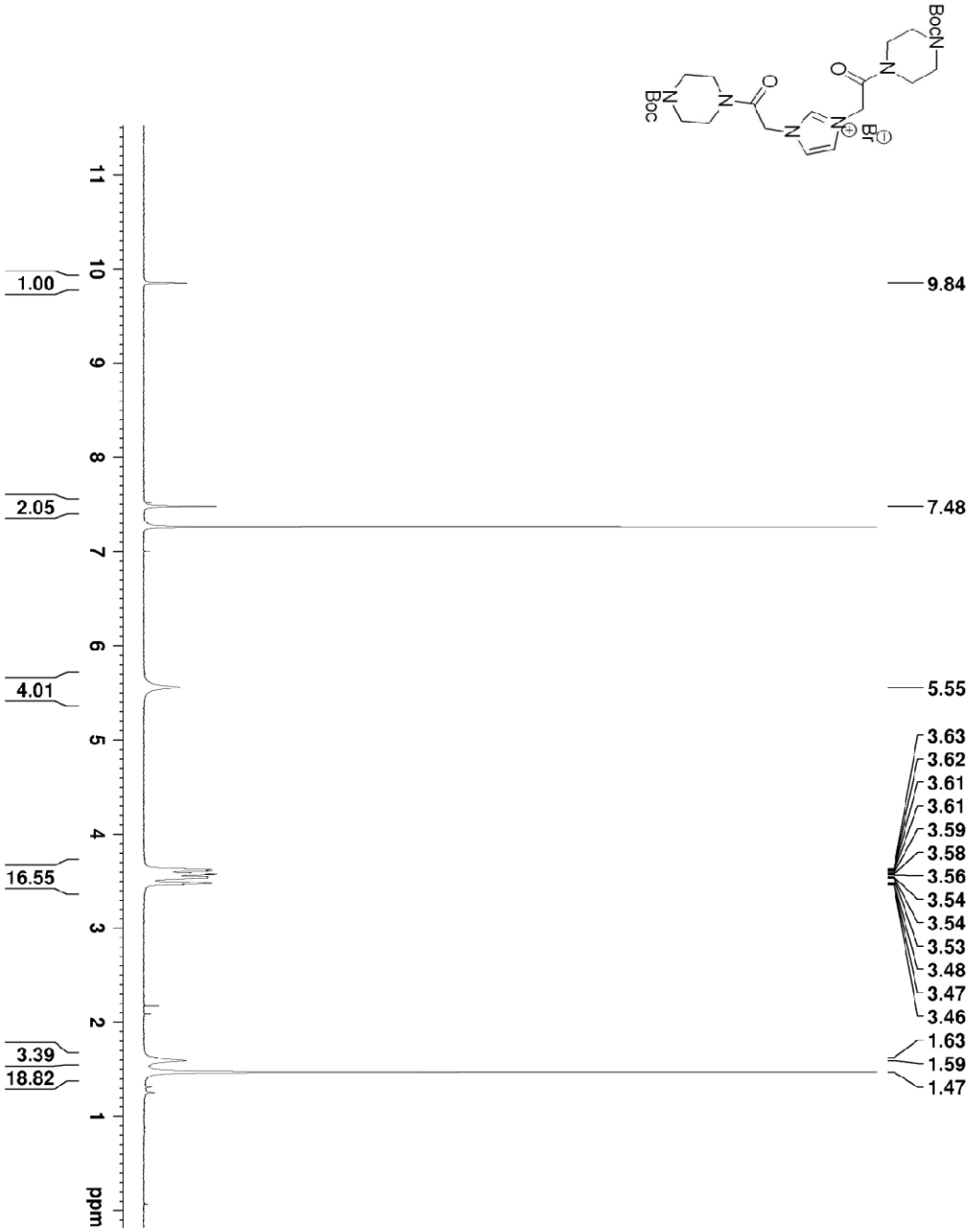
BocN
N
O
N
N
Boc
O
N
N
Br
1.00
2.05
4.01
16.55
3.39
18.82
ppm
9.84
7.48
5.55
3.63
3.62
3.61
3.61
3.59
3.58
3.56
3.54
3.54
3.53
3.48
3.47
3.46
1.63
1.59
1.47

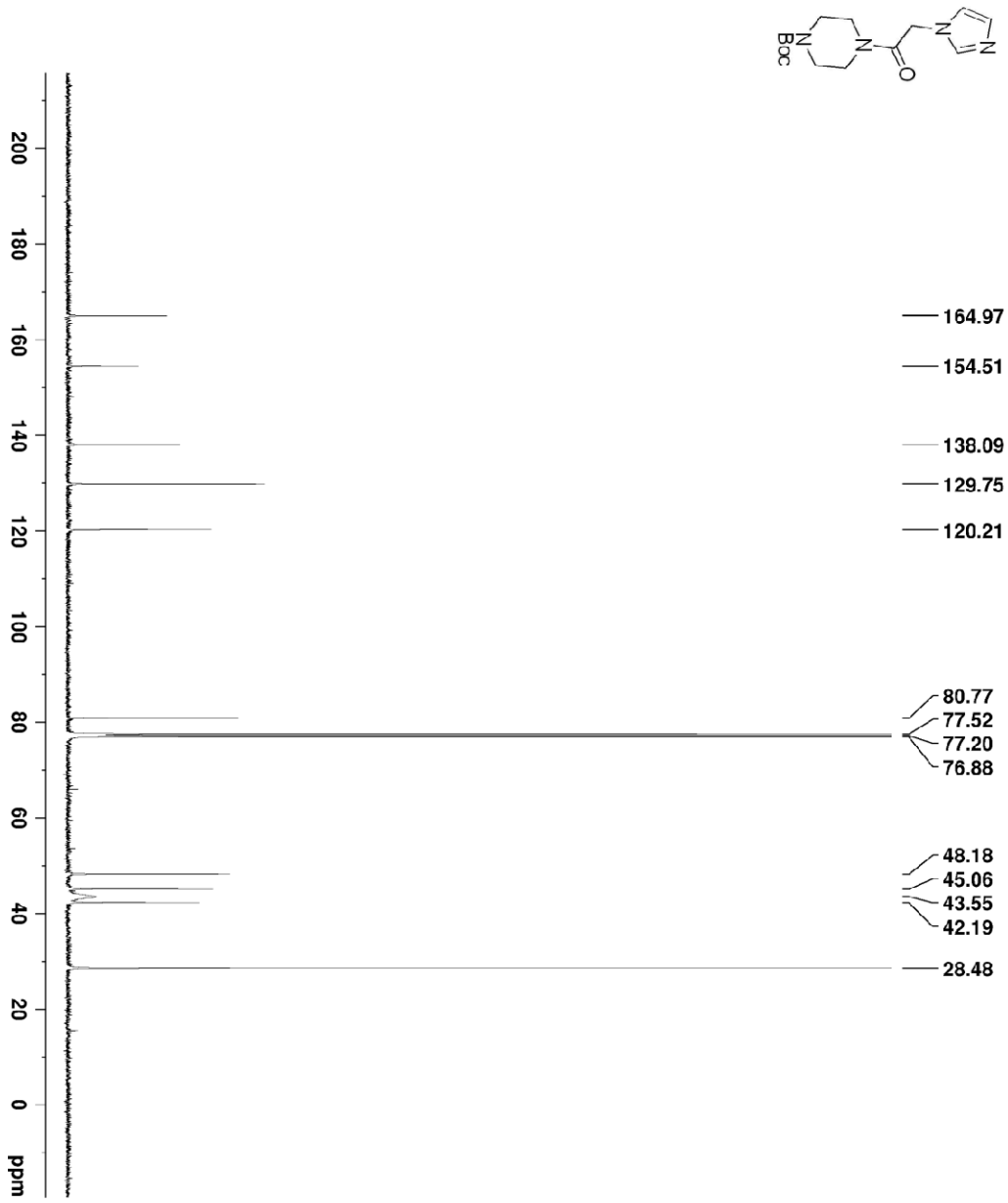
Boc
N
N
O
N
N
200
180
160
140
120
100
80
60
40
20
0
ppm
164.97
154.51
138.09
129.75
120.21
80.77
77.52
77.20
76.88
48.18
45.06
43.55
42.19
28.48

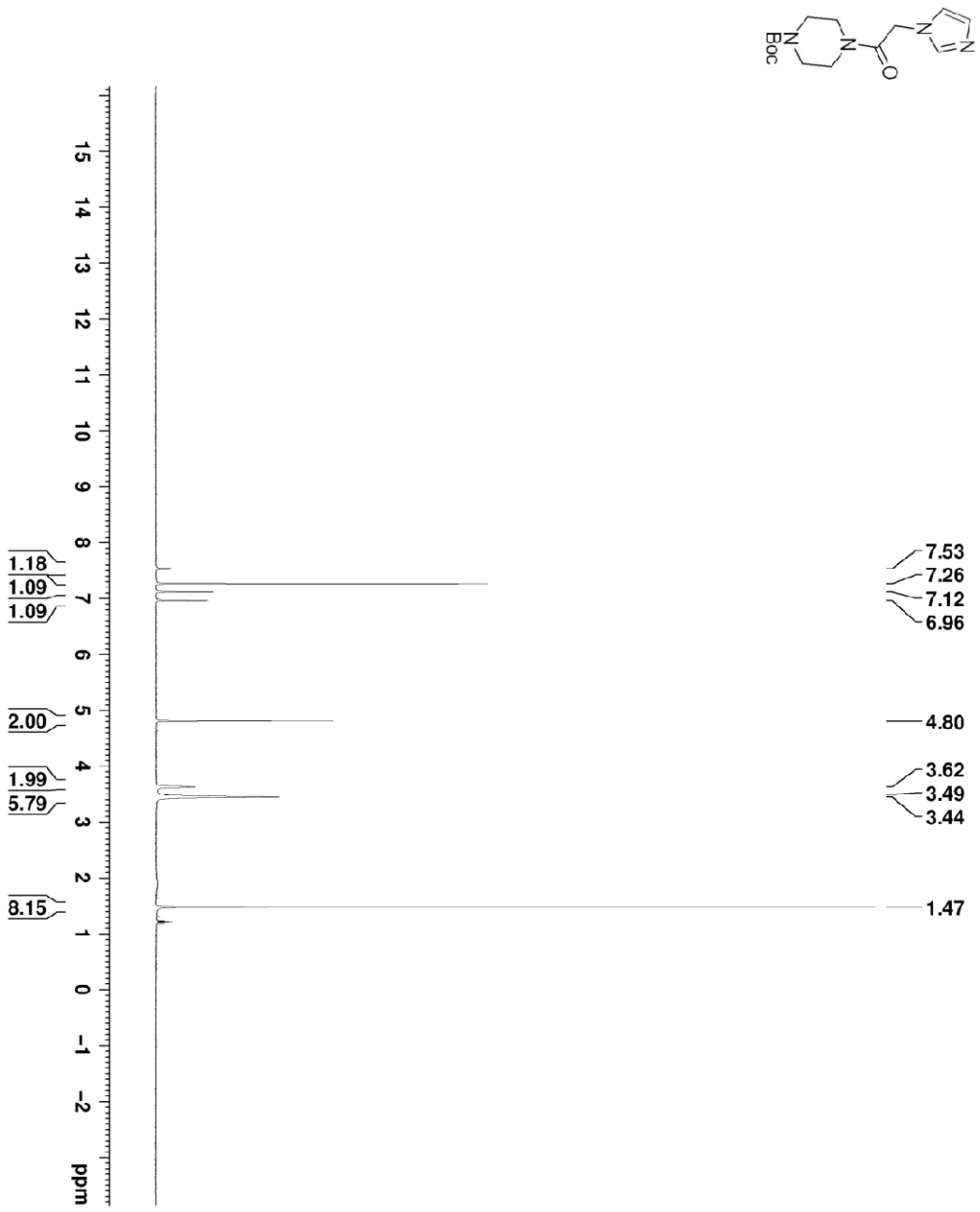
Boc
N
N
O
N
N
7.53
7.26
7.12
6.96
4.80
3.62
3.49
3.44
1.47
1.18
1.09
1.09
2.00
1.99
5.79
8.15
ppm

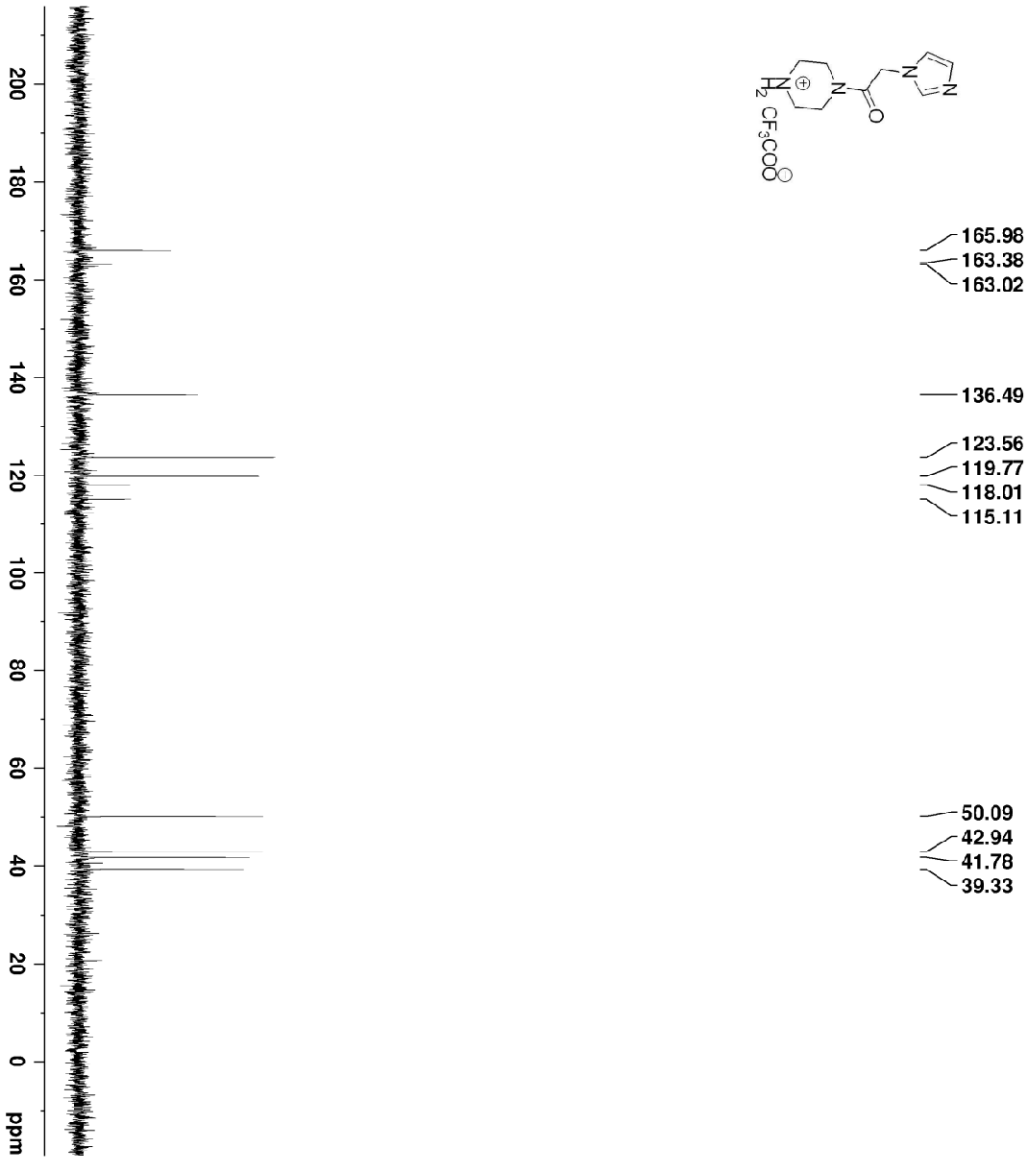
200
180
160
140
120
100
80
60
40
20
0
ppm
165.98
163.38
163.02
136.49
123.56
119.77
118.01
115.11
50.09
42.94
41.78
39.33

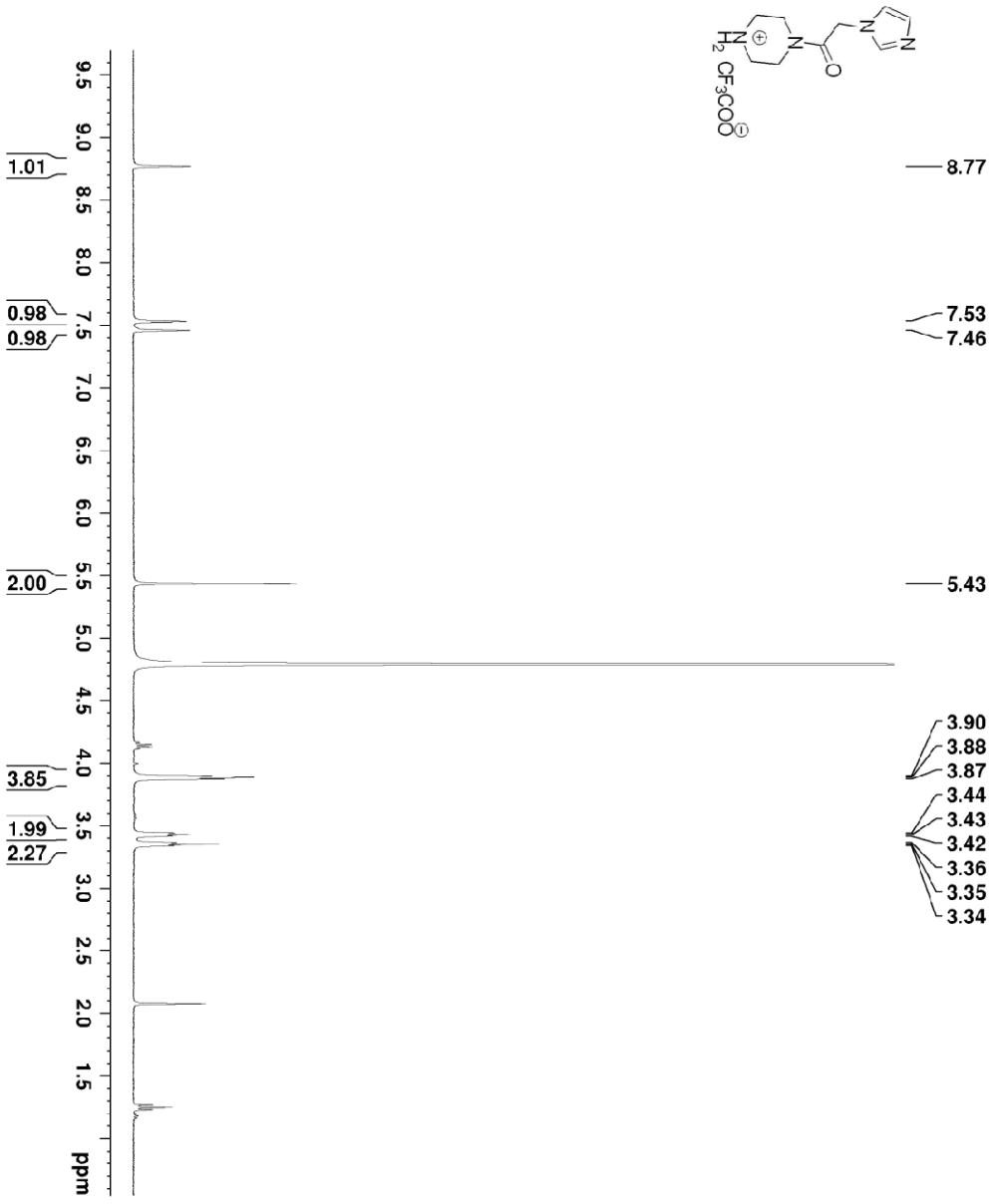
8.77
7.53
7.46
5.43
3.90
3.88
3.87
3.44
3.43
3.42
3.36
3.35
3.34
1.01
0.98
0.98
2.00
3.85
1.99
2.27
ppm

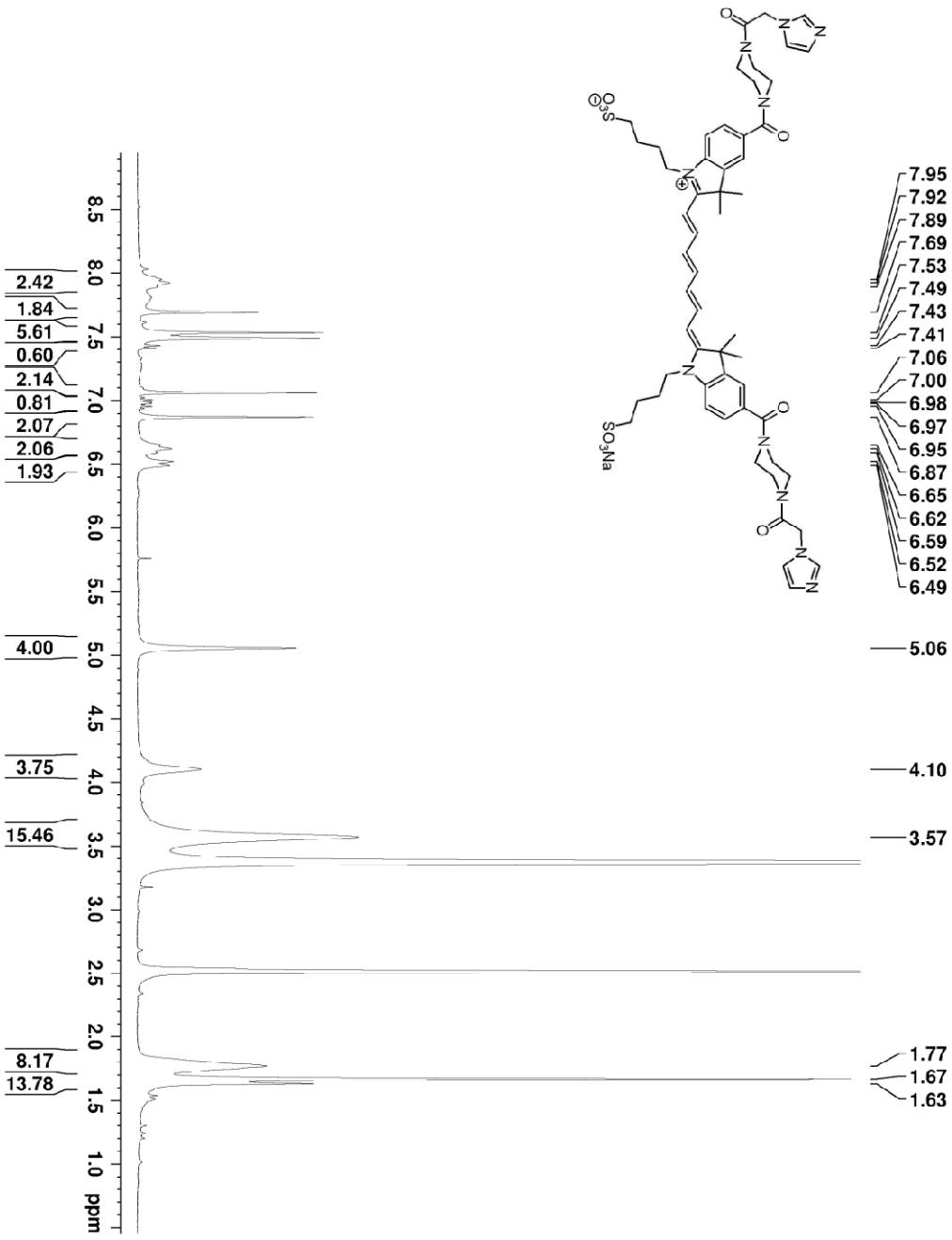
7.95
7.92
7.89
7.69
7.53
7.49
7.43
7.41
7.06
7.00
6.98
6.97
6.95
6.87
6.65
6.62
6.59
6.52
6.49
5.06
4.10
3.57
1.77
1.67
1.63
2.42
1.84
5.61
0.60
2.14
0.81
2.07
2.06
1.93
4.00
3.75
15.46
8.17
13.78
8.5
8.0
7.5
7.0
6.5
6.0
5.5
5.0
4.5
4.0
3.5
3.0
2.5
2.0
1.5
1.0
ppm
SO3Na

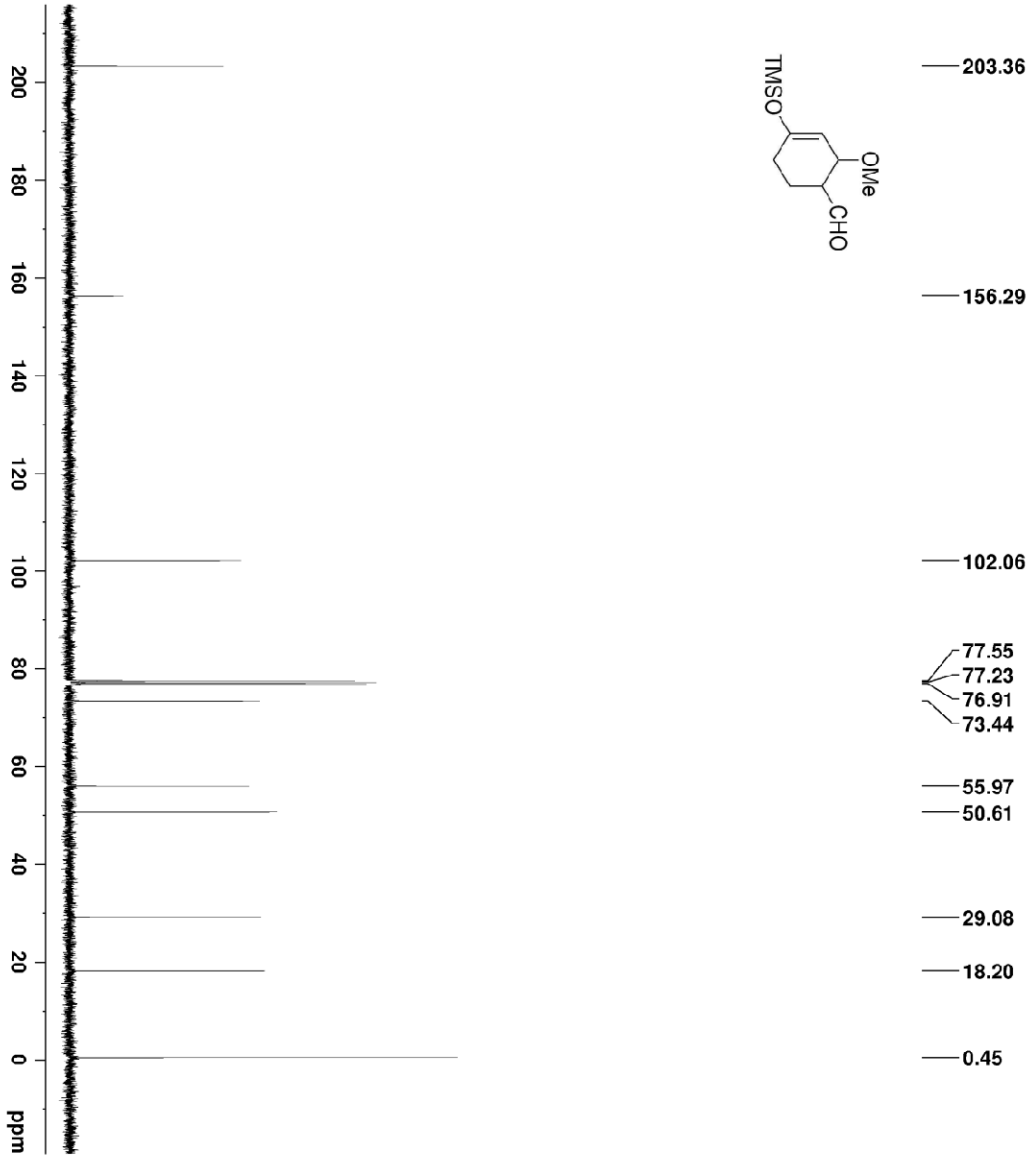
TMSO
OMe
CHO
203.36
156.29
102.06
77.55
77.23
76.91
73.44
55.97
50.61
29.08
18.20
0.45
200
180
160
140
120
100
80
60
40
20
0
ppm

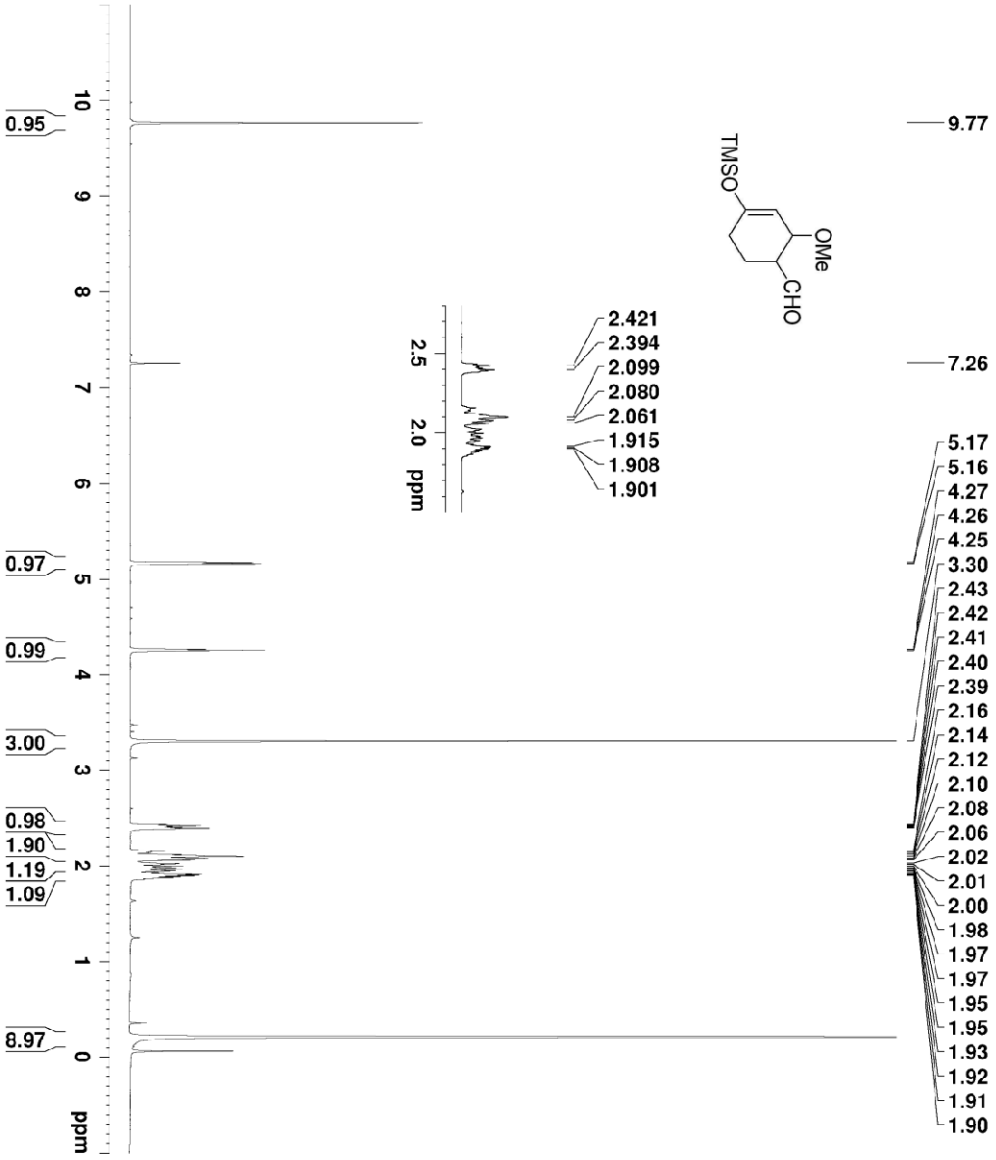
TMSO
OMe
CHO
9.77
7.26
5.17
5.16
4.27
4.26
4.25
3.30
2.43
2.42
2.41
2.40
2.39
2.16
2.14
2.12
2.10
2.08
2.06
2.02
2.01
2.00
1.98
1.97
1.97
1.95
1.95
1.93
1.92
1.91
1.90
2.421
2.394
2.099
2.080
2.061
1.915
1.908
1.901
2.5
2.0
ppm
0.95
0.97
0.99
3.00
0.98
1.90
1.19
1.09
8.97
ppm

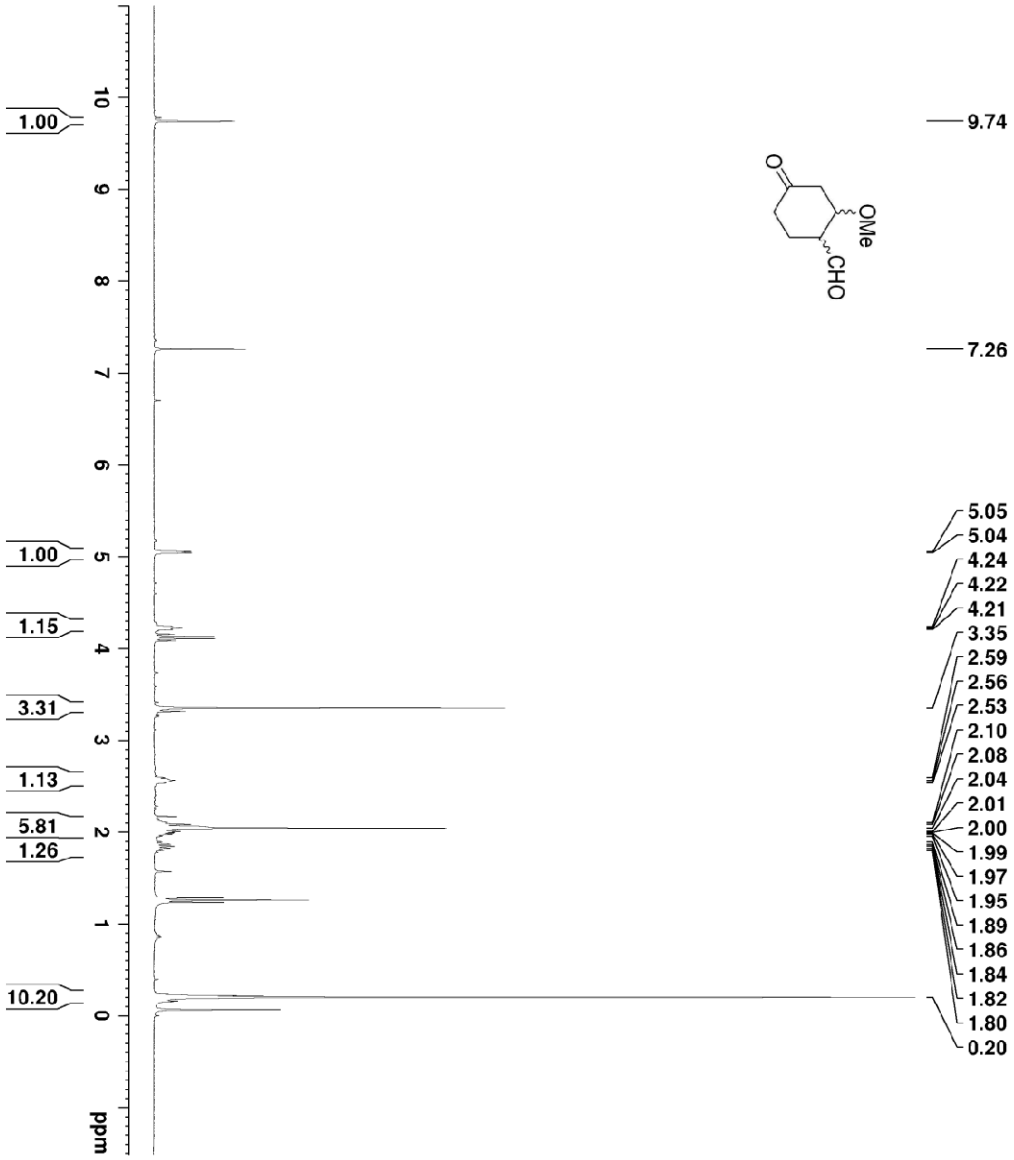
1.00
1.00
1.15
3.31
1.13
5.81
1.26
10.20
ppm
OMe
CHO
9.74
7.26
5.05
5.04
4.24
4.22
4.21
3.35
2.59
2.56
2.53
2.10
2.08
2.04
2.01
2.00
1.99
1.97
1.95
1.89
1.86
1.84
1.82
1.80
0.20

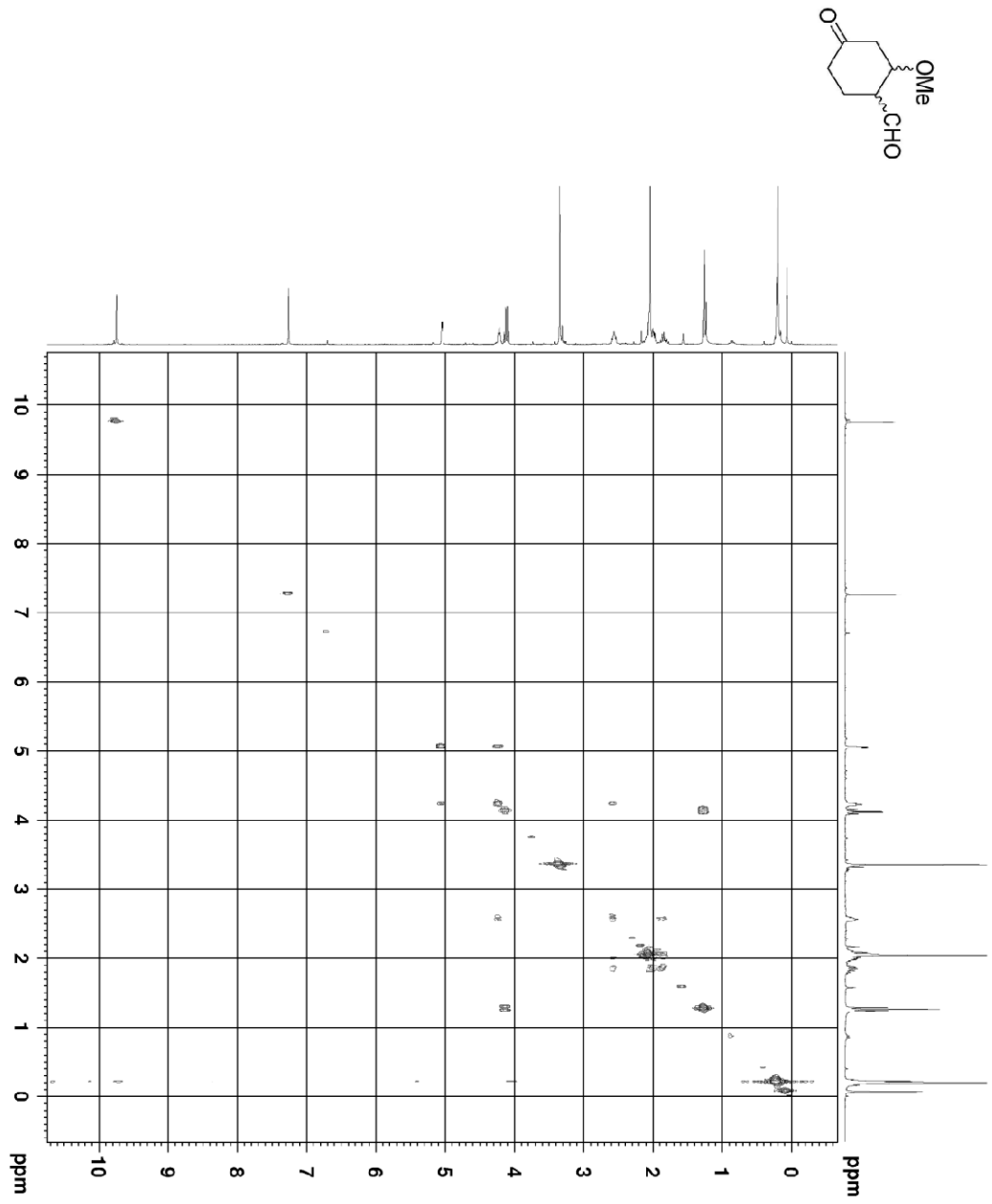
O
OMe
CHO
ppm
10
9
8
7
6
5
4
3
2
1
0

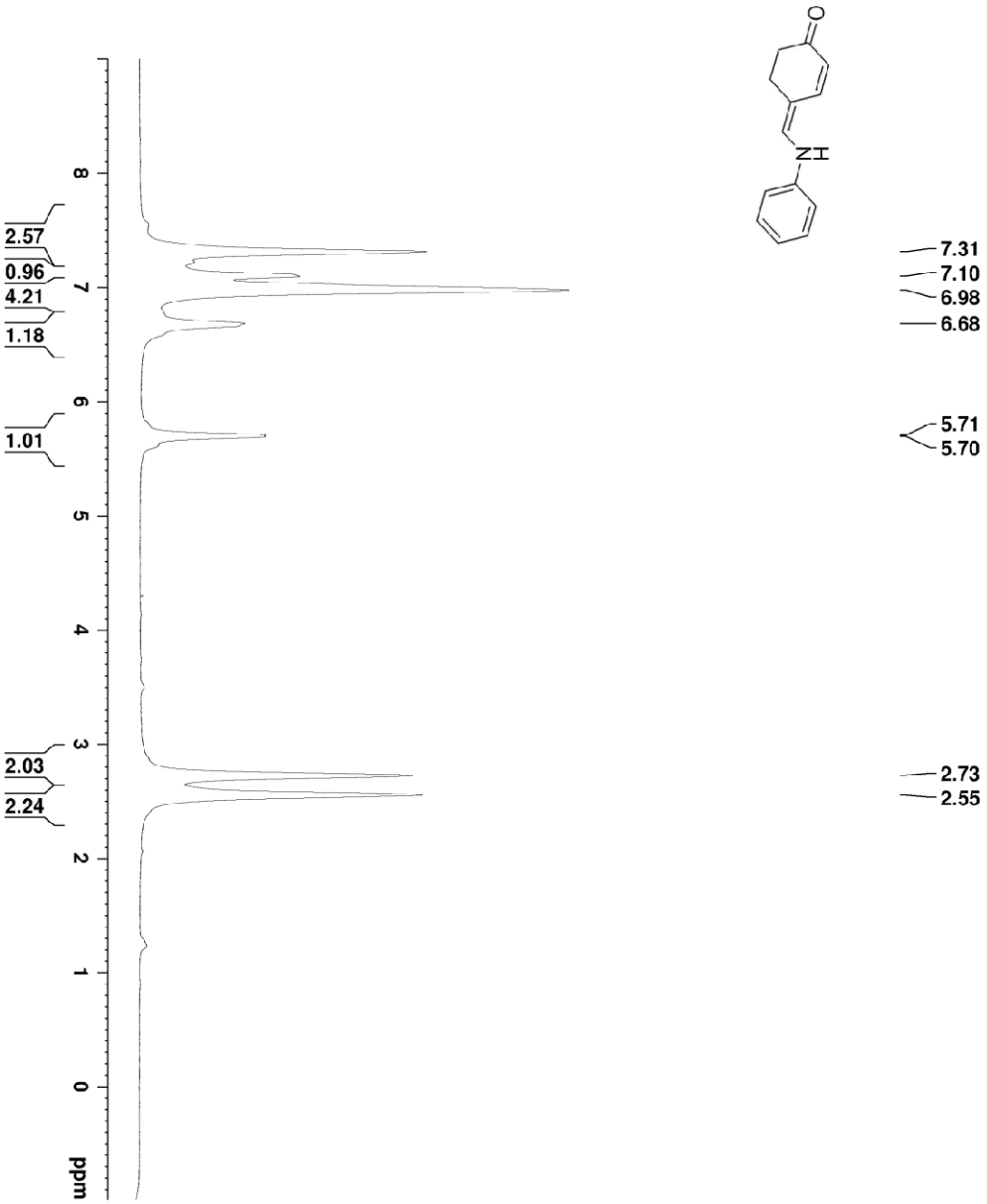
O
NH
2.57
0.96
4.21
1.18
1.01
2.03
2.24
7.31
7.10
6.98
6.68
5.71
5.70
2.73
2.55
8
7
6
5
4
3
2
1
0
ppm

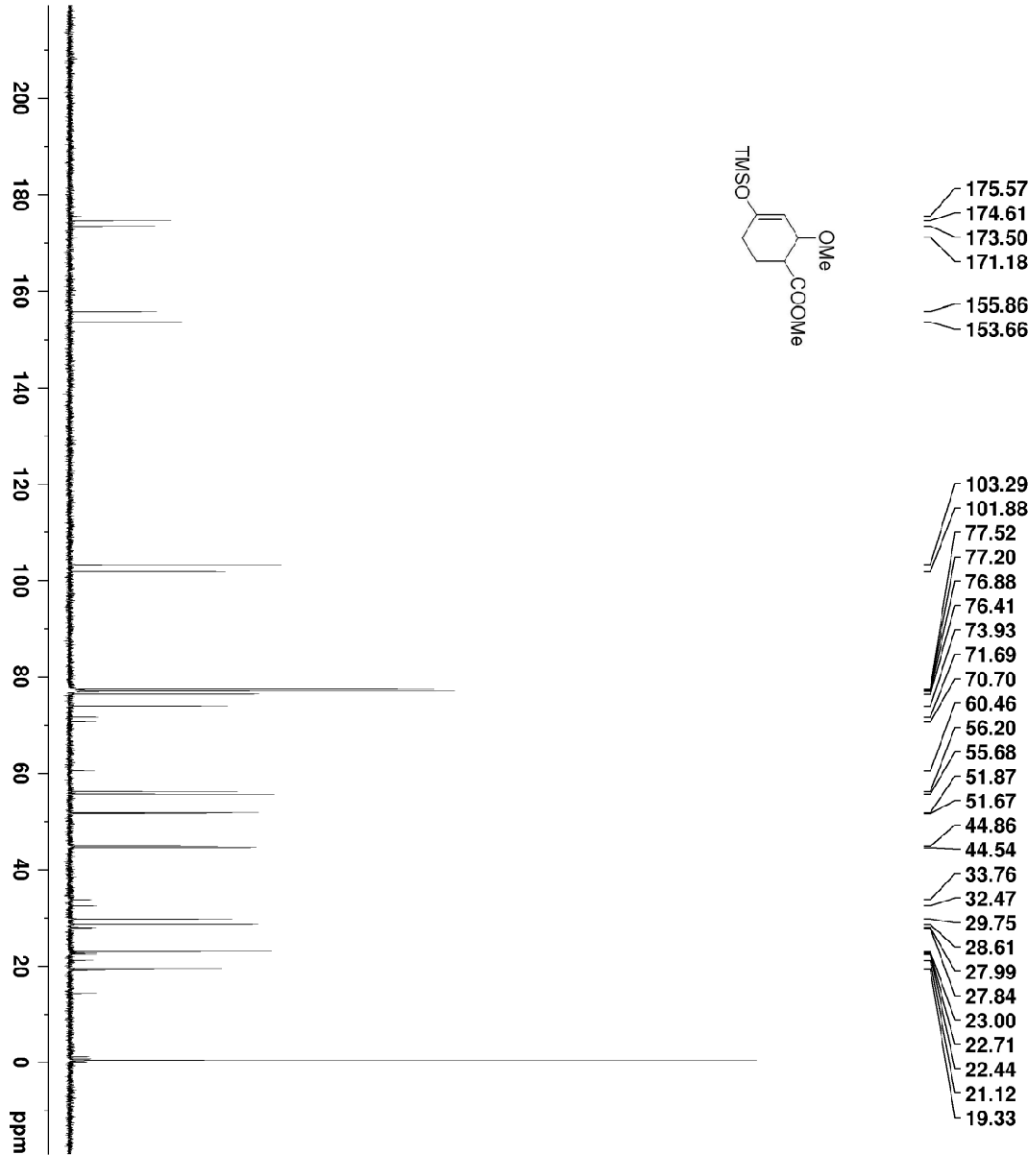
200
180
160
140
120
100
80
60
40
20
0
ppm
TMSO
OMe
COOMe
175.57
174.61
173.50
171.18
155.86
153.66
103.29
101.88
77.52
77.20
76.88
76.41
73.93
71.69
70.70
60.46
56.20
55.68
51.87
51.67
44.86
44.54
33.76
32.47
29.75
28.61
27.99
27.84
23.00
22.71
22.44
21.12
19.33

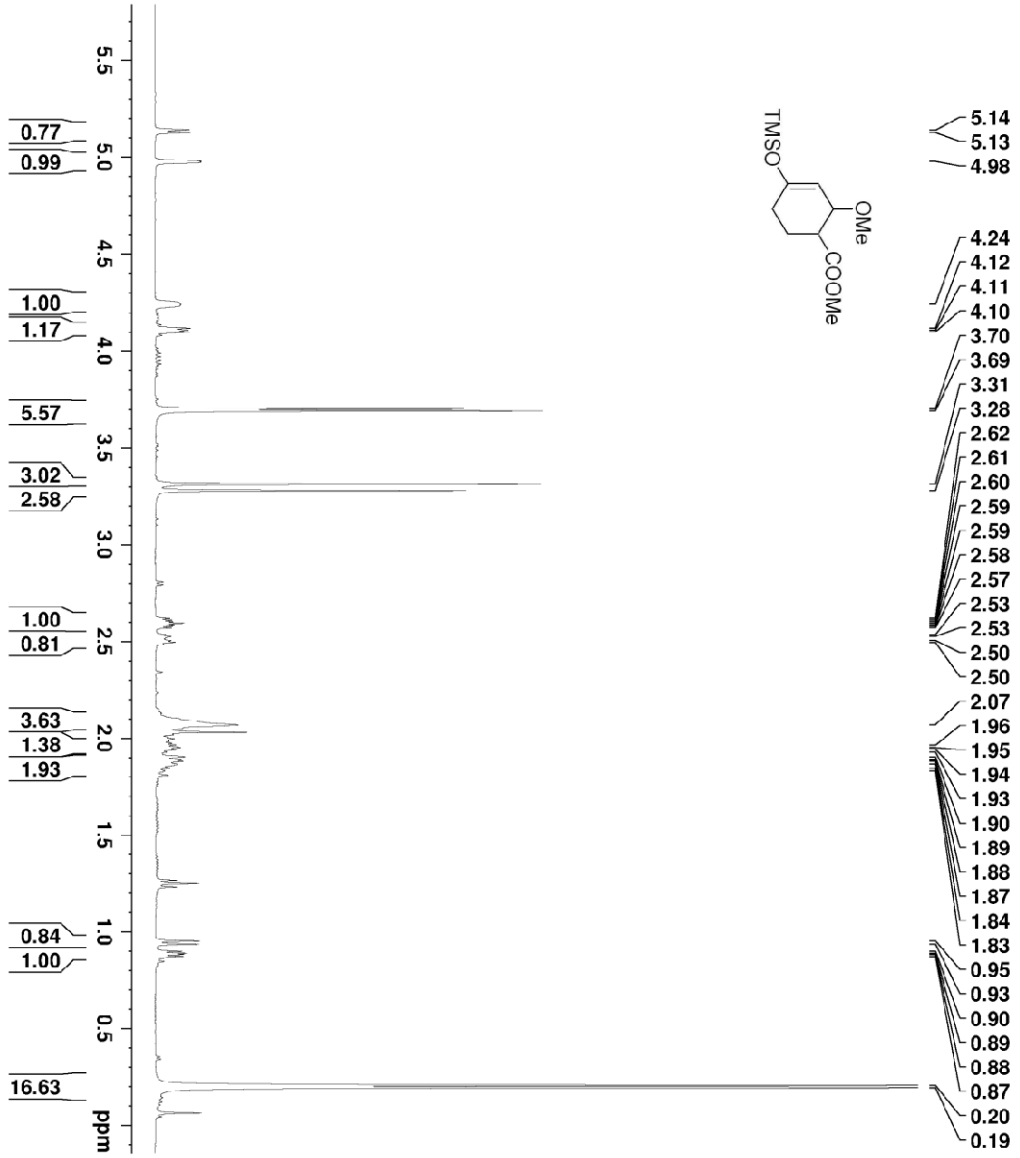
TMSO
OMe
COOMe
0.77
0.99
1.00
1.17
5.57
3.02
2.58
1.00
0.81
3.63
1.38
1.93
0.84
1.00
16.63
5.5
5.0
4.5
4.0
3.5
3.0
2.5
2.0
1.5
1.0
0.5
ppm
5.14
5.13
4.98
4.24
4.12
4.11
4.10
3.70
3.69
3.31
3.28
2.62
2.61
2.60
2.59
2.59
2.58
2.57
2.53
2.53
2.50
2.50
2.07
1.96
1.95
1.94
1.93
1.90
1.89
1.88
1.87
1.84
1.83
0.95
0.93
0.90
0.89
0.88
0.87
0.20
0.19

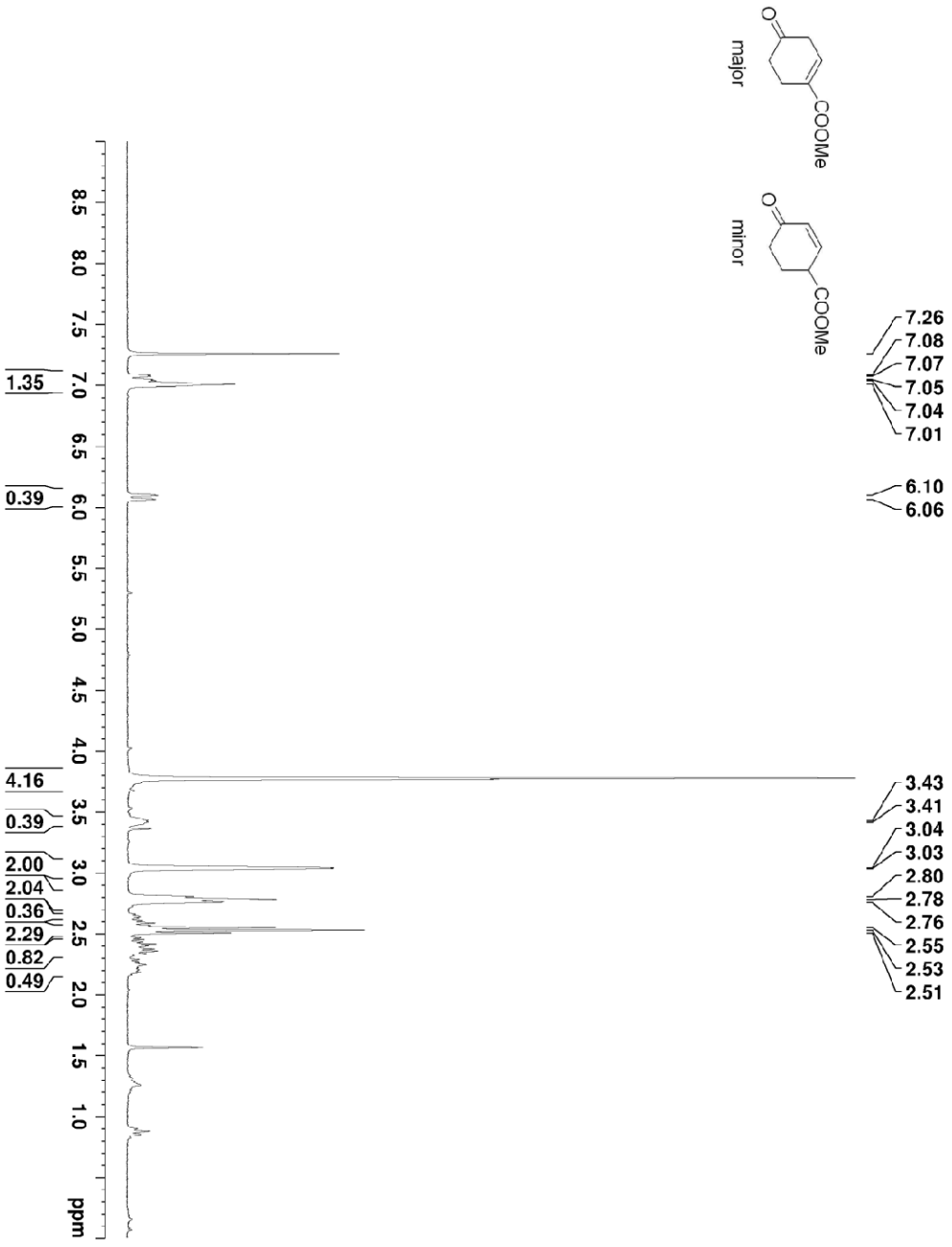
major
COOMe
minor
COOMe
7.26
7.08
7.07
7.05
7.04
7.01
6.10
6.06
3.43
3.41
3.04
3.03
2.80
2.78
2.76
2.55
2.53
2.51
1.35
0.39
4.16
0.39
2.00
2.04
0.36
2.29
0.82
0.49
8.5
8.0
7.5
7.0
6.5
6.0
5.5
5.0
4.5
4.0
3.5
3.0
2.5
2.0
1.5
1.0
ppm

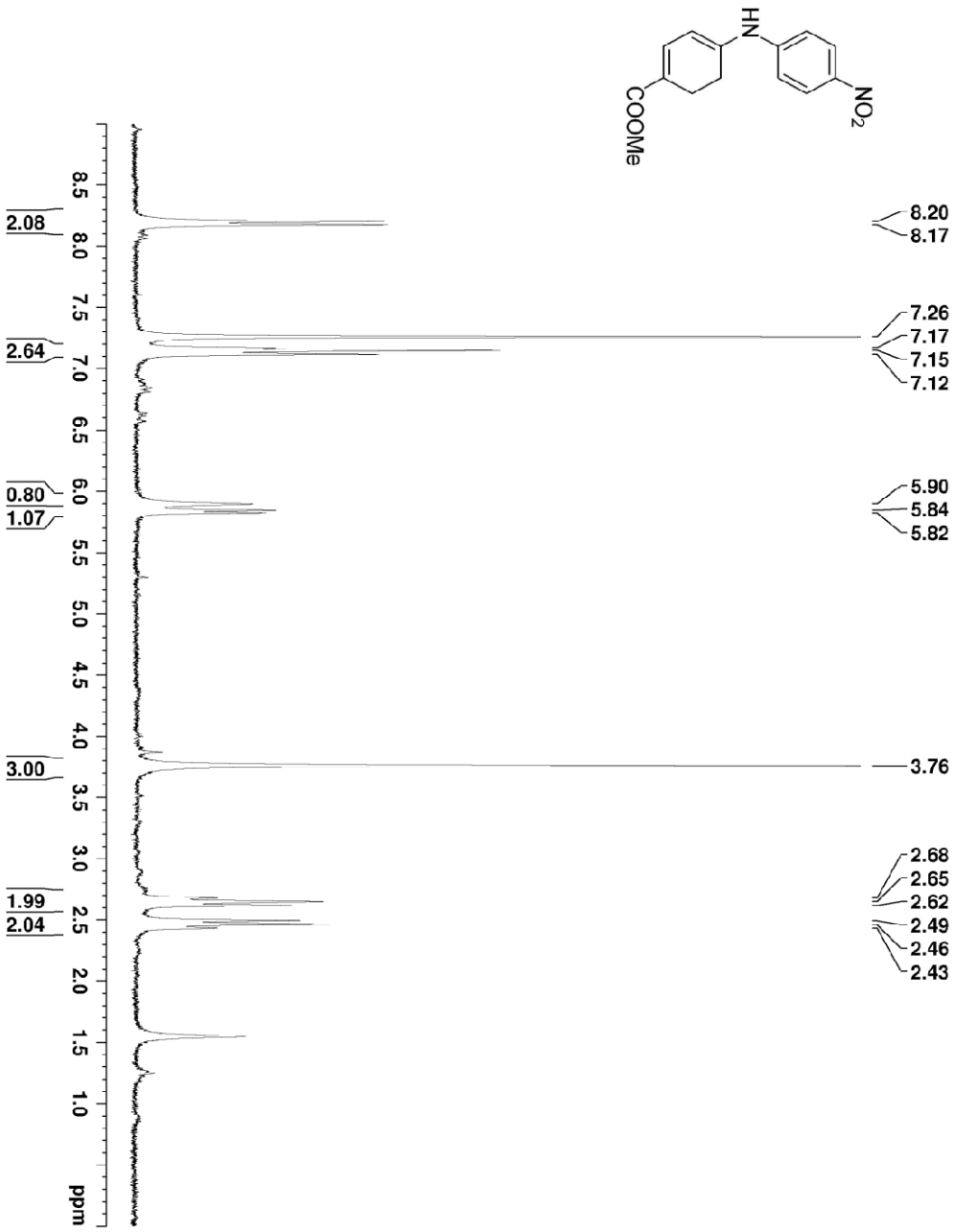
HN
COOMe
NO2
8.20
8.17
7.26
7.17
7.15
7.12
5.90
5.84
5.82
3.76
2.68
2.65
2.62
2.49
2.46
2.43
2.08
2.64
0.80
1.07
3.00
1.99
2.04
ppm

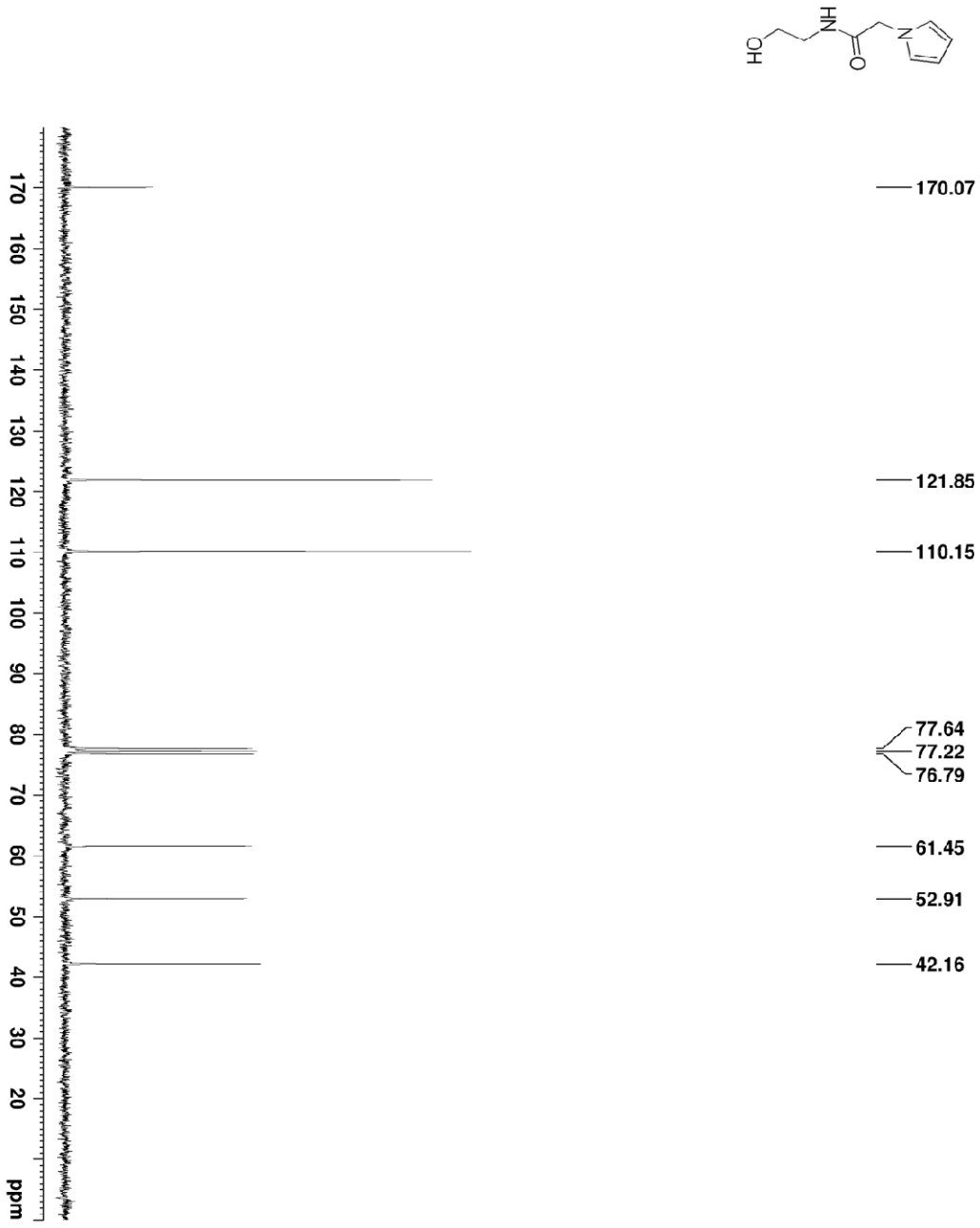
HO
NH
O
N
170.07
121.85
110.15
77.64
77.22
76.79
61.45
52.91
42.16
170
160
150
140
130
120
110
100
90
80
70
60
50
40
30
20
ppm

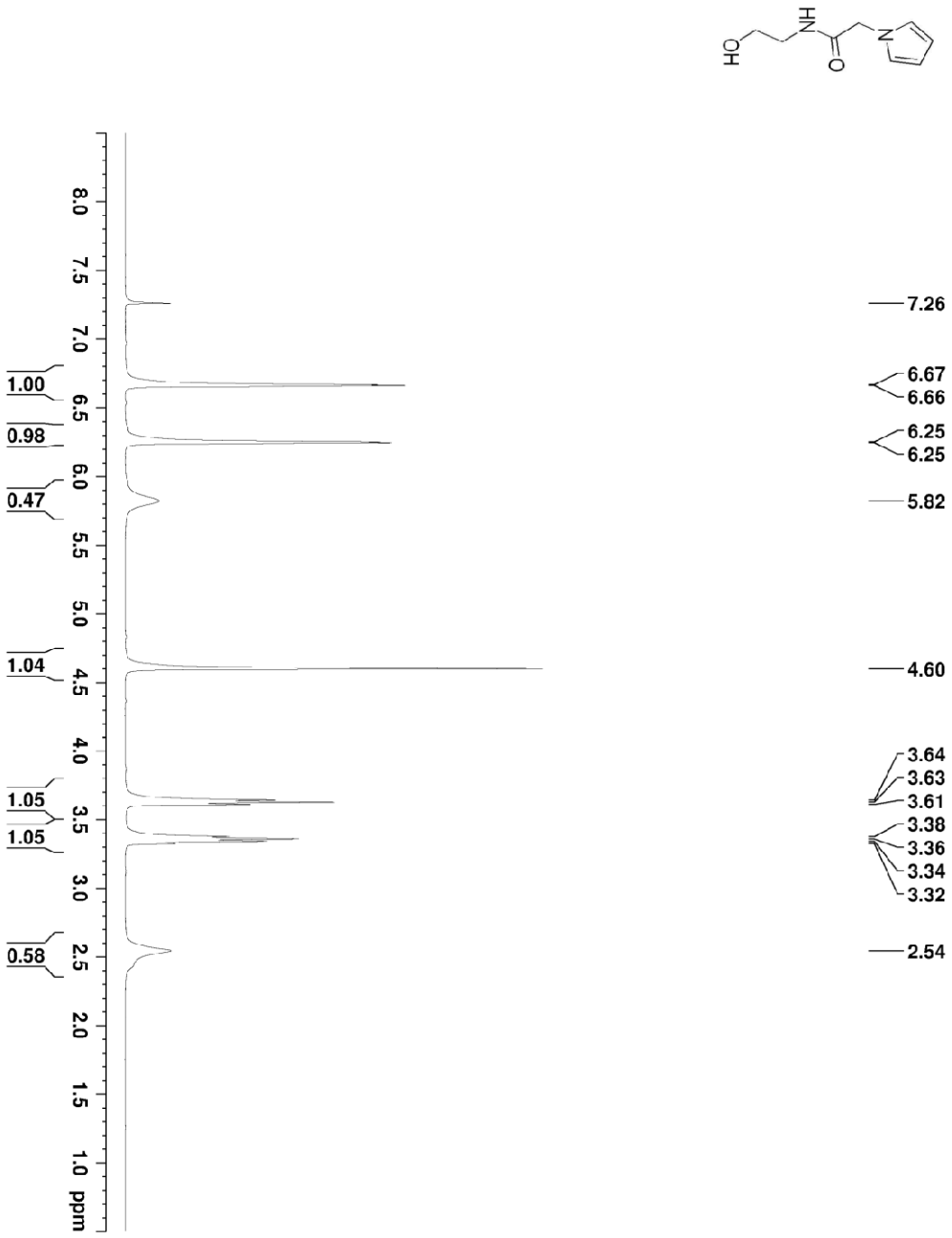
HO
NH
O
N
8.0
7.5
7.0
6.5
6.0
5.5
5.0
4.5
4.0
3.5
3.0
2.5
2.0
1.5
1.0
ppm
1.00
0.98
0.47
1.04
1.05
1.05
0.58
7.26
6.67
6.66
6.25
6.25
5.82
4.60
3.64
3.63
3.61
3.38
3.36
3.34
3.32
2.54

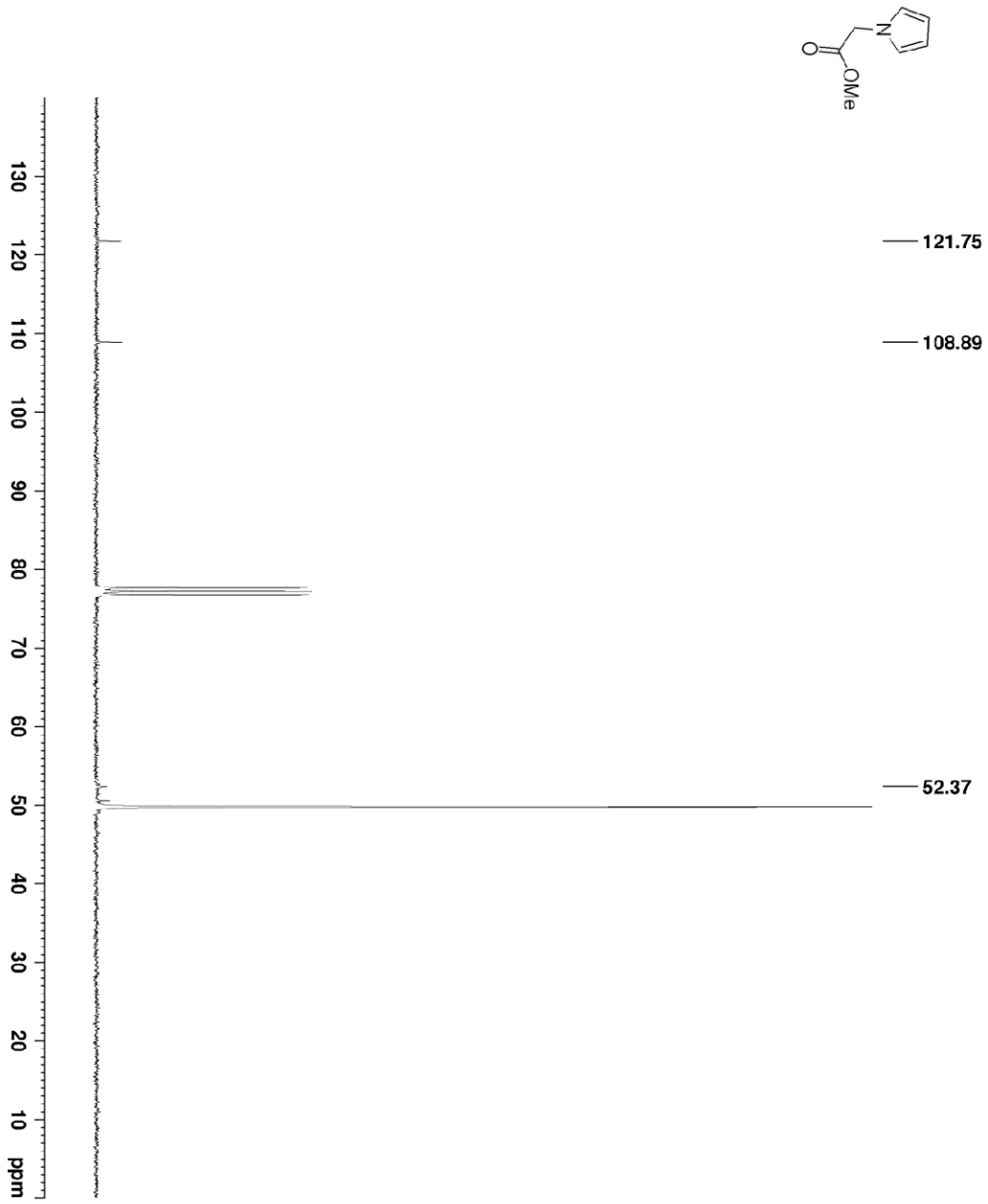
N
O
OMe
121.75
108.89
52.37
130
120
110
100
90
80
70
60
50
40
30
20
10
ppm

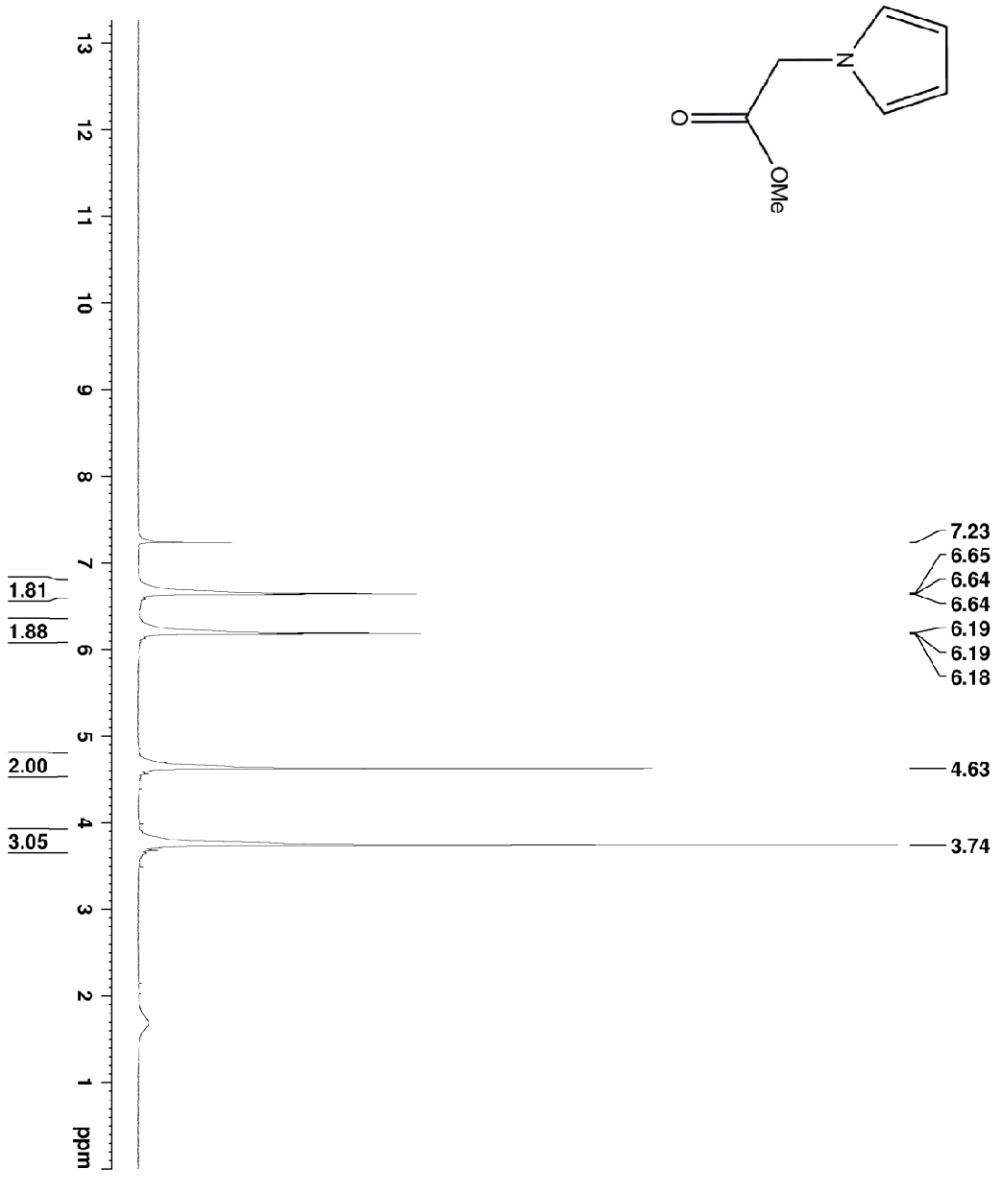
N
O
OMe
7.23
6.65
6.64
6.64
6.19
6.19
6.18
4.63
3.74
1.81
1.88
2.00
3.05
ppm

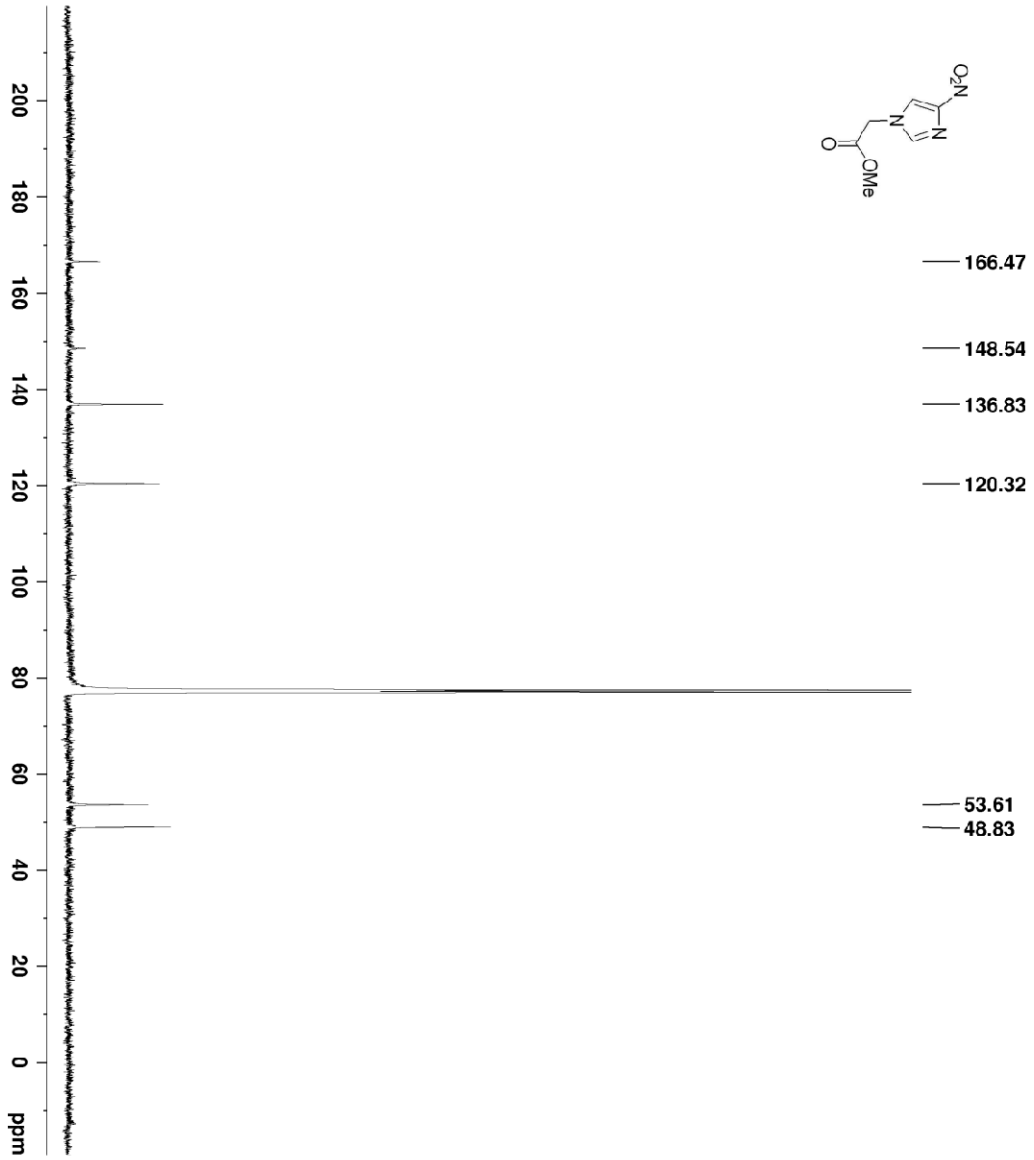
200
180
160
140
120
100
80
60
40
20
0
ppm
O2N
N
N
O
OMe
166.47
148.54
136.83
120.32
53.61
48.83

INFLUENCE OF DISTAL METHYL GROUP ON BASE INDUCED ISOMERIZATION OF TERMINAL ALKYNES

Chapter 6.

KINETICS OF BASE INDUCED ISOMERIZATION OF TERMINAL ALKYNES

6.1 Periodontal disease

Though we clean our mouth every day, it is true that our mouths are always filled with bacterial microflora, which consists of aerobic and anaerobic bacteria. These bacteria form colonies in biofilms on the surface of the tooth. These bacteria combines with other particles and mucus to form a sticky material called “plaque”. Prolonged accumulation of plaque becomes “tartar” which is hard to remove by brushing the teeth. The longer it stays, the more damage it can bring to the teeth. Because of the bacterial inflammation gums become red, swollen and bleeds easily. This type of gum disease is called “Gingivitis”, and it is a mild form of gum disease and easily cured. When gingivitis left untreated, it advances to “Periodontitis”. In this later stage, the body reacts to the bacterial growth along the gum line and the gums pull away from teeth and develop spaces which are called “pockets” (Figure 6.1). When these pockets become severely infected by the bacterial inflammation, the alveolar bones and the supporting tissues are broken down. The damage caused by gingivitis can be reversed with proper treatment whereas complete restoration of supporting tissues in periodontitis is impossible.

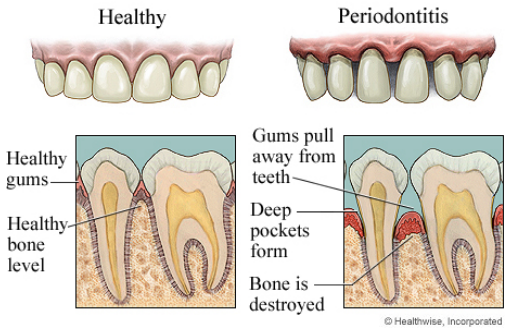

Figure 6.1. Healthy and Periodontitis diseased teeth (source: WebMD)[89]

6.2 Porphyromonas gingivalis and aliphatic alkynes

The anaerobic, Gram-negative organism, *Porphyromonas gingivalis*, is thought to be a major periodontal pathogen associated with inflammatory periodontal disease in adults. Lipid extracts of *P. gingivalis* are known to potentiate prostaglandin secretion from gingival fibroblasts when co-treated with interleukin-1b, and more recent work demonstrated that phosphorylated dihydroceramides, particularly phosphoglycerol dihydroceramides, are the primary biologically active lipid constituents.[90-92] These phosphorylated dihydroceramides have unusual sphinganine base and fatty acid components. The work in Frank Nicholas lab and Smith lab has shown that the dihydroceramides have isobranched C17 and C19 aliphatic chains that comprise the long chain bases in an amide linkage to 3-OH isobranch C17 fatty acids **19**. (Figure 6.2)

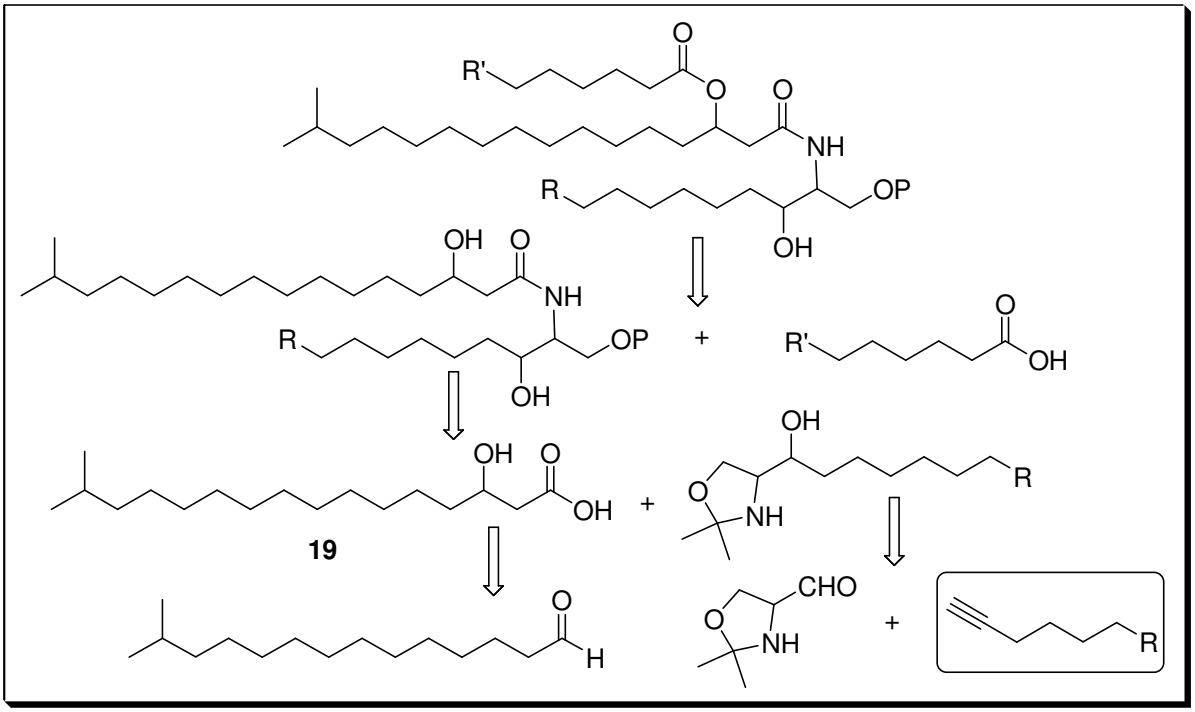

Figure 6.2. Retrosynthesis of phosphorylated dihydroceramides

In previous work, our lab synthesized the putative C17 and C19 long chain bases to prove their structure, and showed them to be isobranched, and that the isobranched aliphatic chains were critical for expression of biological activity.[93] We initially prepared the appropriate dihydroshphingasine derivatives, both isobranched and straight-chain via synthesis of the long-chain terminal alkyne, followed by coupling to Garner's aldehyde. [94,95] Preparation of the straight-chain terminal alkyne was straightforward, but attempts to generate the corresponding isobranched alkyne proved to be difficult. We observed rapid isomerization of the terminal alkyne to the internal alkyne, leading to poor isolated yields of the isobranched alkyne. The base-induced isomerization of triple bonds is well known,[96-101] proceeding through the allene intermediate:[102] In general, strong bases such as $NaNH_2$ convert internal alkynes to terminal alkynes because the equilibrium is shifted by formation of the acetylide ion. With weaker bases such as NaOH (which are not strong enough to

remove the acetylenic proton), the internal alkynes are favored because of their greater thermodynamic stability

If the temperature of the reaction was raised to ambient temperature or above, the base-induced isomerization was rapid, which was not a surprise. This isomerization was easily controlled by temperature control for the straight-chain alkynes, but not for the isobranched alkynes. We observed that long-chain alkynes with a terminal isobranch, distal to the terminal alkyne appeared to isomerize faster than the analogous straight chain alkyne. This isomerization was an interesting reaction and we turned our attention to probe the reason for the reactivity of the isobranched alkyne. We therefore examined the kinetics of the base induced isomerization to gain information that would help us to understand this unusual, and to our knowledge unprecedented observation.

6.3 Synthesis of C17 iso-branch and C18 straight chain external alkynes

To determine the kinetics of base induced isomerization for both the straight-chain terminal alkyne **2** and the iso-branched terminal alkyne **6**, we prepared each by routes that are somewhat different from conditions used in our initial work. Synthesis of the straight-chain alkyne **2** was straightforward and coupling of lithium acetylide with commercially available 1-bromohexadecane **1** in dry DMSO gave 1-octadecyne **2** in 73% yield. We prepared 13-methyl-1-bromotetradecan-1-ol **4** using methodology reported by Singh[103-105] and by Mori, [106] in which the cuprate-mediated coupling reaction of the Grignard reagent prepared *in situ* from 1-bromo-2-methylpropane **3** and commercially available 11-bromoundecan-1-ol. Conversion of 4-methylpentan-1-ol **4** to the corresponding bromide **5** was achieved with NBS and PPh_3 in chloroform. The 1-bromo-4-methylpentane **5** was reacted with lithium acetylide ethylene diamine complex to give 15-methyl-1-hexadecyne **6**.

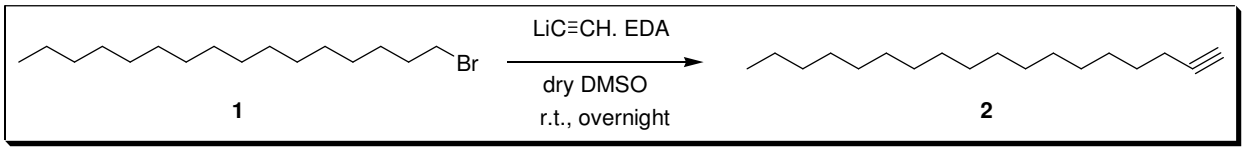

Scheme 6-1. Synthesis of 1-Octadecyne (C-18 straight chain external alkyne, **2**)

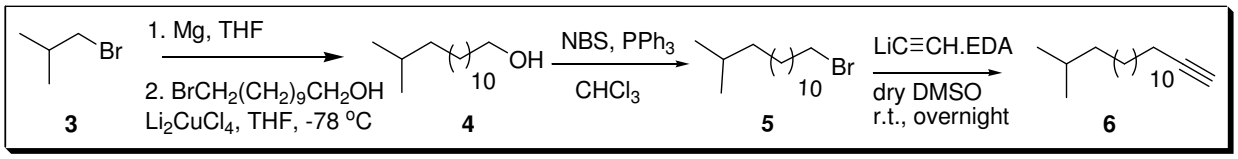

Scheme 6-2. Synthesis of 15-methyl-1-hexyne (C17 iso-branched external alkyne, **6**)

We heated both **2** and **6** with potassium tert-butoxide in DMSO, and observed formation of the internal alkyne, **7** and **8** respectively. In both cases, equilibrium was reached favoring **7** and **8**, with small amounts of **2** and **6**. We determined the equilibrium constants to be K(**6**) = 32.3 and K(**2**) = 46.6, indicating that **2** goes further towards completion relative to the reaction of **6.**

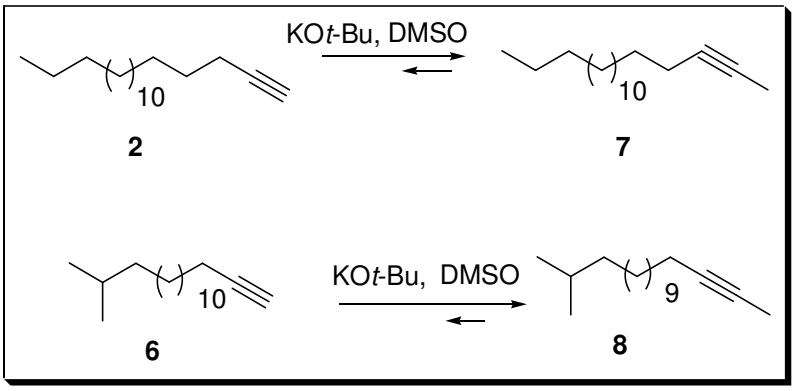

Figure 6.3. Isomerization of **2** and **6**

The base induced isomerization of terminal alkynes to internal alkynes is well known. It was reported that the reaction of 1-hexyne with potassium tert-butoxide, in DMSO at 25-40

°C, isomerized to 2-hexyne in 4 hours.[107] Interestingly, if the reaction was heated to 72 °C for 92 hours, the product was 2,4-hexadiene. Smadja observed a similar isomerization to 2-hexyne with potassium *tert*-butoxide in *tert*-butanol at 143 °C in four hours.[108] In that work, a mechanism was proposed for an equilibrium reaction involving the terminal alkyne, the internal alkyne and an allene intermediate. Indeed, isomerization of internal alkynes to terminal alkynes via a similar allene-mediated mechanism is well known.[109] Therefore, our observations that isomerization of **2** and **6** in DMSO to reach an equilibrium mixture is entirely consistent with previously reported results. A tentative alkyne:allene:alkyne equilibrium can be assembled, adapted from similar work for 1,4-diynes discussed by Mathai, et. al.[110] This diagram indicated that deprotonation of terminal alkyne **8** to give **9** is in equilibrium with α-deprotonation of **8** to give **10** (Figure 6.5). Due to the relatively high pK_a of the α-proton in particular, we believe that *tert*-butoxide reacts with DMSO to generate small concentrations of potassium methylsulfinylmethylide (dimsyl potassium, **14**) as the relevant base, accounting for the pseudo first order behavior. Once formed, anion **10** removes a proton, presumably from DMSO, to give allene **11**. 1,3-Proton transfers have been reported that involve allenes[111-113] and base mediated isomerization of terminal alkynes that involve allenes.[114] Subsequent deprotonation to give **12** is followed by formation of the final product **12**. This mechanistic diagram[115,116] represents the equilibrium mixture that favors the thermodynamically more stable internal alkyne **12**. It is noted that internal alkynes can be isomerized to terminal alkynes with Li diamines. Interestingly, we observed a larger equilibrium constant for the straight chain alkyne **2** when compared to the isobranched alkyne **6**.

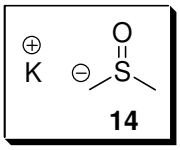

Figure 6.4. Dimsyl potassium

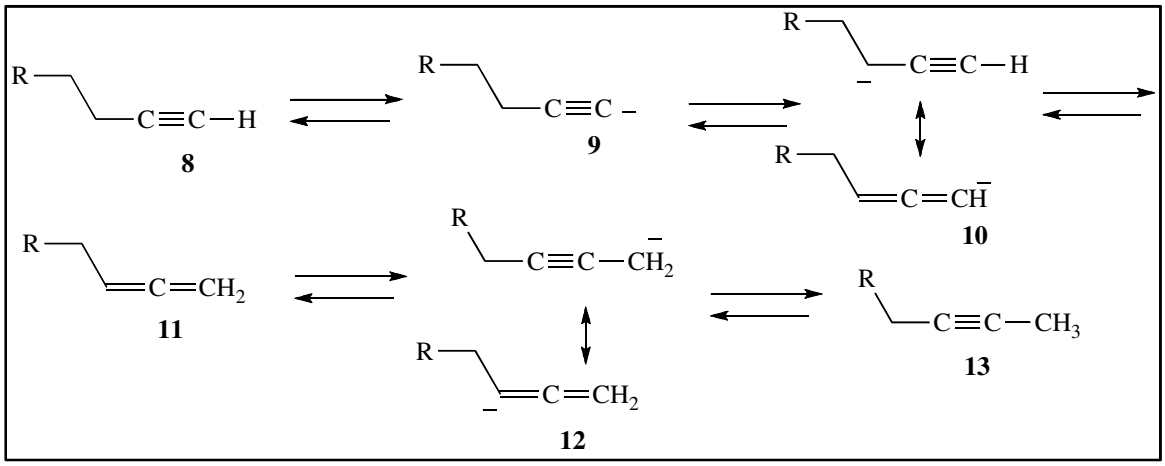

Figure 6.5 Proposed mechanism of terminal alkyne isomerization

Kinetics for isomerization of both **2** and **6** were determined in DMSO at 55 °C and also at 75 °C, temperatures at which reasonable data could be collected. Samples were prepared at 0.042 M alkyne in DMSO. Potassium *tert*-butoxide was added and aliquots were removed at the indicated time intervals shown in the following tables and quenched with water, the products extracted with hexane, and proton NMR data were collected at 300 MHz and 400 MHz.

Table 6-1. Kinetic data for octadec-1-yne **2** at 52-55 °C

Time (min)	Weight of octadec-1-yne **2** (mg)	Weight of octadec-2-yne **7** (mg)	Mmoles of octadec-1-yne **2**	Mmoles of octadec-2-yne **7**	Rel % of octadec-1-yne **2** 52-55 ^{o}C
0	5	0	0.02	0	100
10	4.93	0.07	0.01972	0.00028	98.6
20	4.875	0.125	0.0195	0.0005	97.5
30	4.745	0.255	0.01898	0.00102	94.9
40	4.635	0.365	0.01854	0.00146	92.7
50	4.53	0.47	0.01812	0.00188	90.6
60	4.425	0.575	0.0177	0.0023	88.5
70	4.335	0.665	0.01734	0.00266	86.7
80	4.24	0.76	0.01696	0.00304	84.8
90	4.06	0.94	0.01624	0.00376	81.2
100	4.035	0.965	0.01614	0.00386	80.7
110	3.94	1.06	0.01576	0.00424	78.8
120	3.835	1.165	0.01534	0.00466	76.7
130	3.75	1.25	0.015	0.005	75
190	3.075	1.925	0.0123	0.0077	61.5
250	2.685	2.315	0.01074	0.00926	53.7
260	2.685	2.315	0.01074	0.00926	53.7
310	2.475	2.525	0.0099	0.0101	49.5
370	2.285	2.715	0.00914	0.01086	45.7
430	2.045	2.955	0.00818	0.01182	40.9
600	1.53	3.47	0.00612	0.01388	30.6
660	1.25	3.75	0.005	0.015	25
720	1.035	3.965	0.00414	0.01586	20.7
780	0.91	4.09	0.00364	0.01636	18.2

840	0.86	4.14	0.00344	0.01656	17.2
900	0.745	4.255	0.00298	0.01702	14.9
960	0.665	4.335	0.00266	0.01734	13.3
1020	0.56	4.44	0.00224	0.01776	11.2
1080	0.535	4.465	0.00214	0.01786	10.7
1140	0.485	4.515	0.00194	0.01806	9.7
1200	0.44	4.56	0.00176	0.01824	8.8
1400	0.42	4.58	0.00168	0.01832	8.4
1520	0.38	4.62	0.00152	0.01848	7.6
1800	0.355	4.645	0.00142	0.01858	7.1
1980	0.28	4.72	0.00112	0.01888	5.6
2040	0.21	4.79	0.00084	0.01916	4.2
3600	0.105	4.895	0.00042	0.01958	2.1

Table 6-2. Kinetic data for octadec-1-yne (**2**) at 72-75 °C

Time (min)	Weight of octadec-1-yne **2** (mg)	Weight of octadec-2-yne **7** (mg)	Mmoles of octadec-1-yne **2**	Mmoles of octadec-2-yne **7**	Rel % of octadec-1-yne **2** 73-75 ^{o}C
0	5	0	0.02	0	100
10	4.337	0.663	0.017348	0.002652	86.74
20	3.487	1.513	0.013948	0.006052	69.74
30	2.7775	2.2225	0.01111	0.00889	55.55
40	2.3495	2.6505	0.009398	0.010602	46.99
50	1.852	3.148	0.007408	0.012592	37.04
60	1.5475	3.4525	0.00619	0.01381	30.95
70	1.294	3.706	0.005176	0.014824	25.88
80	1.043	3.957	0.004172	0.015828	20.86
90	0.912	4.088	0.003648	0.016352	18.24
100	0.798	4.202	0.003192	0.016808	15.96
110	0.674	4.326	0.002696	0.017304	13.48
120	0.611	4.389	0.002444	0.017556	12.22
130	0.568	4.432	0.002272	0.017728	11.36
140	0.5055	4.4945	0.002022	0.017978	10.11
150	0.4495	4.5505	0.001798	0.018202	8.99
160	0.443	4.557	0.001772	0.018228	8.86
170	0.4665	4.5335	0.001866	0.018134	9.33
180	0.371	4.629	0.001484	0.018516	7.42

Table 6-3. Kinetic data for methylhexadec-1-yne **6** at 52-55 °C

Time (min)	Weight of 15-methylhexadec-1-yne **6** (mg)	Weight of 15-methylhexadec-2-yne **8** (mg)	Mmoles of 15-methylhexadec-1-yne **6**	Mmoles of 15-methylhexadec-2-yne **8**	Rel % of methylhexadec-1-yne **6** 52-55 °C
0	5	0	0.021186441	0	100
10	3.9	1.1	0.016525424	0.004661017	78
20	3.47	1.53	0.01470339	0.006483051	69.4
30	3.215	1.785	0.013622881	0.007563559	64.3
40	3.14	1.86	0.013305085	0.007881356	62.8
50	2.99	2.01	0.012669492	0.008516949	59.8
60	2.74	2.26	0.011610169	0.009576271	54.8
70	2.59	2.41	0.010974576	0.010211864	51.8
80	2.53	2.47	0.010720339	0.010466102	50.6
90	2.26	2.74	0.009576271	0.011610169	45.2
110	2.24	2.76	0.009491525	0.011694915	44.8
120	1.975	3.025	0.008368644	0.012817797	39.5
140	1.85	3.15	0.007838983	0.013347458	37
200	1.38	3.62	0.005847458	0.015338983	27.6
260	1.065	3.935	0.004512712	0.016673729	21.3
380	0.66	4.34	0.00279661	0.018389831	13.2
500	0.51	4.49	0.002161017	0.019025424	10.2
600	0.26	4.74	0.001101695	0.020084746	5.2
660	0.21	4.79	0.000889831	0.02029661	4.2
720	0.15	4.85	0.000635593	0.020550847	3

Table 6-4. Kinetic data for methylhexadec-1-yne **6** at 72-75 °C

Time (min)	Weight of 15-methylhexadec-1-yne **6** (mg)	Weight of 15-methylhexadec-2-yne **8** (mg)	Mmoles of 15-methylhexadec-1-yne **6**	Mmoles of 15-methylhexadec-2-yne **8**	Rel % of methylhexadec-1-yne **6** 72-75 ^{o}C
0	5	0	0.021186441	0	100
10	3.4945	1.5055	0.014807203	0.006379237	69.89
20	2.6665	2.3335	0.011298729	0.009887712	53.33
30	1.693	3.307	0.007173729	0.014012712	33.86
40	1.5505	3.4495	0.006569915	0.014616525	31.01
50	1.3935	3.6065	0.005904661	0.01528178	27.87
60	1.193	3.807	0.005055085	0.016131356	23.86
70	0.9445	4.0555	0.004002119	0.017184322	18.89
90	0.76	4.24	0.003220339	0.017966102	15.2
100	0.6285	4.3715	0.002663136	0.018523305	12.57
110	0.5415	4.4585	0.002294492	0.018891949	10.83
120	0.4985	4.5015	0.002112288	0.019074153	9.97
130	0.39	4.61	0.001652542	0.019533898	7.8
140	0.375	4.625	0.001588983	0.019597458	7.5
150	0.3725	4.6275	0.00157839	0.019608051	7.45
160	0.3235	4.6765	0.001370763	0.019815678	6.47
170	0.327	4.673	0.001385593	0.019800847	6.54
180	0.3775	4.6225	0.001599576	0.019586864	7.55

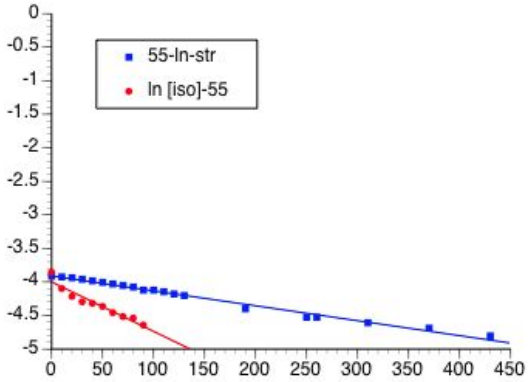

(a) ln[alkyne] at 52-55 °C

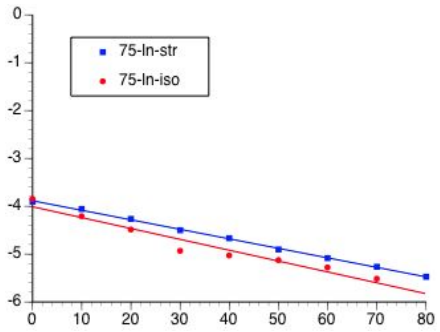

(b) ln[alkyne] at 72-75 °C

Figure 6.6. Plot of ln [**2**] and ln [**6**] versus time (min) at 55 °C and 75 °C.

We initially assumed that the base induced isomerization reaction was a second order reaction between the alkyne and the *tert*-butoxide base, and therefore plotted 1/[alkyne] versus time (in minutes). However, plots of 1/[alkyne] did not show a straight line relationship. As shown in Figure 6.6 plots of ln [alkyne] versus time gave straight line plots. We interpret these results to indicate that the isomerization follows pseudo first order kinetics. If this interpretation is correct, the *tert*-butoxide likely reacts with the DMSO sodium to produce dimsyl sodium, which would be the active base in the reaction and consistent with a pseudo first order process. We have screened a set of solvents which includes polar protic, and aprotic, to understand the role of solvent in the isomerization reaction. Alkyne isomerization was tried at 85 °C and 100 °C. Alkyne isomerization did not happen in any of the solvents, which supports the hypothesis of dimsyl ion **14** formation in the reaction (Table 6-5)

Table 6-5. Terminal alkyne isomerization in different sovents

Alkyne	Solvent	Temperature	Result
2	t-Butanol	85 °C	No Isomerization
	Dimethoxy ethane	85 °C	No Isomerization
	1,4-Dioxane	100 °C	No Isomerization
	Sulfolane	85 °C	No Isomerization
6	t-Butanol	85 °C	No Isomerization
	Dimethoxy ethane	85 °C	No Isomerization
	1,4-Dioxane	100 °C	No Isomerization
	Sulfolane	85 °C	No Isomerization

Based on Figure 6.6, it is clear that isomerization of the isobranched alkyne **6** is faster than that of the straight-chain alkyne **2**. We calculated a pseudo-first order rate constant for reactions done at 55 °C using the slope of the plots in Figure 6.6(a) and obtained a value of -7.38 x 10^{-3} mol^{-1} min^{-1} for the isobranched alkyne **6** and -2.23 x 10^{-3} mol^{-1} min^{-1} for the straight chain alkyne **2**. Kinetic data for the same reactions done at 75 °C are shown in Figure 6.6(b), and gave a rate of -2.27 x 10^{-2} mol^{-1} min^{-1} for **6** and -1.99 x 10^{-2} mol^{-1} min^{-1} for **2**. Although **6** isomerizes about 3.25 times faster than **2**. For both **6** and for **2**, the isomerization does not go to completion, but rather reaches an equilibrium of about 95-97% internal + 3-5% terminal alkyne.

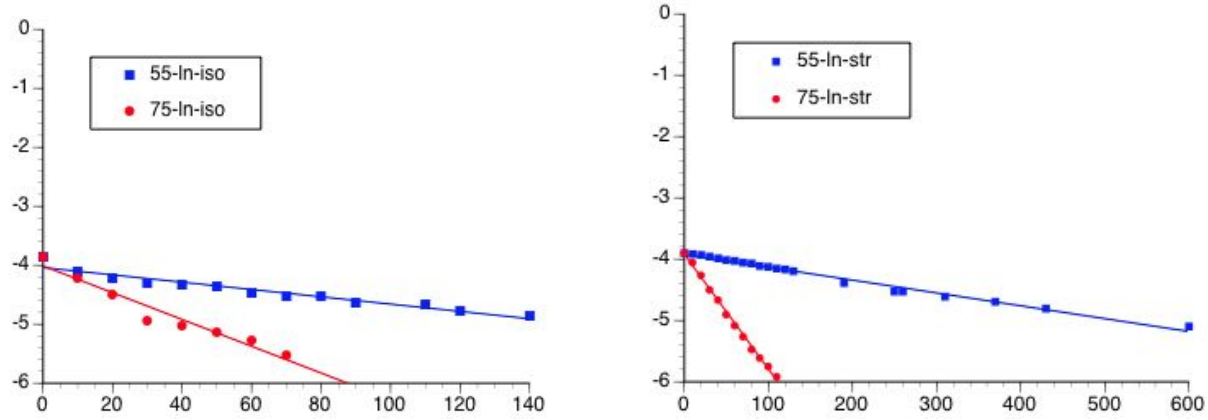

Figure 6.7. Plot of ln [**6**] vs time (min) at 55 °C and 75 °C and ln [**2**] vs time (min) at 55 °C and 75 °C

Using the data at 55 °C and 75 °C, we calculated the activation energy for each alkyne isomerization reaction was calculated using the formula:

$$\ln \frac{k_2}{k_1} = \frac{E_a}{R\left(\frac{1}{T_1} - \frac{1}{T_2}\right)}$$

Where k_2 = rate of alkyne (**2/6**) at T_2 , k_1 = rate of alkyne (**2/6**) at T_1, E_a = activation energy, R = 8.314 J K^{-1} mol^{-1}, T_1 = 55 °C = 328 K and T_2 = 75 °C = 348 K. As shown in Table 6-6, calculations showed that E_a for **2** = 3.19×10^{-3} J mol^{-1}, and E_a for **6** = 2.09×10^{-3} J mol^{-1}. This data suggests that isomerization of the isobranched alkyne is more difficult.

The faster rate of isomerization for **6** relative to **2** is clear, including the lower activation barrier for the reaction. The real question is why does a methyl group at the end of a long carbon chain have an influence of the rate of a reaction at the other end of the molecule? It is reasonable to assume that difference in rate are likely due to some intermolecular interaction that makes the isobranched alkyne more available for reaction, or an intramolecular interaction related to conformation. Bohn's work with relatively short

chain alkynes raises a point that may be relevant to our work. Microwave spectroscopic analysis of several alkynes presented evidence or the presence of an intramolecular CH/Π-interaction that stabilized gauche conformations relative to more open conformations.[117] It is, therefore, possible that long-chain alkynes exist in folded or coiled conformations in relatively large percentages. While speculative, such coiling could bring the distal end of the alkyne into closer proximity to the alkyne unit that is involved in the base-induced isomerization. Simple energy calculations for such coiled conformations of **2** and of **6** indicated that coiled **6** was about 2.4 kJ higher in energy. If correct, the isobranch would tend to be "less coiled" than the straight chain alkyne, presumably making the propargylic carbon and possibly the terminal alkyne proton of the isobranched alkyne more available for reaction with base, leading to a faster rate of isomerization.(Figure 6.8)

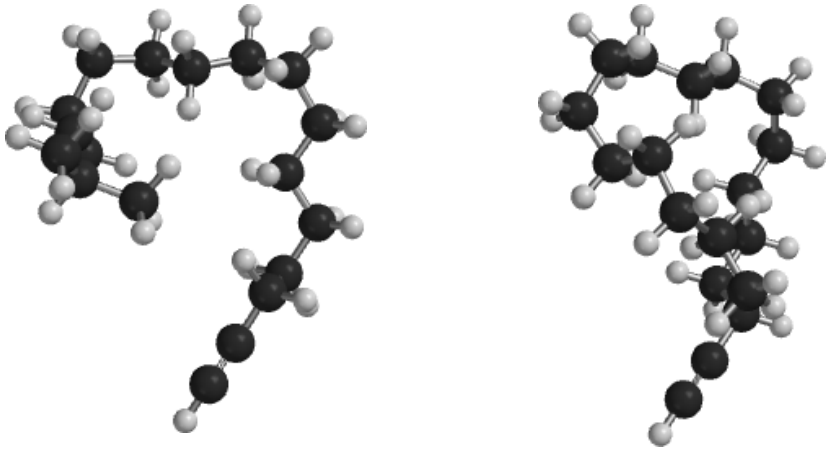

Figure 6.8 Spartan 3D images of coiled conformations of **6** and **2**

Table 6-6. Rate data for **2** and **6** at 55 °C and 75 °C

Alkyne	Pseudo first order rate constant at 55 °C (Mol^{-1} min^{-1})	Pseudo first order rate constant at 75 °C (Mol^{-1} min^{-1})	Activation energy E_a (J Mol^{-1})
2	-2.23×10^{-3}	-18.49×10^{-3}	3.19×10^{-3}
6	-4.64×10^{-3}	-18.75×10^{-3}	2.09×10^{-3}

This proposal is certainly highly speculative, but it is reasonable to assume that difference in rate are likely due to some intermolecular interaction that makes the isobranched alkyne more available for reaction, or an intramolecular interaction related to conformation. To the best of our knowledge, except for Bohn's work, the literature does not provide precedent for either case. Therefore, we present our findings that the presence of a distal methyl group undergoes base-induced isomerization about 3 times faster than the straight chain analog, and offer a possible explanation based on a novel and speculative conformational effect.

To further validate this hypothesis, we synthesized heptadec-1-yne **18** and hexadec-1-yne **16**. The synthesis of each alkyne is straight forward. When the corresponding alkyl bromides **15**, **17** treated with lithium acetylide EDA complex, terminal alkynes **16**, **18** were obtained. To understand the effect of chain length on the isomerization, we studied the kinetics of **16** and **18**.

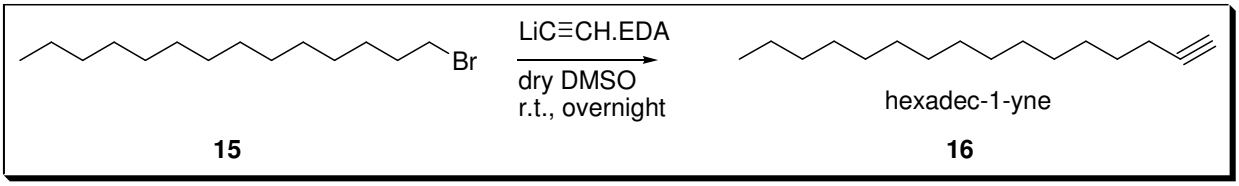

Scheme 6-3. Synthesis of hexadec-1-yne **16**

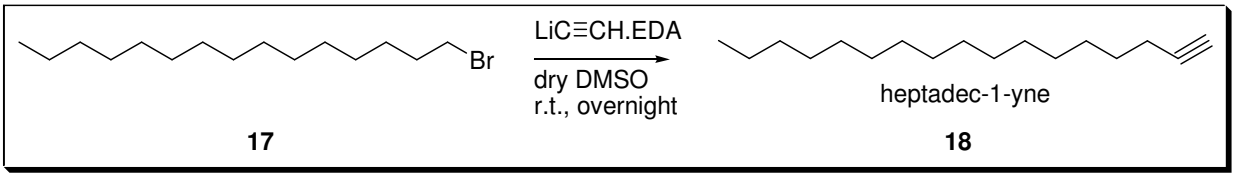

Scheme 6-4. Synthesis of heptadec-1-yne **18**

When we attempted the kinetic studies, we found an interesting observation, the time required for the experiments was much shorter although the trend of isomerization was maintained (the isobranch is faster than straight chain). We ran the experiments with fresh DMSO from a new bottle. To double check our previous results, we ran the kinetics experiments with the old DMSO and the results were repeated as before. We assumed that the old bottle was contaminated with water and calculated the water content in the DMSO using a Karl Fisher Coulometer.[118] The water content in the old DMSO was found to be 4.38%. We rationalized the results to be either water stabilizing the coiled conformations of alkynes or quenching of the dimisyl anion. We don't know the answer yet, but it is clear that the isobranched alkyne isomerizes faster than the straight chain alkyne. This unexpected observation has opened up more questions. If our hypothesis is true, we want to explain how water effects the coiled conformations in solution? To fully understand the effect of water, it is important to look at the energies of coiled conformation of alkynes in presence of water.

Molecular modeling studies that incorporate the hydrophobic interactions between the long aliphatic chains of alkynes and water may be useful. We are collaborating with Dr. Jose Gascon for the molecular modelling experiments on alkynes. After observing the water effect on the isomerization, we conducted the kinetic studies on hexadec-1-yne **16**, heptadec-1-yne **18**, octadec-1-yne **2** and 15-methylhexadec-1-yne **6** with fresh DMSO and the data will be analyzed including the molecular modelling studies.

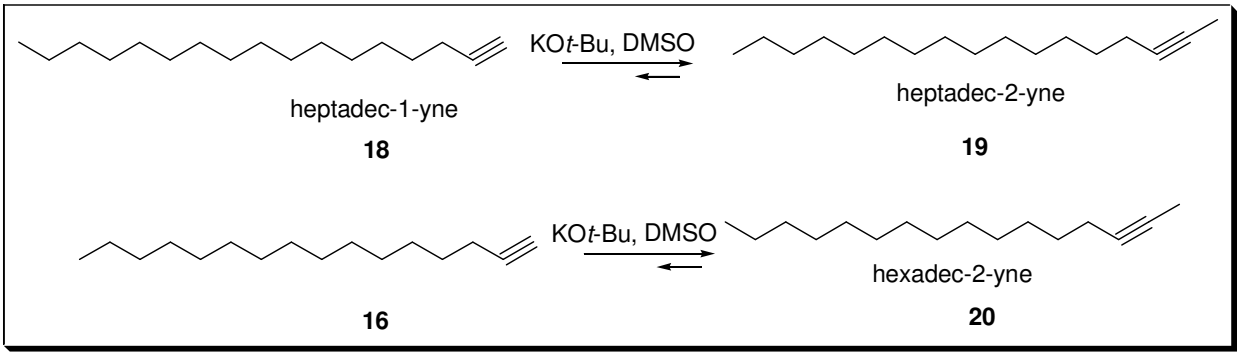

Scheme 6-5. Isomerization of hexadec-1-yne **16**, heptadec-1-yne **18**

6.4 Experimental:

All glassware was flame-dried under nitrogen, and all reactions were performed under a nitrogen atmosphere. All chemicals were purchased from the Aldrich Chemical Co., and used without further purification. The tetrahydrofuran was dried over sodium–benzophenone and distilled immediately prior to its use. The ^{1}H NMR (400 MHz) and the ^{13}C NMR (100.65 MHz) were recorded on a Brücker DRX-400 instrument, in $CDCl_3$ unless otherwise noted, and all chemical shifts are reported relative to tetramethylsilane (TMS) as an internal standard. Infrared spectra were recorded on a JASCO FT/IR-410 instrument, and reported in cm^{-1}. Mass spectra were recorded on a Hewlet-Packard 5970 GC/MS instrument. High resolution mass spectrometry of new compounds was performed on a Micromass VB-QTOF tandem mass spectrometer.

All chemicals were used as received from Aldrich or Acros. All glassware was flame-dried under vacuum, and all reactions in organic solvents were performed under a nitrogen atmosphere, unless otherwise noted. All solvents were dried according to standard procedures. THF was distilled from sodium benzophenone ketyl, methylene chloride was distilled from calcium hydride, and dimethylformamide was vacuum distilled from calcium hydride. Thin-layer chromatography was done on Sorbent Technologies aluminum-backed TLC plates with fluorescent indicator and 0.2 mm silica gel layer thickness, and *p*-anisaldehyde, Phosphomolybdic acid were used as developing agents. Column chromatography was done using 60 Å porosity, 32-63 μm silica gel. ^{1}H and ^{13}C NMR were collected on a Brüker Avance 300 (300.13 MHz ^{1}H, 75.48 MHz ^{13}C), Brüker DRX-400 (400.144 MHZ ^{1}H, 100.65 MHz ^{13}C) or a Brüker Avance 500 (500.13 MHz ^{1}H, 125.65 MHZ

^{13}C). Chemical shifts are given in ppm downfield from TMS in the following format chemical shift, multiplicity (s=singlet, d=doublet, t=triplet, q=quartet, m=multiplet) coupling constant in Hz and Integration. Mass spectroscopy data was collected on a HP 5870B GC/MSD mass spectrometer with an HP-1 column, and high resolution mass spectrometry was done on a Micromass VB-QTOF tandem mass spectrometer. IR spectrums were taken on FT/IR-410/C031560585 JASCO and Nexus 670 FT-IR E.S.P under neat conditions unless and otherwise stated. Melting points were taken on a Uni-melt capillary melting point apparatus and Digimelt MPA160 and recorded to a maximum of 270 °C. For products described as waxy solid, melting points could not be obtained.

Octadec-1-yne (2)

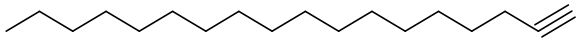

(**2**)

Lithium acetylide (0.3 g, 3.2 mmol) was added to a stirring solution of 1-bromohexadecane **1** (0.5 g, 1.64 mmol) in dry DMSO (3 mL) and the resulting solution was stirred overnight at room temperature. Reaction progress was monitored by TLC. After the reaction completed, the reaction mixture was quenched with 50 mL of H_2O and extracted with diethyl ether (2×25 mL). The organic extracts were washed with water (50 mL), brine and dried over anhydrous $MgSO_4$ and concentrated *in vacuo* to give a crude solid, which was purified by column chromatography (100% hexane) to obtain octadec-1-yne as a clear oil which become white solid up on cooling in an ice bath (0.3 g, 1.20 mmol, 73%);[119] mp: low melting solid (26-27 ºC); IR (neat) 3287, 2915, 2954, 2848, 2115, 1462, 682 cm^{-1}; ^1H NMR (400 MHz, $CDCl_3$) δ 2.18 (td, *J* = 7.1, 2.5 Hz, 2H), 1.93 (t, *J* = 2.5 Hz, 1H), 1.56-1.49 (m, 2 H), 1.40-1.37 (m, 2 H), 1.26 (bs, 24 H), 0.86 (m, 3H); ^{13}C NMR (75 MHz, $CDCl_3$) δ 84.8, 68.2, 32.2, 30.0, 29.9, 29.8, 29.6, 29.4, 29.0, 28.8, 22.9, 18.6, 14.3.

Octadec-2-yne (7)

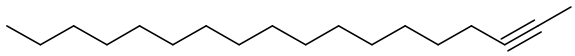

(**7**)

Mp: low melting solid (27-28 °C); IR (neat); 2954, 2912, 2871, 2847, 1470,716 cm^{-1}; ^1H NMR (400 MHz, $CDCl_3$) δ 2.11 (tq, *J* = 5.0, 2.4 Hz, 2H), 1.78 (t, *J* = 2.5 Hz, 3H), 1.50-1.43 (m, 2H), 1.37-1.32 (m, 2H), 1.26 (bs, 24H), 0.88 (m, 3H); ^{13}C NMR (100 MHz, $CDCl_3$)

δ 79.6, 75.4, 32.1, 29.9, 29.7, 29.5, 29.4, 29.3, 29.1, 22.9, 18.9, 14.3, 3.6; HRMS (ESI-TOF): [M+H]+ Calc'd for C_{18} H_{34} *m/z* 251.2739. Found, *m/z* 251.2714.

13-Methyltetradecan-1-ol (4)

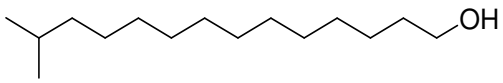

(**4**)

Magnesium turnings (1.52 g, 62.7 mmol) were suspended in dry THF (25 mL) and 1-bromo-2-methyl propane (5.7 mL, 52.5 mmol) was added with vigorous stirring under a nitrogen atmosphere at room temperature. After the reaction mixture started refluxing, another 25 mL of dry THF was added and the reaction mixture was stirred until it cooled to room temperature and turned light brown. In a separate flask LiCl (0.71 g, 16.7 mmol) and $CuCl_2$ (1.09 g, 8.12 mmol) were dissolved in dry THF (15 mL) and stirred for 30 minutes at room temperature. The Grignard solution was cooled to -78 ºC. A solution of 11-bromo-1-undecanol in dry THF (7 mL) was added slowly via syringe, followed by a solution containing the Li_2CuCl_4 salt in THF and the resulting solution was warmed to room temperature and stirred overnight. The reaction mixture was quenched with saturated aqueous ammonium chloride (50 mL), washed with H_2O (50 mL) and extracted with diethyl ether (3×50 mL). The organic extracts were combined and washed with saturated aqueous $NaHCO_3$ (3×50 mL), brine, and dried over $MgSO_4$. The solvent was removed *in vacuo* to give a crude oil which was further purified by flash column chromatography (9:1 petroleum ether: ethylacetate) to yield 13-methyltetradecanol as a white solid (1.44 g, 6.32 mmol, 79%)[120-122]; mp: 30-31 °C; ^{1}H NMR (300 MHz, $CDCl_3$) δ 3.64 (t, *J* = 6.6 Hz, 2H), 1.59-1.47 (m, 4H), 1.26 (bs, 18H) 1.16-1.13 (m, 3 H), 0.86 (d, *J* = 6.6 Hz, 6H); ^{13}C NMR (75 MHz, $CDCl_3$) δ 63.3, 39.3, 33.1, 30.2, 29.9, 29.8, 29.7, 28.2, 27.6, 26.0, 22.9.

1-Bromo-13-methyltetradecane (5)

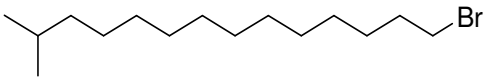

(**5**)

To a stirred solution of 13-methyltetradecanol **4** (1.44 g, 6.32 mmol) in dry dichloromethane (40 mL) was added triphenylphospine (2.38 g, 9.08 mmol). The resulted solution was cooled to 0º C, and *N*-Bromosuccinimide (1.54 g, 8.65 mmol) was added in portionwise and the solution was warmed to room temperature stirred overnight at room temperature. The solvent was evaporated *in vacuo* and the residue was stirred in hexane (50 mL). The resulted slurry was filtered and the cake washed several times with hexane (5×5 mL). The filtrate was concentrated *in vacuo* to give an oil which was purified by flash column chromatography (100% petroleum ether) to obtain 1-bromo-13-methyltetradecane as a clear oil (1.48 g, 5.09 mmol, 81%); ^{1}H NMR (300 MHz, $CDCl_3$) δ 3.37 (td, *J* = 6.9, 2.0, Hz, 2H), 1.89-1.79 (m, 2H), 1.61-1.48 (m, 1H), 1.45-1.40 (m, 2H), 1.27 (bs, 16H), 1.17-1.15 (m, 2H), 0.84 (dd, *J* = 6.7, 2.2 Hz, 6 H); ^{13}C NMR (75 MHz, $CDCl_3$) δ 39.3, 33.7, 33.1, 30.2, 30.0, 29.9, 29.8, 29.7, 29.0, 28.5, 28.2, 27.7, 22.8, 14.3.

15-Methylhexadec-1-yne (6)

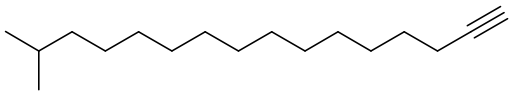

(**6**)

Lithium acetylide EDA complex (0.190 g, 2.05 mmol) was added to the stirring solution of 1-bromo-13-methyltetradecane **5** (0.12 g, 0.41 mmol) in dry DMSO (3 mL) and the resulted solution was at room temperature for overnight. The reaction progress was monitored by TLC. The reaction mixture was quenched with H_2O (30 mL) and extracted

with diethyl ether (3×10 mL). The organic extracts were washed with water (50 mL), brine (50 mL) and dried over anhydrous $MgSO_4$. The solvent was removed *in vacuo* to give 15-methylhexadec-1-yne as an oil, which was purified by column chromatography (straight hexane) to obtain a clear oil (0.075 g, 3.18 mmol, 77%); IR (KBr, CH_2Cl_2) 3315, 2960, 2925, 2855, 2120, 1466, 1261, 1095, 803, 629 cm^{-1}; ^1H NMR (300 MHz, $CDCl_3$) δ 2.17 (td, *J* = 6.9, 2.5 Hz, 2H), 1.92 (t, *J* = 2.6 Hz, 1H), 1.54-1.47 (m, 3H), 1.38 (m, 2H), 1.26 (bs, 16 H), 1.16 (m, 2H), 0.86 (d, *J* = 6.6 Hz, 6H); ^{13}C NMR (75 MHz, $CDCl_3$) δ 84.9, 68.2, 39.3, 30.2, 30.0, 29.9, 29.8, 29.7, 29.4, 29.0, 28.7, 28.2, 27.7, 22.9, 18.6; HRMS (ESI-TOF): [M+H]+ Calc'd for $C_{17}H_{32}$ *m/z* 236.2504. Found, *m/z* 236.2524.[123,124]

15-Methylhexadec-2-yne (8)

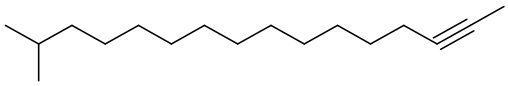

(**8**)

IR (neat); 2921, 2852, 1465, 1383, 1365,720, 698 cm^{-1};^1H NMR (400 MHz, $CDCl_3$) δ 2.11 (tq, *J* = 5.0, 2.4 Hz, 2H), 1.77 (t, *J* = 2.5 Hz, 3H), 1.54-1.43 (m, 3H), 1.37-1.34 (m, 2H), 1.26 (bs, 14H), 1.21-1.12 (m, 2H), 0.86 (d, *J* = 6.6 Hz, 6H); ^{13}C NMR (100 MHz, $CSCl_3$) δ 79.6, 75.4, 39.3, 30.1, 29.9, 29.8, 29.7, 29.4, 29.3, 29.1, 28.2, 27.6, 22.8, 18.9, 3.6; HRMS (ESI-TOF): [M+H]+ Calc'd for $C_{17}H_{32}$ *m/z* 237.2582. Found, *m/z* 237.2582.

Heptadec-1-yne (16)

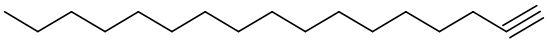

(**16**)

Lithium acetylide EDA complex (0.63 g, 6.86 mmol) was added to the stirring solution of 1-bromopentadecane **17** (1.0 g, 3.43 mmol) in dry DMSO (15 mL) and the resulted solution was at room temperature for overnight. The reaction progress was monitored by TLC. The reaction mixture was quenched with H_2O (30 mL) and extracted with diethyl ether (3×10 mL). The organic extracts were washed with water (50 mL), brine (50 mL) and dried over anhydrous $MgSO_4$. The solvent was removed *in vacuo* to give 15-methylhexadec-1-yne (**6**) as an oil, which was purified by column chromatography (straight hexane) to obtain 15-methylhexadec-1-yne (0.78 g, 2.69 mmol, 78%); IR (neat); 3314, 2921, 2852, 1675, 1654, 1594, 1485,1465, 1432, 1403, 1348, 1306, 1282, 1254, 1207, 1177,1120,1062 cm^{-1}; ^1H NMR (400 MHz, $CDCl_3$) δ 2.18 (td, *J* = 7, 2.5 Hz, 2H), 1.93 (t, *J* = 2.6 Hz, 1H), 1.56-1.49 (m, 2H), 1.40 (m, 2H), 1.26 (bs, 22 H), 0.90-0.86 (m, 3H); ^{13}C NMR (400 MHz, $CDCl_3$) δ 85.0,, 68.2, 32.1, 29.9, 29.8, 29.7, 29.6, 29.3, 29.0, 28.7, 22.9, 18.6, 14.3; HRMS (ESI-TOF): [M+H]+ Calc'd for $C_{17}H_{32}$ *m/z* 237.2582. Found, *m/z* 237.2579.

Heptadec-2-yne (7)

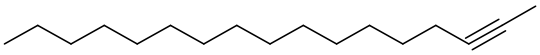

(**7**)

IR (neat); 2920, 2852, 1680, 1601, 1493, 1453, 1348, 1311,1264, 1026 cm^{-1}; ^1H NMR (400 MHz, $CDCl_3$) δ 2.11 (tq, *J* = 5, 2.4 Hz, 2H), 1.78 (t, *J* = 2.5 Hz, 3H), 1.50-1.43 (m, 2H), 1.37-1.34 (m, 2H), 1.26 (bs, 20H), 0.89-0.86 (m, 3H); ^{13}C NMR (100 MHz, $CDCl_3$) δ 79.6,

75.5, 32.1, 29.9, 29.8, 29.7, 29.4, 29.3, 29.1, 22.9, 18.9, 14.3, 3.6; HRMS (ESI-TOF): [M+H]+ Calc'd for $C_{17}H_{32}$ *m/z* 237.2582. Found, *m/z*. 237.2581.

Hexadec-1-yne (18)

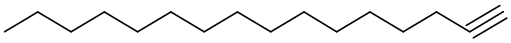

(**18**)

Lithium acetylide EDA complex (0.63 g, 6.86 mmol) was added to the stirring solution of 1-bromotetradecane (**15**) (1.0 g, 3.43 mmol) in dry DMSO (15 mL) and the resulted solution was stirred at room temperature overnight. The reaction progress was monitored by TLC. The reaction mixture was quenched with H_2O (30 mL) and extracted with diethyl ether (3×10 mL). The organic extracts were washed with water (50 mL), brine (50 mL) and dried over anhydrous $MgSO_4$. The solvent was removed *in vacuo* to give 15-methylhexadec-1-yne as an oil, which was purified by column chromatography (straight hexane) to obtain 15-methylhexadec-1-yne (0.78 g, 2.69 mmol, 78%); IR (neat); 3313, 2922, 2852, 1676, 1654, 1592, 1500,1485, 1466, 1430, 1404, 1379, 1350,1308, 1282, 1253,1194, 1178, 1121, 1061, 1028 cm^{-1}; ^1H NMR (400 MHz, $CDCl_3$) δ 2.18 (td, *J* = 7, 2.6 Hz, 2H), 1.93 (t, *J* = 2.6 Hz, 1H), 1.56-1.49 (m, 2H), 1.40-1,37 (m, 2H), 1.26 (bs, 20H), 0.90-0.86 (m, 3H); ^{13}C NMR (100 MHz, $CDCl_3$) δ 84.5, 68.2, 32.1, 29.9, 29.8, 29.7, 29.6, 29.3, 28.7, 22.9, 18.6, 14.3; HRMS (ESI-TOF): [M+H]+ Calc'd for $C_{16}H_{30}$ *m/z* 223.2426. Found, *m/z* 223.2435.

Hexadec-2-yne (20)

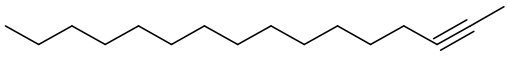

(**20**)

IR (neat); 2920, 2852, 1464 cm^{-1};^{1}H NMR (400 MHz, $CDCl_3$) ^{1}H NMR (400 MHz, $CDCl_3$), δ 2.1 (tq, *J* = 7.8, 5.5 Hz, 2H), 1.78 (t, *J* = 2.5 Hz), 1.50-1.43 (m, 2H), 1.37-1.34 (m, 2H), 1.26 (bs, 18H), 0.88 (t, *J* = 6.6 Hz, 3H); ^{13}C NMR (100 MHz, $CDCl_3$) δ 79.6, 75.5, 32.1, 29.8, 29.7, 29.5, 29.4, 29.3, 29.1, 22.9, 18.9, 14.3, 3.7; HRMS (ESI-TOF): [M+H]+ Calc'd for $C_{16}H_{30}$. *m/z* 223.2426. Found, *m/z* 223.2429.

EXPERIMENTAL WORK FOR OBTAINING THE KINETIC DATA

Kinetic experiments were analyzed by NMR spectroscopy; in order to get the accurate integrations for the signals we have taken into consideration the T1 relaxation times. We ran T1 experiments on alkynes to find the right relaxation times. The T1 experiments ran with the following VDLIST

Table 6-7. VDLIST for T1 experiments

S.No	Variable delay values (sec)
1	0.01
2	0.100
3	0.25
4	0.500
5	1
6	2
7	4
8	8
9	15
10	25

The relaxation times for external and internal alkynes range from 1.296 sec to 8.613 sec. The longest relaxation times were observed for alkyne protons in terminal alkynes and for propargylic protons in internal alkynes. We choose D1 as 30 sec and analyzed the kinetic data for all terminal alkynes (>3*T1) (Table 6-8)

Table 6-8. T1 relaxation of alkyne proton in terminal and terminal methyl in internal alkynes

Alkyne	T1 relaxation times (sec)
hexadec-1-yne (**16**)	7.249
hexadec-2-yne (**20**)	2.830
heptadec-1-yne (**18**)	7.712
heptadec-2-yne (**19**)	2.795
15-methylhexadec-1-yne (**6**)	8.613
15-methylhexadec-2-yne (**8**)	2.680
octadec-1-yne (**2**)	6.740
octadec-2-yne (**7**)	2.776

15-methylhexadec-1-yne (6)

To a solution of 15-methylhexadec-1-yne (0.095 g, 40.2 mmol) in DMSO (10 mL) was added potassium tertiary butoxide (0.045 g, 40.2 mmol) and the resulting solution was heated in an oil bath at 55 °C and 75 °C. Every five minutes 0.5 mL aliquots were collected, quenched with water and extracted with hexane. The organic layer was dried over anhydrous $MgSO_4$ and concentrated *in vacuo* to yield clear oil which was further analyzed by proton NMR using $CDCl_3$ as a solvent.

Octadec-1-yne (2)

To a solution of 15 octadec-1-yne (0.1 g, 40.0 mmol) in DMSO (10 mL) was added potassium tertiary butoxide (0.045 g, 40.0 mmol) and the resulting solution was heated in an oil bath at 55 °C and 75 °C. Every five minutes 0.5 mL aliquots were collected, quenched with water and extracted with hexane. The organic layer was dried over anhydrous $MgSO_4$ and concentrated to yield clear oil which was further analyzed by proton NMR using $CDCl_3$ as a solvent.

The following procedure was followed for the kinetic experiments in fresh DMSO at 70 °C, 40 °C and room temperature:

To a solution of terminal alkyne (25.0 mmol) in DMSO (10 mL) was added potassium tertiary butoxide (0.028 g, 25.0 mmol) and the resulting solution was heated at 70 °C. At regular time intervals 0.1 mL aliquots were collected, quenched with water and extracted with hexane. The organic layer was dried over anhydrous $MgSO_4$ and concentrated to yield clear oil which was further analyzed by proton NMR using $CDCl_3$ as a solvent.

6.5 Appendix (Part II NMR spectrums)

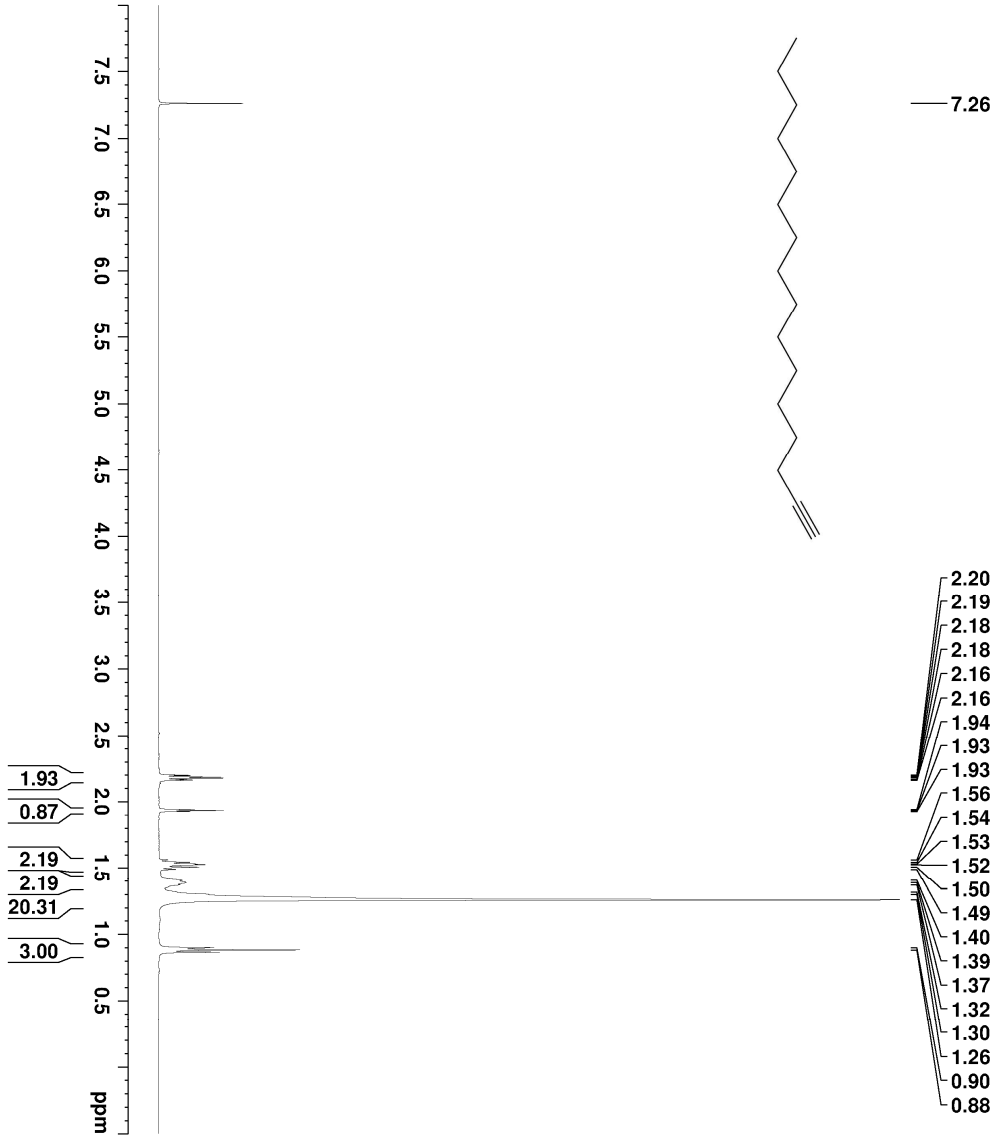
7.26
2.20
2.19
2.18
2.18
2.16
2.16
1.94
1.93
1.93
1.56
1.54
1.53
1.52
1.50
1.49
1.40
1.39
1.37
1.32
1.30
1.26
0.90
0.88
1.93
0.87
2.19
2.19
20.31
3.00
7.5
7.0
6.5
6.0
5.5
5.0
4.5
4.0
3.5
3.0
2.5
2.0
1.5
1.0
0.5
ppm

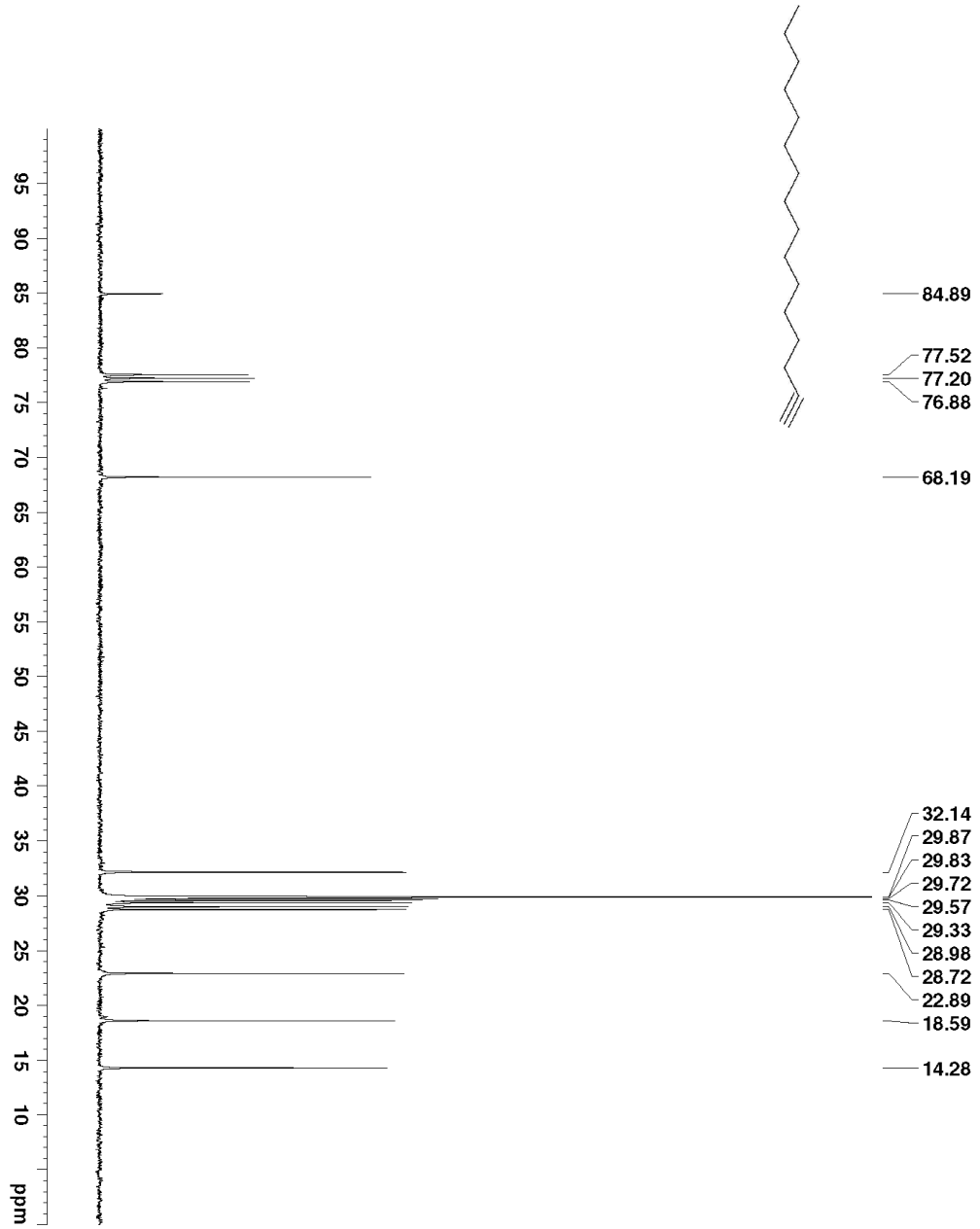
84.89
77.52
77.20
76.88
68.19
32.14
29.87
29.83
29.72
29.57
29.33
28.98
28.72
22.89
18.59
14.28
95
90
85
80
75
70
65
60
55
50
45
40
35
30
25
20
15
10
ppm

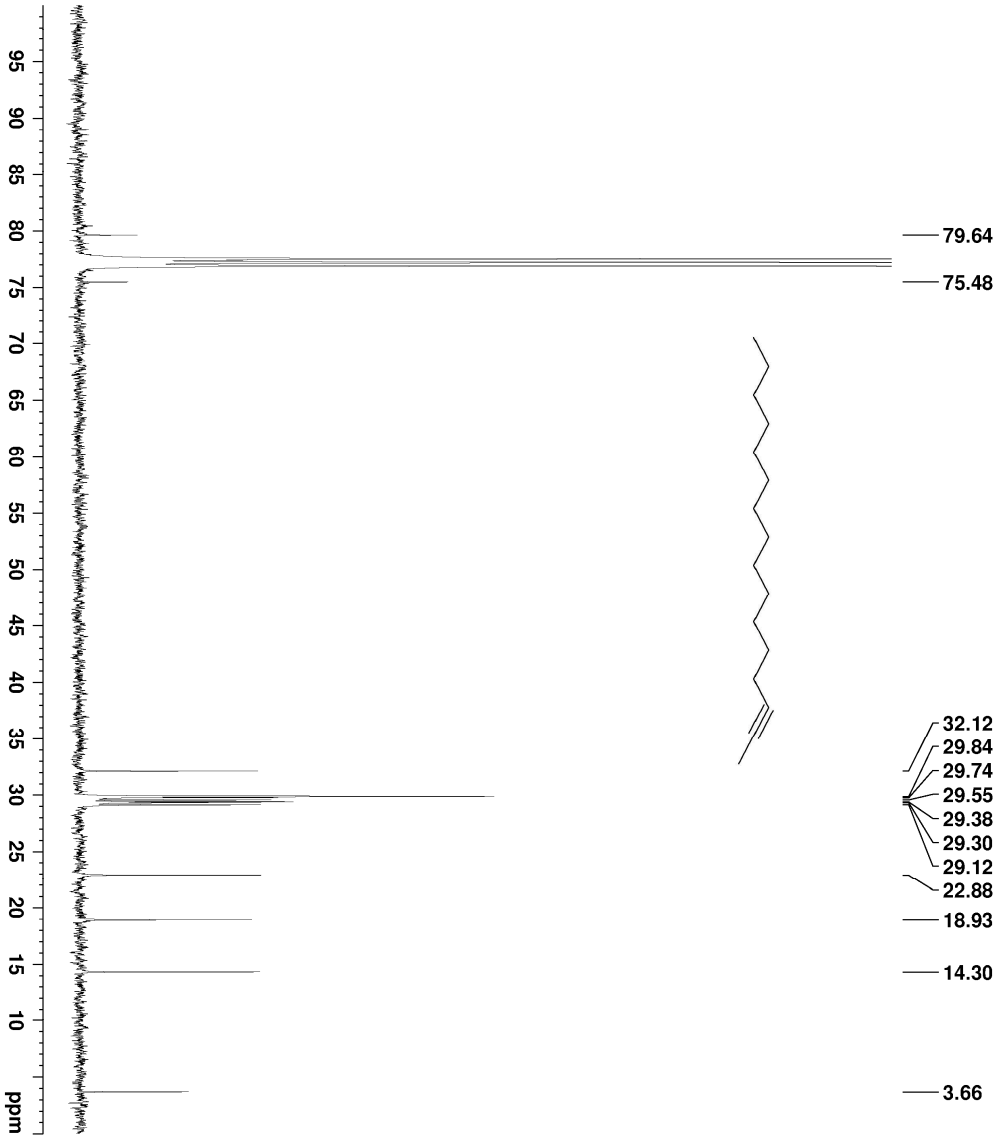
95
90
85
80
75
70
65
60
55
50
45
40
35
30
25
20
15
10
ppm
79.64
75.48
32.12
29.84
29.74
29.55
29.38
29.30
29.12
22.88
18.93
14.30
3.66

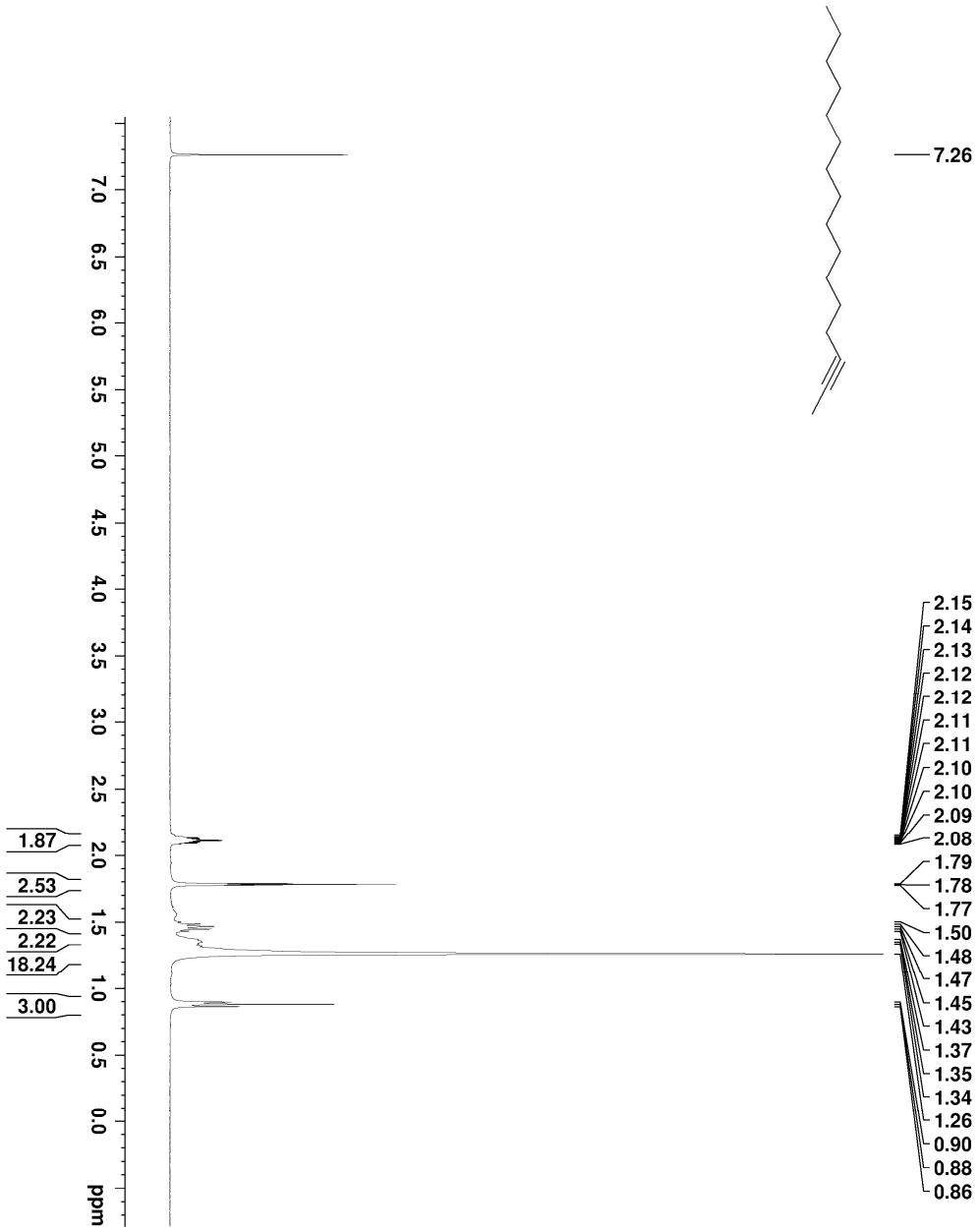
7.26
2.15
2.14
2.13
2.12
2.12
2.11
2.11
2.10
2.10
2.09
2.08
1.79
1.78
1.77
1.50
1.48
1.47
1.45
1.43
1.37
1.35
1.34
1.26
0.90
0.88
0.86
1.87
2.53
2.23
2.22
18.24
3.00
7.0
6.5
6.0
5.5
5.0
4.5
4.0
3.5
3.0
2.5
2.0
1.5
1.0
0.5
0.0
ppm

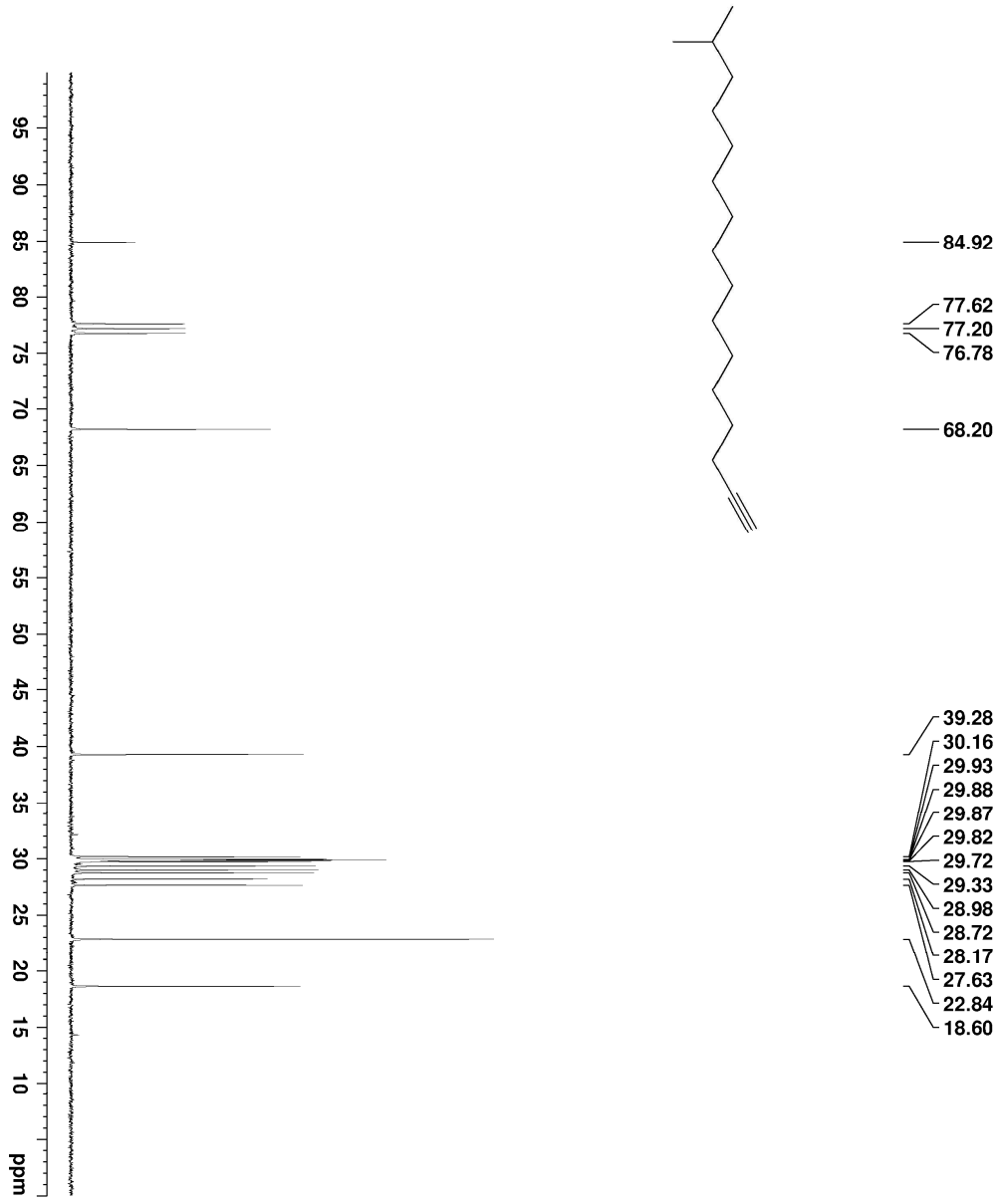
95
90
85
80
75
70
65
60
55
50
45
40
35
30
25
20
15
10
ppm
84.92
77.62
77.20
76.78
68.20
39.28
30.16
29.93
29.88
29.87
29.82
29.72
29.33
28.98
28.72
28.17
27.63
22.84
18.60

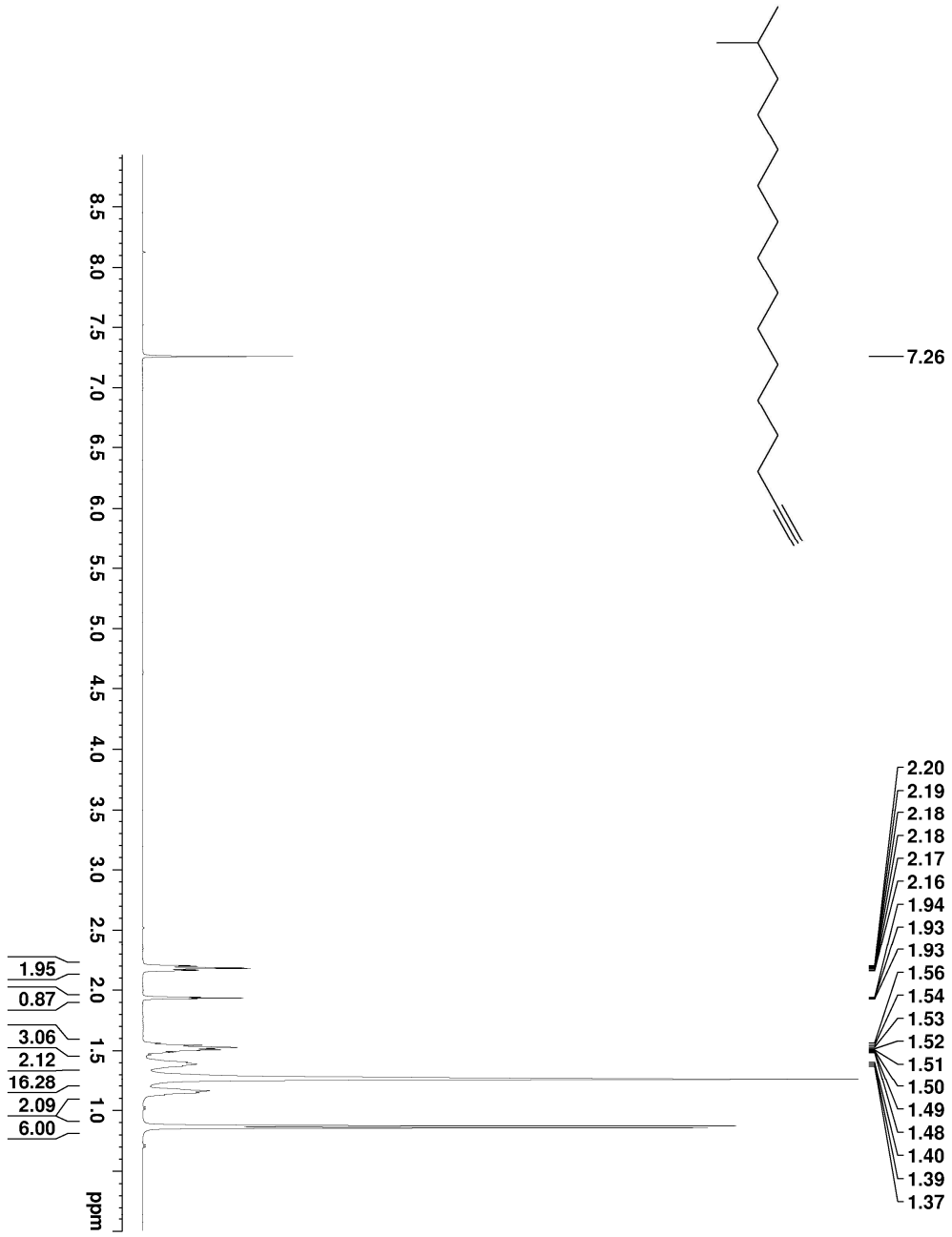
7.26
2.20
2.19
2.18
2.18
2.17
2.16
1.94
1.93
1.93
1.56
1.54
1.53
1.52
1.51
1.50
1.49
1.48
1.40
1.39
1.37
1.95
0.87
3.06
2.12
16.28
2.09
6.00
8.5
8.0
7.5
7.0
6.5
6.0
5.5
5.0
4.5
4.0
3.5
3.0
2.5
2.0
1.5
1.0
ppm

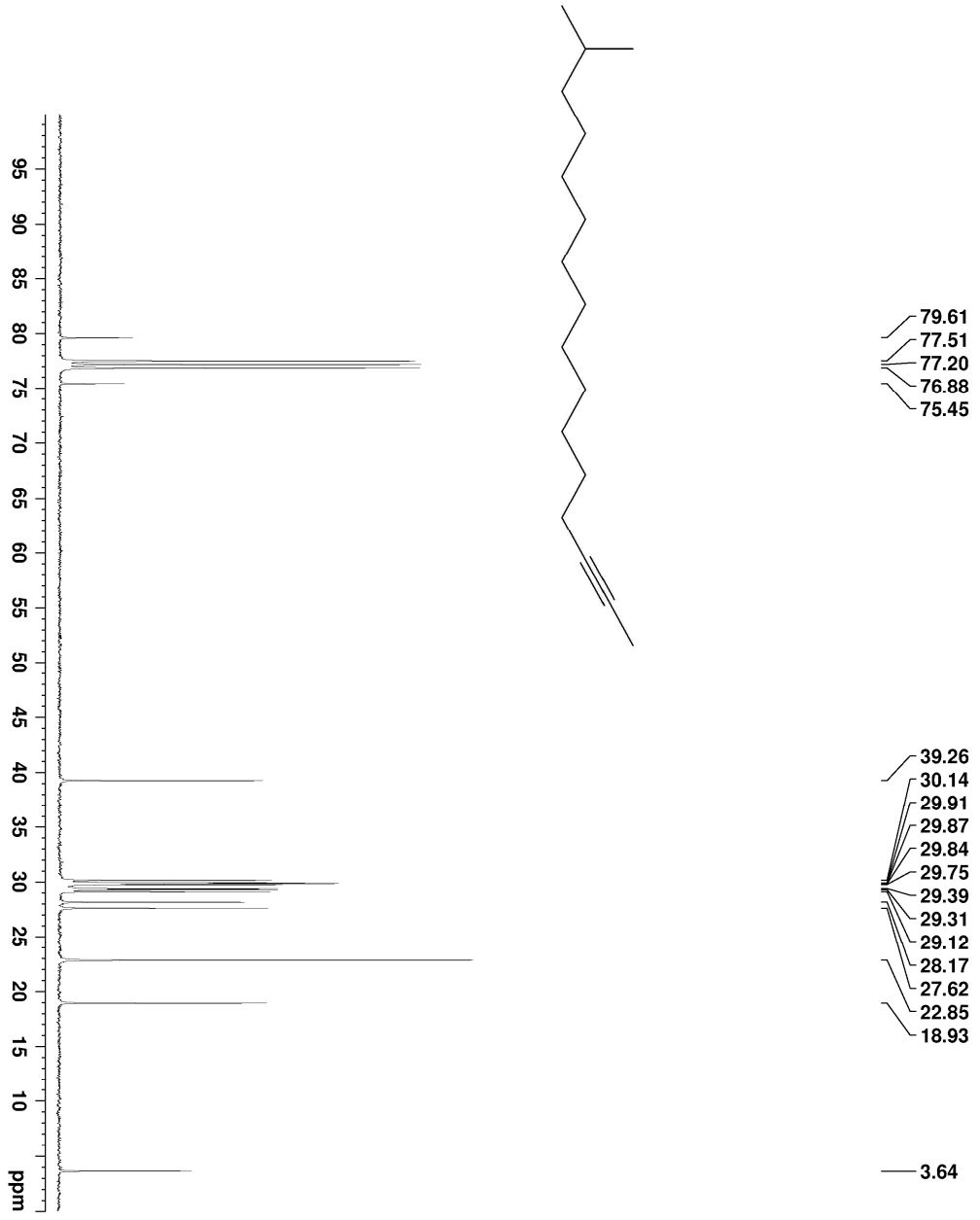
95
90
85
80
75
70
65
60
55
50
45
40
35
30
25
20
15
10
ppm
79.61
77.51
77.20
76.88
75.45
39.26
30.14
29.91
29.87
29.84
29.75
29.39
29.31
29.12
28.17
27.62
22.85
18.93
3.64

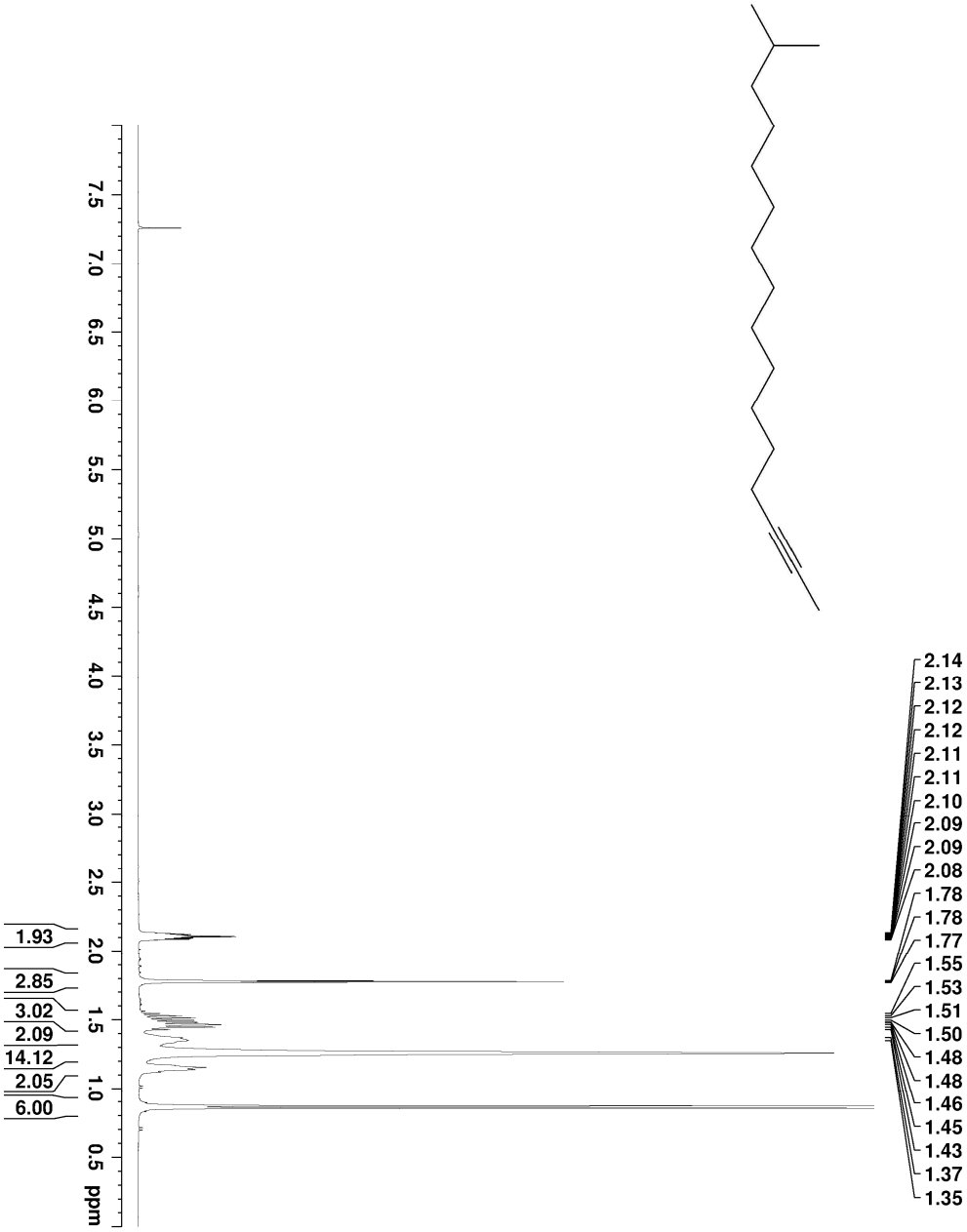
7.5
7.0
6.5
6.0
5.5
5.0
4.5
4.0
3.5
3.0
2.5
2.0
1.5
1.0
0.5
ppm
1.93
2.85
3.02
2.09
14.12
2.05
6.00
2.14
2.13
2.12
2.12
2.11
2.11
2.10
2.09
2.09
2.08
1.78
1.78
1.77
1.55
1.53
1.51
1.50
1.48
1.48
1.46
1.45
1.43
1.37
1.35

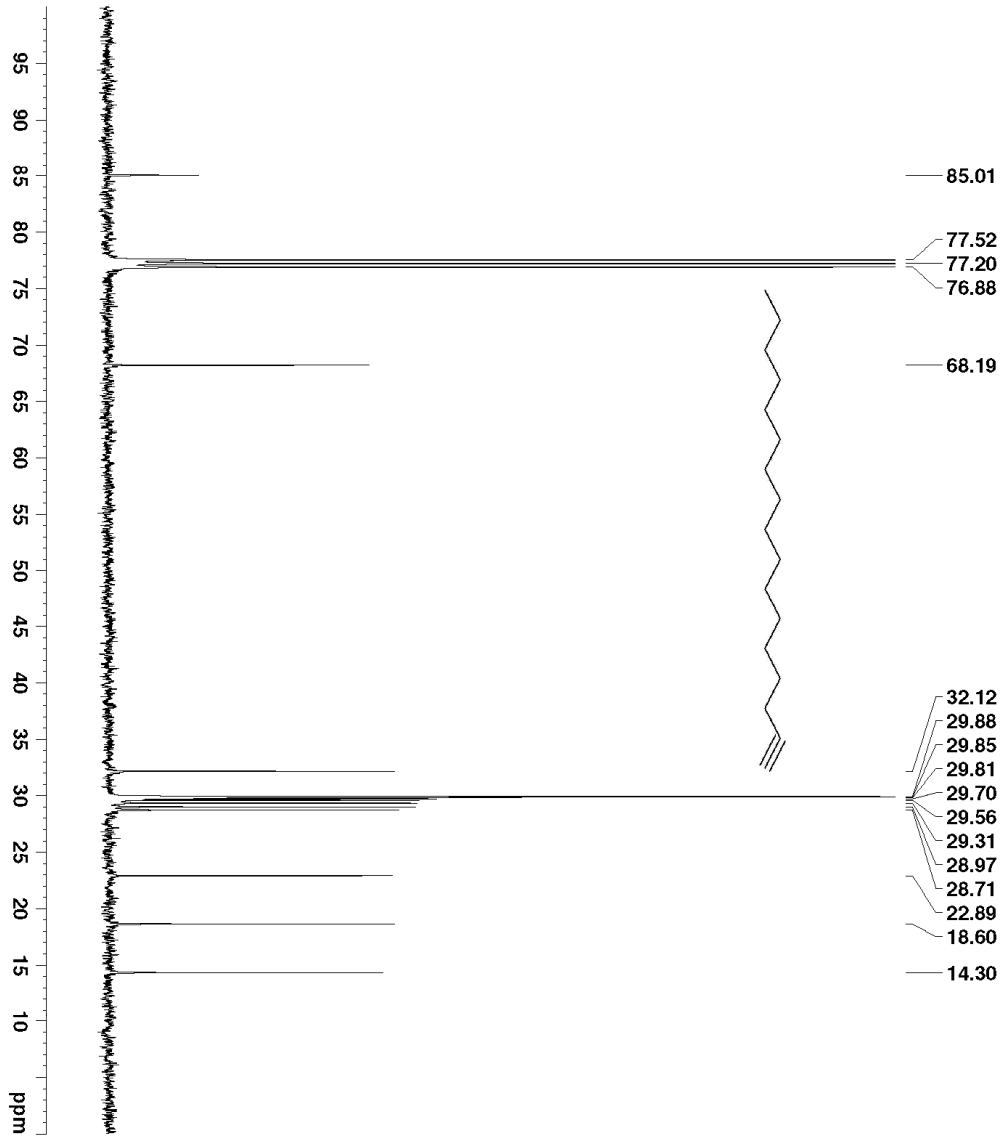
95
90
85
80
75
70
65
60
55
50
45
40
35
30
25
20
15
10
ppm
85.01
77.52
77.20
76.88
68.19
32.12
29.88
29.85
29.81
29.70
29.56
29.31
28.97
28.71
22.89
18.60
14.30

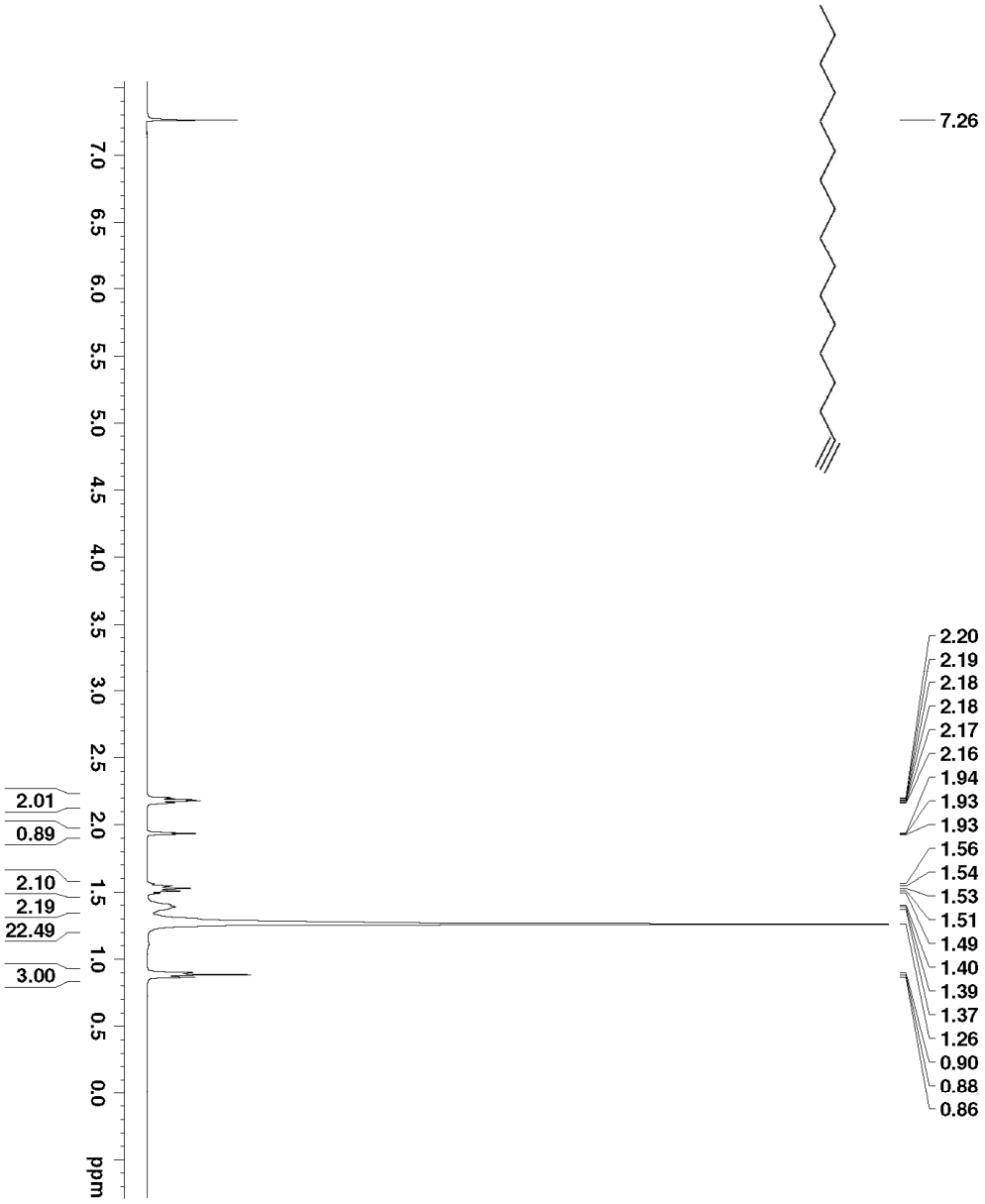
7.26
2.20
2.19
2.18
2.18
2.17
2.16
1.94
1.93
1.93
1.56
1.54
1.53
1.51
1.49
1.40
1.39
1.37
1.26
0.90
0.88
0.86
2.01
0.89
2.10
2.19
22.49
3.00
7.0
6.5
6.0
5.5
5.0
4.5
4.0
3.5
3.0
2.5
2.0
1.5
1.0
0.5
0.0
ppm

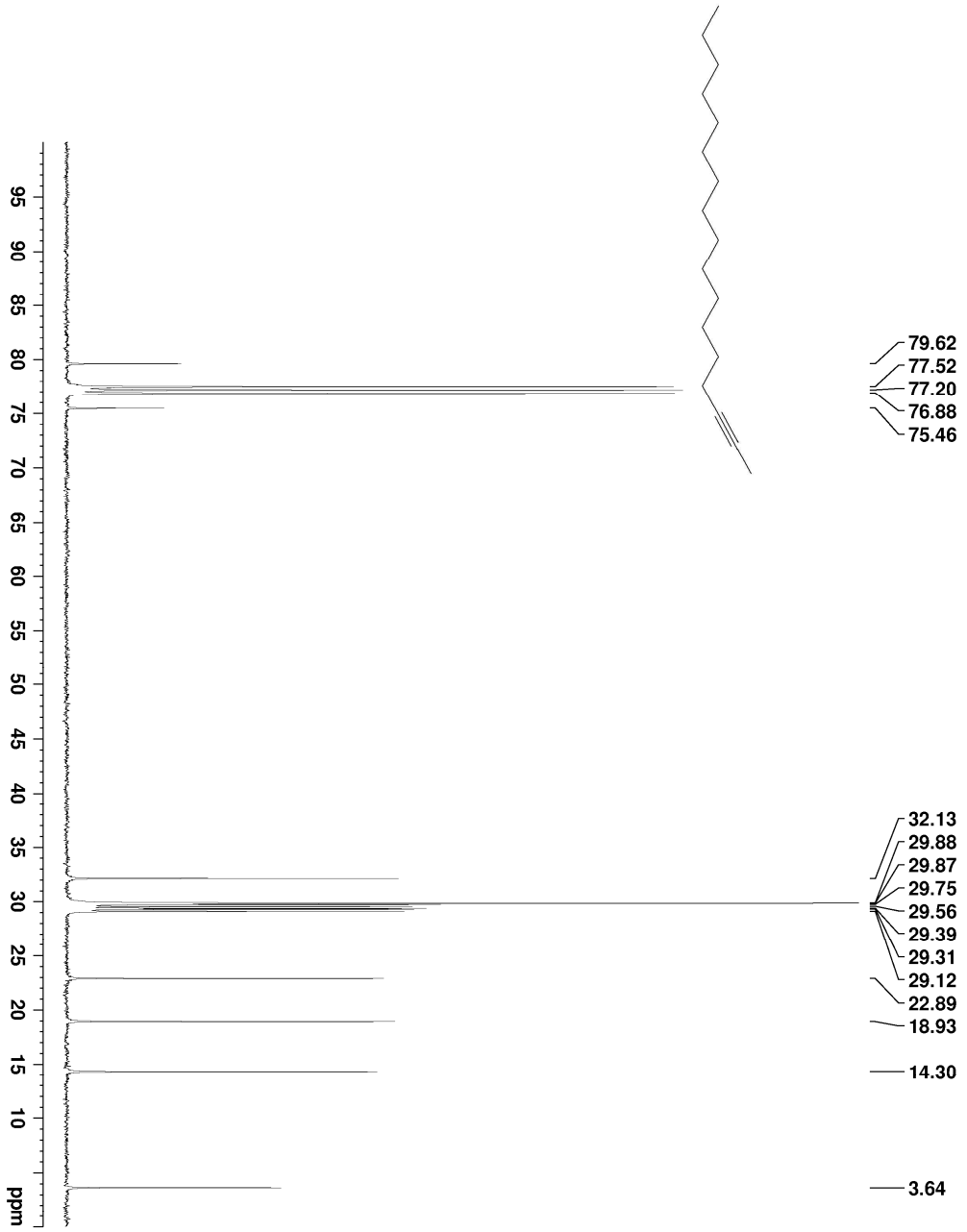
95
90
85
80
75
70
65
60
55
50
45
40
35
30
25
20
15
10
ppm
79.62
77.52
77.20
76.88
75.46
32.13
29.88
29.87
29.75
29.56
29.39
29.31
29.12
22.89
18.93
14.30
3.64

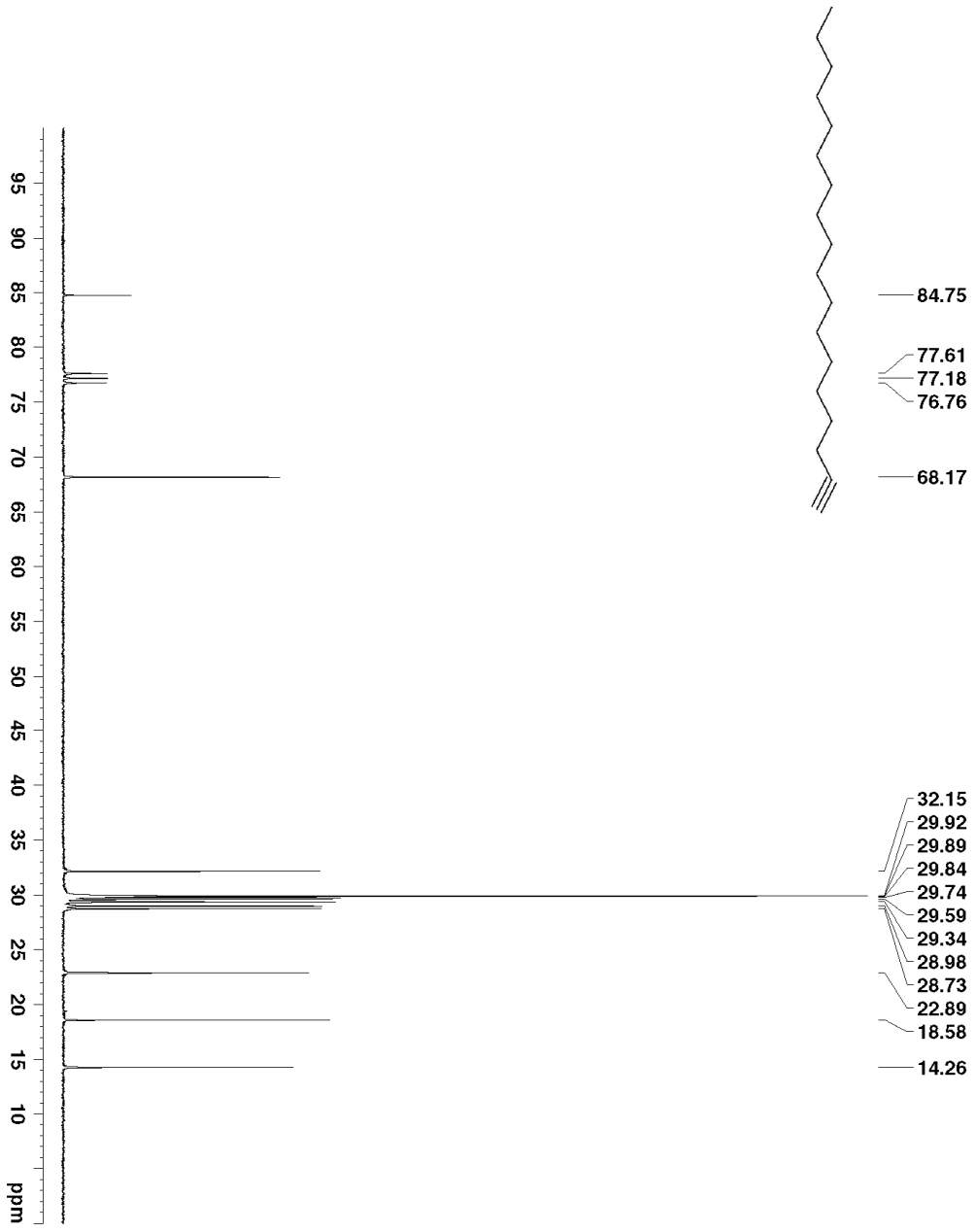
84.75
77.61
77.18
76.76
68.17
32.15
29.92
29.89
29.84
29.74
29.59
29.34
28.98
28.73
22.89
18.58
14.26
95
90
85
80
75
70
65
60
55
50
45
40
35
30
25
20
15
10
ppm

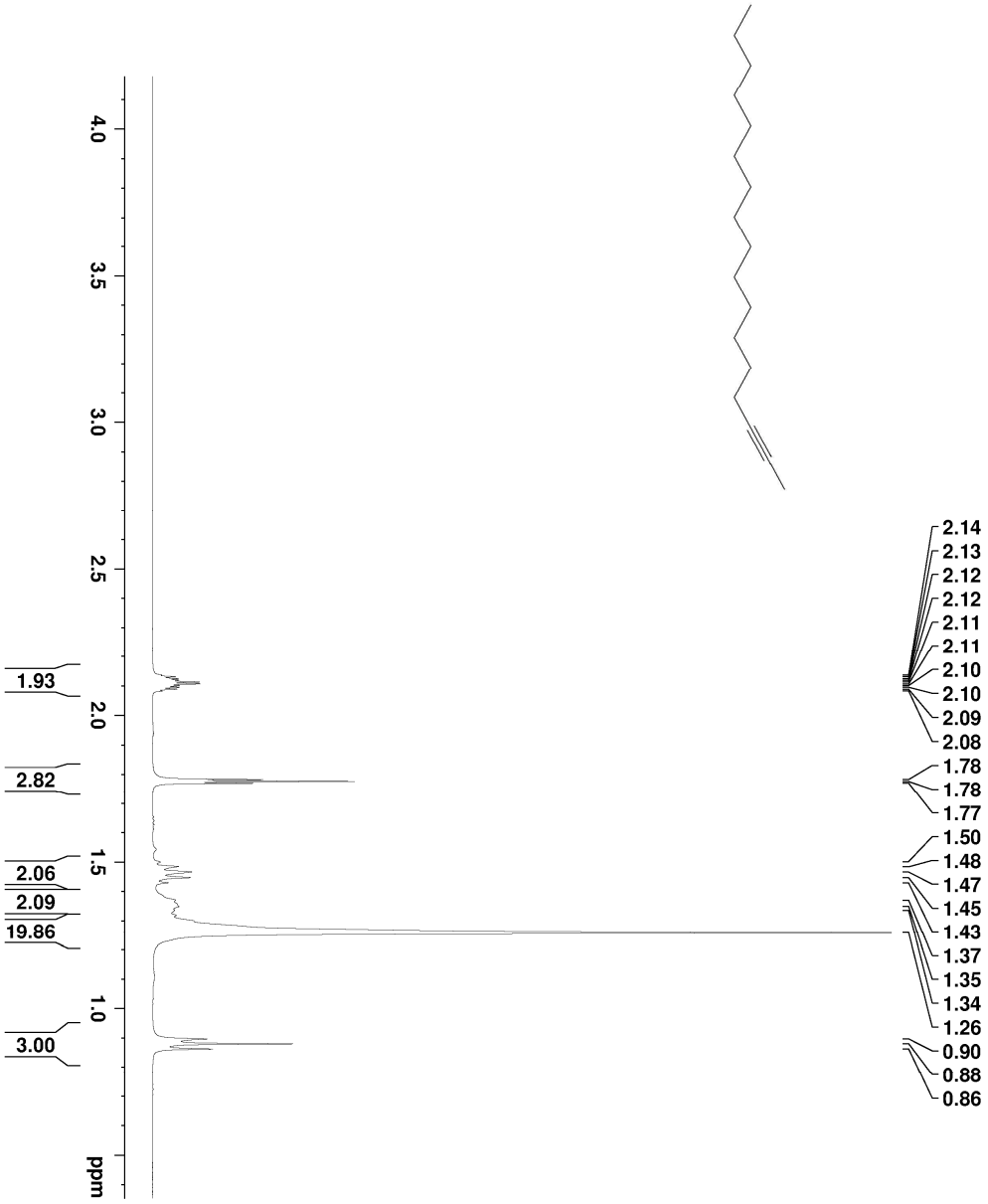
4.0
3.5
3.0
2.5
2.0
1.5
1.0
ppm
1.93
2.82
2.06
2.09
19.86
3.00
2.14
2.13
2.12
2.12
2.11
2.11
2.10
2.10
2.09
2.08
1.78
1.78
1.77
1.50
1.48
1.47
1.45
1.43
1.37
1.35
1.34
1.26
0.90
0.88
0.86

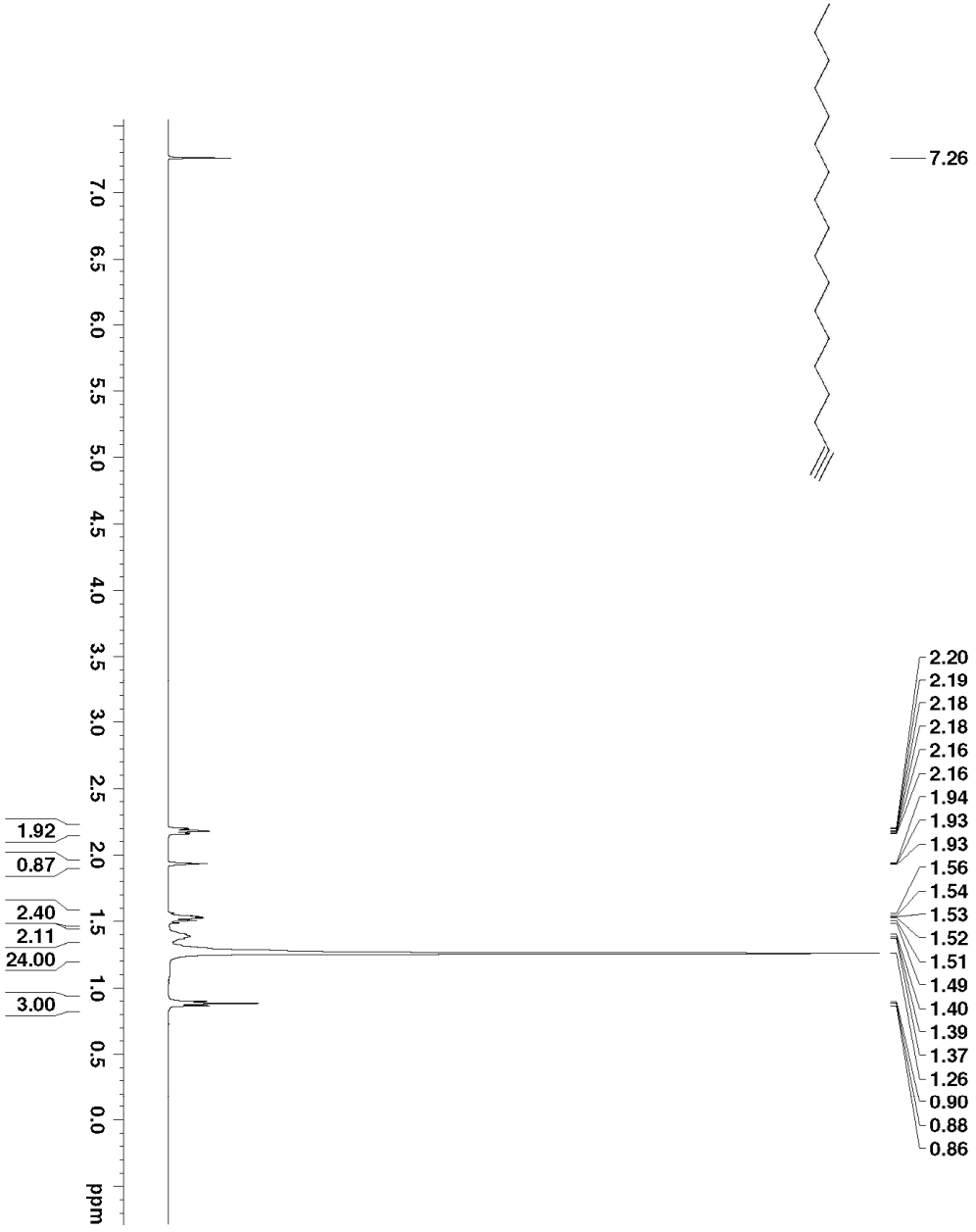
7.26
2.20
2.19
2.18
2.18
2.16
2.16
1.94
1.93
1.93
1.56
1.54
1.53
1.52
1.51
1.49
1.40
1.39
1.37
1.26
0.90
0.88
0.86
1.92
0.87
2.40
2.11
24.00
3.00
7.0
6.5
6.0
5.5
5.0
4.5
4.0
3.5
3.0
2.5
2.0
1.5
1.0
0.5
0.0
ppm

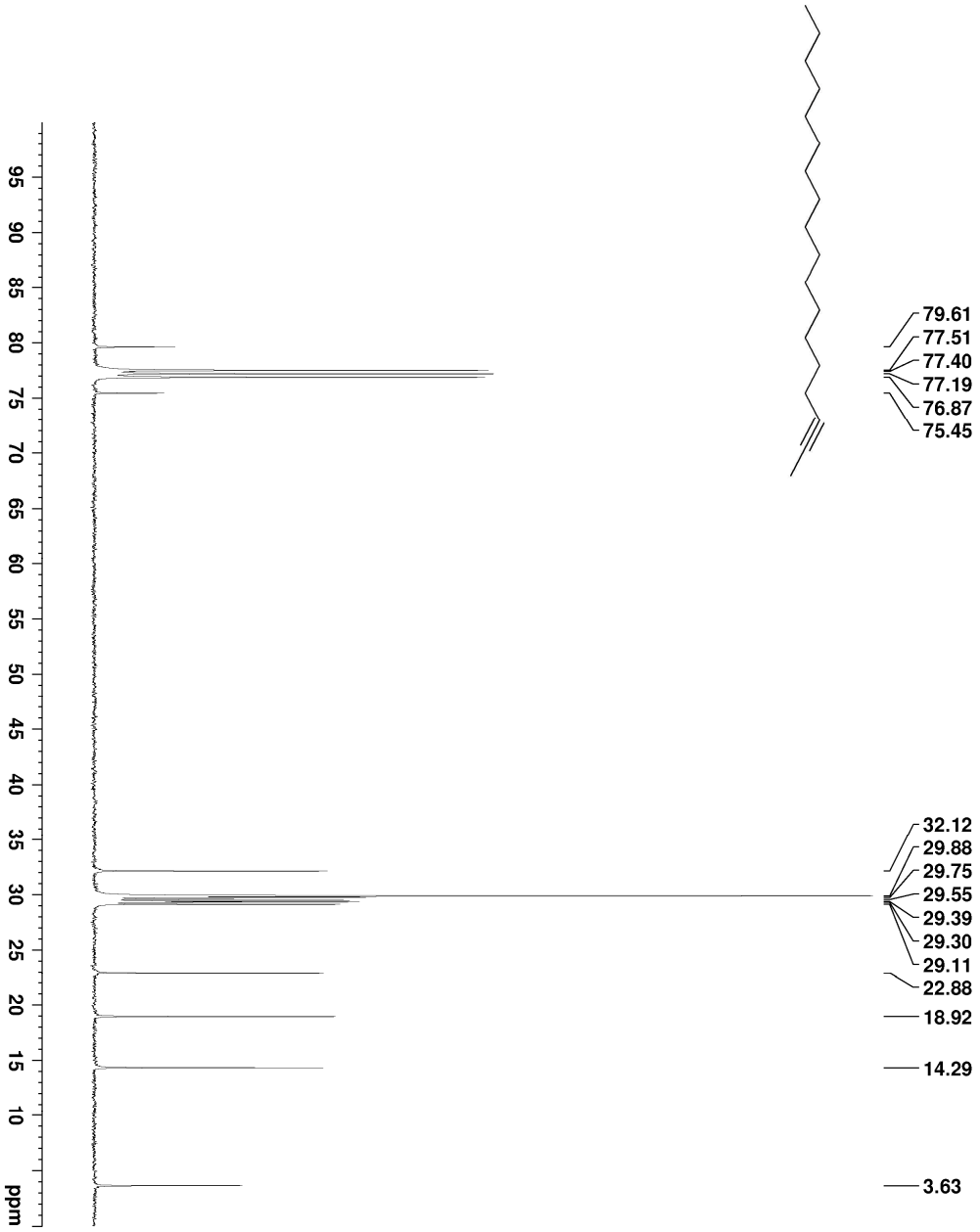
79.61
77.51
77.40
77.19
76.87
75.45
32.12
29.88
29.75
29.55
29.39
29.30
29.11
22.88
18.92
14.29
3.63
95
90
85
80
75
70
65
60
55
50
45
40
35
30
25
20
15
10
ppm

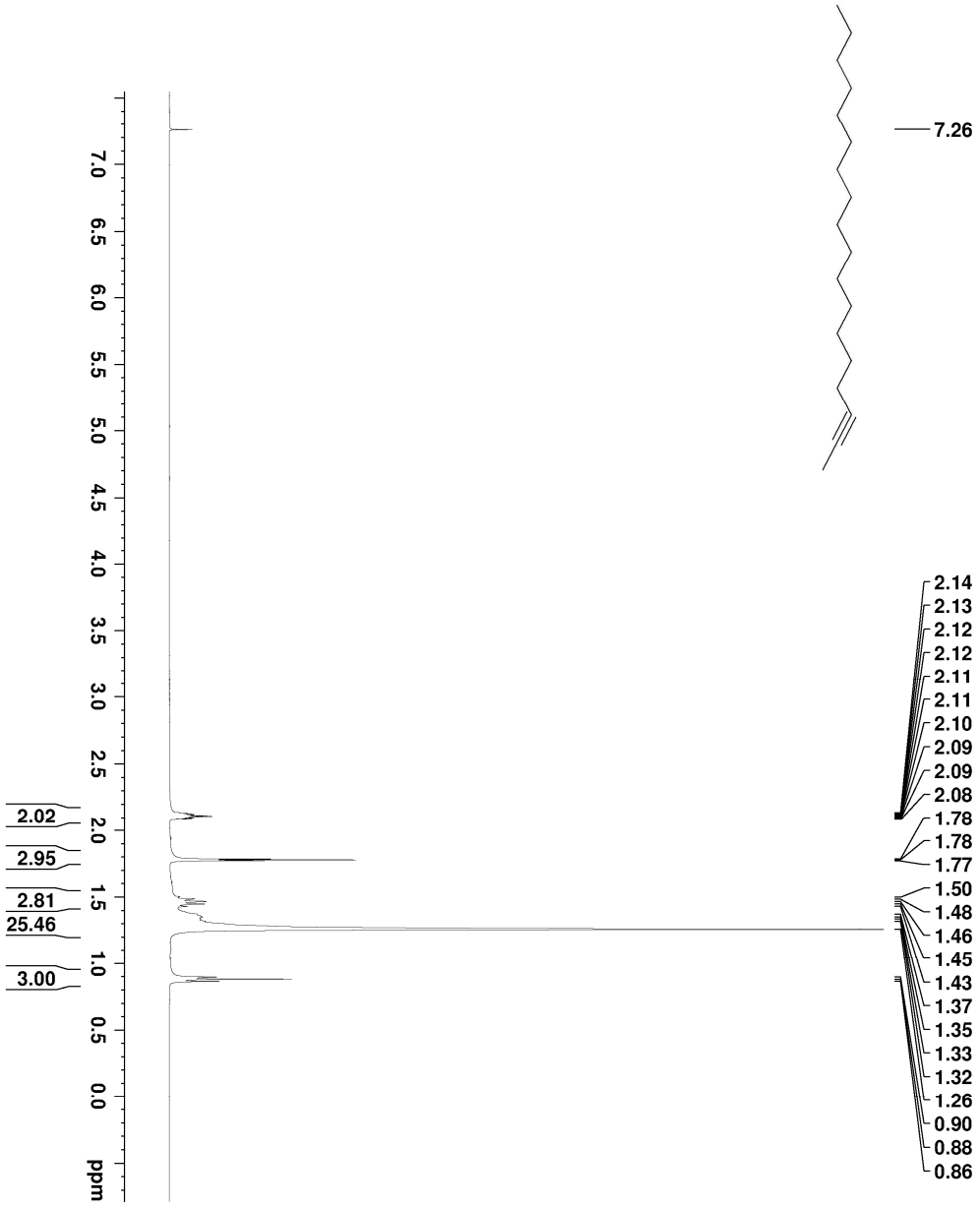
7.26
2.14
2.13
2.12
2.12
2.11
2.11
2.10
2.09
2.09
2.08
1.78
1.78
1.77
1.50
1.48
1.46
1.45
1.43
1.37
1.35
1.33
1.32
1.26
0.90
0.88
0.86
2.02
2.95
2.81
25.46
3.00
7.0
6.5
6.0
5.5
5.0
4.5
4.0
3.5
3.0
2.5
2.0
1.5
1.0
0.5
0.0
ppm

References List:

(1) What Is Cancer? http://www.cancer.org/cancer/cancerbasics/what-is-cancer (accessed 18th March, 2014).

(2) Understanding Cancer Series: Cancer - National Cancer Institute. http://www.cancer.gov/cancertopics/understandingcancer/cancer/page4 (accessed 18th March, 2014).

(3) Metastatic Cancer Fact Sheet - National Cancer Institute. http://www.cancer.gov/cancertopics/factsheet/Sites-Types/metastatic (accessed 18th March, 2014).

(4) A. L. Harris *Nat. Rev. Cancer* **2002**, *2*, 38.

(5) J. M. Brown and W. r. Wilson *Nat. Rev. Cancer* **2004**, *4*, 437.

(6) M. Hockel and P. Vaupel *J. Natl. Cancer Inst.* **2001**, *93*, 266.

(7) P. Vaupel *Sem. Radiat. Oncol.* **2004**, *14*, 198.

(8) S. Kizaka-Kondoh, M. I., H. Harada, and M. hiraoka, *Cancer Sci.* **2003**, *94*, 1021.

(9) Kizaka-Kondoh, S.; Inoue, M.; Harada, H.; Hiraoka, M. *Cancer Science* **2003**, *94*, 1021.

(10) M. Hockel, K. S., C. Knoop, and P. Vaupel, *Cancer Res.* **1991**, *51*, 6098.

(11) D. M. Brizel, G. S. S., L. R. Prosnitz, R. L. Scher, and M. W. Dewhirst, *Int. J. Radiat. Oncol. Biol. Phys.* **1997**, *38*, 285.

(12) Siemann, D. W. *Tumor Microenvironment*; A John Wiley & Sons, Ltd, 2011.

(13) Tatum, J. L.; Kelloff, G. J.; Gillies, R. J.; Arbeit, J. M.; Brown, J. M.; Chao, K. S. C.; Chapman, J. D.; Eckelman, W. C.; Fyles, A. W.; Giaccia, A. J.; Hill, R. P.; Koch, C. J.; Krishna, M. C.; Krohn, K. A.; Lewis, J. S.; Mason, R. P.; Melillo, G.; Padhani, A.

R.; Powis, G.; Rajendran, J. G.; Reba, R.; Robinson, S. P.; Semenza, G. L.; Swartz, H. M.; Vaupel, P.; Yang, D.; Croft, B.; Hoffman, J.; Liu, G.; Stone, H.; Sullivan, D. *Int. J. of Rad. Bio.* **2006**, *82*, 699.

(14) Intes, X.; Ripoll, J.; Chen, Y.; Nioka, S.; Yodh, A. G.; Chance, B. *Med. Phys.* **2003**, *30*, 1039.

(15) Hamer, F. M. *Quarterly Reviews, Chemical Society* **1950**, *4*, 327.

(16) Weissberger A, T. E. *Special topics in heterocyclic chemistry*; wiley, 1977.

(17) Venkataraman, K. *The chemistry of synthetic dyes*; Newyork: Academic press, 1952; Vol. 2.

(18) Hamer, F. *The cyanine dyes and related compounds*; Newyork: Wiley, 1964.

(19) Sternberg, E. D.; Dolphin, D.; Brückner, C. *Tetrahedron* **1998**, *54*, 4151.

(20) Li, X.; Beauvoit, B.; White, R.; Nioka, S.; Chance, B.; Yodh, A. *Proc. SPIE* **1995**, *2389*, 789.

(21) Reynolds, J.; Troy, T.; Mayer, R.; Thompson, A.; Waters, D.; Cornell, K.; Snyder, P.; Sevick-Muraca, E. *Photochem. Photobiol.* **1999**, *70*, 87.

(22) Nioka, S.; Yung, Y.; Schnall, M.; Zhao, S.; Orel, S.; Xie, C.; Chance, B.; Solin, S. *Adv. Exp. Med. Biol.* **1997**, *411*, 227.

(23) Ntziachristos, V.; Yodh, A. G.; Schnall, M.; Chance, B. *PNAS* **2000**, *97*, 2767.

(24) Pavlik, C.; Biswal, N. C.; Gaenzler, F. C.; Morton, M. D.; Kuhn, L. T.; Claffey, K. P.; Zhu, Q.; Smith, M. B. *Dyes and Pigments* **2011**, *89*, 9.

(25) Biswal, N. C.; Pavlik, C.; Smith, M. B.; Aquirre, A.; Kuhn, L. T.; Claffey, K. P.; Zhu, Q. *J. Biomed. Opt.* **2011**, *16*, 066009.

(26) Kedderis, G. L.; Argenbright, L.; Miwa, G. T. *Archives of Biochemistry and Biophysics* **1988**, *262*, 40.

(27) Rauth, A. M. *Int. J. Radiation Oncology Biol. Phys.* **1984**, *10*, 1293.

(28) Splith, K.; Bergmann, R.; Pietzsch, J.; Neundorf, I. *Chem. Med. Chem.* **2012**, *7*, 57.

(29) Rauth, A. M.; McClelland, R. A.; Michaels, H. B.; Battistella, R. *Int. J. Radiation Oncology Biol. Phys.* **1984**, *10*, 1323.

(30) *Br. J. Vener. Dis.* **1978**, *54*, 69.

(31) Asquith, J. C.; Watts, M. E.; Patel, K.; Smithen, C. E.; Adams, G. E. *Radiation Research* **1974**, *60*, 108.

(32) Kizaka-Kondoh, S.; Konse-Nagasawa, H. *Cancer Sci* **2009**, *100*, 1366.

(33) Brown, J. M.; Yu, N. Y.; Brown, D. M.; Lee, W. W. *Int. J. Radiation Oncology Biol. Phys.* **1981**, *7*, 695.

(34) Lindsey, J. S.; Brown, P. A.; Siesel, D. A. *Tetrahedron* **1989**, *45*, 4845.

(35) Terpetschning, E.; Szmacinski, H.; Ozinskas, A.; Lakowicz, J. R. *Anal. Biochem.* **1994**, *217*, 197.

(36) Licha, K.; Riefke, B.; Ntziachristos, V.; Becker, A.; Chance, B.; Semmler, W. *Photochem. Photobiol.* **2000**, *72*, 392.

(37) Pavlik, C.; Biswal, N. C.; Gaenzler, F. C.; Morton, M. D.; Kuhn, L. T.; Claffey, K. P.; Zhu, Q.; Smith, M. B. *Dyes and Pigments* **2011**, *89*, 9.

(38) Gielen AP, S. A. *Collected papers in biochemical pharmacology* **1986**, *35*, 1.

(39) Licha K, R. B., Ntziachristos V, Becker A, Chance B, Semmler W., *Photochem Photobiol.* **2000**, *72*, 392.

(40) Mujumdar SR, M. R., Grant CM, Waggoner AS., *Bioconj. Chem.* **1996**, *7*, 356.

(41) Lindsey JS, B. P., Siesel DA., *Tetrahedron* **1989**, *45*, 4845.

(42) Pham W, L. W., Weissleder R, Tung CH., *Bioconjug. Chem.* **2003**, *14*, 1048.

(43) Neises B, S. W. *Org. Synth.* **1990**, 93.

(44) Pullman A, P. B. *Natl. Acad. Sci.* **1961**, *47*, 7.

(45) Robeson CD, B. W., Dieterle JM, Cawley JD, Baxter JG., *J. Am. Chem. Soc.* **1955**, *77*, 4120.

(46) Brown PK, W. G. *J. Biol. Chem.* **1956**, *222*, 865.

(47) Kizaka-Kondoh S, K.-N. H. *Cancer Sci.* **2009**, *1*, 1.

(48) Kizaka-Kondoh S, I. M., Harada H, Hiraoka M., *Cancer Sci.* **2003**, *94*, 1021.

(49) Xu, Y.; Zanganeh, S.; Mohammad, I.; Aguirre, A.; Wang, T.; Yang, Y.; Kuhn, L.; Smith, M. B.; Zhu, Q. *Journal of Biomedical Optics* **2013**, *18*, 066009.

(50) G. Barker, P. O. B., and K. R. Campos, *Org. Lett.* **2010**, *12*, 4176.

(51) Z. Wang . *Bat. Chem. Biol.* **2008**, *4*, 557.

(52) V. H. Thomas et al. *Expert Opin. Drug. Metab. Toxicol.* **2006**, *2*, 591.

(53) M. J. Neil, A. S., and P. Heckelman, *The Merck Index* **2006**, *14th ed.,*.

(54) C. B. Vu et al. *J. Med. Chem.* **2004**, *47*, 4291.

(55) Ljungkvist, A. S. E.; Bussink, J.; Kaanders, J. H. A. M.; Rijken, P. F. J. W.; Begg, A. C.; Raleigh, J. A.; van der Kogel, A. J. *International journal of radiation oncology, biology, physics* **2005**, *62*, 1157.

(56) Pavlik C, B. N., Gaenzler FC, Morton MD, Kuhn LT, Claffey KP, Zhu Q, Smith; MB. *Dyes and Pigments* **2011**, *89*, 9.

(57) Biswal NC, P. C., Smith MB, Aquirre A, Kuhn LT, Xu Y, Zanganeh S, Claffey KP,; Zhu Q. *J. Biomed. Opt.* **2011**, *16*, 066009.

(58) Biswal NC, G. J., Yuan B, Backer MV, Backer JM, Zhu Q. *J. Biomed. Opt.* **2010**, *15*, 016012.

(59) Suzuki H. Bull. *Chem. Soc. Jpn.* **1959**, *32*.

(60) Berlman IB. *J. Phys. Chem.* **1970**, *74*, 3085.

(61) Ichiro Takahashi, R. M., Kenji Nishiuchi, Minoru Hatanaka, Akihito Yamano, Akiyo Sakushima, and Shinzo Hosoi* *Hetrocycles* **2004**, *63*, 1267.

(62) Pham W, L. W., Weissleder R, Tung CH., *Bioconj. Chem.* **2003**, *14*, 1048.

(63) Reynolds GA, D. K. *J. Org. Chem.* **1977**, *42*, 885.

(64) Slominskii YL, R. I., Tolmachev AI., *Zhur. Organich. Khim.* **1979**, *15*, 400.

(65) Diehl DR, E. A., Ferguson PM, Helber MJ,; Spitzner NV. Eastman Kodak *EP0679939B1; US5451494,* **1995**.

(66) Samanta A, V. M., Dasa R, Chang YT., *Chem. Commun.* **2010**, *46*, 7406.

(67) Samanta A, M. K., Soh KS, Liao X, Vendrell M, Dinish US, Yun SW, Bhuvaneswari; R, K. H., Rautela S, Chung J, Olivo M, Chang YT. *Angew. Chem. Int. Ed.* **2011**, *50*, 6089.

(68) Weissleder R, M. A., Mahmood U, Bhorade R, Benveniste H, Chiocca EA, Basillon JP., *Nat. Med.* **2000**, *6*, 351.

(69) Brahmachari G, L. S. *Tetrahedron Lett.* **2010**, *51*, 2319.

(70) Salon J, S. E., Raszkiewicz A, Patonay G, Strekowski L., *J. Heterocyclic Chem.* **2005**, *42*, 959.

(71) Nagao, Y.; Sakai, T.; Kozawa, K.; Urano, T. *Dyes and Pigments* **2007**, *73*, 344.

(72) Jung ME, K. W. *14* **2006**, 92.

(73) Stark, C. B. W.; Pierau, S.; Wartchow, R.; Hoffmann, H. M. R. *Chem. Eur. J.* **2000**, *6*, 684.

(74) Packer, M. J. e. a.; AstraZeneca AB, Swed.; AstraZeneca UK Ltd.: 2008; Vol. WO2008099145 (A1) — 2008-08-21.

(75) Pavlik, C.; Biswal, N. C.; Gaenzler, F. C.; Morton, M. D.; Kuhn, L. T.; Claffey, K. P.; Zhu, Q.; Smith, M. B. *Dyes and Pigments*, *89*, 9.

(76) Quadrex 007-5-15-0.33F:450C:15mx250umx0.33um; Flow 0.92 mL/min, pressure 0.28329psi, Avg velocity 49.313cm/sec

(77) QUATTRO II (WATERS), MS range 100-650, Capillary 3.50KV, Cone voltage 40V, Desolvation temperature 150C. Sample concentration was 2-3uM in Methanol.

(78) methyl group was overlapped with solvent peak at 3.3 ppm

(79) QUATTRO II (WATERS), MS range 100-650, Capillary 3.50KV, Cone voltage 40V, Desolvation temperature 150C. Sample concentration was 2-3uM in Methanol.

(80) Imaeda, Y.; Kuroita, T.; Sakamoto, H.; Kawamoto, T.; Tobisu, M.; Konishi, N.; Hiroe, K.; Kawamura, M.; Tanaka, T.; Kubo, K. *Journal of Medicinal Chemistry* **2008**, *51*, 3422.

(81) Gordon, R.; Peter, S.; Claire, C.; William, D.; Swarnalatha, G. In *PCT WO2009120094 A3*; Rewcastle: 2009.

(82) We could not get full 13C spectrum of final dye molecules even with 30,000 scans and concentrated samples. It could be due to the aggregation of dyes in the solution.

(83) Nagao, Y.; Sakai, T.; Kozawa, K.; Urano, T. *Dyes and Pigments* **2007**, *73*, 344.

(84) Salon, J.; Ska, E. W.; Raszkiewicz, A.; Patonay, G.; Strekowski, L. *Journal of Heterocyclic Chemistry* **2005**, *42*, 959.

(85) Jung, M. E.; Kim, W. J. *Bioorganic and Medicinal Chemistry* **2006**, *14*, 92.

(86) Kelly, J. M.; Leeper, F. J. *Tetrahedron Letters* **2012**, *53*, 819.

(87) Quirante, J.; Vila, X.; Bonjoch, J. *Synthesis* **2001**, *2001*, 1971.

(88) Junga, M., E. ; Raylea, H., L. *Synth. Commun* **1994**, *24*, 197.

(89) Periodontitis (Advanced Gum Disease). http://www.webmd.com/oral-health/periodontitis-advanced-gum-disease (accessed (March 28th, 2014)).

(90) Nichols, F. C.; Rojanasomsith, K. *Oral Microbiol. Immunol* **2006**, *21*, 84.

(91) Nichols, F. C.; Levinbook, H.; Shnaydman, M.; Goldschmidt, J. *J. Periodont. Res.* **2001**, *36*, 1142.

(92) Nichols, F. C. *J. Lipid Res.* **1998**, *39*, 2360.

(93) Nichols, F. C.; Riep, B.; Mun, J.; Morton, M. D.; Kawai, T.; Dewhirst, F. E.; Smith, M. B. *J. Lipid Res.* **2006**, *47*, 844.

(94) Garner, P.; Park, J. M.; Malecki, E. *J. Org. Chem.* **1988**, *53*, 4395.

(95) Feldhues, M.; Schäfer, H. J. *Tetrahedron* **1985**, *41*, 4213.

(96) Pines, H.; Stalick, W. M. *Base-Catalyzed Reactions of hydrocarbons and Related Compounds*; Academic Press, NY, , 1977.

(97) Théron, F.; Verny, M.; Vessière, R.; Patai, S. *The Chemistry of Carbon-Carbon Triple Bond*; Wiley, NY, 1978.

(98) Bushby, R. J. *Q. Rev. Chem. Soc.* **1970**, *24*, 585.

(99) Iwai, I. *Mech. Mol. Migr.* **1969**, *2*, 73.

(100) Wotiz, J. H.; Viehe, H. *Acetylenes*; Marcel Dekker,: NewYork, 1969.

(101) Vartanyan, S. A.; Babanyan, S. O. *Russ. Chem. Rev.* **1967**, *36*, 670.

(102) Huntsman, W. D. *The Chemistry of Ketenes, Allenes, and Related Compounds*; Wiley: NewYork, 1980.

(103) Fordyce, C. R.; Johnson, J. R. *J. Am. Chem. Soc.* **1933**, *55*, 3368.

(104) Milburn, A. H.; Truter, E. V. *J. Chem. Soc.* **1954**, 3344.

(105) Singh, J.; Arora, A. K.; Kaur, A.; Kad, G. L. *Coll. Czech. Chem. Commun.* **1994**, *59*, 721.

(106) Takikawa, H.; Nozawa, D.; Kayo, A.; Muto, S.; Mori, K. *J. Chem. Soc., Perkin Trans.* **1999**, 2467.

(107) Farmer, M. L.; Billups, W. E.; Greenlee, R. B.; Kurtz, A. N. *J. Org. Chem.* **1966**, *31*, 2885.

(108) Smadja, W. *Ann. Chim.* **1965**, *10*, 105.

(109) Abrams, S. R.; Shaaw, A. C. *J. Org. Chem.* **1987**, *52*, 1835.

(110) Mathai, I. M.; Taniguchi, H.; Miller, S. I. *J. Am. Chem. Soc.* **1967**, *89*, 115.

(111) Bushby, R. J. *J. Quart. Rev., Chem. Soc.* **1970**, *24*, 585.

(112) Hass, E. C.; Mezey, P. G.; Abrams, S. R. *J. Comput. Chem.* **1982**, *3*, 185.

(113) Brown, C. A.; Yamashita, A. *J. Am. Chem. Soc.* **1975**, *97*, 891.

(114) Spence, J. D.; Wyatt, J. K.; Bender, D. M.; Moss, D. K.; Nantz, M. H. *J. Org. Chem.* **1996**, *61*, 4014.

(115) Théron, F.; Verny, M.; Vessiére, R. *The Chemistry of the Carbon-Carbon Triple Bond*; John Wiley and Sons: New York, 1978; Vol. Part I.

(116) Wotiz, J. H.; Barelski, P. M.; Koster, D. R. *J. Org. Chem.* **1973**, *38*, 489.

(117) Restrepo, A. A.; Bohn, R. K. *J. Mol. Struct.* **2007**, *833*, 189.

(118) sample size 1.0 g, drift auto 0.9g/min, content 192.90.6 ppm.

(119) Ulysse, L. G.; Chmielewski, J. *J. Bioorg. Med. Chem. Lett.* **1998**, *8*, 3281.

(120) Erdik, E.; Dusmezkalender, F.; Ozlu, Y. *Synth. React. Inorg. Met. - Org. Chem.* **1993**, *23*, 551.

(121) Tamura, M.; Kochi, J. *Synthesis* **1971**, 303.

(122) Mun, J.; Onorato, A.; Nichols, F. C.; Morton, M. D.; Saleh, A. I.; Welzel, M.; Smith, M. B. *Org. Biomol. Chem.* **2007**, *5*, 3826.

(123) Instrument: AccuTOF (JEOL, Peabody, MA) Source conditions: The DART ion source was operated with helium gas for analysis and nitrogen gas in the standby mode. A small amount of a sample (3–5 μL) was placed into the ion source using a glass melting point stick. Helium (more than 99.999% purity) heated to 250°C was used for ionization. The voltage on the discharge needle of the DART source was 4 kV. Grid voltage 350 V. Mass spec conditions: Orifice 1 temperature 120 °C. Orifice 1 voltage 20 V. Peaks voltage 600 V. The mass spectra were recorded over an m/z range of 60–500 in positive ion mode. PEG 600 was employed for mass calibration.

(124) Instrument: AccuTOF (JEOL, Peabody, MA) Source conditions: The DART ion source was operated with helium gas for analysis and nitrogen gas in the standby mode. A small amount of a sample (3–5 μL) was placed into the ion source using a glass melting point stick. Helium (more than 99.999% purity) heated to 250°C was used for ionization. The voltage on the discharge needle of the DART source was 4 kV. Grid voltage 350 V. Mass spec conditions: Orifice 1 temperature 120 °C. Orifice 1 voltage 20 V. Peaks voltage 600 V. The mass spectra were recorded over an m/z range of 60–500 in positive ion mode. PEG 600 was employed for mass calibration.